

## INFORMATION TO USERS

This manuscript has been reproduced from the microfilm master. UMI films the text directly from the original or copy submitted. Thus, some thesis and dissertation copies are in typewriter face, while others may be from any type of computer printer.

**The quality of this reproduction is dependent upon the quality of the copy submitted.** Broken or indistinct print, colored or poor quality illustrations and photographs, print bleedthrough, substandard margins, and improper alignment can adversely affect reproduction.

In the unlikely event that the author did not send UMI a complete manuscript and there are missing pages, these will be noted. Also, if unauthorized copyright material had to be removed, a note will indicate the deletion.

Oversize materials (e.g., maps, drawings, charts) are reproduced by sectioning the original, beginning at the upper left-hand corner and continuing from left to right in equal sections with small overlaps. Each original is also photographed in one exposure and is included in reduced form at the back of the book.

Photographs included in the original manuscript have been reproduced xerographically in this copy. Higher quality 6" x 9" black and white photographic prints are available for any photographs or illustrations appearing in this copy for an additional charge. Contact UMI directly to order.

**UMI<sup>®</sup>**

Bell & Howell Information and Learning  
300 North Zeeb Road, Ann Arbor, MI 48106-1346 USA  
800-521-0600



University of Alberta

**Modeling the constitutive behavior of sand for the analysis of static liquefaction**

by

S. M. REZA IMAM



A thesis submitted to the Faculty of Graduate Studies and Research in partial fulfillment  
of the requirements for the degree of Doctor of Philosophy

in

Geotechnical Engineering

Department of Civil Engineering

Edmonton, Alberta

Spring 1999



National Library  
of Canada

Acquisitions and  
Bibliographic Services

395 Wellington Street  
Ottawa ON K1A 0N4  
Canada

Bibliothèque nationale  
du Canada

Acquisitions et  
services bibliographiques

395, rue Wellington  
Ottawa ON K1A 0N4  
Canada

*Your file Votre référence*

*Our file Notre référence*

The author has granted a non-exclusive licence allowing the National Library of Canada to reproduce, loan, distribute or sell copies of this thesis in microform, paper or electronic formats.

The author retains ownership of the copyright in this thesis. Neither the thesis nor substantial extracts from it may be printed or otherwise reproduced without the author's permission.

L'auteur a accordé une licence non exclusive permettant à la Bibliothèque nationale du Canada de reproduire, prêter, distribuer ou vendre des copies de cette thèse sous la forme de microfiche/film, de reproduction sur papier ou sur format électronique.

L'auteur conserve la propriété du droit d'auteur qui protège cette thèse. Ni la thèse ni des extraits substantiels de celle-ci ne doivent être imprimés ou autrement reproduits sans son autorisation.

0-612-39543-X

**Canada**

University of Alberta

Library Release Form

Name of Author: Seyed Mohammad Reza Imam

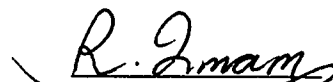
Title of thesis: **Modeling the constitutive behavior of sand for the analysis of static liquefaction**

Degree: Doctor of Philosophy

Year this degree granted: 1999

Permission is hereby granted to the University of Alberta Library to reproduce single copies of this thesis and to lend or sell such copies for private, scholarly, or scientific research purposes only.

The author reserves all other publication and other rights in association with the copyright in the thesis, and except as herein provided, neither the thesis nor any substantial portion thereof may be printed or otherwise reproduced in any material form whatever without the author's prior written permission.



139 Michener Park

Edmonton, Alberta

Canada, T6H 4M4

4/16/99

**University of Alberta**

**Faculty of Graduate studies and Research**

The undersigned certify that they have read, and recommended to the Faculty of Graduate Studies and Research for acceptance, a thesis entitled **Modeling the Constitutive Behavior of Sand for the Analysis of Static Liquefaction** submitted by **S. M. Reza Imam** in partial fulfillment of the requirements for the degree of Doctor of Philosophy in Geotechnical Engineering.



Dr. N. R. Morgenstern  
(Supervisor)



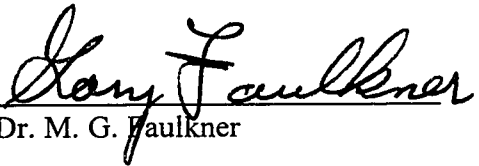
Dr. P. K. Robertson  
(Co-Supervisor)



Dr. D. Chan  
(Co-Supervisor)



Dr. A. E. Elwi



Dr. M. G. Faulkner



Dr. A. J. Whittle  
(External Examiner)

Date 3/28/99

*To Hora, Mohammad and Mohsen and  
To My beloved Mother and late Father*

## **ABSTRACT**

This dissertation examines the constitutive behavior of sand and describes the development of a constitutive model based on this examination. Emphasis is placed on the determination of conditions that lead to unstable strain softening response in undrained shearing of loose sand and modeling the constitutive behavior of sand exhibiting such response. The yield surface was identified an element of the model that significantly influences the predicted response of such materials and is therefore investigated in detail.

Based on the analysis of results of tests on very loose Ottawa sand and following some suggestions in previous literature, it was assumed that the stress ratio at the peak of the capped yield surface of loose sand can be approximated by the stress ratio  $M_p$  measured at the peak of the undrained effective stress path (UESP). Effects of various factors on the yielding behavior of loose sand were therefore investigated by studying the variation of  $M_p$  measured from the UESPs of different sands. Variations of the stress ratio  $M_p$  with factors such as density, mean normal stress, intermediate principal stress, direction of loading, anisotropic consolidation, and soil fabric were examined and formulated. These formulations were used to construct yield surfaces that were functions of the factors mentioned above. Model predictions using these yield surfaces showed that the effects of these factors on the behavior of sand can be accounted for using these yield surfaces. Formulation of the variation of  $M_p$  also made it possible to investigate quantitatively the effects of these factors on the susceptibility of loose sand to collapse and flow failure.



The critical state constitutive model that was developed in this study is capable of predicting the behavior of sand over a wide range of void ratios and confining pressures and subjected to different loading conditions. A unique set of model parameters including a unique ultimate (steady) state line is used in all model predictions. The significant differences in the response of sand to loading in different directions and modes of shearing are modeled using these unique parameters. The two types of directional properties resulting from stress-induced anisotropy and inherent anisotropy are characterized by two separate and independent parameters. The ways in which the predicted behavior is influenced by the two types of anisotropy are also different from each other. Formulation of the hardening rule is based on "state hardening" such that hardening of the material is related to the current "state" rather than the "strain" experienced by the soil from the start of shearing.

## ACKNOWLEDGEMENTS

I would like to express my sincere gratitude to Professor N. R. Morgenstern and Professor P. K. Robertson for supervising this study.

I am deeply indebted to Professor N. R. Morgenstern for his expert guidance, insightful discussions and time allocated to this work. His kindness, remarkable patience and continuous support were essential in making this work a pleasant and satisfying research experience for me.

I wish to express my sincere appreciation to Professor P. K. Robertson for his encouragement, discussions and productive ideas. He provided me with research material and learning opportunities without which this study could not have achieved its goals. The encouragement, discussions, and time provided by Professor D. H. Chan for this research were also invaluable.

I would like to thank Dr. M. Yoshimine from the University of Tokyo for providing me with digital test data on Toyoura sand. The help provided by Professor H. P. Kunzle from the Department of Mathematical Sciences of the University of Alberta with the mathematical aspects of the work is appreciated.

The financial support received from the Ministry of Culture and Higher Education of the Islamic Republic of Iran and the Natural Sciences and Engineering Research Council of Canada (NSERC) are acknowledged. The awards granted by the Coal Mining Research Company and the Mary Louise Imrie scholarship are appreciated.

Finally, I would like to thank my wife Hora Paran and our two sons Mohammad and Mohsen for their patience and understanding. The love and support of my parents and the continuous help of my brother S. Hashem have always been an asset at different stages of my life.

## **TABLE OF CONTENTS**

**Page**

<b><u>CHAPTER ONE: INTRODUCTION</u></b> .....	<b>1</b>
<b>1.1 Constitutive modeling of sand and the analysis of flow liquefaction</b> .....	<b>1</b>
<b>1.2 Initiation of flow liquefaction</b> .....	<b>3</b>
<b>1.3 Constitutive modeling of sand</b> .....	<b>5</b>
<b>1.4 Outline of the thesis</b> .....	<b>8</b>
<b><u>CHAPTER TWO: CONSTITUTIVE MODELING AND LIQUEFACTION OF SAND</u></b> .....	<b>11</b>
<b>2.1 Introduction</b> .....	<b>11</b>
<b>2.2 Modeling the constitutive behavior of sands</b> .....	<b>12</b>
2.2.1 The behavior of sands.....	12
2.2.2 Modeling sand behavior .....	14
2.2.2.1 Elements of a constitutive model for sands.....	14
2.2.2.2 The yield locus of sand.....	16
2.2.2.3 Evaluation of yield functions used in some recent models for sand .....	19
2.2.3 An overview of current constitutive models for sands.....	20
<b>2.3 Liquefaction of granular soils</b> .....	<b>26</b>
2.3.1 Response of a mass of sandy soil to undrained loading.....	26
2.3.2 Flow liquefaction.....	28
2.3.2.1 Flow liquefaction as observed in the field.....	28
2.3.2.2 Experimental studies on flow liquefaction .....	28
2.3.2.3 Empirical criteria for flow liquefaction .....	30
2.3.2.4 Flow liquefaction and instability .....	32
2.3.2.5 Theoretical criteria for instability and flow liquefaction.....	34
<b>2.4 Summary</b> .....	<b>35</b>

## **CHAPTER THREE: YIELDING AND COLLAPSE BEHAVIOR OF SANDS . 47**

<b>3.1 Introduction .....</b>	<b>47</b>
<b>3.2 A yield function for sand, its experimental verification and parameter determination.....</b>	<b>48</b>
3.2.1 A Yield function for sand.....	48
3.2.2 Comparison of the yield function with some experimentally derived yield loci .....	49
3.2.3 Yield function for anisotropically consolidated sand.....	51
<b>3.3 Yield surface of loose Ottawa sand and its relationship to the undrained effective stress path (UESP).....</b>	<b>56</b>
3.3.1 Establishing the yield surface of Ottawa sand.....	56
3.3.2 Yield surface and the undrained effective stress path (UESP).....	58
3.3.3 $M_p$ from drained vs. undrained tests.....	58
<b>3.4 Instability, collapse and undrained softening of loose sand and their relationship to sand yielding.....</b>	<b>60</b>
3.4.1 Shape of the yield surface and the susceptibility of sand to instability and collapse.....	60
3.4.2 Stable collapse of dry sand and unstable collapse of saturated sand in CDS tests: Effect of drainage condition.....	61
3.4.3 Yield surface and slope of the state boundary surface: Effect of consolidation pressure .....	63
3.4.4 Yield surface and the onset of undrained softening in monotonic and cyclic tests: Effect of stress path .....	64
3.4.5 Yield surface and the collapse of anisotropically consolidated sands: Effect of stress ratio at consolidation .....	65
3.4.6 Yield surface and the size of the region of collapsible states: Effect of density.....	65

**CHAPTER FOUR: FACTORS AFFECTING YIELDING OF LOOSE SAND**

**DERIVED FROM THE VARIATION OF  $M_p$ .....81**

**4.1 Introduction .....81**

**4.2 Effect of density .....83**

    4.2.1 Experimental observations .....83

    4.2.2 Formulation of the variation of  $M_p$  with void ratio .....85

    4.2.3 The relation of  $M_p$  with soil strength and dilatancy .....87

**4.3 Effect of mean normal stress .....89**

    4.3.1 Effect of mean normal stress on the stress ratio  $M_p$  .....89

    4.3.2 Formulating the effect of pressure using  $e_n$  and  $\psi_n$  .....92

**4.4 Compression vs. extension .....92**

    4.4.1 Experimental observations .....92

    4.4.2 Formulation of the variations for compression and extension .....93

**4.5 Effect of intermediate principal stress.....94**

    4.5.1 Experimental observations .....94

    4.5.2 Selection of appropriate stress function to account for  $b$  .....97

    4.5.3 Variation of strength at peak with  $b$  in the ROP ..... 100

**4.6 Effect of direction of loading .....103**

    4.6.1 Representation of states of stress corresponding to different directions of loading.....103

    4.6.2 Correlating experimental results..... 106

**4.7 Approximating the combined effects of  $b$  and  $\alpha_\sigma$ .....108**

    4.7.1 Representation of states of stress..... 108

    4.7.2 Implications on stability analysis ..... 112

        4.7.2.1 Stress ratios at which sand is collapsible..... 112

        4.7.2.2 Void ratios at which sand is collapsible: Practical implication of  $e_\mu$  .... 116

**4.8 Effect of anisotropic consolidation.....119**

<b>4.9 Effect of preparation method and soil fabric.....</b>	<b>120</b>
<b>Appendix 4A: Micromechanical phenomena involved in yielding .....</b>	<b>159</b>
4A-1 Shape of the yield surface and its relationship to the mechanisms involved in yielding.....	159
4A-2 Small strain yielding at low shear stress levels.....	160
4A-3 Large strain yielding at high shear stress levels.....	161
4A-4 Observed variation of $M_p$ and the micro-mechanical behavior of sand.....	163
<b>Appendix 4B Representation of the state of stress at peak in principal stress space.....</b>	<b>167</b>
4B-1 Stress states in principal stress space.....	167
4B-2 Variation of strength on the octahedral plane.....	169
4B-3 Accounting for anisotropy of yield-failure strength.....	171

## **CHAPTER FIVE: A CRITICAL STATE CONSTITUTIVE MODEL FOR SAND**

	<b>174</b>
<b>5.1 Introduction .....</b>	<b>174</b>
<b>5.2 Model elements .....</b>	<b>176</b>
5.2.1 The yield surface .....	176
5.2.2 The plastic potential .....	178
5.2.2.1 Pressure and density dependence of stress-dilatancy derived from Rowe's relationship.....	178
5.2.2.2 Determination of the material parameter for Nova's simplified stress-dilatancy relationship.....	183
5.2.2.3 The shape and movement of the plastic potential .....	184
5.2.3 The compression model.....	187
5.2.4 The hardening rule.....	188
5.2.4.1 Size hardening .....	188
5.2.4.2 Shape hardening .....	193
5.2.5 Elasticity .....	193

<b>5.3 Model Calibration .....</b>	<b>196</b>
<b>5.4 Model performance .....</b>	<b>200</b>
5.4.1 Modeling the collapse behavior of very loose Ottawa sand.....	201
5.4.2 Modeling the behavior of Toyoura sand in triaxial compression and extension.....	204
<b>5.5 Summary and conclusions .....</b>	<b>209</b>
<b>Appendix 5A General formulation of the stress-strain relationship for triaxial conditions .....</b>	<b>240</b>

**CHAPTER SIX: FORMULATION OF THE CONSTITUTIVE MODEL IN  
GENERAL STRESS SPACE .....**

<b>6.1 Introduction .....</b>	<b>242</b>
<b>6.2 General formulation of the stress-strain relationship.....</b>	<b>245</b>
6.2.1 General formulation.....	245
6.2.2 Determination of the constitutive relationships using unit tensors .....	248
<b>6.3 Model elements .....</b>	<b>251</b>
6.3.1 The yield function.....	251
6.3.1.1 Stress-induced anisotropy.....	252
6.3.1.2 Structural (inherent) anisotropy.....	254
6.3.1.3 Effect of void ratio and pressure on the yielding behavior .....	258
6.3.2 The “direction” of strain increments .....	260
6.3.2.1 The stress-dilatancy relationship .....	260
6.3.2.2 The stress ratio at phase transformation .....	261
6.3.2.3 Determination of the dilatancy parameter D .....	263
6.3.3 The hardening rules .....	264
6.3.3.1 Size hardening .....	265
6.3.3.2 Shape hardening .....	269
6.3.4 Other model elements.....	269

<b>6.4 Model performance .....</b>	<b>269</b>
6.4.1 Sands modeled and parameters used .....	269
6.4.2 Anisotropically consolidated sand and the effect of direction of consolidation .....	271
6.4.3 Effect of direction of loading .....	273
6.4.4 Effect of mode of shearing .....	274
6.4.5 Effect of soil fabric .....	276
 <b>Appendix 6A: Formulation of the stress-strain relationship.....</b>	<b>301</b>

**CHAPTER SEVEN: SUMMARY, CONCLUSIONS AND RECOMMENDATIONS**

<b>7.1 Summary and conclusions .....</b>	<b>304</b>
<b>7.2 Recommendations .....</b>	<b>311</b>

<b><u>REFERENCES.....</u></b>	<b>314</b>
-------------------------------	------------



**LIST OF TABLES**

**Page**

**CHAPTER FOUR**

**Table 2-1** Properties of sands investigated.....123

**CHAPTER FIVE**

**Table 2-2** Model parameters used in response predictions for Ottawa and Toyoura sands. For Toyoura sand, parameters for peak state are given for moist tamped (MT) samples, and values in parenthesis are for dry deposited (DD) samples. All unit-dependent parameters are given assuming that (p) is substituted in the equations in terms of kPa, except where stated otherwise.....211

**CHAPTER SIX**

**Table 6-3** Model parameters used in response predictions for Toyoura sand and Ham River sand. Parameters are obtained from results of hollow cylinder (HC) tests. Peak parameters for Toyoura sand were obtained from dry deposited (DD) samples. Values of  $a_p$  and  $\phi_{cv}$  obtained for Toyoura sand from results of HC tests were somewhat different from those obtained from triaxial tests (Table 5-1). Parameters for Ham River sand were obtained from results of tests at  $b=0.5$  and therefore, indicate larger strengths in terms of friction angle. Data to determine other parameters for Ham River sand were not available.....279

## **LIST OF FIGURES**

### **CHAPTER ONE**

**Page**

- Figure 1-1** Relationship between the ratio of friction angle at peak strength to residual strength, with porosity obtained from undrained shear tests performed by Castro (1969) on Banding sand (modified after Bishop, 1971)..... 10

### **CHAPTER TWO**

- Figure 2-1** Concepts of critical void ratio (Casagrande, 1936) and ultimate strength as illustrated by Casagrande (1971)..... 36
- Figure 2-2** Undrained behavior of Banding sand in monotonic tests (modified after Castro, 1969)..... 37
- Figure 2-3** Response of loose and dense sand to cyclic loading as illustrated by Ishihara (modified after Ishihara, 1985) ..... 38
- Figure 2-4** Yield loci measured from tests on sands with various densities: ..... 39
- Figure 2-5** Experimental yield stresses obtained for dense sand:..... 40
- Figure 2-6** Flow chart to identify the response of sandy ground to loading (modified after Robertson, 1994). The current thesis addresses the triggering condition for flow liquefaction and the stress-strain behavior of the material after triggering..... 41
- Figure 2-7** Response of a soil element with static shear to monotonic and cyclic loads as illustrated by Robertson (modified after Robertson, 1994) ..... 42
- Figure 2-8** Behavior of very loose sand when stress ratio at collapse is reached under various conditions..... 43
- Figure 2-9** Empirical criteria for the initiation of collapse and instability in granular soils: a) The collapse surface (modified after Sladen et al., 1985); b) The critical stress ratio (CSR) line (modified after Vaid et al., 1990); c) The instability line (modified after Lade et al., 1990); d) The state boundary surface (modified after Sasitharan et al., 1993) ..... 44

<b>Figure 2-10</b> Initiation of strain softening and flow deformation in undrained monotonic and cyclic tests.....	45
<b>Figure 2-11</b> Effect of the rate of volume change imposed on sands on their behavior : a) Strain softening and strain hardening of samples subjected to the same rate of volume change (-0.54) but consolidated to different pressures. Also for the same pressure (900 KPa) softening or hardening can occur depending on the rate of volume change imposed on the soil. b) Softening or hardening of samples subjected to volumetric strain rates smaller or larger than that exhibited by the soil itself at failure (modified after Chu et al., 1993).....	46

### CHAPTER THREE

<b>Figure 3-1</b> Comparison of yield surfaces obtained experimentally with the yield function used in the current study: (a) Dense sand (exp. results obtained from tests on Aio sand) (b) Loose sand.....	67
<b>Figure 3-2</b> Yield surfaces with equal friction angle at peak in compression and extension compared with experimental yield points .....	68
<b>Figure 3-3</b> Yield surface with reduced friction angle at peak in extension, compared with experimental yield stresses .....	69
<b>Figure 3-4</b> Definition of parameters used in the yield surface of anisotropically consolidated sand.....	70
<b>Figure 3-5</b> Yield surfaces for anisotropically consolidated sand compared with average experimental results (a) with equal friction angle at peak in compression and extension (b) with reduced friction angle at peak on the extension side .....	71
<b>Figure 3-6</b> Comparison of experimental yield points with the yield surface in which calculated values of $\alpha$ and $p_\alpha$ are used (reduced friction angle at peak was used on the extension side) .....	72
<b>Figure 3-7</b> Results of a CDS test on very loose dry Ottawa sand: Very small volume change between points A and B, and significant contraction between points B and C. (modified after Skopek, 1994).....	73
<b>Figure 3-8</b> Determination of yield parameters $M_p$ and $p_c$ from tests on Ottawa sand at different void ratios and consolidation pressures (Test data from Skopek, 1994).....	74
<b>Figure 3-9</b> Variation of parameter $M_p$ with void ratio, obtained from CDS tests on dry Ottawa sand.....	75

<b>Figure 3-10</b> Comparison of the undrained effective stress path (UESP) with the shape of the yield surface for a sample of Ottawa sand with a void ratio of 0.805 consolidated to 550 kPa. ....	76
<b>Figure 3-11</b> Variation of $M_p$ with void ratio obtained from CDS tests on dry sand and undrained tests on saturated sand .....	77
<b>Figure 3-12</b> Stress state at collapse of very loose dry and saturated Ottawa sand in CDS tests, compared to the position of the yield surface.....	78
<b>Figure 3-13</b> Factors affecting stress ratio at onset of undrained softening or instability:.....	79
<b>Figure 3-14</b> Differences in stress states at the onset of yielding of loose sands and clayey soils in CDS tests, and accounting for these differences through the use of appropriate shapes for their yield surfaces. ....	80

#### CHAPTER FOUR

<b>Figure 4-1</b> Position of ultimate (steady) state lines (USL) of sands investigated in $e$ - $\ln p$ plane. The USL of Toyoura sand is obtained by regression, using average test results reported by Ishihara (1993). ....	124
<b>Figure 4-2</b> Grain size distribution of sands investigated, as reported in different studies .....	125
<b>Figure 4-3</b> Variation of $M_p$ with void ratio at consolidation for three different sands consolidated to pressures up to 600 kPa. ....	126
<b>Figure 4-4</b> Variation of $M_p$ with state parameter at peak in different sands, consolidated to pressures up to 600 kPa. Note that for some sands the available data covered a limited range of states (as e. g. in Syncrude(2)) or a limited number of data points (as e. g. in Erksak).....	127
<b>Figure 4-5 (a)</b> Variation of $M_p$ with state parameter at peak for all the sands investigated.....	128
<b>Figure 4-6</b> Variation of $M_p$ with void ratio and normalized void ratio in the low and high ranges of pressure. Samples were prepared by Moist Tamping (MT) and dry deposition (DD).....	129
<b>Figure 4-7</b> Variation of $M_p$ with state parameter and normalized state parameter for the low and high ranges of pressure. Samples were prepared by Moist Tamping (MT) and dry deposition (DD).....	130

<b>Figure 4-8</b> Variation of $M_p$ and $\tan\phi_p$ with normalized void ratio ( $e_n$ ) in Triaxial Compression (TC) and Triaxial Extension (TE). Samples were prepared by Moist Tamping (MT) and dry deposition (DD).....	131
<b>Figure 4-9</b> Variation of friction angles at peak for Ottawa sand and Syncrude sand. Void ratios for Syncrude sand were not normalized because the range of pressures was small. Samples were prepared by moist tamping (MT) and water pluviation (WP).....	132
<b>Figure 4-10</b> Effect of direction of loading on $M_p$ for Syncrude sand (data from Wride and Robertson, 1997a), and Toyoura sand. (Data on moist tamped (MT) samples from Verdugo, 1992 and on dry deposited (DD) samples from Yoshimine, 1996).....	133
<b>Figure 4-11</b> Effect of direction of loading and intermediate principal stresses on $\tan\phi_p$ .....	134
<b>Figure 4-12</b> Representation of yield-failure criteria in the octahedral plane.....	135
<b>Figure 4-13</b> Different yield-failure criteria used to correlate stress states at peak for water pluviated (WP) Syncrude sand (data measured from Wride and Robertson, 1997a).....	136
<b>Figure 4-14</b> Different yield-failure functions used to correlate stress states at peak (tests on Moist Tamped (MT) samples from Verdugo, 1992 and Dry Deposited (DD) samples from Yoshimine, 1996).....	137
<b>Figure 4-15</b> Samples of undrained tests used to investigate the effects of $\alpha_\sigma$ and b on $M_p$ for Toyoura sand: (a) effect of $\alpha_\sigma$ (b) effect of b (modified after Yoshimine, 1996).....	138
<b>Figure 4-16</b> Variation of $M_p$ as represented in the reference octahedral plane (ROP). See Appendix 4B for the definition of variables and the analytical form of Matsouka-Nakai failure-yield criteria (data measured from Yoshimine, 1996) .....	139
<b>Figure 4-17</b> Yield loci obtained from contours of equal shear stains in drained True Triaxial Tests (TTT). Stress states at Phase transformation (PT) and failure are also shown (modified after Yamada and Ishihara, 1979).....	140
<b>Figure 4-18</b> Diagrams similar to Figure 4-16 but for Toyoura sand at two other void ratios. "Model" in the legends of the figures refers to the Matsouka-Nakai failure-yield criteria (Data measured from Yoshimine, 1996) .....	141

<b>Figure 4-19</b> (a) The Mohr diagram (b) the reference Mohr diagram and "Reference Mohr Circle" (RMC) used to represent stress states at peak with constant $b$ and different directions of loading $\alpha_\sigma$ .....	142
<b>Figure 4-20</b> Yield and failure surfaces obtained from torsional shear tests in the HC apparatus: (a) Stress paths followed to obtain yield stresses (b) Yield stresses (c) Failure stresses obtained by increasing shear stresses along fixed directions of loading $\alpha_\sigma$ (a and b modified after Pradel et al., 1990 and c modified after Gutierrez et al., 1993).....	143
<b>Figure 4-21</b> Variations of $R_p = \sin\phi_p$ with $\alpha_\sigma$ for Toyoura sand. Void ratios were not normalized since pressures were small (below 100 kPa) (data measured from Yoshimine, 1996). .....	144
<b>Figure 4-22</b> Variations of $R_p = \sin\phi_p$ with $\alpha_\sigma$ for three different sands (Data for Syncrude sand and Fraser River sand measured from Wride and Robertson, 1997a and b).....	145
<b>Figure 4-23</b> Using the reference Mohr diagram to determine $R_p$ from $R'_p$ and $a'_p$ for an arbitrary value of $\alpha_\sigma$ .....	146
<b>Figure 4-24</b> Changes in the relative magnitudes of the three normal stresses with $\beta$ in a true triaxial test (TTT).....	147
<b>Figure 4-25</b> Variation of $M_p$ with $\beta$ for three different densities of Toyoura sand plotted in a polar coordinate. Void ratios were those at consolidation and were not normalized because the confining stresses involved were small. ....	148
<b>Figure 4-26</b> Variation of $M_p$ with $\beta$ in polar coordinate for three different sands .....	149
<b>Figure 4-27</b> Variation of stress ratio at Phase Transformation ( $M_{PT}$ ) with $\beta$ (data measured from Yoshimine, 1996) .....	150
<b>Figure 4-28</b> Evaluation of the susceptibility of loose sand to collapse and flow failure when sheared in different modes.....	151
<b>Figure 4-29</b> Comparisons of regions of collapsible states for dry deposited Toyoura sand consolidated to 100 kPa and three different void ratios .....	152
<b>Figure 4-30</b> Maximum and minimum values of $M_p$ and undrained effective stress paths from which these values are measured. Normalized void ratios corresponding to these limiting values of $M_p$ are also shown. ....	153

<b>Figure 4-31</b> Determination of combinations of void ratio and confining pressures at which sand is collapsible, from the variation of $M_p$ with normalized void ratio. Note that the results shown above are obtained from triaxial compression tests on moist tamped samples (Figure (b) modified after Ishihara, 1993).....	154
<b>Figure 4-32</b> Comparison between values of $M_p$ measured from isotropically consolidated, and anisotropically consolidated sand (Syncrude sand data from Wride and Robertson, CANLEX report, 1997a; Fraser River sand data from Thomas, 1996).....	155
<b>Figure 4-33</b> Effect of soil fabric on the relationship between $M_p$ and the normalized void ratio or normalized state parameter.....	156
<b>Figure 4-34</b> Effect of soil fabric on the variation of $M_p$ for two different sands.....	157
<b>Figure 4-35</b> Effect of preparation method on $M_p$ measured from TC tests on moist tamped samples with different numbers of soil layers: (a) samples prepared using 6-lifts (b) samples prepared using 12-lifts (modified after Riemer, 1992).....	158
<b>Figure 4A-1</b> Aspects of the micro-mechanical behavior of granular materials in small strain: (a) Relative slip required to mobilize full inter-particle friction in chalk (b) Axial strain at failure as a function of axial stress at failure in drained TC tests for materials with different strength (c) Effect of density on the friction angle that should be mobilized ( $\phi_m$ ) along the plane of overall slippage, in order to initiate gross slippage at particle contacts ( $f$ is the inter-particle force and $\theta$ is the angle of contact inclination) (a and b from Billam, 1971).....	165
<b>Figure 4A-2</b> Variation of stress ratio at peak ( $M_p$ ) and at failure ( $M_{max}$ ) in triaxial compression (TC) and extension (TE) for an isotropic soil. Note that the slope $k$ may not be the same in TC and TE.....	166
<b>Figure 4B-1</b> The "reference octahedral plane" (ROP) in principal stress space and representation of stress states at peak on this plane.....	173

## CHAPTER FIVE

<b>Figure 5-1</b> Shape of the yield surface for isotropically consolidated (IC) sand, Anisotropically consolidated sand in compression (ACC) and Anisotropically consolidated sand in extension (ACE).....	212
---	-----

<b>Figure 5-2</b> Correlation of the friction angle at phase transformation (PT) with void ratio and state parameter.....	213
<b>Figure 5-3</b> -Determination of parameter A in Equation 5-14, using Rowe's (1962) stress-dilatancy relationship .....	214
<b>Figure 5-4</b> Evolution of the plastic potential (PP) and the stress ratio at its peak $M_{PT}$ in a drained triaxial compression (TC) test: (1) at phase transformation (PT) ; (2) at peak strength (failure); (3) at ultimate (steady) state (SS) where $M_{PT} = M_{cv}$ .....	215
<b>Figure 5-5</b> Variation of the function $f(p/p_c)$ (Equation 5-28) with the ratio $p/p_c$ .....	216
<b>Figure 5-6</b> Definition of model parameters used to determine friction angles of sand: (a) at the peak of the yield surface (b) at phase transformation (PT).....	217
<b>Figure 5-7</b> Determination of parameters for peak state for moist tamped (MT) and dry deposited (DD) samples of Toyoura sand.....	218
<b>Figure 5-8</b> Determination of the compressibility parameter $\beta$ (Pestana and Whittle, 1995) using compression data on Ottawa and Toyoura sands. Ottawa sand data shown with hollow markers are from Sasitharan (1993) and those with solid marker from Vaid et al. (1985). Toyoura sand data from Ishihara (1993). Samples were prepared using moist tamping (MT), water pluviation (WP) and dry deposition (DD) methods.....	219
<b>Figure 5-9</b> Predicted vs. measured response of very loose Ottawa sand ( $e=0.808$ , $D_r=4\%$ ) consolidated isotropically to 515 KPa in drained triaxial compression test (Note: Different horizontal and vertical scales used in (b) for clarity). .....	220
<b>Figure 5-10</b> Predicted and Measured responses of very loose Ottawa sand ( $D_r = 4\%$ ) in undrained triaxial compression tests. The two tests with $p_c = 550$ kPa and $p_c = 350$ kPa were used for general model calibration. The test with $p_c=100$ kPa was predicted, and no experimental data were available for comparison.....	221
<b>Figure 5-11</b> Predicted vs. measured responses of very loose Ottawa sand ( $D_r = 2\%$ ) in a drained $p = \text{const.}$ test starting from a state on the post-peak portion of the undrained effective stress path.....	222
<b>Figure 5-12</b> Predicted vs. measured responses of very loose Ottawa sand ( $D_r = 2\%$ ) in a drained triaxial compression test starting from a state on the post-peak portion of the undrained effective stress path (Note: (c) not to scale).....	223



<b>Figure 5-13</b> Predicted and measured responses of very loose dry Ottawa sand ( $D_r = -8\%$ ) in a CDS test. Note that the deviatoric stress was not strictly constant during this test because of the loading method used, as explained in Chapter 3.....	224
<b>Figure 5-14</b> Model predictions illustrating the effect of void ratio on the susceptibility of sands to collapse in CDS tests .....	225
<b>Figure 5-15</b> Predicted vs. measured response of Toyoura sand with a void ratio of 0.833 and consolidation pressure of 100 to 2000 kPa in undrained triaxial compression (Note: (b) not to scale) .....	226
<b>Figure 5-16</b> Predicted vs. measured response of Toyoura sand with a void ratio of 0.735 and consolidation pressures of 100 to 2000 kPa in undrained triaxial compression (Note: (b) not to scale). .....	227
<b>Figure 5-17</b> Effect of compressibility parameter $\beta$ (Pestana and Whittle, 1995) on the predicted response of Toyoura sand at different void ratios consolidated to $p = 3000$ kPa loaded in undrained triaxial compression. ....	228
<b>Figure 5-18</b> Predicted and observed behavior of loose Toyoura sand consolidated to 100 and 1000 kPa and subjected to undrained triaxial compression loading. ....	229
<b>Figure 5-19</b> Complete liquefaction of very loose Toyoura sand with zero minimum strength in undrained triaxial compression. ....	230
<b>Figure 5-20</b> Model predictions including and beyond measured data for Toyoura sand in undrained triaxial compression (test data from Yoshimine, 1996) ((a) not to scale).....	231
<b>Figure 5-21</b> Measured vs. predicted response of samples of Toyoura sand with different initial densities consolidated to 500 KPa and sheared in drained triaxial compression (Data from Verdugo et al., 1996).....	232
<b>Figure 5-22</b> Measured vs. predicted response of samples of Toyoura sand with different initial void ratios, consolidated to 100 kPa and sheared in drained triaxial compression (Data from Verdugo et al., 1996).....	233
<b>Figure 5-23</b> Model predictions and measured data for undrained triaxial extension tests on Toyoura sand. Notice the difference between measured and predicted responses at larger strain levels (Data from Yoshimine, 1996).....	234

<b>Figure 5-24</b> Model predictions and test data on the complete liquefaction of Toyoura sand at void ratios of 0.86 or more ( $D_r=30\%$ or less ) in undrained triaxial extension (Data from Yoshimine, 1996).....	235
<b>Figure 5-25</b> Differences between drained behavior of Toyoura sand consolidated to 500 kPa and sheared in triaxial compression and extension (Note: (c) not to scale). .....	236
<b>Figure 5-26</b> Differences between undrained behavior of samples of Toyoura sand having the same state, but sheared in triaxial compression and extension (Data from Yoshimine, 1996). .....	237
<b>Figure 5-27</b> Differences between the stress-strain response, and the amount of strain required to reach the ultimate state in undrained triaxial compression and extension.....	238
<b>Figure 5-28</b> Predicted differences between undrained response of Toyoura sand at a void ratio of 0.86 to loading in triaxial compression and extension: strong dilatancy in compression and complete liquefaction in extension.....	239

## CHAPTER SIX

<b>Figure 6-1</b> Shape of the yield surface in principal stress space when principal directions of stress and anisotropy coincide. ....	280
<b>Figure 6-2</b> Effect of stress induced anisotropy on the position of the yield surface of sands. Note that the stress state at phase transformation (PT) is not affected by changes in the stress ratio at anisotropic consolidation (modified after Cambu and Lanier, 1988). .....	281
<b>Figure 6-3</b> Definition of parameters used to model the effect of inherent anisotropy on the yield behavior .....	282
<b>Figure 6-4</b> Effect of $b$ and $\alpha_\sigma$ on the variation of friction angle at peak with void ratio, as measured from hollow cylinder tests .....	283
<b>Figure 6-5</b> Effect of intermediate principal stress ( $b$ ) on the variation of friction angle at phase transformation (PT) with state parameter as measured from hollow cylinder test.....	284
<b>Figure 6-6</b> Effect of stress state on the variation of stress ratio at phase transformation ( $M_{PT}$ ) with void ratio, as represented in the octahedral plane .....	284
<b>Figure 6-7</b> Undrained response of anisotropically consolidated loose Toyoura sand to shearing in triaxial compression .....	285

<b>Figure 6-8</b> Effect of consolidation pressure on the behavior of anisotropically consolidated loose Toyoura sand.....	286
<b>Figure 6-9</b> Predicted and observed behavior of a sample of very dense Toyoura sand consolidated anisotropically at $K_0 = 0.37$ . .....	287
<b>Figure 6-10</b> Behavior of Toyoura sand consolidated in compression and sheared in extension (Data from Hyodo et al., 1994) .....	288
<b>Figure 6-11</b> Effect of direction of loading on the undrained response of anisotropically consolidated Toyoura sand consolidated to different densities. ....	289
<b>Figure 6-12</b> Effect of direction of consolidation on the response of loose Toyoura sand to undrained shear in triaxial compression and triaxial extension. ...	290
<b>Figure 6-13</b> Effect of direction of loading on the undrained behavior of Toyoura sand with $e=0.86$ sheared under $b=0.25$ in the hollow cylinder apparatus.....	291
<b>Figure 6-14</b> Predicted drained response of Toyoura sand with $e=0.86$ and $b=0.25$ sheared under different values of $\alpha$ in the hollow cylinder apparatus.....	292
<b>Figure 6-15</b> Measured and predicted response of loose Ham River sand to drained shear with $b=0.5$ in the hollow cylinder apparatus.....	293
<b>Figure 6-16</b> Effect of direction of loading on the void ratio of Toyoura sand that leads to complete undrained collapse .....	294
<b>Figure 6-17</b> Effect of void ratio on the undrained response of Toyoura sand in simple shear .....	295
<b>Figure 6-18</b> Effect of mode of shearing on the undrained response of Toyoura sand with $e=0.85$ .....	296
<b>Figure 6-19</b> Effect of mode of shearing on the undrained response of Toyoura sand with $e=0.75$ .....	297
<b>Figure 6-20</b> Observed (top) and predicted (bottom) difference between the undrained effective stress path of Toyoura sand prepared by moist (wet) tamping (MT) and dry deposition (DD).....	298
<b>Figure 6-21</b> Observed (top) and predicted (bottom) difference between the undrained effective stress path of Toyoura sand prepared by moist (wet) tamping (MT) and water pluviation (sedimentation) (WP). ....	299
<b>Figure 6-22</b> Observed (top) and predicted (bottom) difference between the stress-strain behavior of Toyoura sand prepared by moist (wet) tamping and water pluviation (sedimentation). ....	300

## *Chapter 1*

# **1 Introduction**

## **1.1 Constitutive modeling of sand and the analysis of flow liquefaction**

Geotechnical engineers have often been less concerned about deformation problems in structures made of or built on sand, as compared to clay. Stability analysis of such structures, on the other hand, has not posed significant difficulties in most cases. These, in addition to the complexity of the constitutive behavior of sand and the difficulty of normalizing sand behavior, has resulted in the constitutive modeling of sand lagging behind that of clay. Although many constitutive models have been presented for sand in the last few decades, a number of important issues related to modeling sand behavior have either remained unresolved or have been addressed only recently.

Constitutive modeling of clay, on the other hand, has often been influenced by the Cambridge models. Formulations in the general framework presented by the Cam Clay series (e. g. Roscoe et al., 1958) have often resulted in satisfactory modeling of the behavior of isotropic clay. Such formulations, however, have not been as successful in modeling the behavior of sand.

In many instances, the study of the constitutive behavior of sand is made in the context of liquefaction. "Liquefaction," although defined by various authors to refer to a

number of somewhat different phenomena, generally refers to the condition at which saturated sand changes from a state of solid consistency to that close to a liquid. This condition is realized once the effective stress becomes very small or close to zero such that the soil mass exhibits very small or no shearing resistance. The importance of liquefaction was particularly highlighted by the 1964 earthquake in Niigata, Japan. Numerous studies regarding the behavior of sandy soils as related to liquefaction have been carried out since then. These studies, which were mainly pioneered by H. B. Seed and his collaborators at the University of California at Berkeley, devoted a substantial amount of effort to establishing methods of predicting the occurrence of liquefaction and evaluating its consequences, and focused on liquefaction due to earthquake shaking.

Advances in computing technology, together with the development of new numerical techniques to solve large and complicated problems, have provided the possibility of conducting detailed analyses of the behavior of sand structures, including the behavior of sand during liquefaction. Such analyses require a realistic account of the constitutive behavior of sand to be used in the numerical analysis.

The condition defined above as “liquefaction” may occur under a variety of different circumstances. A detailed description of these circumstances, including the different loading types and soil states under which such a condition can be realized are given in Chapter 2. An important circumstance under which liquefaction occurs is the one associated with “flow liquefaction.” Flow liquefaction is the result of the rapid loss of strength of very loose sand that exhibits a drop in shear strength in undrained loading. Flow liquefaction of the soil can cause catastrophic flowslide of soil structures if sufficiently large portions of the soil mass exhibit loss of strength during loading.

Numerous liquefaction flowslides were observed in the early stages of the development of modern soil mechanics and were termed “spontaneous liquefaction” (Terzaghi, 1925), but the triggering mechanism and the circumstances under which these slides occurred remained unclear. These flowslides occur in a very short period of

time and give little or no warning before turning the material into a highly mobile mass that travels long distances, sometimes in the order of several kilometers.

Gu et al. (1993) analysed the failure of the lower San Fernando Dam that occurred in 1971 following an earthquake. They modeled the stress-strain relationship of the soil during undrained collapse by a hyperbolic function and used a triggering criterion in the form of a "collapse surface" (Sladen et al., 1985). They showed that the stress redistribution resulted from the strain softening of the liquefied material is the main reason for the flow failure. Their analysis also indicated that the size of the liquefied zone after stress redistribution might be much larger than that of the initial liquefied zone that is produced by direct earthquake shaking. They concluded that a post-earthquake deformation analysis may be an essential part of any stability analysis of structures subjected to this type of liquefaction. This is because stability may be lost as a result of the re-consolidations and stress re-distributions that may occur in the soil mass following its initial loading.

The above example suggest that proper analysis of soil structures subjected to flow liquefaction requires employing a realistic stress-strain relationship that can accurately replicate the behavior of loose collapsible granular materials. It is also important to have a proper account of the conditions under which such failures can be initiated.

## **1.2 Initiation of flow liquefaction**

Liquefaction flowslides can be triggered by static or dynamic loads. The possibility of triggering such slides by dynamic loading is well known, but the fact that such slides can be triggered by static loads is not as well realized. Morgenstern (1994) cited a number of such slides that occurred without the soil mass being subjected to any dynamic loading, referring to them as "static liquefaction." There is a general lack of understanding of the instability and the associated runout mechanics in such slides.

Safety factor calculations carried out on such soil masses using conventional methods suggest that they are stable.

Studies performed by Morgenstern (1967) into the mechanics of submarine landslides indicated that the initiation of such slides was consistent with the mobilization of the undrained shear strength of the loose cohesionless sediments. Knowledge of the undrained shear strength of loose sands and the stress condition at the mobilization of the peak strength is therefore important in the analysis of such slides.

A number of criteria have been introduced recently to predict the conditions under which flow liquefaction initiates. Details of these criteria are given in Chapter 2. These criteria generally require determination of the stress ratio or friction angle at the point where peak strength is reached in undrained loading. While these criteria have mostly been defined based on results of triaxial compression tests, both field and laboratory evidence indicate that other modes of shearing, such as simple shear and triaxial extension can also have significant effects. In soils exhibiting anisotropic behavior, responses to loading in different directions or different modes of shearing can differ significantly. In such soils, therefore, stress states at which the peak of the undrained effective stress path is reached should be known for a wide range of loading conditions and soil states.

Bishop (1971) showed that for very loose sand, the peak undrained shear strength can occur at a friction angle that may be significantly smaller than the friction angle at failure. By comparing undrained effective stress paths of Ham River sand subjected to triaxial compression and extension, he showed that the orientation of the principal stresses can have important effects on the undrained strength of loose sand. The effect of anisotropic consolidation on the undrained strength was also emphasized. He further showed that the unique relationship between void ratio and failure strength of soils assumed in the critical state soil mechanics is not applicable to the undrained shear strength of sand, since the ratio of the friction angle at peak strength to that at residual strength depends on sand density. He used results of Castro's (1969) undrained tests on

**Banding Sand** to show that as the porosity of sand increases, this ratio decreases (Figure 1-1).

Apart from Bishop's (1971) work cited previously, limited information is available on the effect of various factors such as density, consolidation stresses, direction of loading, mode of shearing (e. g. simple shear, plane strain, etc.) and soil fabric on the friction angle at peak undrained strength of loose sand. To evaluate the possibility of occurrence of flow liquefaction in a soil mass, it is also important to have a quantitative measure of these variations, and a relationship among values of peak strength for various conditions. Qualitative descriptions regarding variations of peak strength with some of the factors mentioned above were given by some researchers, but they are often not usable in a quantitative analysis.

### **1.3 Constitutive modeling of sand**

It was stated in Section 1.1 that constitutive modeling of sand has suffered a number of shortcomings despite the introduction of numerous models in the past few decades. An overview of current constitutive models for sand is presented in Section 2.1.3 together with some of the difficulties of modeling sand behavior and the limitations of current formulations. In addition to the need for a suitable stress-strain formulation in any liquefaction analysis of loose sand, such formulations constitute an important part of the requirements of solving general deformation problems in sand.

The main shortcomings of current constitutive models for sand can be listed as follows:

1-Many of the current models have been either presented in, or validated by, results of triaxial tests, sometimes only for triaxial compression conditions. While in some cases the models have been extended theoretically for general stress conditions, the performance of the models for the other conditions of loading is either unknown or poor. The following reasons seem to have contributed to this trend:



- a. While the data base for triaxial compression tests is enormous, results for other modes of shearing are not as readily available.
- b. Test data on some of the other modes of shearing, such as the triaxial extension are not as reliable as those of triaxial compression, because of the increased susceptibility of test specimens to non-uniform deformation.
- c. Modeling the behavior in other modes of shearing requires taking into account some aspects of sand behavior that are not well quantified or formulated. One important aspect is soil anisotropy. While anisotropy may not have significant effects on some aspects of sand behavior (e. g. soil strength, soil deformability at large strains, etc.) it can affect some other aspects significantly. Anisotropy seem to have substantial effects on the response of loose sand to undrained loading and the drained stress-strain behavior at small strain levels. Taking anisotropy into account often results in significant increase in model complexity and/or calibration efforts.

2-In more comprehensive models, calibration often involves the determination of parameters that are either difficult to obtain from conventional test results, or have no clear physical meaning.

3-In many models, shapes of yield surfaces have been chosen approximately. In very loose sand, this can cause imprecise modeling of the collapse behavior for drained and undrained conditions as will be seen in Chapter 3.

4-While sand usually exists in-situ in a state of anisotropic consolidation, constitutive models often deal with isotropically consolidated soils.

5-Except for some recent models, most sand models do not recognize the existence of the ultimate (steady) state condition at large strain.

6-In many models, parameters are determined for a certain state of the soil and are applicable only for a limited range of densities and/or pressures. As a result, re-calibration of the model is required for other soil states.

7-Recent models that attempt to formulate the behavior of sand over a wide range of pressures and densities often use the ultimate (steady) state line (USL) as a reference line by which different soil states are normalized. Such models generally use the USL obtained from triaxial compression tests to model sand behavior. However, the determination of this line in practice is often difficult, and its uniqueness for different modes of shearing has not been ascertained. These difficulties can cause significant problems in the performance of constitutive models that rely heavily on the USL for predicting the response of soil to loading in different conditions.

8- Constitutive models that attempt to predict the behavior of sand over a wide range of states and loading conditions, are often very complicated and difficult to use by an average geotechnical engineer. Such complexities may result from their mathematical formulation, choice of model parameters or conceptual complexities in the functioning of the model.

Considering the issues discussed above regarding flow liquefaction and constitutive modeling of sand, the present research work focused on the following two areas:

1-Study of the variation of the stress state or friction angle at the peak of the undrained effective stress path for different soil states and loading conditions. This study will be carried out using an extensive data base consisting of published results of undrained tests on a variety of sands at different densities, consolidation stresses, loading conditions and soil fabrics. Observed variations will be formulated such that they can help in assessing the susceptibility of loose sand at various states subjected to different loading conditions, to flow liquefaction. Results of the formulations will be related to the constitutive behavior of sand and used in the development of a constitutive model for sand that emphasizes on modeling the behavior of loose sand.

2-Development of a constitutive model that can predict the behavior of granular materials over a wide range of states and loading conditions using a unique set of

parameters. The model is developed in an attempt to overcome some of the limitations of current models that were stated earlier. The model, while being applicable to a wide range of states, addresses some aspects of sand behavior that are especially important in loose, liquefiable sand.

## **1.4 Outline of the thesis**

The thesis is comprised of seven chapters. In Chapter 2 the response of granular soils at different states to various loading conditions is reviewed, and existing constitutive models that have been developed to predict these responses are examined. Responses of sandy soils subjected to various loading conditions are explained, and currently available criteria for predicting the initiation of flow liquefaction are introduced and evaluated.

Chapter 3 mainly deals with the yielding of sand in triaxial stress space, and introduces methods of determination of parameters that appear in a yield function that will be used in modeling sand behavior. Comparison is also made between yield stresses obtained from this yield function and those obtained from other studies. The capability of the yield function to determine the effects of void ratio, inherent anisotropy and anisotropic consolidation on the yield stresses of sand is examined. It is shown that for very loose sand, the yield surface closely resembles the undrained effective stress path (UESP). This result is used in Chapter 4 to determine the position of the yield surface of sand at a variety of states subjected to different loading conditions. The yield function is then used to explain a number of observations reported in the literature regarding the instability and collapse of loose sand subjected to a variety of loading conditions.

In Chapter 4, stress states corresponding to the peak of the UESP of different sands at different fabrics, void ratios, consolidation stresses and loading conditions are examined. Based on the result obtained in Chapter 3 regarding the proximity of the stress state at the peak of the yield surface and the UESP, stress states at the peaks of the

UESPs are used to formulate effect of the above factors on the yielding behavior. These formulations are used in constitutive modeling of sand in Chapters 5 and 6.

In Chapter 5 a constitutive model for sand is presented for triaxial stress conditions. The model uses the results obtained in Chapter 4 regarding the yielding behavior of sand. The model is able to predict the behavior of sand over a wide range of states subjected to drained and undrained shearing in triaxial compression and extension conditions. The response of very loose collapsible Ottawa sand to a variety of loading paths in the triaxial apparatus including  $p=\text{const.}$ ,  $q=\text{const.}$ , and triaxial compression in two-stage undrained to drained tests is modeled successfully. The model demonstrates the ability to predict the remarkable differences in the response of loose sand to loading in triaxial compression and extension, with a unique set of model parameters, including a unique ultimate (steady) state line. Some aspects of the behavior of sand in triaxial extension tests that seem to have been obscured by the limitations of the available testing equipment are examined, using model predictions.

The model is extended for generalized stress conditions in Chapter 6. The effect of loading direction on the drained and undrained behavior of sand is predicted and compared with observed behavior. The effect of anisotropic consolidation on the behavior of sand is also modeled. Differences in responses of sand to shearing in different modes, including triaxial compression, triaxial extension, simple shear and plane strain are compared and effects of density on these differences are evaluated. The complete liquefaction of sand in undrained loading that occurs at different densities depending on loading direction is predicted by the model. Differences in the response of sand having different fabrics to undrained loading are also compared and modeled. All model predictions were made using a unique set of model parameters including a unique USL as in the triaxial formulation. In the formulation of the yield surface in this chapter, results obtained from Chapter 4 were used.

Chapter 7 summarizes the important findings and conclusions of the work. Suggestions for further studies are also made.

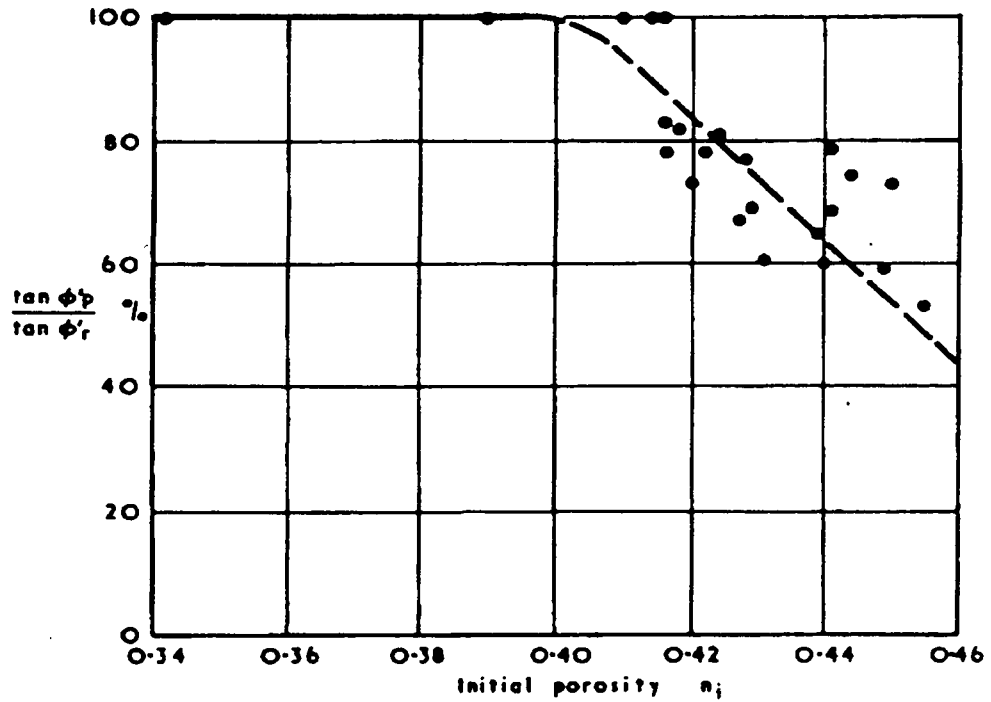


**Figure 1-1** Relationship between the ratio of friction angle at peak strength to residual strength, with porosity obtained from undrained shear tests performed by Castro (1969) on Banding sand (modified after Bishop, 1971).

## *Chapter 2*

# **2 Constitutive modeling and liquefaction of sand**

## **2.1 Introduction**

Appropriate stress-strain relationships are needed to solve any deformation problem in sand. Such relationships are also an important component of the liquefaction analysis of loose sandy soils. Liquefaction damage, in particular, liquefaction flowslides are the most important problems faced in structures made of or built on loose sandy soils. Therefore, constitutive models for sand are expected to be particularly suitable for the analysis of such problems, and to address issues that are of more relevance to the behavior of sands prone to such failures. Liquefaction flowslides can be triggered by static or dynamic loads. Much has been said and done on the liquefaction analysis of sand subjected to dynamic loading but the currently available information on methods of analysis for static liquefaction is less comprehensive.

In this chapter, the response of sand to loading is first reviewed, and elements of modeling of sand behavior are summarized. Yielding of sand is then discussed in detail because of its importance in modeling the behavior of loose sand and relationship to flow liquefaction, as will be seen later in Chapter 3. An overview of current constitutive models will then be presented. The liquefaction of sand is examined, and various conditions and circumstances leading to liquefaction failures are explained. Current methods of analysis of the stability of sandy soils subjected to flow liquefaction are reviewed.

## 2.2 Modeling the constitutive behavior of sands

### 2.2.1 The behavior of sands

Figure 2-1 shows the response of a sample of sand to drained shearing in a direct shear test as illustrated by Casagrande (1975). It can be seen that during shearing, an initially loose sample exhibits a gradual increase in strength (increase in shear stress) such that its strength approaches an ultimate value referred to as the “ultimate strength” (Figure 2-1-a). At the same time, void ratio of the sample decreases and approaches a value denoted by the “critical void ratio” (CVR) (Figure 2-1-c). For a dense sample of the same sand, on the other hand, strength increases rapidly to a maximum value (peak strength-Figure 2-1-a ) and then decreases gradually towards the “ultimate strength” reaches by the loose sample. Void ratio of this sample increases towards the CVR approached by the loose sample.

Casagrande (1936) presented the concept of CVR in relation to volume changes associated with the shearing of sands. Based on his observations and intuition, he suggested that when samples of very loose and dense sands are sheared in a drained condition, the void ratio of both samples approaches a value that is constant and independent of their initial void ratios. He referred to this constant void ratio as the “critical void ratio.” Later, he (Casagrande, 1975) suggested that the variation of the CVR with normal stress can be represented by a single curve in the  $e$ - $\log \sigma_n$  plane that he called the E-line (Figure 2-1-b). The concept of CVR was extended to clays by Roscoe and his co-workers and was used in a series of constitutive models based on a framework known as the “critical state soil mechanics” (see e. g. Roscoe et al., 1958).

Studies performed by Bjerrum et al. (1961) showed that loose sand can exhibit very brittle postpeak behavior if subjected to undrained shearing. Castro's (1969) load-controlled tests on Banding Sand also showed that very loose sands can lose a significant portion of their strength if loaded undrained, and reach a state of constant strength that can be much smaller than the peak strength (Figure 2-2-a). He referred to

this loss of strength as “liquefaction,” since it can cause the soil to behave like a liquid with very small shear strength. The small strength and high positive pore pressures that developed due to the contractive tendency of the sample remained nearly unchanged while shear strain increased. However, samples at lower void ratio but still loose experienced temporary loss and subsequent increase in strength (Figure 2-2-b), while in dense samples (Figure 2-2-c), strength increased monotonically with axial strain.

Poulos (1971) referred to a state at which a particulate material undergoes continuous deformation under constant effective stress, constant void ratio and constant velocity, as the “steady state of deformation”. Considering the definitions of the CVR and the steady state of deformation, and following Castro’s (1969) observations on the undrained behavior of very loose sands, Castro and his co-workers (see e. g. Castro and Poulos, 1977) suggested that a “Steady State Line” (SSL) exists in the void ratio ( $e$ ) vs. mean normal stress ( $p$ ) plane that represents the locus of states at which the soil experiences continuous deformation at constant volume and constant stresses. They suggested that this line is unique for a certain soil regardless of drainage condition or the type of tests. If the initial state of a sample of sand is above the SSL in the  $e$ - $p$  plane, the sample will have a tendency to contract upon shearing. However, if the initial state is below the SSL, the sample will tend to dilate.

The undrained response of isotropically consolidated loose and dense sand to cyclic loading is shown in Figure 2-3 as illustrated by Ishihara (1985). The “phase transformation” (PT) lines defined by Ishihara (1975) as the loci of states in the plane of shear stress ( $\tau$  or  $q$ ) vs. normal stress ( $\sigma$  or  $p$ ) where the behavior changes from contractive to dilative are also shown. Samples at contractive states develop positive pore pressures during loading, and their stress paths move towards the origin. Dilative samples, on the other hand, move away from the origin because of the negative pore pressures developed. The tendency of both loose and dense sand to contract at small strains leads to the development of positive pore pressures and the movement of the stress path towards the origin. In subsequent cycles, the stress path of the loose sample continues its movement towards the origin, finally reaching a state of essentially zero



effective stress where it has very small stiffness and experiences substantial deformations due to the applied loads (Figure 2-3-A-a). The achievement of the condition of zero effective stress, referred to as the “initial liquefaction” (Seed, 1983), in the dense sample does not result in the development of substantial shear strain. The dense sample, however, has smaller stiffness at stress ratios below PT, but experiences an increase in stiffness and reduction in the development of shear strain as the stress ratio increases beyond the PT point (Figure 2-3-c). For these samples, therefore, the increase in shear strains with the number of cycles is gradual (Figure 2-3-B-a). Note that in cases of both loose and dense sand discussed above, the samples do not lose strength but experience degradation in their stiffness that can be large or small depending on their densities. The development of strains due to the degradation of stiffness without loss of strength was termed “cyclic mobility” by Casagrande (1970).

## 2.2.2 Modeling sand behavior

### 2.2.2.1 *Elements of a constitutive model for sands*

A plasticity-based constitutive model for sand includes at least three main elements:

- a) A “yield surface” that defines the yielding stresses or the direction of loading;
- b) A “flow rule” that defines the direction of plastic flow or a “plastic potential function” that can be used to determine such directions;
- c) A “hardening rule” that defines the evolution of the yield surface with strains.

In modeling the behavior of isotropic clays, it is often assumed that the direction of loading coincides with the “direction” of plastic strains. This assumption, referred to as the “associative flow rule,” can lead to realistic modeling of the behavior of such soils.

However, sands are well known for their non-associative plastic behavior. This was shown by Poorooshasb et al. (1966) in triaxial tests and further demonstrated by Lade et al. (1973) among others. This behavior necessitates the establishment of yield surfaces

and plastic potentials for sand separately. The establishment of the plastic potential is less problematic since measurement of strains is an easy task. The identification of yield points from stress-strain curves, on the other hand, is less straightforward. In some constitutive models, other criteria such as contours of equal plastic work or normalized plastic work have been used to define yield surfaces (see e. g. Moroto, 1976; Lade and Kim, 1988).

On the other hand, some constitutive models establish shapes of plastic potentials based on stress-dilatancy relationships and assume that the yield surfaces are either identical (e. g. Jefferies et al., 1993) or have mathematically similar forms (e. g. Pastor and Zienkiewicz, 1985; di Prisco and Nova, 1993) to the plastic potentials. Such yield surfaces can have shapes that are generally similar to the experimentally derived yield curves, but the degree of their accuracy in representing the actual yielding behavior of sand at different densities and loading conditions is often unknown.

Other models relate the yield behavior to the failure of the soil, even though yielding and failure seem to be governed by different physical processes since, unlike yielding, failure is the result of instability. Experimental evidence suggest that yield surfaces and failure surfaces may have somewhat different shapes in the octahedral plane (Yamada and Ishihara, 1979) and intersect in a meridian plane (Lade and Prabucki, 1995).

In sand, failure stresses have traditionally been of more interest to geotechnical engineers and have been studied more frequently than yield properties, since sandy soils often cause less deformation problems than clayey soils. This, however, may not be the case for loose sand, especially in the context of liquefaction. As will be seen in Chapter 3, the position of the yield surface of loose sand may have an important bearing on the stress ratio at which undrained softening, and subsequently sand liquefaction occurs.

For clays, ellipses have often been used as yield surfaces, while for sand, the more complex yielding behavior, in addition to the difficulties cited above, has caused modelers to use a wide range of shapes, many of which depict the actual yield behavior

only approximately. Since hardening also affects the predicted stress-strain behavior, combinations of yield surfaces and hardening rules are used such that reasonable predictions of sand behavior are produced. Such a procedure may produce reasonable results for a limited range of states and loading conditions, but the ability of such yield surfaces to model a wider range of responses is questionable.

Because of the importance of the yield surface in modeling sand behavior and that it is, in fact, the element that distinguishes many constitutive models from each other, and since it is one of the focuses of the current study, a review of past studies regarding yielding of sand is provided here.

### 2.2.2.2 *The yield locus of sand*

The simplest shape used as a yield locus of granular soils is a straight line radiating from the origin of the stress space that corresponds to a constant stress ratio  $\sigma_1/\sigma_3$  or  $\eta=q/p$ , where  $q=\sigma_1-\sigma_3$  is the deviatoric stress and  $p$  is the mean normal stress. Although this shape was used in many constitutive models (e. g. Matsuoka 1974, Lade and Duncan 1975, Matsuoka and Sakakibara 1987, Manzari and Dafalias 1997) because of its simplicity, experimental evidence indicates that such a shape cannot accurately depict the yielding of sands at various states and loading conditions. In addition to evidence for the curvature of the yield locus with increasing pressure, straight lines cannot predict plastic deformations along stress paths such as proportional loading along a constant stress ratio (see e. g. Lade and Durcan, 1976; Lade, 1977).

From tests on dense Ottawa sand, Poorooshab (1971) obtained the following yield locue for sands:

$$f = \eta + m \ln p = \text{const.} \quad 2-1$$

in which  $m$  is a constant material property that was equal to 0.6 for the sand he tested. A more comprehensive study conducted by Tatsuoka and Ishihara (1974) showed that while the above equation is in general suitable, it needs two modifications. Firstly, the

yielding behavior is affected by density, and the yield locus becomes less curved (i. e. closer to a straight line) as the sand becomes looser. Secondly, even for dense sands, the above equation “gives a somewhat larger curvature in yield locus” compared to what they obtained. No closed form function for the yield curves was suggested in their study, but they used the following relationship for the yield locus:

$$\eta = F(p) + \eta_0 \quad 2-2$$

in which  $\eta_0$  is an initial reference stress ratio and  $F(p)$  is a function that determines the curvature of the yield locus and is a function of the void ratio (Figure 2-4-d). The study by Tatsuoka and Ishihara (1974), which was limited to yielding in terms of shear strains and at high stress ratios, is still a key reference with which yield functions used in constitutive modeling of sands are often compared (see e. g. Lade and Kim, 1988; Lade et al., 1995).

The above yield surfaces were obtained for high stress ratios close to failure and did not deal properly with yielding at small stress ratios close to the hydrostatic stress line. This issue was addressed in a semi-experimental procedure adopted by Nova and Wood (1978) in which they derived the following relationship to define a yield surface in a p-q stress plane:

$$\varepsilon_v^p + D \varepsilon_s^p = \text{const.} \quad 2-3$$

in which  $\varepsilon_v^p$  and  $\varepsilon_s^p$  are the volumetric and shear plastic strains that develop from the beginning of a drained loading, and  $D$  is a parameter that accounts for the coupling between the volumetric and shear strains. In subsequent publications (Nova and Wood, 1981), it was found that  $D$  increases with density and decreased to zero in sufficiently loose liquefiable sand. Shapes obtained from the analysis of results of drained tests using the above procedure were similar to those obtained from Equation 2-1 in the region of high stress ratios, but bent to form an elliptical cap at low stress ratios.

A study on the yielding of isotropically consolidated (IC) and anisotropically consolidated (AC) dense sand over a wide range of stresses was performed by Yasufuko

et al. (1991-a) in the triaxial apparatus. Yield stresses were identified as points where marked changes in the slope of the variation of each of the  $\eta$ - $\varepsilon$ ,  $\eta$ - $v$ ,  $\eta$ - $k_m$  and  $\eta$ - $W$  curves occurred. Axial and volumetric strains are denoted here by  $\varepsilon$  and  $v$  respectively,  $k_m$  is the normalized plastic energy (Moroto, 1976) and  $W$  is the total plastic energy dissipated during the shearing process. Since the sand tested was dense, yield points in many cases were obtained from stress-strain curves that showed very gradual changes in curvature, therefore, yield points had to be obtained by approximation. Good general agreement, however, was observed among the four criteria used to identify yield points (Figure 2-5), although some scatter existed.

From the yielding stresses they measured, Yasufuko et al. (1991-a) obtained the following equation for the yield surface of an AC sand:

$$f = (\eta - \alpha)^2 + 2 N (N - \alpha) \ln (p/p_0) = 0 \quad 2-4$$

in which  $N$  and  $\alpha$  are the stress ratios  $q/p$  at points where the slope  $dq/dp$  is zero and infinity respectively,  $p$  is the mean normal stress and  $p_0$  is the mean normal stress at  $\eta = \alpha$ . Yasufuko et al. (1991-b) suggested that  $\alpha$  varies during shear, and its initial value  $\alpha_0$  can be obtained through the determination of experimental mean value of the ratio of plastic strain increments  $dv^p/de^p$  measured during anisotropic consolidation. Equation 2-4 reduces to the following form for IC sand:

$$f = \eta^2 + 2 N^2 \ln (\hat{p}/p_0) = 0 \quad 2-5$$

Based on experience with different kinds of sandy soils, Yasufuko et al. (1991-a) suggested that  $N$  is a material parameter that is relatively constant, and is approximately equal to  $0.7M$  where  $M$  is the stress ratio at critical state. It was suggested by Yasufuko et al. (1991-b) that the value of  $N$  in compression ( $N_c$ ) for a specific sand can be determined from a drained load-unload test by identifying the yield point during reloading.

The value of  $N$  in extension ( $N_e$ ) was related to that in compression ( $N_c$ ), assuming an equal friction angle at peak in compression and extension:

$$N_e = \frac{-3N_c}{(3 + N_c)} \quad 2-6$$

It should be noted that the study described above was conducted on dense sand and did not include the effect of density on the yielding behavior.

The studies reviewed above were limited to the yielding of sand in the meridian plane (the plane in the principal stress space that contains the hydrostatic axis). Experimental studies have also been conducted on the yielding behavior of sand in the octahedral plane (the plane normal to the hydrostatic axis). Examples are the studies by Yamada and Ishihara (1979), Cambu and Lanier (1989), Pradel et al. (1990) and Gutierrez et al. (1993). Such studies have often resulted in shapes for the yield locus in the octahedral plane that resemble circles at an early stage of shearing which changes to a rounded triangle at higher strain. More details regarding these studies and the shape of the yield surface in the octahedral plane will be given in Chapters 4 and 6 where necessary.

### 2.2.2.3 *Evaluation of yield functions used in some recent models for sand*

A number of recent constitutive models have used functions that produce capped shapes to represent yield surfaces in principal stress space. Depending on the way the functions are defined, the yielding parameters they employ, and the way the yielding parameters are related to soil properties, the ability of such yield functions to represent the actual yielding behavior of sand varies. Some of these functions are reviewed below.

A function producing a cap-shaped yield surface is adopted in a model by Lade and Kim (1988) that can be defined by three parameters. The shape represents isotropic yielding and is not intended to model effects of inherent or stress-induced anisotropy.

Another isotropic capped yield surface with a simple mathematical form is defined by Nova (1988). This yield surface is extended by di Prisco and Nova (1993) to include effects of stress-induced anisotropy. To this end, new stress variables are defined in general stress space and substituted in the equation of the isotropic yield surface to account for the effect of stress-induced anisotropy.

Changes in the shape of the capped yield surface defined by Pestana (1994) are primarily governed by changes in the tangent to the surface at the origin of the stress space. This tangent is related to sand strength at failure, which is in turn related to density through a proposed relationship. The yield function can account for the effect of stress-induced anisotropy is also used for silty and clayey soils.

The shape used by Crouch et al. (1994) is a complex combination of curves that are segments of ellipses and a hyperbola smoothly connected to produce a capped yield surface with a tensile region. The segmented yield function was adopted to provide flexibility in matching the yielding behavior of different soils including the yielding of both clays and sands

It is noted that since derivatives of yield functions generally appear in an incremental formulation of stress-strain relationships, increased complexity of yield surfaces can result in complexities in such formulations and difficulties in the implementation of such relationships in a numerical code.

### 2.2.3 An overview of current constitutive models for sands

Perfect plasticity has long been used in solving engineering problems related to soil strength (Terzaghi, 1948, Meyerhof, 1951). This method, however, is not suitable for predicting soil deformations (Drucker and Prager, 1952) and work-hardening plasticity

is a more appropriate framework for modeling the stress-strain relationship of soils (Drucker et al., 1957).

Hvorslev (1937) showed that in saturated clays, the strength at failure is independent of stress history and is a function of the effective normal stress and current void ratio on the failure surface. Based on Hvorslev's (1937) work and Gibson's (1953) test results, Roscoe, Schofield and Wroth (1958) defined a yield surface in the three dimensional space of "effective normal stress ( $p$ ), shear stress ( $q$ ), void ratio ( $e$ )." This surface enveloped all stress paths of a clay sample as it was sheared and contained the latter parts of all these stress paths. By establishing an equation for the yield surface of normally consolidated clays, Roscoe, Schofield and Thurairajah (1963, 1965) developed the first comprehensive constitutive model for clays, which they called "Cam clay." This model (currently called the Original Cam Clay, OCC model) was later seen to overestimate strains at small stress ratios, and a "Modified Cam Clay" (MCC) model suggested by Burland (1965) employed a modified stress-dilatancy relationship and hence a different shape for the yield surface. Later, Roscoe and Burland (1968) used separate intersecting yield surfaces for shear and volumetric strains to account for shear strains that developed inside the yield surface of the MCC.

The OCC, MCC and their improved versions mentioned above assumed that regardless of stress paths followed, soils reach a unique state at large strain, which was called the "critical state" (Casagrande, 1936). The unique relationship between void ratio and stress that existed at this state, and also between void ratio and the size of the yield surface, helped to formulate the behavior of remoulded clays with different void ratios and stress within the same framework. Subsequent developments in constitutive modeling of clays (e. g. by Prevost, 1977; Mroz et al., 1978; Pietruszczak and Mroz, 1981; Dafalias and Herrmann, 1982 and 1986; Whittle and Kavvadas, 1994) involved using new concepts of plasticity to model various aspects of clay behavior, mostly focusing on modeling their response to cyclic loading. In most of these developments, the new concepts were still introduced within the critical state framework.



This framework, however, is not as successful in modeling the behavior of sand as in clay. One important reason is the lack of a unique relationship between void ratio and the size of the yield surface. Unlike clays, sands do not have a unique normal consolidation line in the usual ranges of stresses. Another limitation in applying Cam Clay models to sands is that the dilatancy relationships used in these models do not accurately correspond to sand behavior. It has been shown (e. g. Rowe, 1962) that sands follow a stress-dilatancy relationship that is different from those used in the Cam clay models. These discrepancies have resulted in the development of numerous constitutive models for sands that either totally abandon the critical state framework or use a modified version of it.

Following some studies on the constitutive behavior of sands, Lade and Duncan (1975) developed a constitutive model that was shown (Lade and Duncan, 1975, 1976) to be able to capture the behavior of sands in drained true triaxial tests (TTT). Predictions of this model for sand behavior in torsional shear tests, however, were not satisfactory. Lade (1977) later introduced a work-softening law and curved yield surfaces into the model in order to improve its performance, which included a better account for the behavior of dense sands. He showed that the improved model can predict the behavior of loose and dense sands in drained and undrained triaxial compression tests. A single hardening model was later introduced by Kim and Lade (1988) and Lade and Kim (1988) that used capped yield surfaces and plastic potentials, and was shown to produce good predictions for the drained behavior of sands in triaxial compression (TC) and TTT.

Vermeer (1978) used Rowe's (1962) stress-dilatancy relationship to develop a double hardening model with separate volumetric and shear yield surfaces. This model could predict the behavior of loose sands in  $p$ -constant, simple shear and also drained and undrained triaxial compression tests.

To overcome the problem of non-uniqueness of the relationship between the yield surface and void ratio in sands, Nova (1977) suggested that in addition to volumetric

strains (or void ratio changes), shear strains will also influence the hardening of sands. A model presented by Nova and Wood (1979) for the triaxial stress space simulated triaxial compression tests. An isotropic model for monotonic loading in the general stress space was presented later by Nova (1988) and was shown to produce satisfactory simulations of the drained behavior of sands in some stress paths in the Hollow Cylinder and TTT apparatus. This model was extended by diPrisco and Nova (1993) to include the effects of anisotropic consolidation. New stress parameters were introduced in formulating the extended model.

A growing interest in modeling the behavior of sands in cyclic loading has developed since the early 1970s, when earthquake-induced cases of liquefaction of saturated loose sands and large settlements and tilting of structures built on sandy soils received more attention.

Various modeling techniques were used to account for the physical phenomena involved in cyclic loading. Mroz (1967) defined certain rules for the movement of a collection of “nested yield surfaces” of metals in order to prevent their intersection. His work and the work of Iwan (1967) on the multiple yield surfaces were the basis for a number of “multi-surface” models for soils (e. g. Joyner and Chen, Prevost, 1977, 1978, 1985). The use of multiple yield surfaces, however, requires that the size and position of these surfaces be traced throughout the entire deformation process. This resulted in some difficulties when implementing such models in numerical calculations. The concept of “bounding surface plasticity” was introduced by Dafalias (1975) and Dafalias and Popov (1975) to simplify this concept. They used an inner “yield surface” and an outer “bounding surface” that enclosed the yield surface to model the behavior of metals in cyclic loading.

A constitutive model by Ghaboussi and Momen (1979, 1982) was able to simulate experimental results presented by Castro (1969) and Ishihara (1975). Zienkiewicz and Mroz (1984) suggested that unit vectors be defined for the directions of loading (i. e. normals to yield surfaces) and plastic strain increments. The plastic modulus had to be

defined directly without the imposition of the consistency condition. This information could be used to determine the constitutive matrix required for calculating the stress-strain relationship. This framework, referred to as “generalized plasticity,” was used in the model by Pastor et al. (1985). It was shown in Pastor et al (1991) and Zienkiewicz et al. (1990) that the model can predict the behavior of loose and medium dense sand in drained and undrained shearing in a general stress path. Some difficulties, however, were encountered in the use of this model (Zienkiewicz et al., 1993) due to the lack of imposition of the consistency condition.

The model proposed by Poorooshasb and Pietrusczak (1985, 1986) and its simplified version (Pietrusczak and Stolle, 1987) were mainly aimed at simulating the behavior of loose sands in cyclic loading. Both models were shown to be able to produce simulations in agreement with results of cyclic triaxial tests on loose sand. The models, especially in their original forms, are complicated and therefore are difficult to use in numerical simulations for the analysis of soil deformation.

The multi-yield surface model presented by Prevost (1985) is simple in its formulation and has been shown to be able to simulate the behavior of sands in drained simple shear and cyclic loading. The model uses open-ended yield surfaces that cannot predict plastic strains under constant stress-ratio loadings. Lacy and Prevost (1987) later extended the model to account for this type of loading but at the expense of adding complexity to the model. Both of these models have the same unsatisfactory characteristics mentioned above for all multi-surface models when implementing them in a numerical scheme.

The models reviewed above for sands are not presented in the critical state framework because they do not use the critical state as an ultimate state to which the shearing processes converge. These models need separate calibrations and parameter determinations for different initial states. This is in variance with the clay models based on the critical state framework, which can predict the behavior of clay with different initial void ratios and stresses, using a single set of material parameters.

Jefferies (1993) presented a constitutive model for sands that can simulate sand behavior with different initial densities and stresses with a unique set of material parameters. The model used the steady state of sands as a condition to which all distortional processes converge. This simple isotropic plasticity model is based on the concept of normality of plastic strain rate vector to the yield surface, and has been validated for triaxial compression tests.

Compared to Jefferies' (1993) model, the critical state model proposed by Crouch and Dafailas (1994-a) can perhaps be considered to be on the other extreme in terms of generality and complexity. This model uses a two-slope steady state line in the  $e - \ln p$  plane and a purely volumetric hardening law. Crouch and Dafailas (1994-b) showed that the model can simulate the behavior of clays, silts, and sands in monotonic and cyclic loading over a wide range of densities and consolidation stresses with a unique set of parameters. In the principal stress space, the shape of the yield surface in the octahedral plane and meridian plane (the plane containing the hydrostatic axis) is constructed by combining different curves that join together to produce the shape required for fitting experimental results. The model in its most general form requires 32 parameters, but the number of parameters that need to be determined can reduce to 8 if the rest of the parameters are assumed to take on some default values.

Unlike the models presented by Jefferies (1993) and Crouch and Dafalias (1994) in which the position of the steady state line (SSL) in the  $e-p$  space should be given as an input and used as a reference to compare different states of the soil, the model presented by Pestana (1994) uses a "Limiting Compression Curve" (LCC) as a reference. The LCC is defined as a straight line in the high-pressure region of the  $\ln e - \ln p$  plot to which all compression curves converge regardless of their initial void ratios. The model predicts the monotonic response of cohesive and granular soils with a unique set of parameters regardless of the soil's initial state. It has been shown that this model is able to produce predictions in agreement with the observed behavior of granular soils for a wide range of stresses and densities in undrained triaxial compression and give

reasonable qualitative predictions of soil behavior in drained triaxial compression condition.

It should be noted that constitutive models that can cope with the behavior of a wide range of soils, especially when they are formulated to capture the response to both monotonic and cyclic loading, are often very complicated. They usually require a large number of parameters that are sometimes difficult to determine or relate to the well-known soil properties. Such parameters often need to be obtained by curve fitting.

## **2.3 Liquefaction of granular soils**

### **2.3.1 Response of a mass of sandy soil to undrained loading**

Robertson (1994) used a flow chart (Figure 2-6) to illustrate the conditions that may arise from subjecting a mass of sandy soil to different types of loading. It can be seen from this flow chart that strain softening material are prone to "flow liquefaction" that may be triggered by monotonic or cyclic loading. Depending on the duration and intensity of the applied loads and the geometry of the ground, flow deformations triggered by such loads may develop temporarily and lead to subsequent stabilization, or continue until the complete collapse of the soil mass. One objective of this thesis is the examination of conditions that lead to the initiation (triggering) of flow liquefaction, and the formulation of the stress-strain relationship of the liquefiable soil.

Typical undrained responses of sand at different states subjected initially to a static shear  $q_{ST}$ , and loaded monotonically or cyclically are shown in Figure 2-7 as illustrated by Robertson (1994). Static shear can result from in-situ ground stresses that are functions of the position of the soil element and the geometry of the ground.

In monotonic loading, a very loose sand at an initial state lying far above the SSL in the  $e$ - $p$  plane (sample SS in Figure 2-7) undergoes monotonic reduction in strength (i. e.

strain softening, SS) as it moves towards the steady state. If the soil mass is composed entirely of such material and subjected to a load larger than its ultimate undrained shear strength  $s_u$ , it experiences complete collapse. Such failure, termed “flow liquefaction.” (Robertson, 1994) can also be triggered by cyclic loading, as will be seen later.

If the state of the sample is such that it lies slightly above the SSL in the  $e$ - $p$  plane (sample LSS Figure 2-7), it experiences limited reduction in strength (i.e. limited strain softening, LSS) followed by an increase in strength up to the steady state. In cases in which the state of the sample lies below the SSL, (sample SH Figure 2-7) the strength of the sample increases continuously (i. e. strain hardening, SH) until the corresponding steady state is reached. If a mass of soil composed of SH or LSS material is subjected to undrained loading smaller than its ultimate strength, it may not experience complete collapse since the shear strength of the soil increases upon shearing. However, in the case of materials with LSS behavior, large deformations may develop without leading to a total collapse of the soil mass.

The response of sandy ground to cyclic loads is mainly governed by the soil’s initial state and the amplitude of the applied cyclic loads (Figure 2-7). If loose sand with SS behavior in monotonic loads is subjected to cyclic loads higher than its corresponding  $s_u$ , it may experience flow liquefaction as the stress state moves towards the origin of the stress plane. This is because as the stress path moves to the left, it will follow a stress path close to its UESP in monotonic test, leading to a reduction in soil strength and the occurrence of “flow liquefaction” in a mass of soil, as will be shown later.

Denser sand subjected to stresses smaller than the steady state strength experience small strains that develop gradually as the number of cycles increases. Strain-controlled monotonic loading of such material leads to an increase in their strength as the stress state moves towards the steady state line (LSS or SH response) (Figure 2-7). A soil mass composed of such material and subjected to cyclic loading may experience large or small deformations, depending on soil density and intensity of the load. Such a response was termed “cyclic mobility” by Casagrande (1970) as mentioned before.

It may be noted from the above discussion that “flow liquefaction” can take place in sandy soils that are sufficiently loose such that they experience softening (reduction in strength) when subjected to undrained loading. Both monotonic and cyclic loading can lead to flow liquefaction. In the following section, this type of failure and the condition under which it occurs are examined in more detail.

## 2.3.2 Flow liquefaction

### 2.3.2.1 *Flow liquefaction as observed in the field*

The distinguishing characteristics of failures currently known as “flow liquefaction” have been recognized since the early stages of the development of modern soil mechanics (see e.g. Terzaghi, 1925; Casagrande, 1936). Terzaghi (1956) observed that submarine slopes composed of sediments of coarse sand and gravel remain stable at slope angles up to the angle of repose. However, slopes made of fine-grained cohesionless or almost cohesionless sediments failed at angles significantly smaller than their angle of repose. He referred to such failures as “spontaneous liquefaction.”

Studies performed by Morgenstern (1967) on submarine landslides indicated that the initiation of such slides is consistent with the mobilization of the undrained shear strength of the material. Numerous observations on the occurrence of similar slides in natural and man-made slopes composed of loose granular soils have been made since then. Such slides were triggered by either static or dynamic loads (see e. g. Koppejan et al., 1948; Bishop, 1973; Sladen et al., 1985b; Seed et al., 1986; McKenna, 1992).

### 2.3.2.2 *Experimental studies on flow liquefaction*

Although the occurrence of liquefaction flowslides has been documented since long ago, a clear account of the conditions under which such failures initiate, and practical criteria to evaluate the possibility of their occurrence were not introduced until recently.

Laboratory tests have revealed that an important aspect of the behavior of loose granular soils is that they can exhibit a dramatic change in their behavior at a certain stress ratio (friction angle) that can be much smaller than their stress ratio at failure. Under undrained condition, the rate of generation of pore pressures increases rapidly and softening starts at such a stress ratio regardless of whether it is reached due to monotonic or cyclic loading (see e. g. Castro, 1969-Figure 2-2-a for monotonic and Figure 2-8-a for cyclic). In drained loading, significant volume contraction can initiate at such a stress ratio (Skopek, 1994). Some experimental studies revealing such behavior are summarized below.

Eckersley (1990) induced a series of model flowslides in coal mine tailings by slowly raising the water level. He noticed that failure initiated at a stress ratio that was close to the stress ratio at the peak shear strength of the material obtained from undrained triaxial compression tests. Eckersley suggested that the generation of pore pressures was the result of failure and not its cause.

Sasitharan et al. (1994-a) performed drained stress-controlled constant deviatoric stress (CDS) tests on samples of very loose saturated Ottawa sand. Collapse of the sample took place once a stress ratio corresponding to the post peak of the UESP was approximately reached (Figure 2-7-c). The CDS stress path was imposed by applying a constant load at the top of the sample using a hanger while the effective mean normal stress was gradually reduced.

Skopek et al. (1994) showed that when very loose dry Ottawa sand is loaded in triaxial compression to a certain shear stress, and then subjected to CDS loading under load-controlled condition, significant volume contraction occurs when a certain stress ratio is reached (Figure 2-8-b). Anderson and Riemer (1995) observed similar behavior. They also reported that the amount of contraction becomes smaller as the initial density increases, and disappears if the initial density is increased beyond a certain value. Detailed explanations regarding the above CDS tests on saturated and dry Ottawa sand will be given in Chapter 3.



Such a change of behavior at a certain stress ratio has been attributed by some researchers to the collapse of the metastable structure of such soils (Terzaghi, 1956; Bjerrum et al., 1961); the attainment of a flow structure after the peak undrained strength of the soil is passed (Casagrande, 1971); the different behavior exhibited by certain types of sands called “quick sands” as opposed to “normal sands” (Hanzawa, 1980), or the “collapsiveness of the sand skeleton” associated with a “very rapid change in compressibility with respect to shear strains,” which is more pronounced in soils with certain grain size distribution and grain shape (Alarcon-Guzman et al., 1988).

### *2.3.2.3 Empirical criteria for flow liquefaction*

Sladen et al. (1985) introduced the concept of “collapse surface” to determine the condition under which flow liquefaction initiates. They suggested that for samples of very loose sand at a certain void ratio, the peak points of the UESPs lie on a straight line in the  $p$ - $q$  plane that passes through the steady state point corresponding to that void ratio. The position of the line changes with void ratio, but its slope remains constant. The combination of an infinite number of lines corresponding to different void ratios constitutes a surface in the  $p$ - $q$ - $e$  space, which they called the “collapse surface” (Figure 2-9-a). A necessary condition for the initiation of collapse is that the state of the soil lies on this surface regardless of the drainage condition under which the surface is reached.

From the inspection of the shape of the UESP of anisotropically consolidated (AC) sands, Sladen et al. (1985) suggested that the slope of the collapse surface may be greater in AC sands. They observed that AC sands “often fail almost immediately upon loading under undrained condition, i.e. they reach the collapse surface during drained consolidation” (Sladen et al., 1985).

Vaid and Chern (1985) suggested that the peak points of the UESPs, which marked the initiation of contractive behavior, lie on a line of constant stress ratio  $q/p$ , which they termed the “critical stress ratio” (CSR) line (Figure 2-9-b). They suggested that

liquefaction of very contractive sand occurs when the CSR is reached regardless of whether the applied load is monotonic or cyclic (Vaid et al., 1989). In cases in which sand exhibits limited softening in undrained shear, limited liquefaction associated with a temporary increase in pore pressure and axial strain occurs when the CSR is reached. This is followed by a decrease in pore pressure and a subsequent increase in shear strength up to the steady state. Vaid et al. (1989) suggested that the CSR is unique for a certain type of sand in triaxial compression regardless of the initial void ratio or the stress ratio at consolidation. However, under triaxial extension the CSR increases as void ratio decreases.

Alarcon-Guzman et al. (1988) performed torsional cyclic shear tests on loose Ottawa sand. They observed that strain softening in cyclic loading occurs at stress ratios that are higher than the CSR defined by Vaid et al. (1985). They noticed that during cyclic loading, once the state of stress reaches the UESP obtained from monotonic tests, an abrupt increase in the rate of generation of pore pressures and shear strains initiates. They concluded that the UESP obtained from monotonic tests constitutes a “collapse boundary” that determines the condition under which strain softening behavior initiates in cyclic loading (Alarcon-Guzman et al., 1988) (Figure 2-10-a). Similar results were obtained by Ishihara (1991) and Hyodo et al. (1994) but from tests on anisotropically consolidated Toyoura sand (Figure 2-10 b and d).

Canou et al. (1994) investigated the initiation of undrained softening in monotonic and cyclic loading conditions using tests on loose Houston RF sand. They noticed that the stress ratio at the start of softening under cyclic loading is close to but slightly higher than that obtained from monotonic tests (Figure 2-10-c).

Lade (1992) showed that whenever the state of a loose fine sand in a meridian plane lies above a line connecting the top points of the yield surfaces, the sand is in an unstable condition and may collapse due to a small perturbation. This line, which for very loose sand was assumed to pass through the origin, was called the “instability line” (Figure 2-9-c). Lade (1992) suggested that for very loose sand this line is very close to

the line connecting the top points of the UESPs. Using the concept of the instability line, Lade (1992) showed that certain submarine slopes can become unstable under very small slope angles and even level ground under  $K_0$  consolidation may destabilize due to a small disturbance. A more recent experimental investigation by Bopp and Lade (1996) involving tests at high pressures suggested that initial relative density has a small effect on the slope of the instability line obtained from triaxial compression and extension tests. They observed that the slope of the line decreases slightly due to a decrease in initial relative density.

Sasitharan et al. (1993) showed that a state boundary surface (SBS) exists for very loose sand in the  $p$ - $q$ - $e$  space that separates states that are attainable by the soil from those that cannot be attained. A SBS is a surface that envelops all possible states of the soil and is itself a yield surface (Roscoe et al., 1958). Sasitharan et al. (1993) approximated the SBS of loose Ottawa sand by a straight line in the  $p$ - $q$  plane that was the common tangent to the UESPs of samples having the same void ratio, but consolidated to different pressures (Figure 2-9-e). This line passed through the steady state stress corresponding to the common void ratio of the samples. Such an approximation provided substantial convenience in evaluating the susceptibility of very loose sand consolidated to a limited range of pressures, to instability and collapse.

Sasitharan et al. (1993) showed that the stress path of a sample of very loose sand cannot cross the SBS but is forced to stay on this surface once the surface is reached. Collapse and/or instability may take place if the applied loads and drainage condition do not allow the stress path to remain on the SBS. Skopek et al. (1994) showed that very loose sand may experience significant volume contraction when the SBS is encountered.

#### *2.3.2.4 Flow liquefaction and instability*

Lade and his co-workers (e. g. Lade et al., 1988) showed that dense dilating sand remained stable when loaded into a region of high shear stresses where Drucker's

stability postulate (Drucker, 1951, 1956, 1959) is violated. However, loose contractive sand became unstable when subjected to the same loading condition but prevented from drainage. Instability involved a sudden increase in pore pressure and axial strain and the development of a runaway condition that brought the sample to failure without further loading. However, when the sample was loaded to low shear stress level, it remained stable and developed only a small axial strain and pore pressure that was attributed to a small volumetric creep. Under fully drained condition, however, the sample remained stable regardless of its density and the stress level imposed. Lade et al. (1988) concluded that when the state of stress of a contractive sand lies on the portion of the yield surface that opens up in the outward direction of the hydrostatic axis, instability initiates if drainage is prevented.

Chu et al. (1993) followed a procedure similar to that of Lade et al. (1988) and showed that instability may also occur in dilative sand. They concluded that if a rate of dilation is imposed on a soil that exceeds the rate of dilation exhibited by the soil itself, pre-failure strain softening occurs (Figure 2-11-a) which may lead to instability. Similar observation was made by Uchida and Vaid (1994) in strain path tests. Pre-failure strain softening depended on several factors including the initial confining pressure. The higher the pressure was, the greater was the tendency for softening, provided that the imposed rate of dilation remains the same (Chu et al., 1992)(Figure 2-11-a). By conducting pairs of tests under stress-controlled and strain-controlled conditions, Chu et al., (1993) showed that instability occurs under stress-controlled condition in samples that exhibited softening under strain-controlled condition. They concluded that strain softening is a necessary condition for the occurrence of instability. Chu et al. (1992, 1993) also showed that, as suggested by Vardoulakis (1979), the strain softening observed in drained triaxial compression tests on dense sand is not a material property but is a result of the development of non-uniform strains and shear band.

Lade et al. (1993) performed tests in which water was injected into a sample of dilating sand, forcing it to dilate at a certain rate, while the applied load was kept constant. Instability occurred when the imposed rate of dilation exceeded the rate that

was exhibited by the soil during drained loading. In this case, the effective confining stress decreased, and instability initiated. They concluded that unlike compressive soils in which the occurrence of instability is self sustained and unconditional under undrained condition, in dilating sand, decrease in load-carrying capacity depends on the reduction of the effective confining stress and is therefore, conditional. In fact, if at any stage during the test, the injection of water into the sample is stopped, the sample remains perfectly stable (Lade et al., 1993).

### 2.3.2.5 *Theoretical criteria for instability and flow liquefaction*

The stress-strain relationship of an elastoplastic material can be written in the following form:

$$d\boldsymbol{\varepsilon} = \mathbf{C} d\boldsymbol{\sigma} \quad 3-21$$

in which  $d\boldsymbol{\varepsilon}$  and  $d\boldsymbol{\sigma}$  are tensors of strain and stress increments respectively and  $\mathbf{C}$  is the fourth order elastoplastic compliance tensor. As long as the material is in the hardening regime and deforms uniformly without any restraint on the development of strains, the above equation gives an increment of strain for any increment of stress and the material remains stable. In sand obeying non-associative flow plasticity, this is true regardless of the sign of the second increment of plastic work  $d^2W$  (Lade et al., 1988).

Pradel and Lade (1990) showed that in an elastoplastic material with non-associative flow rule, a small increase in deviatoric stress cannot be matched by a reaction from the material, if the constitutive matrix becomes singular. Certain relationships among material parameters and the state of stress can lead to such condition. They showed that this condition existed in cases in which instability was observed in experiments.

Peters (1991) showed that while the determinant of the stiffness matrix is positive and sand is in the hardening regime, individual stiffness terms can become negative, leading to instability. For dilative sand, he showed that this condition prevails when a strain rate that is more dilative than that measured in a drained test is imposed on the material.

Molenkamp (1991) showed that instability develops when the smallest real eigenvalue of the constitutive matrix becomes zero and subsequently negative during stress-controlled loading. He showed that under uniform deformation conditions, instability occurs sooner if soils become more contractive, or less able to drain.

Di Prisco and Nova (1994) investigated the condition under which the shear stiffness of an infinite submerged sandy slope at a certain depth becomes zero. They showed that this condition may be realized when the inclination of the slope is much smaller than the angle of repose, but larger than the value obtained from Lade's (1992) instability line or Hill's (1958) criteria (i. e. the positive definiteness of the stiffness matrix). They concluded that steep submarine slopes can therefore exist in nature, but a load of small intensity (but not infinitesimal) may give rise to their failure.

## **2.4 Summary**

The behavior of sandy soils and the importance of proper modeling of the constitutive behavior of sand were examined in this chapter. It was indicated that constitutive models for sand should be capable of predicting the behavior of loose sands satisfactorily because such sands are prone to flow liquefaction. The yield surface was identified as an important model element that affects the predicted behavior of loose sand significantly. Yield loci obtained from experimental studies and yield functions used in some recent constitutive models for sand were discussed and evaluated. Constitutive models for sand were then reviewed and evaluated. Major shortcomings of most current constitutive models for sand were listed in Chapter 1 and therefore, were not repeated in this chapter.

The occurrence of flow deformations in loose, sandy soils was also examined in this chapter. Empirical criteria for predicting the initiation of collapse and flow deformation were reviewed. While some of the current criteria discuss effects of a number of factors on the stress state at the onset of collapse and instability, effects of many factors are either not studied or not quantified.

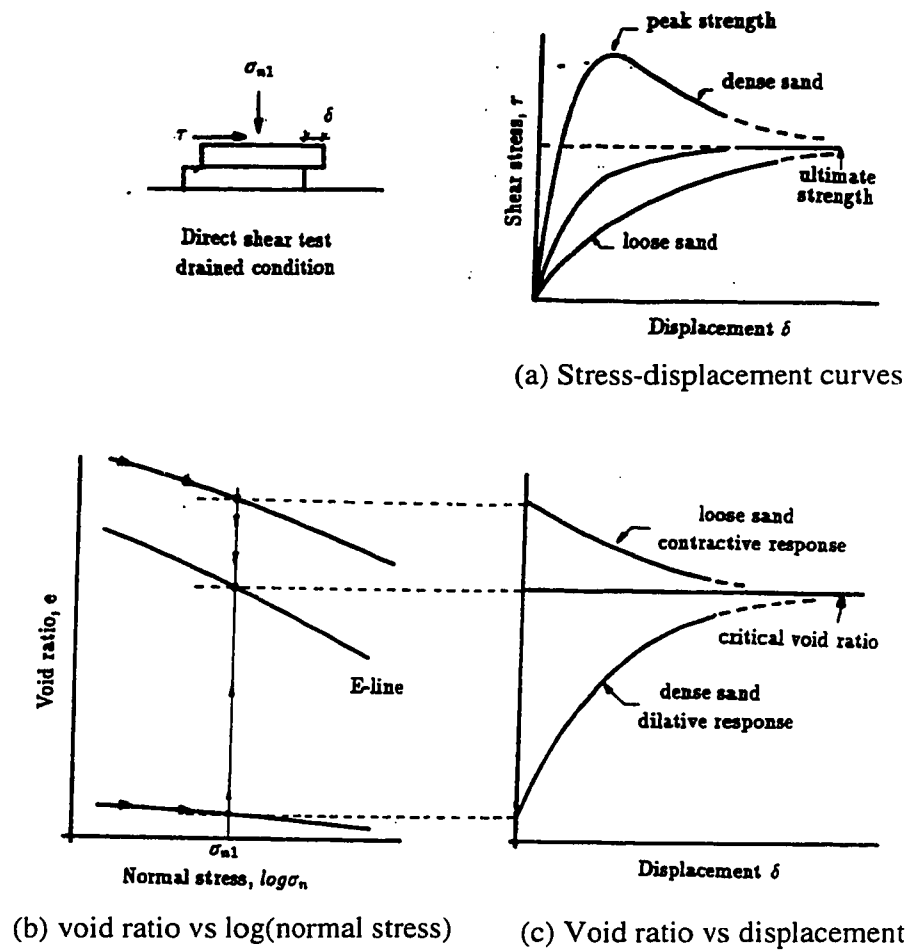
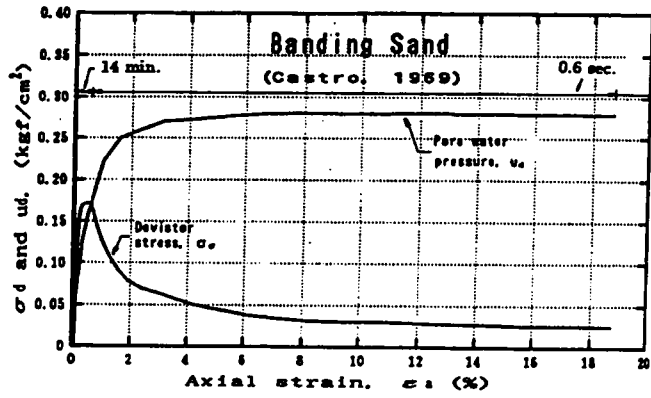
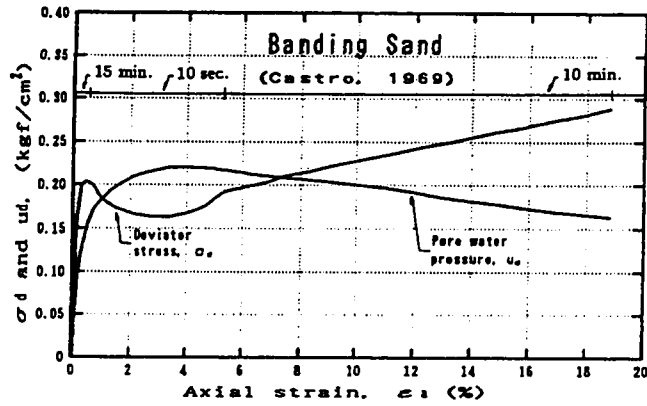


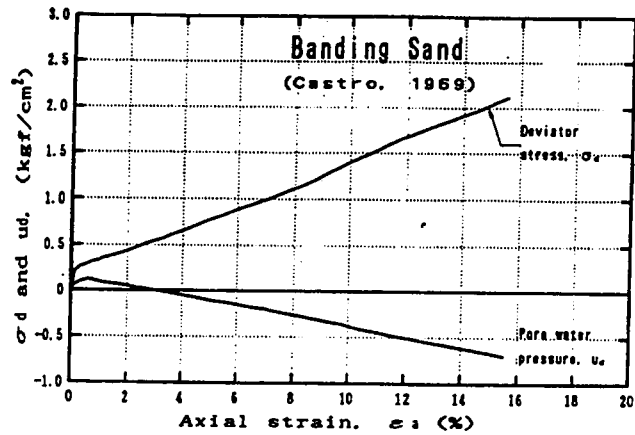
**Figure 2-1** Concepts of critical void ratio (Casagrande, 1936) and ultimate strength as illustrated by Casagrande (1971)



(a) Very loose sand



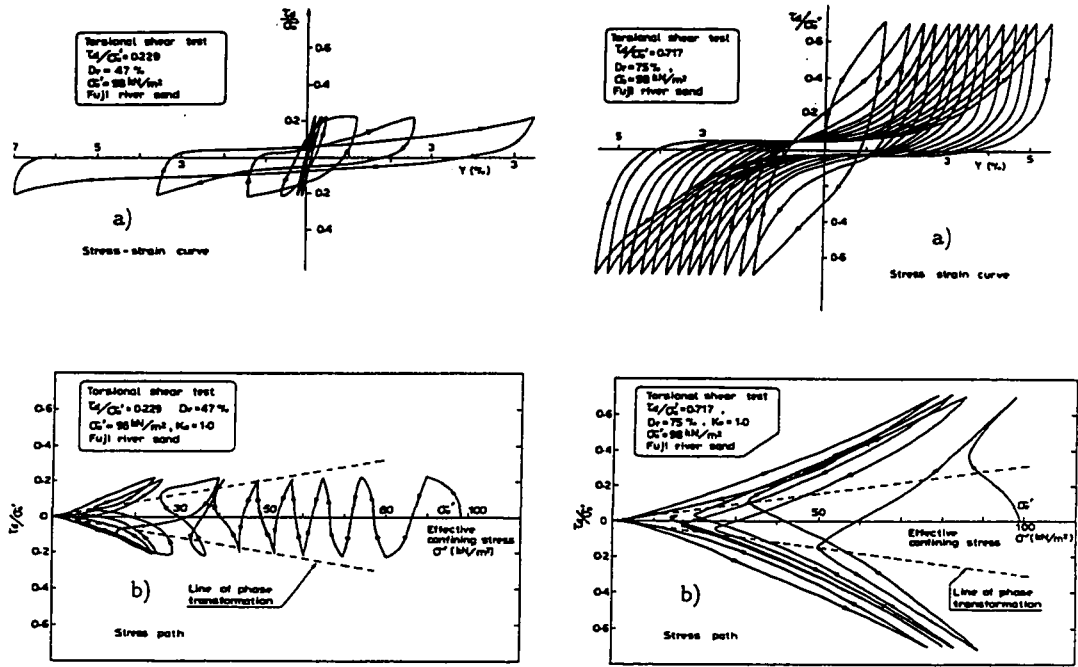
(b) Loose sand



(c) Dense sand

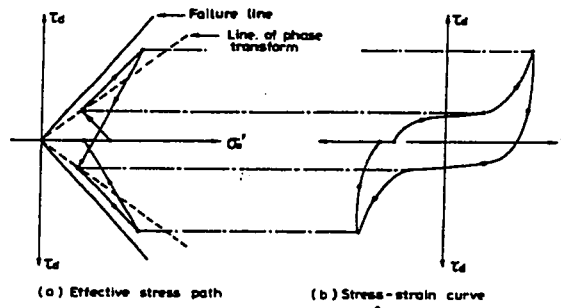
**Figure 2-2** Undrained behavior of Banding sand in monotonic tests (modified after Castro, 1969)





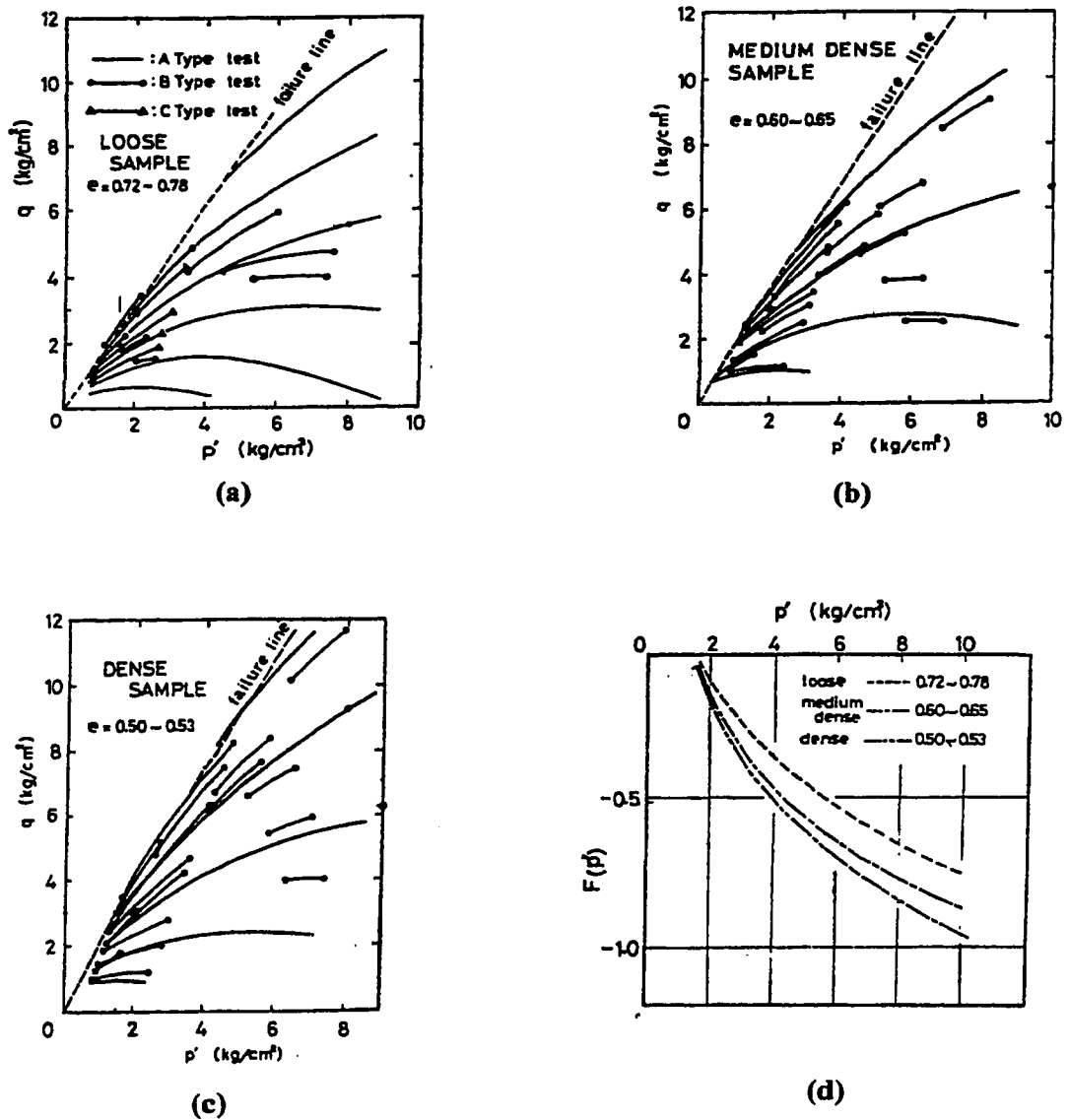
A) Loose sand

B) Dense sand



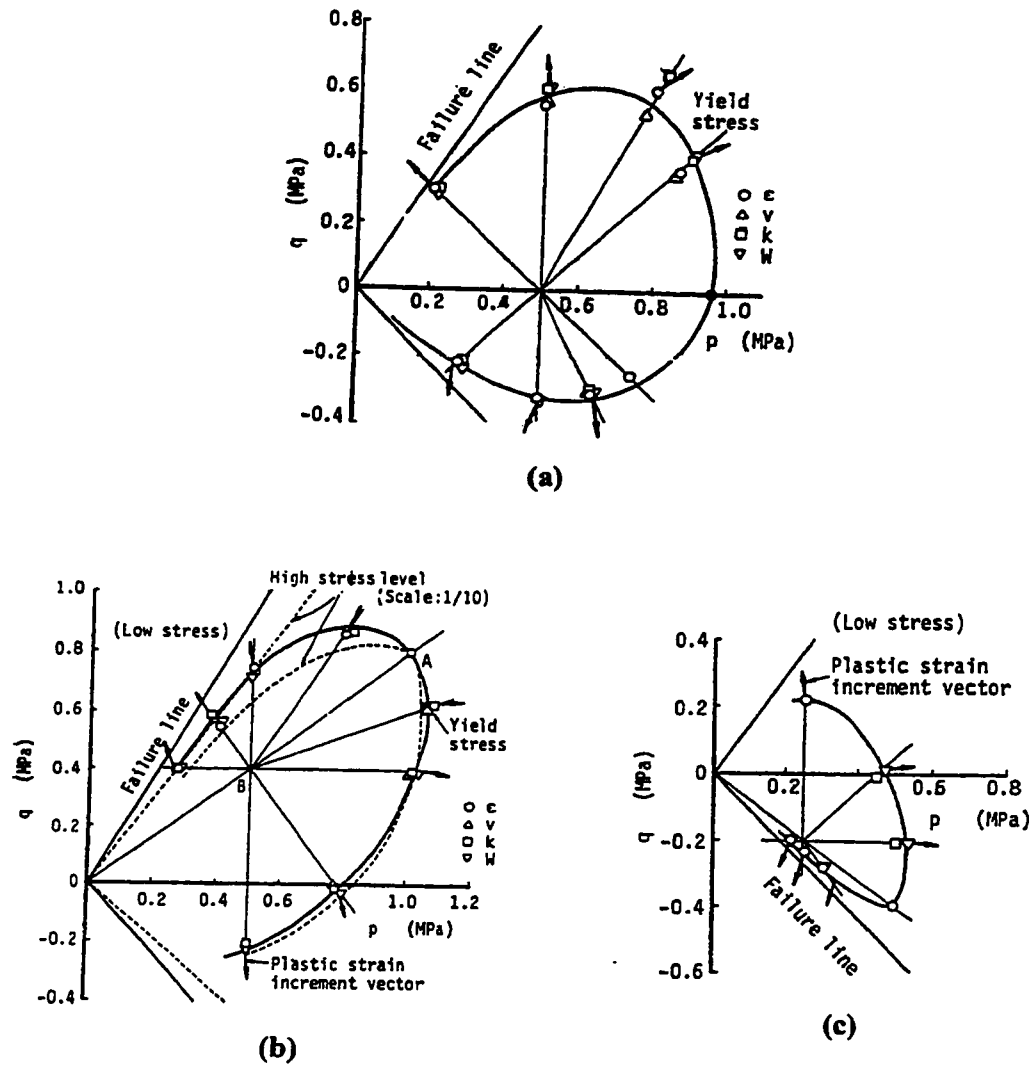
C) Stress path and stress-strain during one cycle

Figure 2-3 Response of loose and dense sand to cyclic loading as illustrated by Ishihara (modified after Ishihara, 1985)



**Figure 2-4** Yield loci measured from tests on sands with various densities:

(a) Loose (b) Medium dense (c) Dense (d) function  $F(p)$  accounting for the curvature of the yield loci and the effect of density (modified after Tatsouka and Ishihara, 1974)



**Figure 2-5** Experimental yield stresses obtained for dense sand:

(a) Isotropically consolidated

(b) Anisotropically consolidated in compression along stress ratio 0.8

(c) Anisotropically consolidated in extension along stress ratio -0.8

(modified after Yasufuko et al., 1991-a)

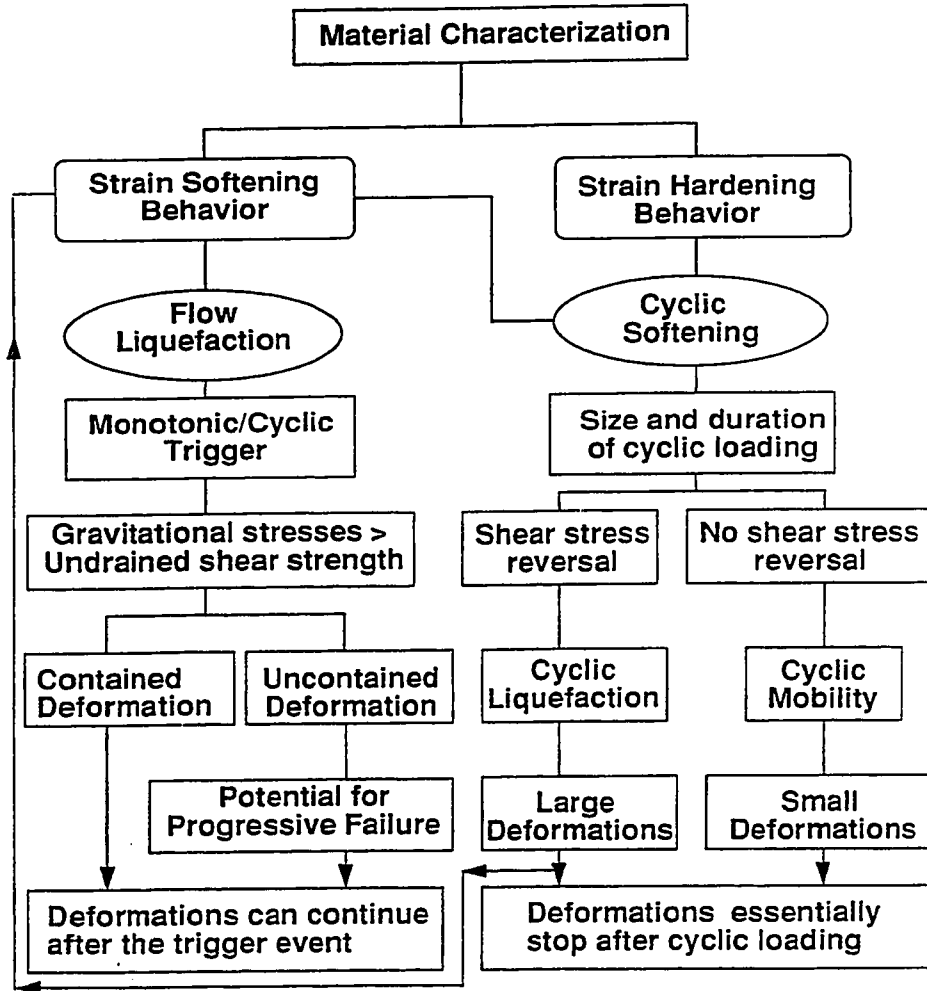


**Figure 2-6** Flow chart to identify the response of sandy ground to loading (modified after Robertson, 1994). The current thesis addresses the triggering condition for flow liquefaction and the stress-strain behavior of the material after triggering

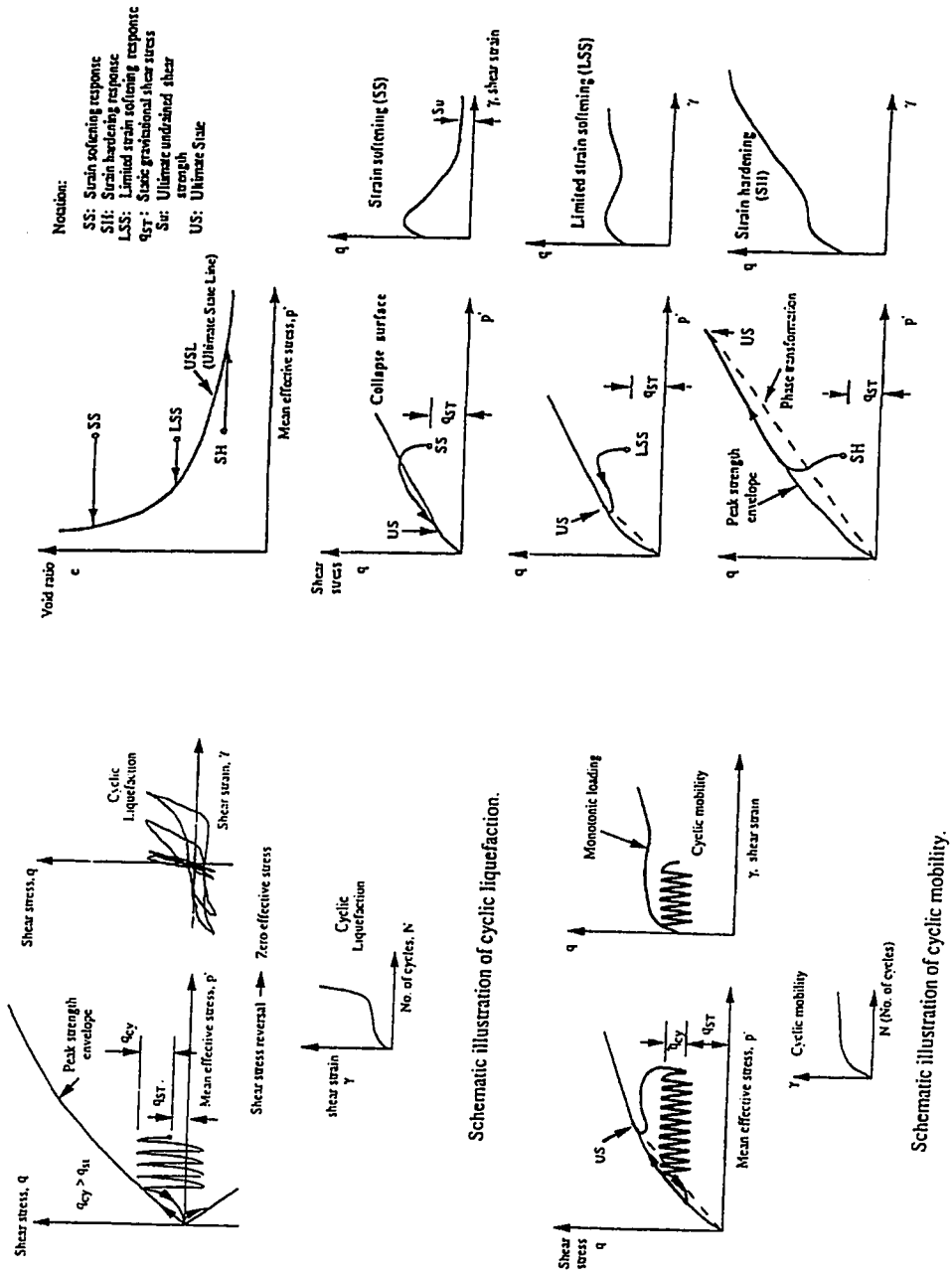
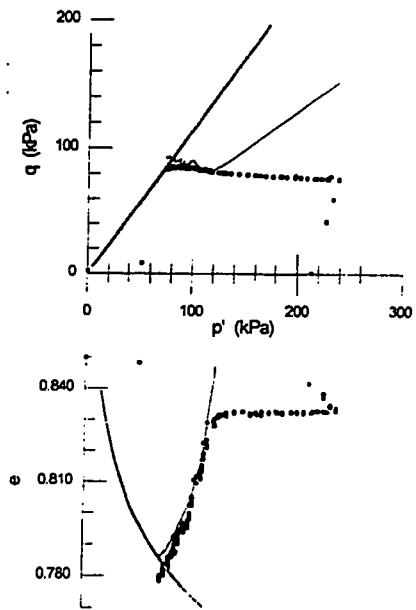
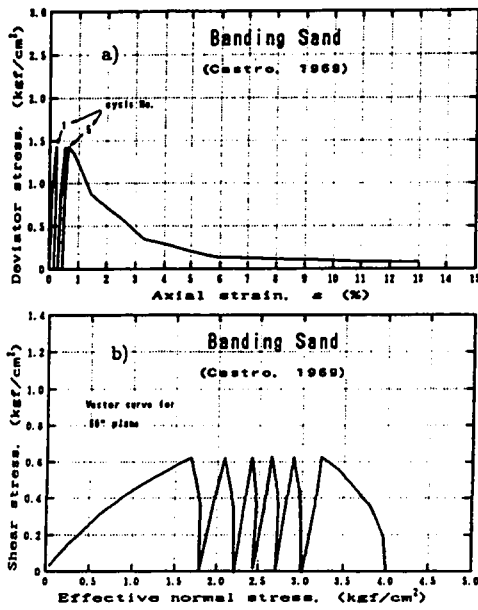
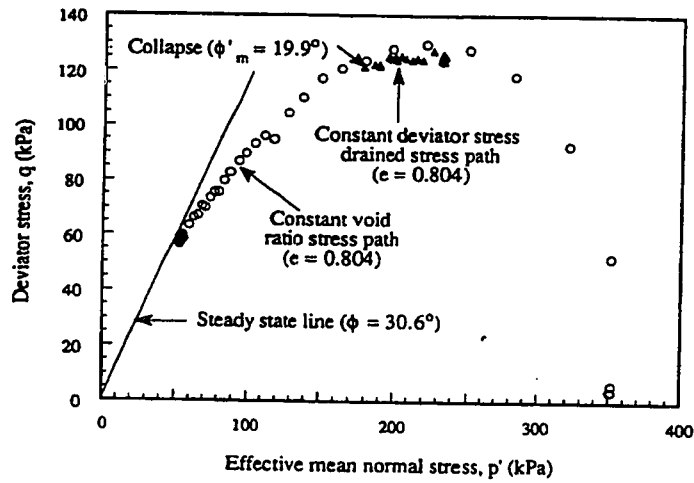


**Figure 2-7** Response of a soil element with static shear to monotonic and cyclic loads as illustrated by Robertson (modified after Robertson, 1994)



a) Liquefaction in cyclic test (modified after Castro, 1969)

b) Significant contraction in CDS test on dry sand (modified after Skopek, 1994)



c) Collapse in CDS test on saturated sand (modified after Sasitharan et al, 1994)

**Figure 2-8** Behavior of very loose sand when stress ratio at collapse is reached under various conditions

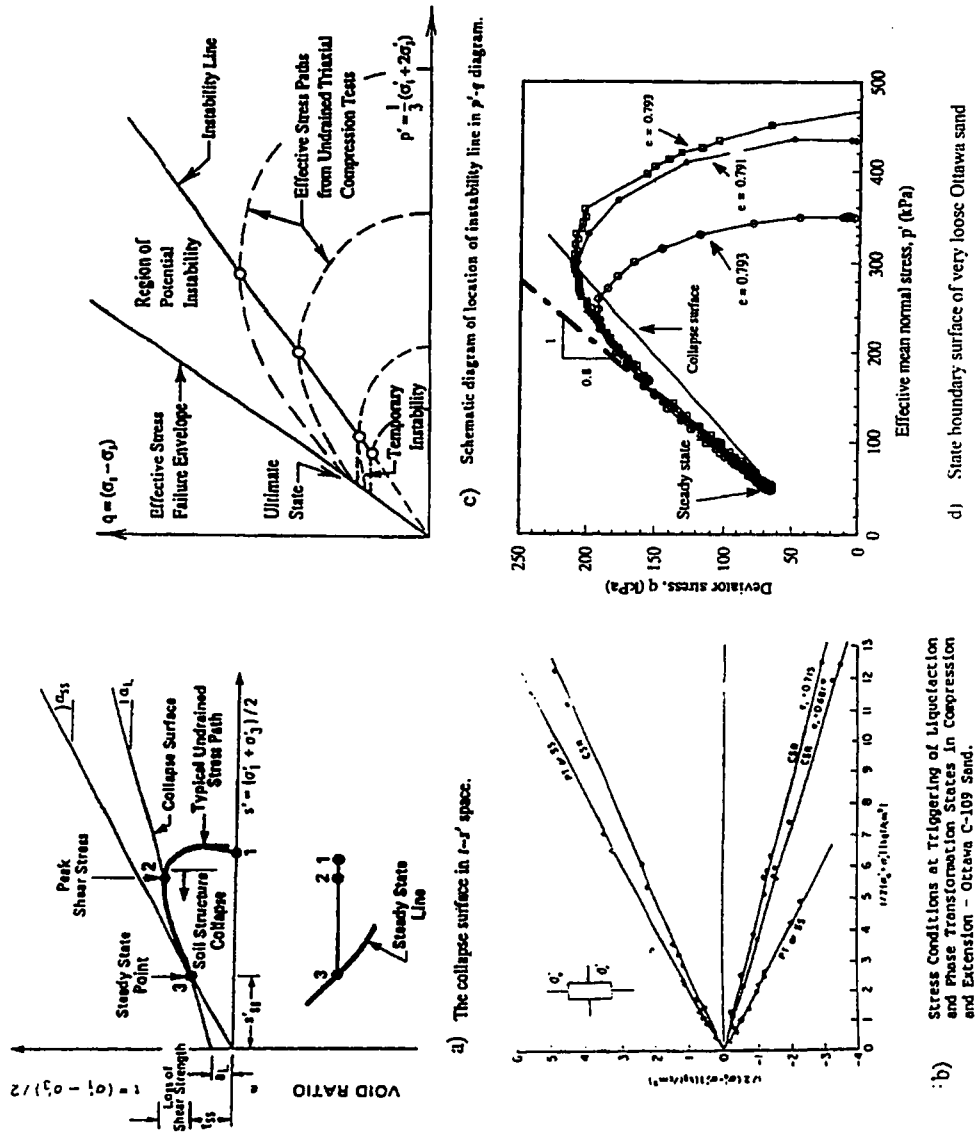
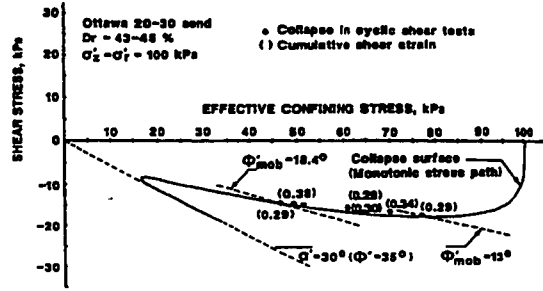
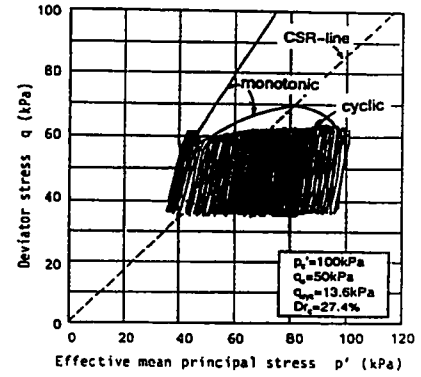


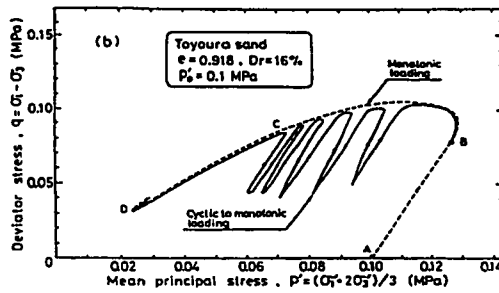
**Figure 2-9** Empirical criteria for the initiation of collapse and instability in granular soils: a) The collapse surface (modified after Sladen et al., 1985); b) The critical stress ratio (CSR) line (modified after Vaid et al., 1990); c) The instability line (modified after Lade et al., 1990); d) The state boundary surface (modified after Sasitharan et al., 1993)



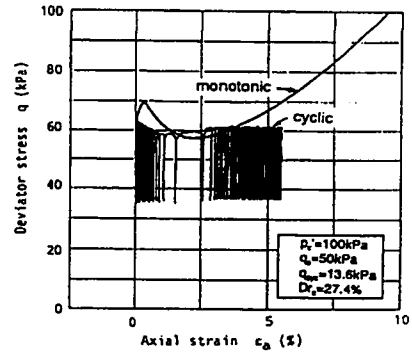
a) Stress condition at the initiation of strain softening behavior in undrained cyclic tests (modified after Alarcon-Guzman et al., 1988)



(a)

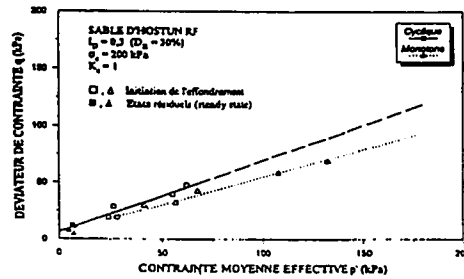


b) Comparison of stress paths followed in undrained monotonic and cyclic tests (modified after Ishihara, 1991)



(b)

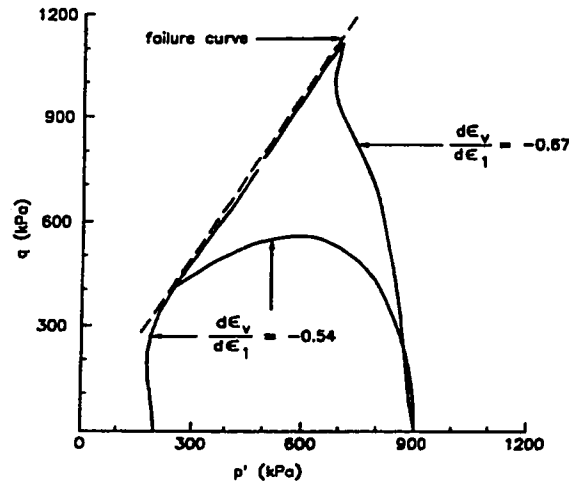
d) Occurrence of small flow deformations during cyclic loading and its relationship to the undrained effective stress path in monotonic loading (modified after Hyodo et al., 1993)



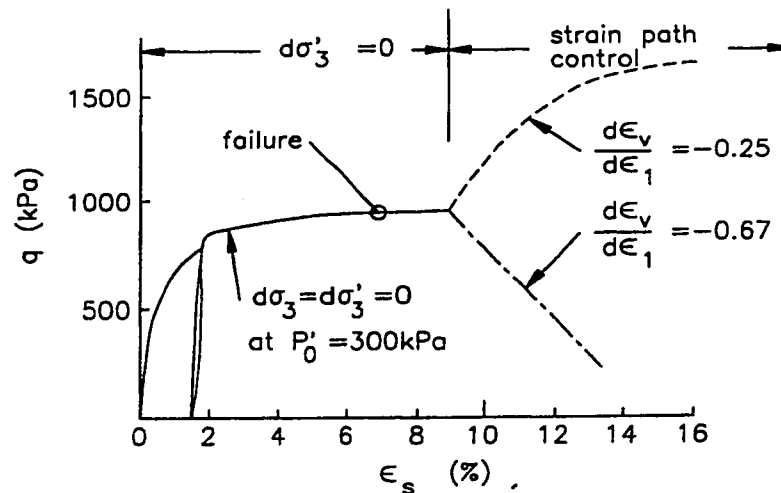
c) Stress state at the initiation of softening observed in cyclic and monotonic tests (modified after Canon et al., 1993)

**Figure 2-10** Initiation of strain softening and flow deformation in undrained monotonic and cyclic tests





a) Stress paths



b) Stress-strain in post-failure strain path tests

**Figure 2-11** Effect of the rate of volume change imposed on sands on their behavior : a) Strain softening and strain hardening of samples subjected to the same rate of volume change (-0.54) but consolidated to different pressures. Also for the same pressure (900 KPa) softening or hardening can occur depending on the rate of volume change imposed on the soil. b) Softening or hardening of samples subjected to volumetric strain rates smaller or larger than that exhibited by the soil itself at failure (modified after Chu et al., 1993)

## *Chapter 3*

### **3 Yielding and Collapse behavior of sands**

#### **3.1 Introduction**

It was noted in Chapter 2 that the yield surface is an important element of a constitutive model for sands. In a constitutive model that, among other aspects of sand behavior, is intended to address various aspects of the behavior of loose sands, yield surface should be used that can account for the yielding of loose sands appropriately. An important aspect of the behavior of loose sands is their susceptibility to “flow liquefaction.” Therefore, a clear understanding of the conditions that lead to “flow liquefaction” and their relationship to the constitutive behavior of the material needs to be established. This chapter will therefore, include the following subjects:

1-Using results of previously published tests on very loose Ottawa sand, the yielding of granular soils and the effect of density on the yielding behavior are examined. A yield function is adopted for sands and methods of determination of its parameters are described. Comparison is then made between this yield surface and the results of some previously published experimental studies reviewed in Chapter 2.

2-The yield function used for isotropically consolidated (IC) sand is extended to include the effect of anisotropic consolidation. Method of determination of the parameters of the extended function from the stress state at consolidation is examined.

Results of this procedure are then compared with yield stresses of an anisotropically consolidated (AC) sand obtained from experiment.

3-The relationship between the shape of the yield surface and the shape of the undrained effective stress path (UESP) of loose sand is investigated. Results of this comparison are used in this chapter to explain a number of observations reported in past literature regarding the stress ratio at the onset of collapse and instability of very loose sands. Factors affecting this stress ratio are examined and experimental evidence is presented from the literature. Results of this comparison is also used in Chapter 4 to locate the position of the yield surface of loose sands at a variety of states and loading conditions.

It is noted that in this chapter, derivations, investigations and discussions are made for triaxial conditions. Extension to general states of stress is made in the chapters that follow where needed.

## **3.2 A yield function for sand, its experimental verification and parameter determination**

### **3.2.1 A Yield function for sand**

A yield function with the following analytical form is adopted. Comparison of its geometric representation with yield functions reviewed previously will be made later:

$$f = \eta^2 - k^2 \left[ 1 - \left( \frac{p}{p_c} \right)^{\frac{1}{2}} \right] = 0 \quad 3-1$$

in which  $\eta = q/p$  is the ratio of deviatoric stress  $q = \sigma_1 - \sigma_3$  to mean normal stress  $p = (\sigma_1 + \sigma_2 + \sigma_3)/3$ ,  $p_c$  is the maximum value of  $p$ , and  $k$  is a material parameter. Yield

functions having similar analytical forms (see e. g. Pestana-Nascimento, 1994) or geometric representations (see e. g. di Prisco et al., 1993) have frequently been used in constitutive modeling of sands recently. Yield parameters and degrees of complexity of yield functions, however, have varied in different models.

By assigning numerical values for the pressure  $p_c$  and the material parameter  $k$  in Equation 3-1, a specific yield surface is defined. Representation of such a surface in the  $p$ - $q$  plane (Figure 3-2) exhibits a peak. Assuming that the material parameter  $k$  is independent of the stresses  $p$  and  $q$ , and denoting the stress ratio at peak by  $M_p$ , application of the condition  $\frac{dq}{dp} = 0$  leads to:

$$k^2 = 5 M_p^2 \quad 3-2$$

In what follows, the above yield function is compared with results of the experimental studies on the yielding of sand reviewed in Chapter 2, and variations of  $p_c$  and  $M_p$  are examined.

### 3.2.2 Comparison of the yield function with some experimentally derived yield loci

Figure 3-1 shows the shape of the yield locus given by Equation 3-1, along with the experimentally derived yield loci reviewed in Chapter 2. Yield stresses obtained by Yasufuko et al. (1991-a) from tests on dense Aio sand (void ratio of 0.65 to 0.67) are also shown in the same figure. This reference describes Aio sand as an angular to sub-angular sand composed mainly of Quartz and feldspar. Its maximum and minimum void ratios are 1.05 and 0.58 respectively. Yield parameters and initial yield stresses were selected such that all yield loci passed through one of Yasufuko et al.'s (1991-a) yield points (point A in Figure 3-1-a). The ability of different yield functions to predict other yield stresses were then compared with each other. It can be seen that for the

region of high stress ratios  $q/p$ , shapes of yield functions represented by Equations 3-1 and 2-5 are similar to those of Equations 2-1 and 2-2 obtained experimentally. However, compared to Equation 2-5, Equation 3-1 produces smaller curvature for this region, which is in a better agreement with the observed yield stresses. It can be seen that yield functions without a cap cannot predict yield stresses at small stress ratios (closer to the  $p$ -axis) appropriately.

Similar data were not available for loose sand but an initial yield point A1 (Figure 3-1-b) was assumed that corresponded to an expected smaller stress ratio at yielding. Smaller values of  $N$  and  $M_p$  were used in Equations 2-5 and 3-1 respectively to make these yield surfaces pass through point A1. It can be seen that the shape represented by Equation 2-1 obtained from tests on dense sand differs from the other shapes significantly. The version of Equation 2-2 that was obtained from tests on loose sand, however, predicts yield stresses at the region of high stress ratios that are close to those obtained from the two capped curves up to the point of peak  $q$ . It can be seen that for both dense and loose sand, a straight line provides a suitable approximation of yield stresses in the region of high stress ratios close to the origin. Capped yield surfaces on the other hand, can provide good approximations of yield stresses at high and low stress ratios, provided appropriate parameters are used to account for sand density. In what follows, Equations 3-1 and 2-5 that seem to provide better account of yielding of sands are examined in more detail and compared to each other.

From a best fit to their experimental data, Yasufuko et al. (1991-a) obtained a stress ratio at peak  $N_c = 1.015$  for their yield function (Equation 2-5). The same value was therefore used for  $M_{p,c}$  in Equation 3-1 and the two yield curves along with average experimental yield stresses were plotted in Figure 3-2. It can be seen that on the compression side, yield stresses at high stress ratios close to failure are generally overestimated by both equations while those near the top of the yield surface of IC sand are slightly underestimated. Equation 3-1, however, gives slightly better general fit to the measured yield points. On the other hand, yield stresses on the extension side are overestimated substantially by both equations. It is noted that for Equation 3-1, the

value of  $M_p$  at extension ( $M_{p,e}$ ) was obtained from that in compression ( $M_{p,c}$ ) assuming that the friction angle at peak is the same in compression and extension, as suggested by Yasufuko et al. (1991-a):

$$M_{p,e} = -\frac{3M_{p,c}}{(3 + M_{p,c})} \quad 3-3$$

which results in  $M_{p,e} = N_e = -0.75$ .

To obtain a better fit to the measured data, a value of  $M_{p,e} = -0.5$  was used in Equation 3-2 and the yield curve was replotted in Figure 3-3. It can be seen that the agreement is improved significantly. This reduction in stress ratio can be attributed to the existence of some anisotropy in the yielding behavior of this "dense" sand that can be accounted for by a reduction in the friction angle at peak on the extension side. Evidence of such anisotropy in "loose" sand is also demonstrated in the next chapter.

### 3.2.3 Yield function for anisotropically consolidated sand

Equation 3-1 adopted for the yield function of an isotropically consolidated (IC) sand can be modified to account for anisotropic consolidation. It is often noticed (e. g. by Cambu and Lanier, 1988; Yasufuko et al., 1991-a) that if sand is consolidated anisotropically, its yield surface moves in the direction of anisotropic consolidation. In such cases, therefore, a procedure is needed by which changes in the position of the yield surface resulting from anisotropic consolidation can be accounted for.

If the point at which the slope  $dq/dp$  becomes infinity (i. e. where  $p = p_c$  in IC sand) moves away from the hydrostatic axis and lies on a line with stress ratio  $\alpha$ , maximum yield pressure will be at this point rather than the pressure  $p_c$  at which the soil is consolidated (Figure 3-4). This largest pressure will be denoted by  $p_\alpha$  here and is in general, not known but depends on the consolidation stress history and the stress ratio

$\alpha$ . This stress ratio determines the degree of stress-induced anisotropy of the yielding behavior. In this case, Equation 3-1 for the yield surface of IC sand should be written in the following form such that at  $p = p_\alpha$ , we have  $\eta = \alpha$ :

$$f = (\eta - \alpha)^2 - k^2 \left[ 1 - \left( \frac{p}{p_\alpha} \right)^{\frac{1}{2}} \right] = 0 \quad 3-4$$

To determine the relationship between the stress ratio  $M_p$  and the parameter  $k$  in the above equation, the slope  $dq/dp$  obtained from the above equation is equated to zero:

$$\frac{dq}{dp} = \frac{5\eta^2 - 6\eta\alpha + \alpha^2 - k^2}{4(\eta - \alpha)} \quad 3-5$$

The parameter  $k^2$  in Equation 3-4 can now be determined from  $\frac{dq}{dp} = 0$ :

$$k^2 = 5 M_p^2 - 6 M_p \alpha + \alpha^2 \quad 3-6$$

Note that for  $\alpha = 0$ , the above equation reduces to Equation 3-2 obtained for IC sand.

Figure 3-5-a compares the yield surface defined by Equation 3-4 with the yield stresses of anisotropically consolidated (AC) dense Aio sand obtained by Yasufuko et al. (1991-a). Values of  $M_{p,c} = 1.015$  and  $M_{p,e} = -0.75$  equal to those initially used for IC sand were substituted in this equation. It can be seen that while good agreement generally exists between measured and predicted yield stresses on the compression side, the same is not true for the extension side. Similar observation was made earlier in the case of IC sand. Use of  $M_{p,e} = -0.5$ , however, led to better agreement on the extension side (Figure 3-5-b). As with the case of IC sand, this reduction in yield strength may be attributed to the inherent anisotropy that existed in the material prior to the application of the consolidation stresses. The example reviewed here suggest

that this anisotropy in yielding can be accounted for using suitable values for  $M_{p,c}$  and  $M_{p,e}$  regardless of stress ratio at consolidation. This is because anisotropic consolidation did not seem to affect  $M_{p,c}$  and  $M_{p,e}$ . It will be shown in Chapter 4 that similar conclusion is reached when  $M_p$  is measured from undrained tests on IC and AC loose sand.

Equation 3-5 shows that while the slope  $\frac{dq}{dp}$  is infinity at  $\eta = \alpha$ , the slope of the yield surface is not the same in triaxial compression and extension. This is true even in IC sand, because the slope is a function of the stress ratio at peak  $M_p$  which may not be the same in triaxial compression and extension.

It should be noted that in comparing Equation 3-4 with experimental yield stresses, a stress ratio  $\alpha$  equal to that obtained experimentally by Yasufuko et al. (1991-a) was substituted in this equation. The parameter  $\alpha$  that accounts for the effect of stress induced anisotropy on the yield stresses and its corresponding pressure  $p_\alpha$  cannot in general be obtained from initial soil and consolidation states. Yasufuko et al. (1991-b) suggested that  $\alpha$  varies during shearing and its initial value  $\alpha_0$  can be obtained from the experimental mean value of the plastic strain increment vector  $du^p/d\varepsilon^p$  measured during anisotropic consolidation. In the following, a convenient procedure for the determination of  $\alpha$  is presented without the introduction of new material parameters or the need for additional stress-strain data. In this procedure,  $\alpha$  is calculated from the stress ratio at consolidation ( $\eta_c$ ) and the stress ratio at peak ( $M_p$ ), both of which known for any loading condition and soil state. The determination of  $M_p$  will be discussed in detail later in this chapter and in Chapter 4. Due to lack of sufficient experimental data regarding the evolution of  $\alpha$ , and since only monotonic loading is considered in the current study, it is assumed here that this stress ratio remains constant during shearing provided that the number and size of stress reversals is small.

From Figure 2-5 (Chapter 2) it can be seen that in the three different stress ratios at consolidation shown, the slopes  $dq/dp$  of the yield surface at the end of consolidation



(i. e. where  $p = p_c$  and  $\eta = \eta_c$ ) are nearly perpendicular to the slope  $\eta_c$ . At this point we will therefore have:

$$\frac{dq}{dp} = -\frac{1}{\eta_c} \quad 3-7$$

For given values of  $M_p$  and  $\eta_c$  the stress ratio  $\alpha$  can be obtained from the following relationship derived from Equations 3-5, 3-6 and 3-7:

$$\alpha = \left[ \frac{5(\eta_c^2 - M_p^2) + 4}{6\eta_c(\eta_c - M_p) + 4} \right] \eta_c \quad 3-8$$

Experimental results indicated that  $M_p$  is not the same in compression and extension. In using Equation 3-8, therefore, the value of  $M_p$  corresponding to the appropriate loading condition should be used.

Note that from the geometry of the yield surface (Figure 3-4) it may be noticed that the condition  $|M_p| > |\eta_c| > |\alpha|$  should always be satisfied. Results of anisotropic consolidation tests on the compression side discussed earlier satisfied these conditions and suggested that the  $M_p$  is not affected by anisotropic consolidation. However, in cases of anisotropic consolidation along stress ratios higher than  $M_p$ , the value of  $M_p$  may increase due to anisotropic consolidation and become close to, but slightly larger than  $\eta_c$  (comparisons are made in terms of absolute values of stress ratios). This can be noticed by comparing the extension sides of Figure 2-5-a and Figure 2-5-c and will be discussed further in Section 4.8.

Anisotropic properties exhibited by  $\alpha$  are expected to develop in the same direction as  $\eta_c$  and therefore, the sign of  $\alpha$  (positive in compression and negative in extension) should be the same as the sign of  $\eta_c$ . This means that if sand is consolidated anisotropically in the compression side, the yield surface will shift in the compression

side, and the same is true about the extension side. The term in the big bracket in Equation 3-8 should therefore, be always positive. Because of the geometry of the yield surface, this condition may not always be satisfied and when the consolidation stresses are small compared to  $M_p$  it may not hold. In this case, the yield behavior is close to that of an IC sand and a value of  $\alpha = 0$  can be adopted.

Equation 3-8 was used to calculate  $\alpha$  for Yasufuku et al.'s (1991-a) tests in which  $\eta_c = 0.8$  in compression. If the experimental value of  $M_{p,c} = 1.015$  is substituted in Equation 3-9, a value of  $\alpha = 0.579$  is obtained that is close to Yasufuku et al.'s (1991-a) experimentally derived value of  $\alpha = 0.5$ .

The maximum yield pressure  $p_\alpha$  depends on  $\alpha$  and  $\eta_c$ . When sand is consolidated anisotropically, the consolidation pressure  $p_c$  is generally known and  $p_\alpha$  can therefore be calculated using Equations 3-4, 3-6 and 3-8:

$$p_\alpha = \left( \frac{5\eta_c^2 - \alpha\eta_c + 4}{4(\eta_c^2 + 1)} \right)^2 p_c \quad 3-9$$

Using the above equation results in  $p_\alpha = 1055$  kPa for Yasufuku et al.'s (1991-a) test data in which  $p_c = 1000$  kPa and  $\eta_c = 0.8$ , if  $\alpha = 0.579$  calculated previously is used. Substituting these calculated values of  $\alpha$  and  $p_\alpha$  in Equation 3-4 for the yield surface provided very good agreement between the yield curve and the experimental yield stresses (Figure 3-6).

Conclusions made so far in this chapter can be summarized as follows:

1-Stress ratios at the peak of the yield surface ( $M_p$ ) in TC and TE do not always correspond to the same friction angle, the difference being apparently a result of structural (inherent) anisotropy of the sand. The friction angle at peak measured on the extension side was smaller than that obtained from compression tests.

2-The stress ratio  $\alpha$  and the maximum yield pressure  $p_\alpha$  were obtained from the stress ratio at consolidation  $\eta_c$  and the stress ratio at peak  $M_p$  without the need for further stress-strain data or the introduction of new material parameters.

3-The stress ratio at peak  $M_p$  does not seem to be affected by stress induced anisotropy. This was found true both on the compression and on the extension sides provided that the stress ratio at anisotropic consolidation is not more than  $M_p$ .

### **3.3 Yield surface of loose Ottawa sand and its relationship to the undrained effective stress path (UESP)**

#### **3.3.1 Establishing the yield surface of Ottawa sand**

A series of tests were performed by Skopek (1994) on very loose samples of “dry” Ottawa sand prepared by the moist tamping technique. Ottawa sand is a subrounded uniform quartzic sand with maximum and minimum void ratios of 0.82 and 0.50 respectively according to the ASTM D2049 method. Void ratios greater than the above maximum value, however, were achieved by moist tamping. Details of the loading procedure and method of sample preparation are given in Skopek (1994).

In these tests, isotropically consolidated samples were loaded in TC using a hanger that exerted a constant axial force to the top of the sample, while allowing free development of strains without the interference of the hydraulic loading system. Deviatoric stress applied by the weight of the hanger was then kept constant while the confining pressure was gradually reduced. This procedure caused the sample to be subjected to a nearly constant deviatoric stress (CDS) throughout this portion of the test until the steady state condition was reached. The actual deviatoric stress, however, slightly increased during the CDS stress path because of the gradual reduction in the confining pressure that reduced the force applied to the top platen. Ten such CDS tests

were performed by Skopek (1994) at initial consolidated void ratios ranging between 0.789 and 0.833 and confining pressures between 190 and 300 kPa.

Results of a typical test are shown in Figure 3-7. It can be seen that very small volume change occurred in the earlier part of the CDS stress path before a certain point was reached at which void ratio started decreasing substantially. Although not shown here, axial strains exhibited similar behavior in that they remained nearly unchanged before a certain point where they started developing at high rates (Skopek, 1994). This behavior continued until steady state was reached. Similar behavior was observed in other tests. It can be noticed that the point at which volume contraction started (point B in Figure 3-7) is where the current yield surface that was established after the application of the full deviatoric stress (point A) was encountered again. Between points A and B, the sample was in the elastic domain of the current yield surface, experiencing unloading. Between points A and B, very small change in void ratio (a very small increase due to rebound) takes place. However, compared to the subsequent plastic volume changes, void ratio can practically be assumed constant between these two points.

From each CDS test, two points similar to A and B can be identified that belong to a yield surface that passes through these points. This yield surface corresponds to the void ratio and consolidation pressure of the sample during unloading between these two points. For these IC samples, the two yield parameters of Equation 3-4 (i. e. the pressure  $p_c$  and the stress ratio  $M_p$ ) can be obtained for each test from the position of points A and B. Figure 3-8 shows the determination of these parameters for two of the CDS tests.

Values of  $p_c$  and  $M_p$  were determined for all CDS tests on dry sand. It was noticed that  $M_p$  was a function of the nearly constant void ratio of the sample between points A and B. Figure 3-9 shows the variation of  $M_p$  with this void ratio. It can be seen that on average, a linear relationship exists and  $M_p$  is inversely related to void ratio. For the sand tested, this relationship was estimated by the following equation:

$$M_p = 3.7425 - 3.8723e \quad 3-10$$

Substituting this relationship in Equation 3-6, the yield surface of IC Ottawa sand can be obtained as a function of the consolidation pressure  $p_c$  and void ratio:

$$f = \eta^2 + (3.7425 - 3.8723e)^2 (1 - (p/p_c)^{1/2}) = 0 \quad 3-11$$

in which  $e$  is the void ratio. A more general form for the variation of  $M_p$  and the form of the yield function will be introduced in Chapter 4. The form given above, however, is intended to be used it in the next section.

### 3.3.2 Yield surface and the undrained effective stress path (UESP)

Sasitharan et al. (1994) performed a series of undrained monotonic TC tests on samples of Ottawa sand prepared in the same way used by Skopek (1994) in dry sand. Consolidated void ratios varied from 0.791 to 0.809 and consolidation pressures from 350 to 550 kPa. Results of a typical test at a void ratio of 0.805 and a consolidation pressure of 550 kPa are shown in Figure 3-10 (triangular marks). The yield surface corresponding to the same void ratio and consolidation pressure, obtained from CDS tests on dry samples (Equation 3-11) is also shown for comparison. It can be seen that at such loose state, the UESP closely resembles the yield surface corresponding to the same void ratio and consolidation pressure.

### 3.3.3 $M_p$ from drained vs. undrained tests

Figure 3-10 suggested that the shape of the UESP of loose Ottawa sand is close to the shape of the yield surface. Therefore, values of  $M_p$  obtained from drained CDS tests on dry Ottawa sand (from Skopek, 1994) were plotted in Figure 3-11 against void

ratio, together with those measured from peak points of the UESPs (from Sasitharan et al., 1994). Data from tests in which the sample was not sufficiently contractive and therefore, a clear peak was not distinguished in its UESP were not included. It can be seen that results obtained from the two different procedures are in good agreement with each other, suggesting that  $M_p$  may be obtained from either method. These results are another indication of the proximity of the peaks of the yield surface and the UESP.

Lade (1992) suggested that in loose sand the peak point of the UESP occurs slightly after but very close to the peak point of the yield surface. Although this suggestion was repeated in several subsequent publications (e. g. in Lade, 1994; Bopp and Lade, 1997) no experimental verification was presented for the suggestion in these publications.

The results obtained above are also consistent with the suggestion of Nova and Heuckel (1981) in that loose sand experience very small or no hardening due to shear strain. In modeling the behavior of sand at different densities, they noticed that the parameter  $D$  in Equation 2-3 (Chapter 2) for the yield surface should be reduced or even equated to zero in the case of loose sand. A small value of  $D$  is equivalent to small hardening and a  $D = 0$  implies no hardening due to shear strain. In undrained shearing of loose sands having  $D = 0$ , no hardening due to plastic shear strain and small hardening due to “plastic” volumetric strain takes place, forcing the UESP to follow the current yield surface approximately.

The example shown in Figure 3-10 and the suggestion of Nova and Heuckel (1981) indicate that in loose sand, the post-peak portion (PPP) of the UESP is also close to the front portion (FP, where stress ratios are high) of the yield surface. In sufficiently loose sand these two portions may practically coincide. This coincidence may explain some observations that have been reported in past literature regarding the significance of the PPP of the UESP (PPP-UESP) in locating stress ratios at which undrained softening or instability initiate. The following sections further discuss this issue.

### **3.4 Instability, collapse and undrained softening of loose sand and their relationship to sand yielding**

#### **3.4.1 Shape of the yield surface and the susceptibility of sand to instability and collapse**

A number of empirical criteria for assessing the condition under which instability and collapse initiates were reviewed in Section 2.3.2.3 (Chapter 2). These criteria generally define lines in the  $p$ - $q$  stress plane that determine states of stress at which instability, collapse or undrained softening can initiate. Some of these criteria suggest that the position of this line is fixed and some others introduce qualitative descriptions regarding the effects of a number of factors on the position of the line.

In the sections that follow, collapse and instability of loose Ottawa sand as observed by Sasitharan et al. (1993) and Skopek et al. (1994) are examined and their relationship with yielding of this sand is investigated. The yield surface obtained previously for Ottawa sand (Equation 3-11) is used in this investigation. Factors affecting the stress ratio at the onset of soil collapse and the size of the zone of collapsible states (Figure 3-13-a) are discussed by examining the shape of the yield surface studied earlier. It is shown that the stress ratio at the onset of instability is influenced by all the factors that affect the position of the yield surface discussed previously. Effects of drainage condition, consolidation pressure, stress path, stress ratio at consolidation, and void ratio on collapse potential are examined in this chapter. Effects of some other factors that influence the stress ratio  $M_p$ , and consequently the shape of the yield surface, including the direction of loading, the intermediate principal stress and soil fabric will be investigated in Chapter 4.

### 3.4.2 Stable collapse of dry sand and unstable collapse of saturated sand in CDS tests: Effect of drainage condition

Figure 3-7 showed that when very loose Ottawa sand is subjected to CDS loading it undergoes significant contraction upon reaching the yield surface. Skopek et al. (1994) showed that in this case strains may not develop smoothly but at certain points large volume reductions accompanied by significant axial strain were experienced by the soil in a short period of time. Such discontinuous response represents collapse of the soil with no loss of stability since the applied load is fully carried by the sample. Similar behavior was observed by Anderson and Riemer (1995) in loose sand. It seems unlikely that these drops in void ratio are results of sand creep since they resemble irregular and varying rates of volume contractions, while sand creep is expected to develop at a smaller and more regular rate. These collapses might have other causes such as the stick-slip phenomena that has been observed frequently in tests involving direct measurement of the interparticle friction of sands (see e. g. Procter and Barton, 1974) or the collapse of an unstable honeycomb structure that such very loose sands may have.

Similar stress paths were imposed by Sasitharan (1993) on saturated samples of very loose Ottawa sand (Figure 3-12- triangular marks). In these tests samples were consolidated isotropically and sheared undrained to a certain stress level (point A) before the peak was reached. Back pressure was then set equal to the current pore pressure, and drained shearing along a CDS stress path in a way similar to that explained earlier for dry sand was initiated. Two such tests were performed. Sasitharan et al. (1993) showed that in both tests once the stress state reached a point corresponding to the PPP of the UESP of a sample at the same void ratio and confining pressure, the sample was no longer able to sustain the applied load and collapsed vigorously (point B).

In order to investigate the cause of collapse at point (B), test #16 was selected from Skopek's (1994) CDS tests on "dry" sand such that void ratio and stress state at point



(A) was very close to Sasitharan et al.'s (1993) CDS test, and its results were also shown in Figure 3-12. It can be seen from this figure that upon CDS loading, the stress state at point B where collapse occurred is very close to the stress state at which significant contraction started in dry the sand. The yield surface of the two samples after consolidation is also plotted in the same figure using Equation 3-11. It can be seen that collapse of the samples has actually occurred when the yield surface was reached (Figure 3-12). It was shown previously that for sufficiently contractive sand, the shape of the UESP is very close to that of the yield surface. This is consistent with the observation made by Sasitharan (1993) that collapse occurred once the PPP of the UESP was encountered.

The occurrence of instability in a "drained" test is not consistent with the experimental investigation of Lade et al. (1988). In Lade et al.'s (1988) tests, samples brought to the condition of potential instability remained stable as long as they were allowed to drain. Upon closure of the drainage valve, however, a small volumetric creep produced small pore pressures that initiated instability.

Although Sasitharan et al.'s (1993) tests were nominally "drained", full drainage could not be maintained during the rapid volumetric collapse of the very loose sample. This inability of the material to develop volumetric strains freely resulted in its instability, because in this case, the behavior is similar to an undrained or semi-drained response. In such cases, the material cannot harden sufficiently by a reduction in its void ratio and therefore, fails to provide the required reaction to the applied loads. Since in very loose sand the amount of hardening due to shear strain is very small, the sample is forced to follow a stress path very close to the current yield surface, leading to a reduction in its shear strength.

The condition discussed above can occur when the "time rate" of the volume reduction required to provide the necessary reaction to the applied loads is more than the "time rate" of the volume reduction that the material can experience, given the drainage capacity of the soil. The drainage capacity of the soil is a function of the

permeability of the soil, boundary conditions and the geometry of the soil mass. It does not seem likely that the high rate of volume reduction that was required to cause instability in Sasitharan et al.'s (1993) "drained" tests was produced by creep as in Lade et al.'s (1988) "undrained" tests. Volumetric collapse of the soil similar to that observed in tests on dry sand, however, could have led to the observed instability.

Differences in drainage condition can be the reason why some submarine slopes consisting of gravel remained stable at slope angles much higher than slopes in similar environments, but made of fine sands (Terzaghi, 1956). Morgenstern (1994) noted that collapse has been generally observed in soils with permeabilities less than about  $10^{-2}$  cm/sec and suggested that further research is needed to refine this value.

### 3.4.3 Yield surface and slope of the state boundary surface: Effect of consolidation pressure

From shapes of yield surfaces of sand (Figure 3-13-b) it can be seen that yield surfaces of samples having the same void ratio but consolidated to different pressures converge at their FPs. In such cases if variations in the consolidation pressure are not significant the FPs will be close to each other and may be approximated by a straight line. For very loose sand, in which the shape of the yield surface and the UESP are close to each other, the common tangent to UESPs of samples sheared at the same void ratio but within a limited range of confining pressures will lead to a similar result. It was mentioned in Section 2.3.2.3 that Sasitharan et al. (1993) used this latter procedure to define a state boundary surface (SBS) that was used to determine states at which collapse initiates.

Sasitharan et al. (1993) obtained a slope of 0.8 for the SBS of loose Ottawa sand from results of tests at void ratios between 0.791 and 0.809, and consolidation pressures between 350 and 550 kPa. Skopek (1994), however, obtained a slope of 0.6

for this SBS from results of his CDS tests at void ratios between from 0.789 and 0.833 and consolidation pressures between 190 and 300 kPa. Consolidation pressures were therefore, higher in Sasitharan et al.'s (1993) tests resulting in an increase in the slope of the FP of the yield surfaces (see Figure 3-13-b) of his samples. The increase in the slope of the SBS obtained by Sasitharan et al. (1993) compared to that of Skopek (1994) may have therefore, resulted from differences in the range of pressures at which their tests were conducted.

#### 3.4.4 Yield surface and the onset of undrained softening in monotonic and cyclic tests: Effect of stress path

Studies reviewed in Chapter 2 (Figure 2-10) suggested that in undrained shearing of loose sand, the stress ratio at the onset of softening is higher in cyclic tests compared to monotonic tests. These studies also indicated that the locus of stress ratios at the onset of softening coincided approximately with the position of the PPP of the UESP obtained from monotonic tests. Sasitharan et al.'s (1994) monotonic CDS tests discussed previously also showed that undrained softening starts at a stress ratio close to the position of the PPP of the UESP. Although such observations have frequently been reported in the literature, the reason for the PPP of the UESP of monotonic tests in locating stress states at the onset of softening has not been clarified. Yielding of loose sand and its relationship to the UESP discussed previously may provide an explanation.

In cyclic loading tests or monotonic CDS tests, the initial consolidation of the sample produces a yield surface encompassing a region in the  $p$ - $q$  plane inside which only small strains (shear or volumetric) can develop. Upon the application of the cyclic or the CDS loading, the stress path enters this region and moves towards the FP of the current yield surface (see Figure 3-13-c). As the FP of the yield surface is encountered, undrained softening in cyclic tests or instability in CDS tests on saturated sand initiates, if the condition remains undrained. Because of the proximity of the

yield surface and the UESP of loose sand, the stress ratio at the onset of undrained softening can be approximated by the PPP of the UESP, as is widely observed.

If soil is loaded monotonically without unloading, on the other hand, undrained softening can occur once the stress ratio corresponding to the peak strength ( $M_p$ ) is first achieved. In cyclic and CDS tests discussed above,  $M_p$  is achieved while the soil is still inside the elastic (small strain) region. In this cases undrained softening will not occur until the elastic region is crossed and the FP of the yield surface, which corresponds to a stress ratio higher than  $M_p$ , is encountered (Figure 3-13-c).

### 3.4.5 Yield surface and the collapse of anisotropically consolidated sands: Effect of stress ratio at consolidation

Based on their experimental observations, Sladen et al. (1985) noted that the stress ratio at the onset of undrained softening, instability or collapse may be larger in AC sands compared to IC sands. Di Prisco and Nova (1995) presented test results that lead to a similar conclusion. This difference can result from the effect of anisotropic consolidation on the yielding of sands. Figure 3-13-d shows that the slope of the FP of the yield surface is higher in AC sand compared to IC sand. Similar differences are frequently observed in the PPP of the UESP of AC and IC samples (see e. g. Di Prisco and Nova, 1995)

### 3.4.6 Yield surface and the size of the region of collapsible states: Effect of density

Results of CDS tests on dry sand showed that yielding of IC loose sand starts at stress ratios that can be significantly smaller than the stress ratio at ultimate state ( $M_{us}$ ). In loose sand the stress ratio at ultimate state is close to the stress ratio at phase transformation (PT) (Ishihara, 1975), at which sand behavior changes from contractive

(undrained softening) to dilative (undrained hardening) (see Chapter 5). The position of the FP of the yield surface, at which yielding in CDS tests starts, is controlled by  $M_p$ . As void ratio decreases,  $M_p$  increases, indicating that a higher stress ratio is required to initiate instability. In sand that is not sufficiently loose, the stress ratio  $M_p$  is close to the stress ratio at PT ( $M_{PT}$ ), and no undrained softening will therefore take place. The region between the FP of the yield surface (controlled by the stress ratio  $M_p$ ) and the stress ratio  $M_{PT}$  is the locus of states at which instability or collapse can occur. The size of this region increases with the increase in void ratio, indicating an increase in the susceptibility of the soil to instability. In sand that is not sufficiently loose (also in remoulded clay), stress ratios  $M_p$  and  $M_{PT}$  (or  $M_c$  in clay) are very close to each other or may coincide, eliminating any possibility of pre-failure collapse or instability (Figure 3-13-e).

Elliptical yield surfaces with the steady state (ultimate state) line passing through the top of the ellipse, as in the modified Cam Clay model (Roscoe and Burland, 1968), will not produce a region of potential collapse since in this case, stress ratios  $M_p$  and  $M_{PT}$  (which is equal to  $M_{us}$  here) coincide. This difference in the shape of yield surfaces of sand and clayey soils is consistent with results of the CDS tests on very loose dry sand reported earlier, and the observations of Anderson et al. (1995). In CDS tests on dry sand yielding started prior to  $M_{PT}$  (Figure 3-14). In clays subjected to a CDS stress path, however, yielding did not start until a stress ratio very close to that of the steady state was achieved (see Anderson et al., 1995).

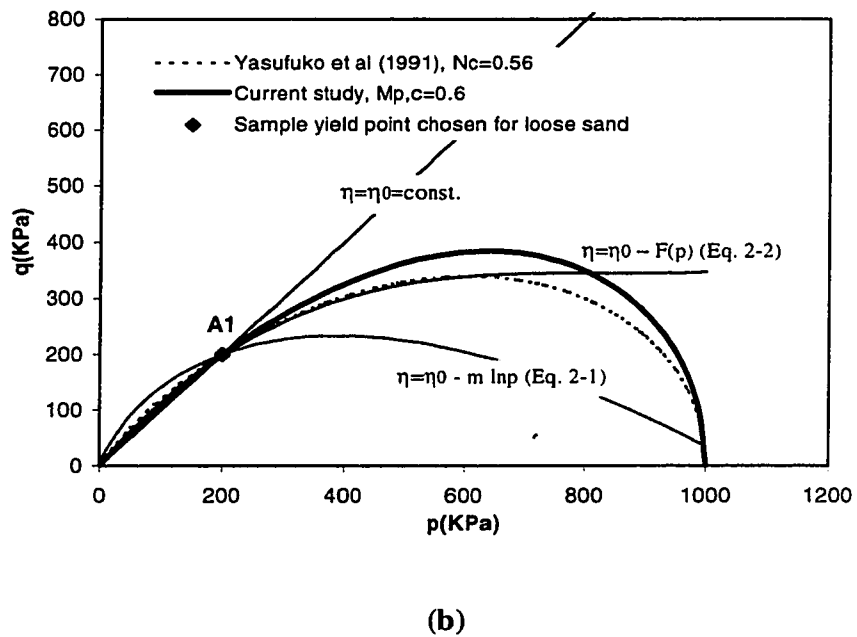
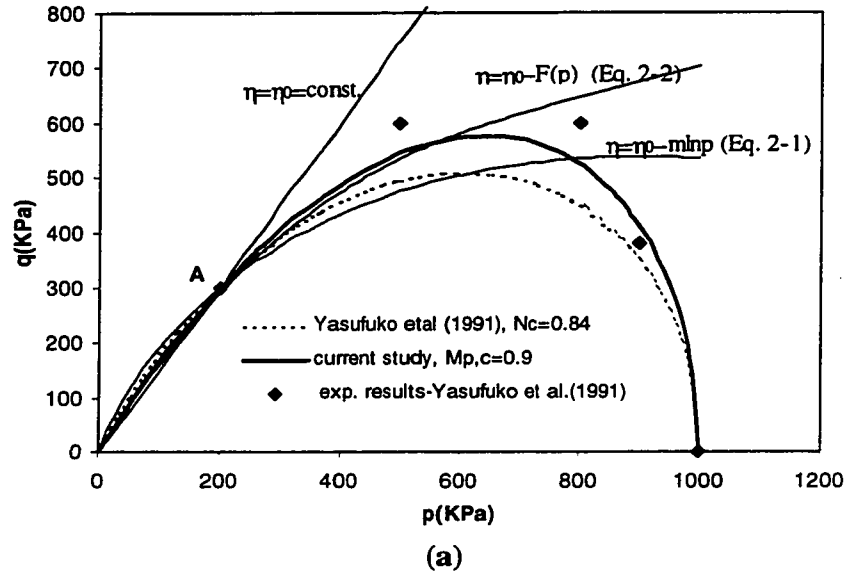


**Figure 3-1** Comparison of yield surfaces obtained experimentally with the yield function used in the current study: (a) Dense sand (exp. results obtained from tests on Aio sand) (b) Loose sand

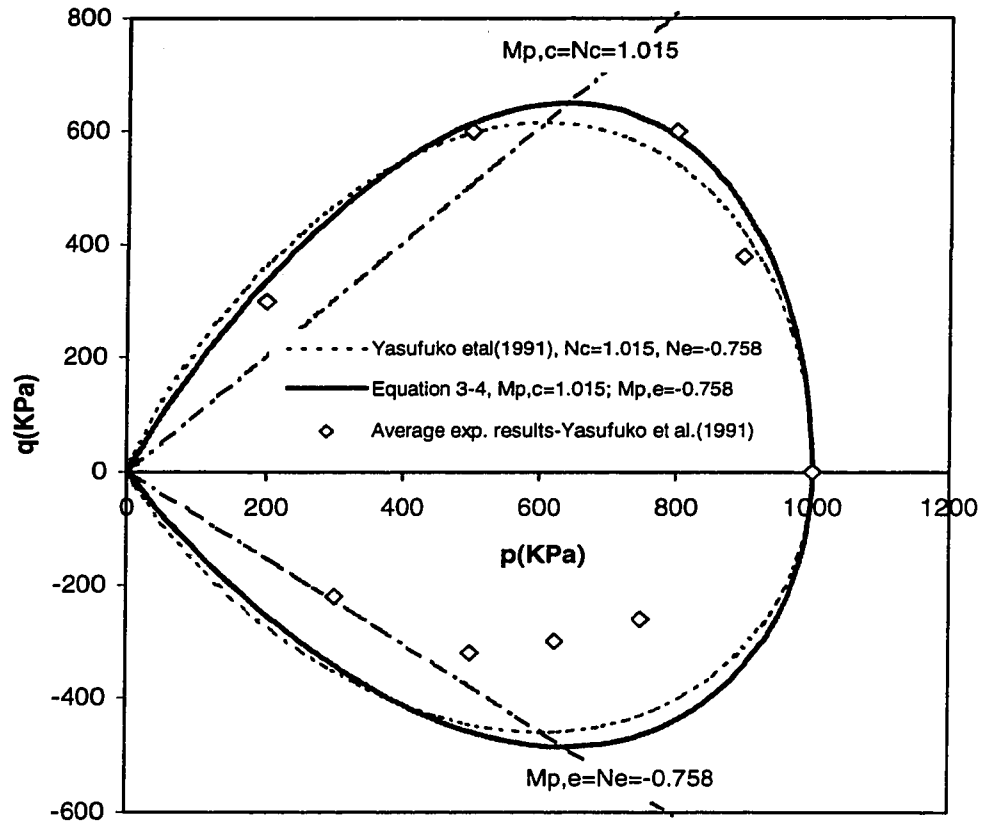


**Figure 3-2** Yield surfaces with equal friction angle at peak in compression and extension compared with experimental yield points

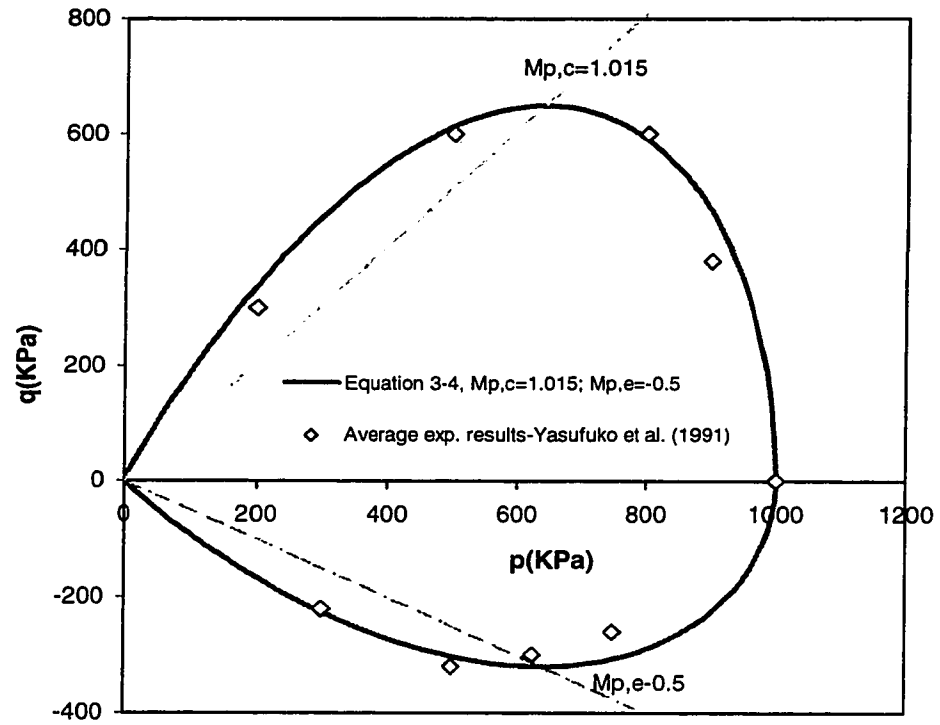


**Figure 3-3** Yield surface with reduced friction angle at peak in extension, compared with experimental yield stresses



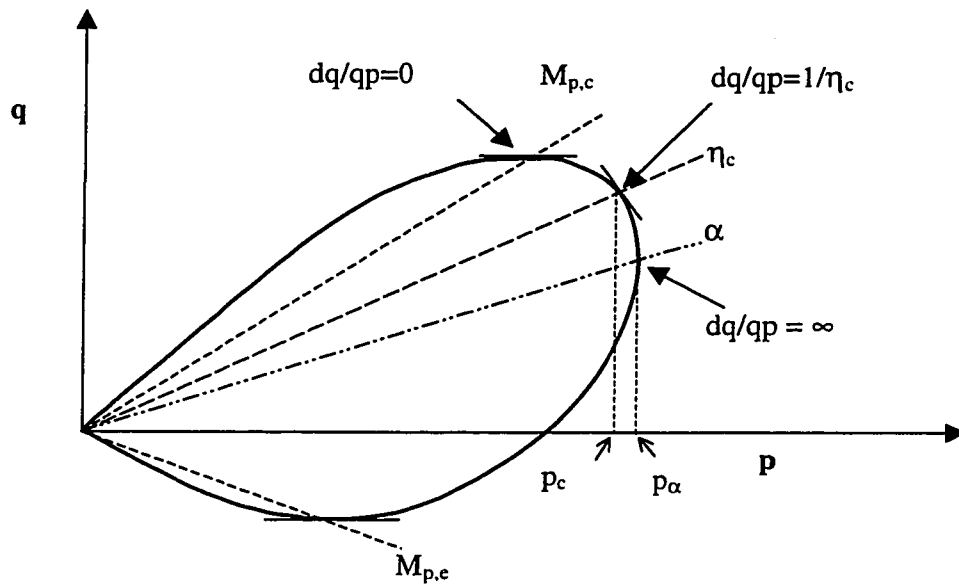


**Figure 3-4** Definition of parameters used in the yield surface of anisotropically consolidated sand

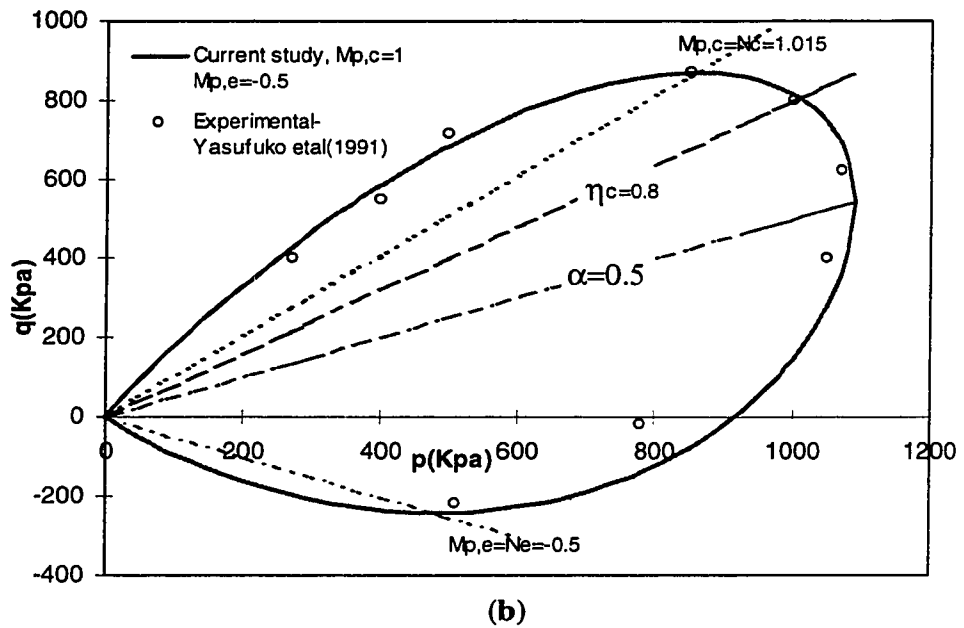
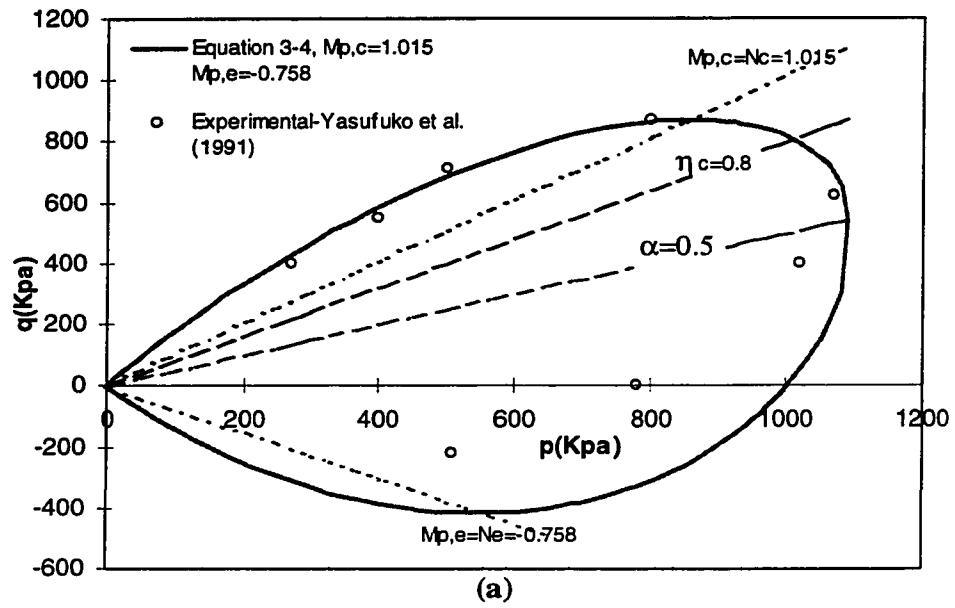


**Figure 3-5** Yield surfaces for anisotropically consolidated sand compared with average experimental results (a) with equal friction angle at peak in compression and extension (b) with reduced friction angle at peak on the extension side

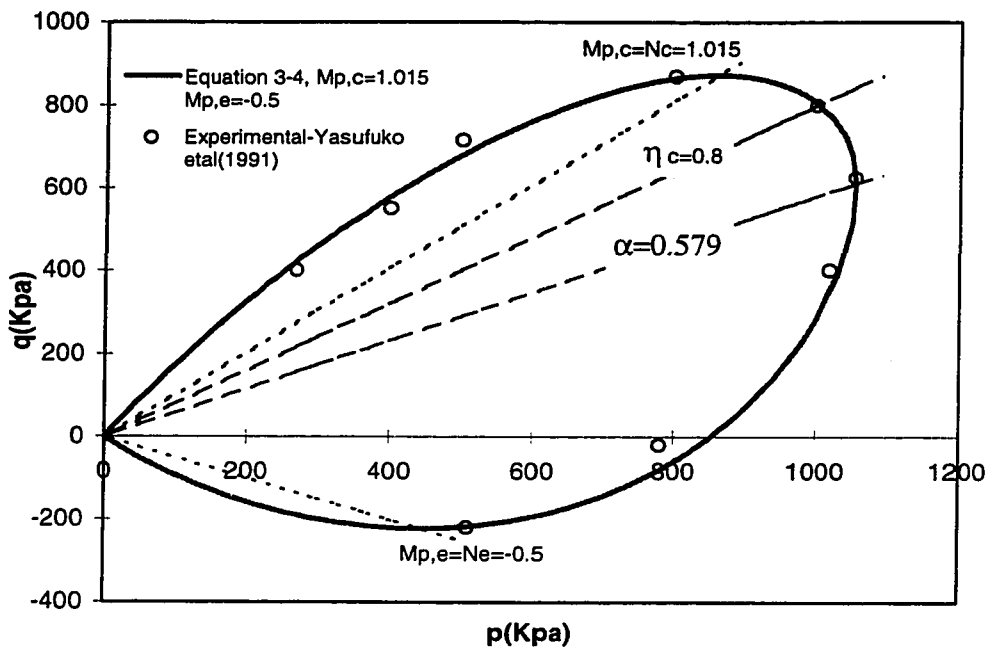


**Figure 3-6** Comparison of experimental yield points with the yield surface in which calculated values of  $\alpha$  and  $p_\alpha$  are used (reduced friction angle at peak was used on the extension side)

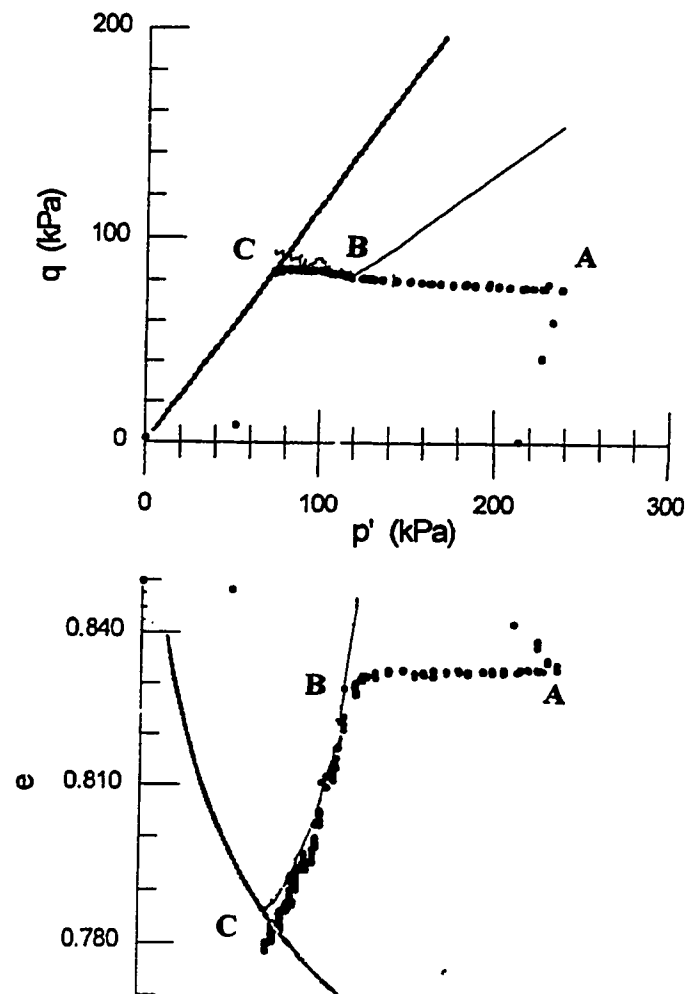


**Figure 3-7** Results of a CDS test on very loose dry Ottawa sand: Very small volume change between points A and B, and significant contraction between points B and C. (modified after Skopek, 1994)

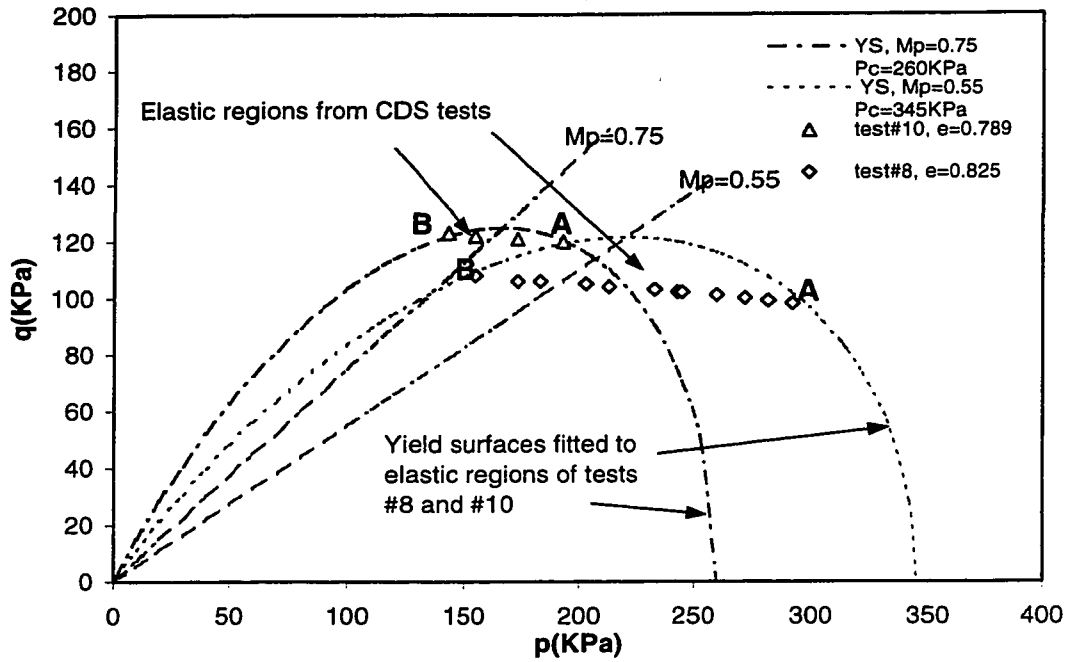


**Figure 3-8** Determination of yield parameters  $M_p$  and  $p_c$  from tests on Ottawa sand at different void ratios and consolidation pressures (Test data from Skopek, 1994)

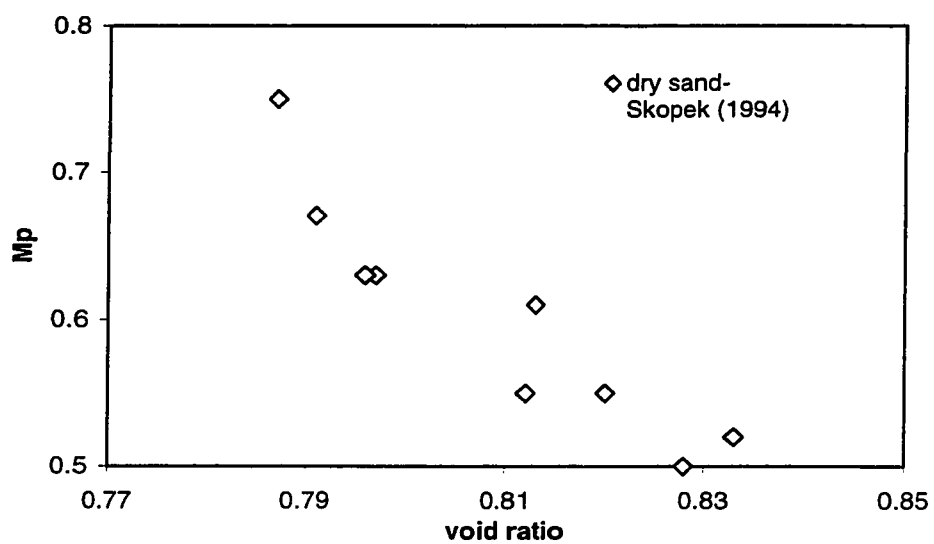


**Figure 3-9** Variation of parameter  $M_p$  with void ratio, obtained from CDS tests on dry Ottawa sand

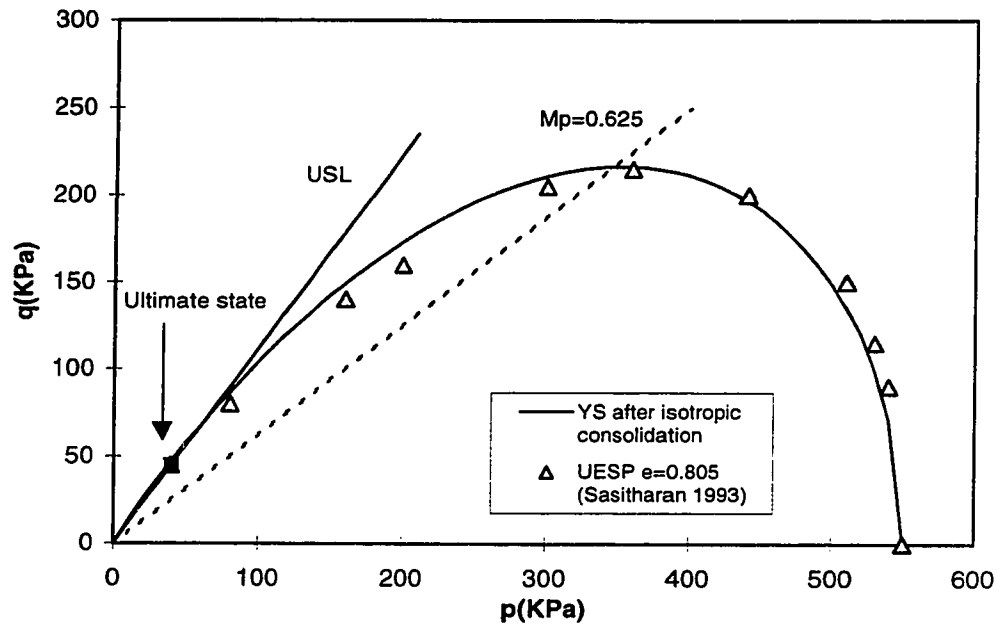


**Figure 3-10** Comparison of the undrained effective stress path (UESP) with the shape of the yield surface for a sample of Ottawa sand with a void ratio of 0.805 consolidated to 550 kPa.

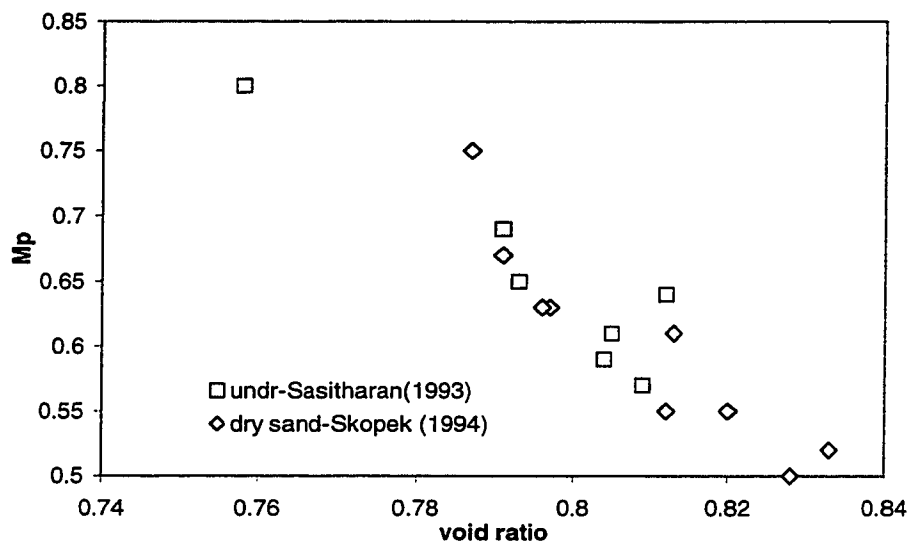


**Figure 3-11** Variation of  $M_p$  with void ratio obtained from CDS tests on dry sand and undrained tests on saturated sand



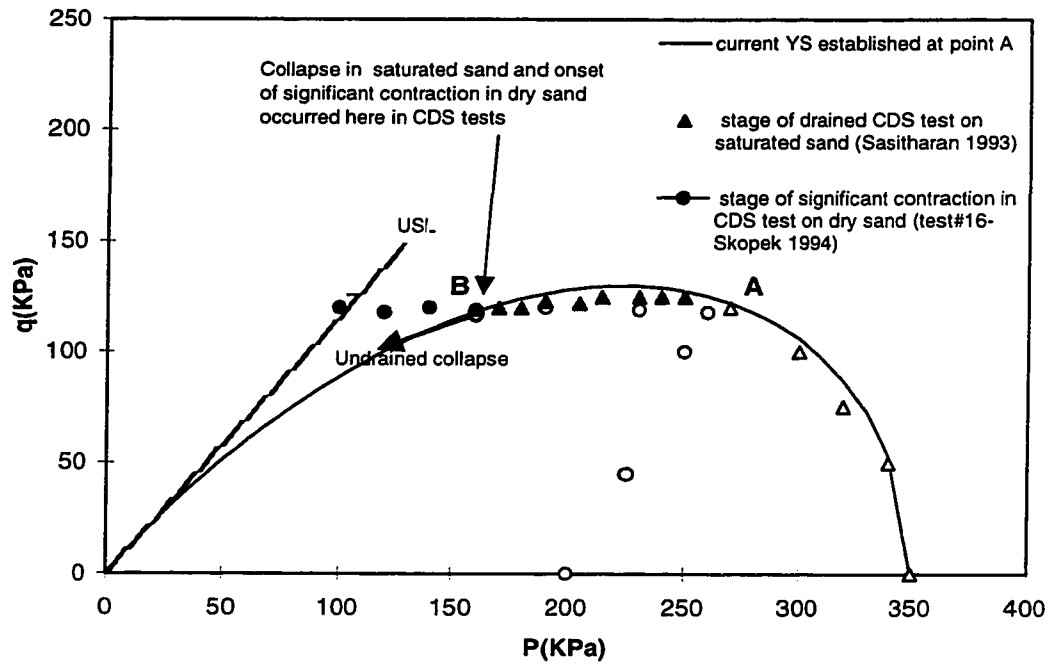


**Figure 3-12** Stress state at collapse of very loose dry and saturated Ottawa sand in CDS tests, compared to the position of the yield surface.

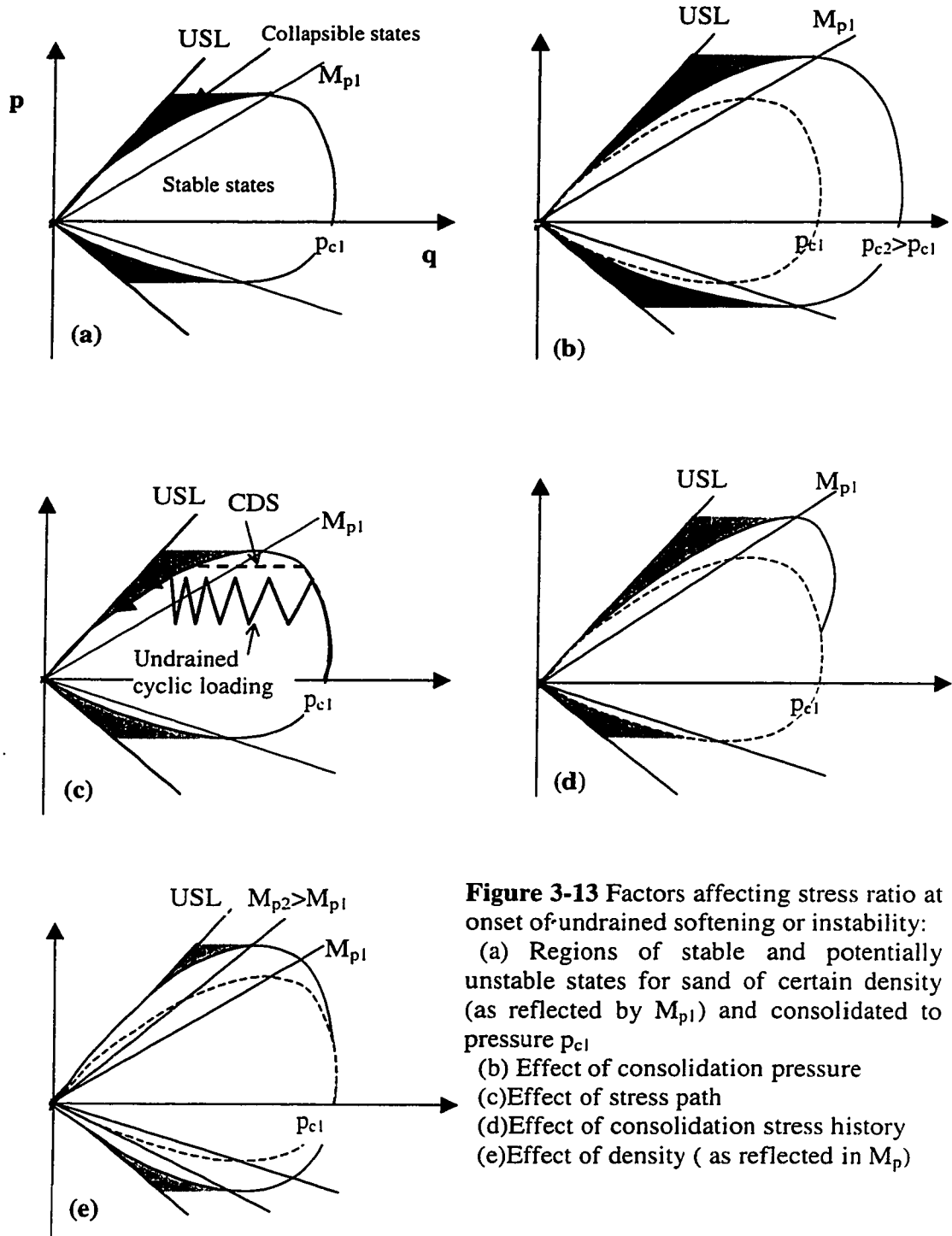


**Figure 3-13** Factors affecting stress ratio at onset of undrained softening or instability:

(a) Regions of stable and potentially unstable states for sand of certain density (as reflected by  $M_{p1}$ ) and consolidated to pressure  $p_{c1}$

(b) Effect of consolidation pressure

(c) Effect of stress path

(d) Effect of consolidation stress history

(e) Effect of density (as reflected in  $M_p$ )

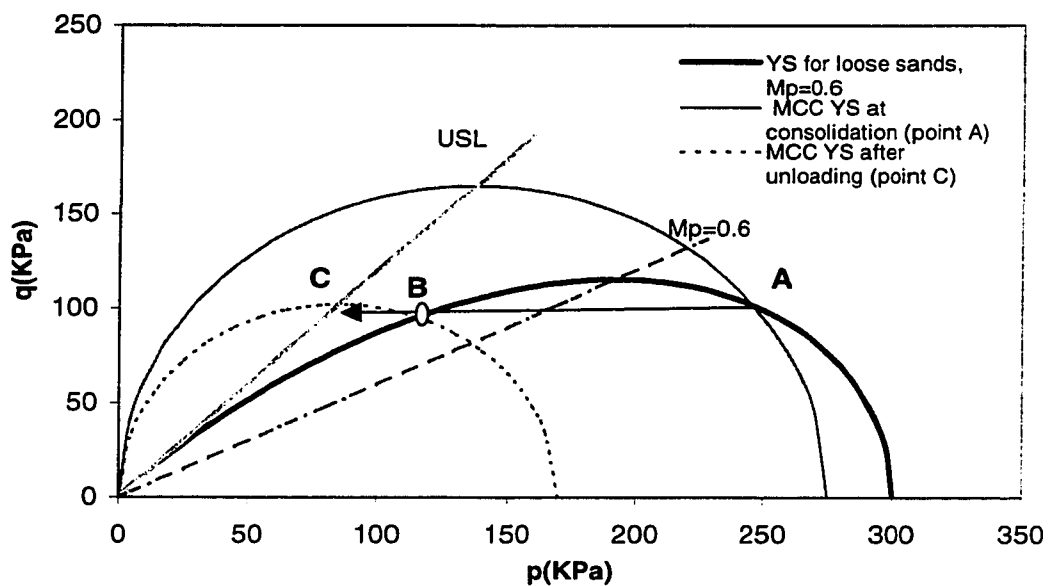


**Figure 3-14** Differences in stress states at the onset of yielding of loose sands and clayey soils in CDS tests, and accounting for these differences through the use of appropriate shapes for their yield surfaces.

## Chapter 4

# **4 Factors affecting yielding of loose sand derived from the variation of $M_p$**

## **4.1 Introduction**

By comparing the undrained effective stress path (UESP) of very loose Ottawa sand with the yield surface of the same sand, it was shown in Chapter 3 that in sufficiently contractive sand, the shape of the yield surface can be approximated by the shape of the UESP. In undrained tests on sands that are sufficiently contractive to exhibit a peak in their UESPs, the peak point of the yield surface can be approximated by the peak point of the UESP. The proximity of the peaks was also shown previously using results of tests on very loose Ottawa sand.

In this chapter, an extensive data base consisting of published results of undrained shearing of a variety of sands, consolidated to different states and subjected to a range of loading conditions, was used to determine stress ratios at peak ( $M_p$ ). This stress ratio is defined as  $M_p = q_p/p_p$  in which  $q_p = (\sigma_1 - \sigma_3)_p$  is the deviatoric stress, and  $p_p = (\sigma_1 + \sigma_2 + \sigma_3)/3$  is the mean normal stress that are measured at the peak point of the UESP. The investigation was carried out for the following purposes:

1-In constitutive modeling of sand, the flow rule or the shape of the plastic potential is examined at any soil state and loading condition by measuring increments of strain.

Investigation of yielding of sand, on the other hand, is not as convenient. The following difficulties often arise in investigating yielding behavior:

- a. Establishment of yield surfaces often requires unconventional tests with complex stress paths (see e. g. Poorooshasb, 1971; Yasufuko et al., 1991; Pradel et al., 1990).
- b. In many cases, the identification of yield points is not straightforward, and requires some approximations that influence the validity and accuracy of the outcome.
- c. Loading soils, often causes changes in their properties, making it difficult to reach different yield points belonging to the same yield locus, while the soil has a constant value of a certain soil property (void ratio, fabric, etc.)

Because of these difficulties, in constitutive modeling of sands, some generic shapes are often used for yield surfaces, accompanied by, sometimes complex formulations of model parameters to account for the effects of various factors on the constitutive behavior. In many instances, effects of such factors are not clearly related to measurable soil properties. The study of the variation of  $M_p$  helps determine the effect of various factors on the yielding behavior.

2-The variation of  $M_p$  has been the subject of some studies in the past in the context of flow failures. However, these studies have often been done qualitatively, and the effects of some factors on the variation of the stress ratio at peak are either not investigated, or not quantified. Formulation of the variation of  $M_p$  with various factors can also be important in the context of evaluating and analyzing liquefaction flow failures.

3-It will be seen later that the variation of  $M_p$  is also closely related to the variation of soil strength at failure. While the study of sand strength is sometimes obscured by the limitations of the available testing equipment and the non-uniformities developed in the sample in certain tests (e. g. in triaxial extension and hollow cylinder tests), the stress ratio  $M_p$  occurs at small strain where non-uniformities are still absent. The study of its variation, therefore, helps understanding the variation of soil strength, as well as the yielding behavior, especially in cases in which measurements of soil strength are difficult or dubious.

In what follows, values of  $M_p$  measured from UESPs of a variety of sands at different states subjected to different loading conditions are plotted, and their variations are investigated. Physical properties of the sands investigated are given in Table 4-1, Figure 4-1, and Figure 4-2. Variations of  $M_p$  with a number of factors are studied and possible physical phenomena responsible for these variations are examined to interpret the variations. These variations are then formulated using suitable state indices and presented in the form of yield surfaces for sand. Results of these formulations are compared with those reported in other studies, in cases where such studies exist. In the next two chapters, these formulations are incorporated in a constitutive model for sand, and it is shown that use of these yield surfaces leads to realistic predictions of the effects of different factors on sand behavior. Implications of these findings on the stability analysis of sand subjected to flow liquefaction are also discussed in this chapter.

## 4.2 Effect of density

### 4.2.1 Experimental observations

It was shown in Chapter 3 that the stress ratio  $M_p$  obtained from drained or undrained tests on Ottawa sand decreased with the increase in void ratio. Figure 4-3 shows this variation along with data from undrained tests on Toyoura sand (Verdugo, 1992) and Syncrude sand (Wride and Robertson, 1997). Syncrude sand is a tailings sand that results from the extraction of bitumen from oil sand. The tests used here are those in which the sand exhibited a clear peak in its UESP in  $p$ - $q$  plane. Results shown in Figure 4-3-c belong to tests that were conducted at Laval University and the University of Alberta (U of A), with sample dimensions (height to width  $H/D$ ) of 1:1 and 2:1 respectively. These samples were prepared by moist tamping (MT) at both universities. Consolidation pressures for Ottawa, Toyoura and Syncrude sands ranged between 290 and 550 kPa, 100 and 500 kPa, and 200 and 600 kPa respectively. It can be seen that for these ranges of pressures, the relationship between  $M_p$  and void ratio for all these sands is approximately linear. For Syncrude sand, results obtained by the two universities

using different  $H/D$  ratios and different end restraints (lubricated end platen were used at Laval University, and conventional platen at the U of A) are quite consistent. It will be shown later (Figure 4-34-c) that another series of test results obtained independently at the University of British Columbia (UBC) are also consistent with those discussed here. This remarkable agreement may have resulted from the fact that  $M_p$  occurs at small strain. At such strain level, non-uniformities are unlikely to develop, and end restraints do not seem to affect the results substantially.

In order to compare results from different sands in a unified framework, data from the above three sands were plotted in Figure 4-4, along with those from two other sands, namely, Fraser River sand and Erksak sand. In this figure, variations of  $M_p$  were plotted against the state parameter (Been and Jefferies, 1985) at peak rather than the void ratio. The state parameter is defined as the difference between the current void ratio and the ultimate (steady) state void ratio of the soil, corresponding to the current pressure. In the case of Syncrude sand, two different studies, namely Sladen and Handford (1987) and Wride and Robertson (1997), reported different USLs (Figure 4-1). Figure 4-2-b shows that the grain size distributions of samples used in the two studies were in fact, somewhat different. Results of each study were therefore, normalized by the USL obtained in the same study, before plotting them in Figure 4-4. If the USL obtained in one of the studies is used to normalize both data series, two distinct and different variations will be obtained. Figure 4-5 shows such an exercise with the USL obtained by Sladen and Handford (1987) used for the normalization.

From Figure 4-4, the following observations can be made:

1. The stress ratio  $M_p$  and accordingly, the mobilized friction angle at peak decreases with the increase in the state parameter.
2. For the sands investigated, variations of  $M_p$  with state parameter followed similar trends. Although some scatter was observed in the variations, they were normalized nearly within the same trend.

3. The slopes of variation of  $M_p$  with the state parameter at peak  $k_\psi = -\frac{dM_p}{d\psi_p}$  are close to each other for the sands for which sufficient data were available.

It is interesting to note that Jefferies (1993) in his gathering of an extensive data base consisting of about 28 different sands, obtained a nearly linear relationship between the maximum soil dilatancy  $\frac{dv}{de}$  (or maximum soil strength at failure), and the state parameter at maximum dilatancy. Variation of the stress ratio at the peak of the UESP, or peak of the yield surface (i. e.  $M_p$ ) with state parameter at peak is, therefore, similar to that of maximum strength at failure. This similarity can be the result of the similarity of the physical phenomena leading to this variation. Appendix 4A explains evidence suggesting that the stress ratio  $M_p$  divides stress combinations leading to small strain yielding, from those causing large strain yielding. Small strain yielding may result from small inter-particle slippage, before the mobilization of the shear stresses needed for gross slippage. Large strain yielding, on the other hand, may result from gross slippage at particle contact that occurs when high shear stresses are mobilized at the contact point.

#### 4.2.2 Formulation of the variation of $M_p$ with void ratio

It was shown in the previous sections that the variation of  $M_p$  with the state parameter or void ratio for the sands investigated could be approximated by a straight line. It is shown in Appendix 4A that this trend of variation is consistent with the effect of dilatancy on soil strength. Figure 4-4 shows that for the sands investigated, at  $\psi = 0$ , the mobilized friction angle at peak is close to the inter-particle friction angle of quartz-based sands (see Appendix 4A). Note that the condition of  $\psi = 0$  at peak is different from the condition of constant volume shearing, the difference is explained in Section 4.2.3. Note that the maximum values of  $M_p$  measured from tests in which sand just



started to exhibit a peak in its UESP, were not the same in different sands. In rounded quartzic-based sands such as Ottawa, Erksak and Toyoura sands, this maximum was close to the inter-particle friction angle of Quartz and occurred close to  $\psi = 0$ . In Syncrude Sand that is angular and in Fraser River Sand that has a higher constant volume friction (see Table 4-1), this maximum value of  $M_p$  was larger and occurred at  $\psi < 0$ .

If the value of  $M_p$  at  $\psi = 0$  is denoted by  $M_\mu$ , the variation of  $M_p$  with  $\psi$  can be written in the following form:

$$M_p = M_\mu - k_\psi \psi \quad 4-1$$

in which  $k_\psi$  is a material constant representing the slope of variation.

In the absence of a well-defined ultimate state line, or where it is more convenient, the variation of  $M_p$  can be determined in terms of void ratio in the following form:

$$M_p = M_\mu - k_e (e - e_\mu) \quad 4-2$$

in which  $e_\mu$  is the void ratio corresponding to the stress ratio  $M_\mu$ ,  $e$  is the current void ratio and  $k_e$  is the slope of the  $M_p$ - $e$  plot.

It should be noted that the stress ratio  $M_\mu$  in the above equations is used as a reference value to define the position of the line determining the variation of  $M_p$ , and it is not necessary that it corresponds to the actual inter-particle friction angle of the sand. However, the notation  $M_\mu$  was used here to refer to the proximity of this value to the inter-particle friction angle as observed from the current results. When using Equation 4-2 in modeling sand behavior in the next chapters, we will use a value for  $M_\mu$  that corresponds to a friction angle that is a few degrees (e. g. seven degrees) smaller than the constant volume friction angle of the soil. The constant volume friction angle can be

measured conveniently for any soil and is often determined in routine sand characterizations. Such value of  $M_p$  often corresponds to the maximum stress ratio that can be measured from the UESPs. Once  $M_\mu$  is selected, its corresponding void ratio  $e_\mu$  can be determined from the variation of  $M_p$  with void ratio obtained from experimental results. The value of  $M_\mu$  in Equation 4-1, however, cannot be selected arbitrarily since it is the stress ratio that corresponds to  $\psi = 0$ , and should be determined from test results.

It is to be noted that Equations 4-1 and 4-2 were obtained based on results of TC tests on sands consolidated to pressures that are normally encountered in most practical problems (e. g. pressures in the order of 100 to 600 kPa). In cases where higher pressures are involved, or where other loading directions, consolidation stress histories, or stress states are involved, the above equation may need to be modified. Investigation of the effects of these factors on the variation of  $M_p$  and formulation of these variations are presented in the following sections.

#### 4.2.3 The relation of $M_p$ with soil strength and dilatancy

Effects of void ratio, angle of inter-particle friction  $\phi_\mu$ , and soil dilatancy on the variation of  $M_p$  were investigated in the previous sections. These variations are examined in Appendix 4A in the context of the micro-mechanical behavior of sand. The strength of sand at failure ( $M_f$ ), on the other hand, is also influenced by these effects, and the variations of  $M_p$  and  $M_f$  with the factors mentioned above follow a similar trend.

Been and Jefferies (1985) showed that peak strength  $M_f$  or maximum dilatancy of sands decreased with the increase in state parameter. Jefferies (1993) approximated the variation of maximum dilatancy with  $\psi$  by a linear relationship, and Wood et al. (1994) formulated the variation of  $M_f$  with  $\psi$  in the following form:

$$M_f = M_{cv} - k\psi \quad 4-3$$

in which  $M_f$  is the maximum attainable stress ratio for a sand with the current state parameter  $\psi$ ,  $M_{cv}$  is the constant volume (critical or ultimate state) stress ratio, and  $k$  is a material parameter.

The above equation has the same form as Equation 4-1 obtained for  $M_p$ . However, at  $\psi = 0$ , where no tendency for volume change is expected, Equation 4-1 yields a mobilized stress ratio  $M_p = M_\mu$ , while Equation 4-3 corresponds to a mobilized stress ratio  $M_f = M_{cv}$ . This difference, which is based on experimental observations, may be a result of the difference between the conditions at peak and at constant volume shearing. Soil failure and its corresponding stress ratio  $M_f$  occur while the soil is undergoing shear deformation and is therefore, in motion. If soil deforms at a state of no tendency for volume change, the mobilized stress ratio correspond to that of the constant volume  $M = M_{cv}$ . The stress ratio at peak, on the other hand, occurs when soil is on the verge of gross inter-particle slippage, but is not experiencing any movement yet. Under such conditions, if the soil has no tendency for volume change, the mobilized stress ratio will correspond to  $M_\mu$ , since unlike the case of constant volume deformation, no gross inter-particle movement is actually taking place at this state.

Equations 4-1 and 4-3 are in fact similar to the following form of the stress-dilatancy relationship suggested by Nova (1979) :

$$\eta = M_{cv} - \mu d \quad 4-4$$

in which  $\eta$  is the current stress ratio,  $\mu$  is a positive material constants and  $d = \frac{dv}{d\varepsilon}$  is the dilatancy of the soil. This relationship suggests that soil strength as represented by  $\eta$  increases linearly with dilatancy.

## 4.3 Effect of mean normal stress

### 4.3.1 Effect of mean normal stress on the stress ratio $M_p$

Equations 4-1 and 4-2 were derived from test data on samples sands consolidated to pressures up to 600 kPa. Confining pressures encountered in practical use often vary within this range. However, it is necessary in some cases to examine the behavior of sand at higher pressures. Some of these cases are as follows:

1. A number of in-situ tests induce high pressures in the ground in the region that is being tested. However, soil properties obtained from such tests are often used for the normal range of pressures that is usually encountered in practice. It is useful, therefore, to have a unique framework in which soil behavior can be examined over a wider range of pressures.
2. In order to study the behavior of soils around penetrometers, properties of soils at high pressures are needed.
3. A number of practical applications require knowledge of soil behavior at higher pressures. Examples are high dams, deep tunnels, nuclear reactors etc.
4. In studying the steady (ultimate) state of sands, it is frequently necessary to apply high pressures to soil samples in order to make them reach their ultimate state. Only very loose sands reach their ultimate state in the normal range of consolidation pressures.

At higher pressures, the linear relationship between  $M_p$  and  $\psi$ , or  $M_p$  and void ratio, derived previously from experiments, is no longer applicable. Figure 4-6 shows results obtained from tests on Toyoura sand consolidated to pressures from 100 and 3000 kPa. Compared to the normal range of pressures, values of  $M_p$  measured from high-pressure tests are smaller. This is consistent with a reduction in soil dilatancy and hence soil strength at peak, due to increase in pressure. Similar effect of pressure on the strength of soils at failure has been reported in the literature frequently.

Figure 4-6-a shows that looser samples consolidated to lower pressures have the same value of  $M_p$  as denser samples consolidated to high pressures. For a certain value of  $M_p$ , therefore, increase in pressure causes reduction in the corresponding void ratio, which can result from the compression caused by the application of pressure. It is possible, therefore, to normalize values of void ratio to a common reference pressure  $p_r$  such that reductions in void ratio due to increases in pressure can be accounted for. The reference pressure  $p_r$  may be chosen to be very small, such that normalization leads to comparison of void ratios of samples at their initial value  $e_i$  at preparation. In this case, all samples prepared at the same initial void ratio and lying on the same normal consolidation line (NCL) will have the same normalized void ratio  $e_n$  regardless of the confining pressure that is applied to them subsequently. Such void ratio is in fact a "reference void ratio" corresponding to the "reference pressure" selected.

A difficulty in the determination of  $e_n$ , however, is that the consolidation behavior of sands is complex. Unlike clay, the slope of the NCL of sand in the  $e$ - $\ln p$  plane is not unique, but is a function of density and pressure. The simplified version of a comprehensive compression model for sand, suggested by Pestana and Whittle (1995) is used here to define the NCL of sands. This simplified model uses only one material parameter to determine soil compressibility at different densities and pressures. A more detailed description of this compression model is given in Chapter 5. The simplified model can be written in the following form:

$$\ln(e/e_i) = -e_i^{2.5} \beta (p/p_a) \quad 4-5$$

in which  $e_i$  and  $e$  are the initial and current void ratios respectively,  $p$  is the current pressure,  $p_a$  is the atmospheric pressure and  $\beta$  is a material parameter that can be obtained by fitting test data on sand compressibility, starting from different initial void ratios. When a very small reference pressure is selected (e. g.  $p_r = 1$  kPa), the normalized void ratio  $e_n$  will be equal to  $e_i$ , and can be calculated directly from Equation 4-5 for any given pressure  $p$  and void ratio  $e$ .

Figure 4-6-b shows the same data shown in Figure 4-6-a, but with void ratio on the abscissa substituted by  $e_n$  defined above. It can be seen that compared to using  $e$ , the correlation of  $M_p$  with  $e_n$  reduces the scatter in the data significantly, and the data measured from the high pressure tests, fall very close to, or on those obtained from the low pressure tests.

When  $\psi$  was used as an abscissa, on the other hand, values of  $M_p$  measured from high pressures tests plotted above those of low pressure (Figure 4-7-a). This results from the fact that at higher pressures, the slope of the ultimate state line (USL) in the  $e - \ln p$  plane increases significantly, resulting in unusually higher values of  $\psi$  at higher pressures as can be seen in (Figure 4-7-a). The increase in the slope of the USL is often attributed to the crushing of soil particles that causes an increase in soil compressibility. To correlate values of  $M_p$  with  $\psi$  for various levels of pressure, it is necessary, therefore, to account for changes in soil compressibility at different pressures. It was noticed that by subtracting the amount of void ratio change caused by compressibility from the value of  $\psi$  at any pressure, the correlation was improved significantly. This change in void ratio is in fact the difference between the current void ratio and the normalized void ratio discussed previously. In this case, a common reference pressure  $p_r$  should be selected as for  $e_n$ .

It is possible, therefore, to define the states of soil samples consolidated to different pressures in terms of this "normalized state parameter"  $\psi_n$  that is defined as follows:

$$\psi_n = \psi - (e_n - e) \quad 4-6$$

where  $e_n$  is the normalized void ratio corresponding to the current pressure, and  $e$  and  $\psi$  are the current void ratio and state parameter.

Figure 4-7-b shows the same data plotted in Figure 4-7-a but with  $\psi$  substituted by  $\psi_n$  defined above. It can be seen that compared to the correlation with  $\psi$ , the relationship of

$M_p$  with  $\psi_n$  shows significantly smaller scatter, and data measured from high pressure tests plot closer to those from low pressure tests.

### 4.3.2 Formulating the effect of pressure using $e_n$ and $\psi_n$

To generalize Equations 4-1 and 4-2 for a wider range of pressures, these equations will be written in the following forms in terms of the normalized values of the state parameter  $\psi_n$  and void ratio  $e_n$ :

$$M_p = M_\mu - k_{\psi,n} \psi_n \quad 4-7-a$$

$$M_p = M_\mu - k_{e,n} (e_n - e_\mu) \quad 4-7-b$$

where  $k_{\psi,n}$  and  $k_{e,n}$  are values obtained from plots of  $M_p$  vs.  $\psi_n$  and  $e_n$  respectively.

## 4.4 Compression vs. extension

### 4.4.1 Experimental observations

In Figure 4-8-a, the data plotted in Figure 4-8-b are shown along with similar data, but obtained from dry deposited (DD) samples sheared in Triaxial Extension (TE), and reported by Yoshimine (1996). It can be seen that values of  $M_p$  measured from TE generally plot below those of TC, and the slope of variations is somewhat smaller in TE. Plotting the same data in terms of  $\tan\phi_p$  (Figure 4-8-b), which is the coefficient of friction at peak resulted in closer slopes of variation for the TC and TE data. It is noted, however, that TC and TE samples were prepared by different methods, and this may cause some difference in  $\tan\phi_p$ , as will be seen later. Figure 4-5-b also shows that for TC and TE, the maximum  $\phi_p$ , which was measured from tests in which the soil just

started to exhibit undrained softening, and also the minimum  $\phi_p$ , which was measured from tests exhibiting complete liquefaction of the soil, are close to each other.

Results of drained tests on dense "Aio sand" reported by Yasufuko et. al. (1991), and discussed in Chapter 3, showed similar decrease in  $\phi_p$  at TE. Unlike the current study where UESPs were used to approximate yield stresses, yield surfaces were constructed by direct determination of yield stresses in the Yasufuko et. al. (1991).

#### 4.4.2 Formulation of the variations for compression and extension

Figure 4-9 compares values of  $\tan\phi_p$  obtained from TC and TE for two other sands investigated previously. Enough data over the full range in which the soils exhibited softening in undrained shear, were not available, but the trend of the existing data is similar to that observed in Toyoura sand.

From the data presented so far, the variation of  $\tan\phi_p$  with  $\psi_n$  in compression and extension can be obtained from the following relationships:

$$\begin{array}{ll} \text{in TC} & \tan\phi_p = \tan\phi_\mu - k_{\psi,n} \psi_n & 4-8-a \\ \text{and in TE} & \tan\phi_p = \tan\phi_\mu - a_p - k_{\psi,n} \psi_n & 4-8-b \end{array}$$

If the normalized void ratio is used for the correlation, we will have:

$$\begin{array}{ll} \text{in TC} & \tan\phi_p = \tan\phi_\mu - k_{e,n} (e_n - e_\mu) & 4-9-a \\ \text{and in TE} & \tan\phi_p = \tan\phi_\mu - a_p - k_{e,n} (e_n - e_\mu) & 4-9-b \end{array}$$

in which  $\phi_\mu$  is the inter-particle friction angle at peak and  $a_p$  is the difference between  $\tan\phi_p$  in compression and extension. Experimental observations reported earlier suggested that slopes of variation of  $\tan\phi_p$  with  $\psi_n$  or  $e_n$  in TC and TE may be assumed to be the same. It is possible, however, to use different slopes in the above relationships.



if experimental results necessitated. In cases where pressures change in a limited range, it may not be necessary to use normalized values in Equations 4-8 and 4-9. Because of the difficulties associated with the determination of the steady state line, using  $e_n$  or  $e$  may be more convenient than using  $\psi$  or  $\psi_n$ . In the following correlations, therefore,  $e_n$  or  $e$  will be used, depending on the range of pressures involved.

## 4.5 Effect of intermediate principal stress

### 4.5.1 Experimental observations

In the previous section, it was noticed that the strength at peak of the UESP determined in terms of  $\tan\phi_p$ , was smaller when measured from TE tests, compared to TC. Two factors differentiate TC and TE tests from each other: First is the relative magnitude of the intermediate principal stress ( $\sigma_2$ ) compared to the major ( $\sigma_1$ ) and minor ( $\sigma_3$ ), often determined in terms of  $b$  defined below (Bishop, 1971):

$$b = \frac{\sigma_2 - \sigma_3}{\sigma_1 - \sigma_3} \quad 4-10$$

The second is the direction of application of  $\sigma_1$  relative to the direction of soil deposition, often determined in terms of the angle  $\alpha_\sigma$  between the two directions.

TC, therefore, corresponds to  $b = 0$  and  $\alpha_\sigma = 0$  degrees, and TE to  $b = 1$  and  $\alpha_\sigma = 90$ . In a general loading condition,  $b$  can vary between 0 and 1, and  $\alpha_\sigma$  between 0 and 90 degrees. Considering the possible range of variation of  $b$  and  $\alpha_\sigma$ , TC and TE, therefore, correspond to the two extreme modes of shearing. Since in a general loading condition,  $b$  and  $\alpha_\sigma$  may vary arbitrarily within the ranges given above, it is necessary to investigate their effects on  $M_p$  separately. The hollow cylinder (HC) apparatus provides

such possibility, since tests with constant  $b$  and constant  $\alpha_\sigma$  can be conducted in this apparatus.

UESPs from TC, TE and HC tests are often presented in terms of the "stress difference"  $q'$  vs.  $p$ . The stress difference  $q'$  will be defined for any stress condition as follows:

$$q' = \sigma_1 - \sigma_3 \quad 4-11$$

and the corresponding stress ratio  $M'$  is obtained from:

$$M' = q'/p \quad 4-12$$

In TC, TE and HC test, value of  $b$  and  $\alpha_\sigma$  are known or given. From results of such tests, principal stresses at peak can be obtained using the following relationships:

$$\sigma_1 = p + q'(2-b)/3 \quad 4-13-a$$

$$\sigma_2 = p - q' + 2q'(1+b)/3 \quad 4-13-b$$

$$\sigma_3 = p - q' + q'(2-b)/3 \quad 4-13-c$$

Note that the intermediate principal stress  $\sigma_2$  does not appear in the definition of the stress difference  $q'$ . The "deviatoric stress"  $q$ , is therefore defined in the principal stress space as:

$$q = \left[ \frac{1}{2} \left( (\sigma_1 - \sigma_2)^2 + (\sigma_1 - \sigma_3)^2 + (\sigma_2 - \sigma_3)^2 \right) \right]^{1/2} \quad 4-14$$

and the corresponding stress ratio  $M$  will be:

$$M = q/p \quad 4-15$$

Values of  $q$  and  $q'$  (and consequently, values of  $M$  and  $M'$ ), will be the same for TC and TE, where  $b = 0$  and  $1$  respectively, but will be different from each other for other values of  $b$ . For an arbitrary value of  $b$ ,  $q$  and  $q'$  are related by the following equation:

$$q = (1-b+b^2)^{1/2} q' \quad 4-16$$

Stress ratios at peak  $M'_p$ , determined in terms of stress difference  $q'$ , can therefore be converted to their generalized values  $M_p$  for any value of  $b$ , from the following equation:

$$M_p = (1-b+b^2)^{1/2} M'_p \quad 4-17$$

Figure 4-10- a shows the variation of  $M'_p$  for Syncrude sand measured from TC, TE and HC tests. HC tests were performed with a  $b = 0.5$  (that is intermediate between those of TC and TE), and values of  $\alpha_\sigma$  varied between 0 and 90 degrees. It can be seen that although the value of  $b$  is different from those of TC and TE, as  $\alpha_\sigma$  changes from 0 to 90 degrees  $M'_p$  moves from a value close to TC to that close to TE. This shows that the direction of loading as reflected by  $\alpha_\sigma$  has a major effect on  $M'_p$ , and accounts for a substantial part of the observed difference in  $M'_p$  between TC and TE. Figure 4-10 -b shows a similar plot for Toyoura sand but with  $b$  parameters having values equal to 0 and 0.5. Available HC data did not cover the full range of  $\alpha_\sigma$  for Toyoura sand, since tests with certain combinations of  $b$  and  $\alpha_\sigma$  produced unacceptable non-uniformities in the HC sample, and were therefore not performed. The existing data, however, show a trend similar to that observed in Syncrude sand.

In the above comparisons, the commonly used stress difference ( $q'$ ), and the corresponding stress ratio ( $M'$ ), were used. However, to formulate the variations of stress state at peak with  $b$  and  $\alpha_\sigma$ , it is necessary to use suitable stress variables in which all relevant stress components are taken into consideration. In this section, the effect of  $b$  is investigated and formulated, and in the next section, the effect of  $\alpha_\sigma$  will be accounted for.

#### 4.5.2 Selection of appropriate stress function to account for b

A suitable stress function  $f$  for taking into account the effect of  $b$  on the variation of stress state at peak, is expected to have the following two properties:

- a) It should properly account for the effect of  $b$  and normalize its effect. Therefore, the function should have the same numerical value regardless of  $b$ . Differences in its value due to differences in  $\alpha_\sigma$  should be dealt with separately.
- b) The variation of the numerical value of the function with  $e$  (or  $\psi$ ) should be uniform (e. g. should have the same slope) regardless of  $b$ . This will ensure straightforward formulation of the variation of the stress function with void ratio.

The following two functions have been used so far in formulating the variations of stress state at peak in TC and TE:

$$f = M'_p = \frac{q'}{p} = \frac{\sigma_1 - \sigma_3}{(\sigma_1 + \sigma_2 + \sigma_3)/3} \quad 4-18$$

$$f = \tan\phi_p \quad 4-19$$

It was noted previously that unlike  $M'_p$ , determining stress states at peak in terms of  $\tan\phi_p$ , satisfied the second condition approximately. The first condition is investigated below for cases with varying values of  $b$ .

In Figure 4-11-a, the same data shown in Figure 4-10-a are re-plotted in terms of  $\tan\phi_p$ . In comparing HC data ( $b=0.5$ ) with those of TC ( $b=0$ ) and TE ( $b=1$ ), it can be seen that values of  $\tan\phi_p$  are somewhat larger when  $b=0.5$ , than the average trend of samples subjected to the same  $\alpha_\sigma$ , but with values of  $b$  other than 0.5. This may be realized by comparing  $\tan\phi_p$  from HC for  $\alpha_\sigma=0$ , with that of TC; and for  $\alpha_\sigma=90$  with TE. In Fig 4-8-b, the same results shown in Figure 4-10 -b for Toyoura sand, are re-

plotted in terms of  $\tan\phi_p$ . Similar conclusions can be made regarding the HC data with  $b=0.5$ , compared to the TC and TE, where  $b$  is 0 and 1 respectively. Note, however, that the HC data point with  $b = 0$ , and  $\alpha_\sigma = 0$ , is close to the TC data points.

In Figure 4-11-b if the HC data points corresponding to the same  $\alpha_\sigma$ , but for  $b=0$  and  $b=0.5$  are connected by straight lines, slopes of these lines will be larger than the slope of variation of  $\tan\phi_p$  with  $e_n$  measured from TC and TE tests. This indicates that a stress state corresponding to  $b=0.5$  results in values of  $\tan\phi_p$  that are larger than those corresponding to  $b=0$  or  $b=1$ .

The Mohr-Coulomb failure criteria can be determined in terms of a constant mobilized friction angle  $\phi$ , in the following form:

$$\sin\phi = \frac{\sigma_1 - \sigma_3}{\sigma_1 + \sigma_3} = C_{M-C} \quad 4-20$$

This equation shows that determination of strength in terms of friction angle neglects the effect of the intermediate principal stress  $\sigma_2$ . When "failure strength" of sands is measured in terms of friction angle, larger values are frequently obtained when  $b$  is about 0.5 than when  $b$  is 0. Test results comparing friction angles at failure for  $b=1$  and  $b \neq 1$ , however, are contradictory (see e. g. Bishop, 1971; Lade, 1975; Matsouka, 1974). It seems, therefore, that the variation of "strength at peak"  $M_p$  with  $b$ , follows a trend similar to that of "strength at failure". The stress ratio  $M_p$ , however, occurs at smaller strains, where non-uniformities and localizations that can potentially affect measured values of strength at failure, are absent.

From the observations made previously, it may be concluded that the friction angle can not account for the effect of  $b$  on soil strength at peak properly. In order to investigate a suitable function, and following the observations regarding the similarity of strength at peak with strength at failure, the data shown in Figure 4-10, were re-plotted in terms of the following combinations of stress invariants:

$$f = (J_2/I_1^2) = C_{D-P} \quad 4-21-a$$

$$f = (I_1^3/I_3) = C_{L-D} \quad 4-21-b$$

$$f = (I_1 I_2/I_3) = C_{M-N} \quad 4-21-c$$

in which  $I_1$ ,  $I_2$  and  $I_3$  are the first, second and third invariants of stress, and  $J_2$  is the second invariant of deviatoric stress. The invariants of stress can be determined in terms of the principal stresses as the follows:

$$I_1 = \sigma_1 + \sigma_2 + \sigma_3 \quad 4-22-a$$

$$I_2 = \sigma_1 \sigma_2 + \sigma_1 \sigma_3 + \sigma_2 \sigma_3 \quad 4-22-b$$

$$I_3 = \sigma_1 \sigma_2 \sigma_3 \quad 4-22-c$$

$$J_2 = [(\sigma_1 - \sigma_2)^2 + (\sigma_2 - \sigma_3)^2 + (\sigma_1 - \sigma_3)^2]^{1/2} / 6 \quad 4-23$$

Figure 4-12 shows the geometric representations of the functions defined by Equations 4-21 in the octahedral plane, together with the locus of a constant friction angle (Equation 4-20). Relationships representing variations of strength given by these functions, when projected in the octahedral plane are given in Appendix 4C. In the octahedral plane, Equation 4-21-a represents a circle that was suggested by Drucker-Prager as the yield surface of soils, and Equations 4-21-b and c are rounded triangles suggested by Lade-Duncan (1975) and Matsuoka-Nakai (1974) respectively as failure surfaces.

Values of  $C_{D-P}$ ,  $C_{L-D}$  and  $C_{M-N}$  were calculated from Equation 4-21 by substituting stress states at peak shown in Figure 4-10. Values of  $C$  were plotted against void ratio as shown in Figure 4-13. It is noticed from Figure 4-13-a that the difference in  $b$  between the TC and HC results at  $\alpha_\sigma = 0$ , is clearly reflected by a reduction in the value of  $C_{D-P}$  for the HC test, compared to that of the TC. The value of  $C_{D-P}$  is a measure of the radius of the circle in the octahedral plane shown in Figure 4-12. It can therefore be concluded that tests with  $b=0.5$  will result in a smaller radius for this circle, compared to TC tests where  $b=0$ . On the other hand, it was noted previously that when the strength at peak is

determined in terms of friction angle, higher values of  $\tan\phi_p$  were obtained for  $b=0.5$  than for  $b=0$ . A suitable stress function, therefore, is one that produces strengths at  $b=0.5$  between those given by Equations 4-20 and 4-21-a. Equations 4-21-b and 4-21-c introduce such a variation, since as can be seen in Figure 4-12, these equations produce strengths that lie between those given by Equations 4-20 and 4-21-a. Figure 4-13-b and c show that regardless of  $b$ , values of  $C_{M-N}$  and  $C_{L-D}$  for HC tests vary more consistently between TC and TE, indicating a better account for the effect of  $b$ .

Note that functions given by Equations 4-20 and 4-21 are isotropic functions and do not provide the possibility of accounting for the effect of anisotropy on the yield/failure strength. These isotropic functions are used here merely to account for the effect of the intermediate principal stress and to isolate and identify the effect of anisotropy. The effect of anisotropy is investigated and formulated in the next section (Section 4.6) after suitable functions are found to account for  $b$ .

In Figure 4-14, the data shown in Figure 4-10-b obtained from tests on Toyoura sand are presented in forms similar to those in Figure 4-13. Although data for some values of  $\alpha_\sigma$  were not available to allow direct comparison between HC results with those from TC and TE, similar behavior to that of Syncrude sand can be inferred in general.

Data presented so far helped identify suitable shapes that can represent the variation of  $M_p$  with the intermediate principal stress or  $b$ . In order to verify the suitability of such shapes for different values of  $\alpha_\sigma$  and at all possible values of  $b$ , it is necessary to compare results from tests with the same  $\alpha_\sigma$ , but with  $b$  varying between 0 and 1. Such results are investigated in the next section.

### 4.5.3 Variation of strength at peak with $b$ in the ROP

The point where the peak of the UESP is reached, does not always correspond to the same value of  $p$ . Therefore, stress states at peak, obtained from different tests, can not

be shown on the same octahedral plane. A "reference octahedral plane" (ROP) was therefore defined in the principal stress space, that intersects the hydrostatic axis at  $A(1,1,1)$ . Stress ratios  $M_p$  can be shown on this plane as distances from point A to the intersection of lines having stress ratio  $M_p$  in the principal stress space (see Appendix 4B).

The effects of loading direction and intermediate principal stress on the undrained behavior of Toyoura sand were studied by Yoshimine (1996) using the HC apparatus. Three ranges of void ratios were selected and tests with constant  $b$  and constant  $\alpha_\sigma$  were performed for each range. Certain combinations of  $b$  and  $\alpha_\sigma$  were selected such that unacceptable non-uniformities would not develop in the HC sample. Combinations of  $b$  and  $\alpha_\sigma$ , therefore, did not cover their full possible range. All samples were consolidated isotropically to 100 kPa before being sheared (Figure 4-19). Stress ratios  $M_p$  were calculated for any test with given values of  $b$  and  $\alpha_\sigma$ , by measuring values of  $p_p$  and  $q'_p$ , and using Equations 4-13 to 4-15. Stress states were then located on the ROP.

Figure 4-16 shows results calculated as described above, and obtained from samples with void ratios of about 0.82. Curves representing variations of strength as obtained from the M-N yield-failure criteria are also plotted in the same figure. From this figure, the following observations can be made:

1. Results of tests with the same  $\alpha_\sigma$  but different  $b$  represent curves that are similar in their shapes to those obtained from the L-D or M-N criteria for the yield-failure surfaces. This indicates that the variation of stress state at peak with  $b$  follows a trend similar to that of yield/failure.
2. For the same intermediate principal stress and soil density, as  $\alpha_\sigma$  increases, the soil exhibits lower strength at peak that is represented by lower values of  $M_p$ .
3. Curves of constant  $\alpha_\sigma$  are not centered on the origin of the ROP, but are translated in the direction of  $s_1/p$ .



4. Although the number of available data points was not large enough to facilitate a definitive conclusion, the current data indicated that the amount of translation was nearly the same for all values of  $\alpha_\sigma$ .

Use of the L-D yield-failure curves was equally appropriate and did not alter the above conclusions. Since the soil was not pre-sheared and is therefore not expected to exhibit any stress induced anisotropy, the translations in the yield curves can be attributed to the soil's inherent anisotropy.

Changes in the strength of the soil due to inherent anisotropy are often related to changes in the direction of loading  $\alpha_\sigma$ . It is interesting to note, however, that although each curve in Figure 4-16 corresponds to a constant  $\alpha_\sigma$ , strong anisotropy effects are exhibited by the soil, merely due to loading along different  $\theta$  (i. e. different  $b$ ). Similar results were obtained by Yamada and Ishihara (1979) from "drained" true triaxial tests (TTT) when samples were loaded radially along different  $\theta$ , starting from the origin of the octahedral plane. Unlike the current study in which peak points of the UESPs were used to locate yield points, they located yield loci by connecting points of equal shear strain, and obtained shapes of yield surfaces with translated origins (Figure 4-17).

Figure 4-18 shows results of tests similar to those shown in Figure 4-16, but for two other ranges of densities. Conclusions similar to those made from Figure 4-16 can also be made from this figure.

Translation of the center of the yield curves due to anisotropy can be represented by a vector  $a$  ( $a_1, a_2, a_3$ ) in the ROP with components  $a_1, a_2$  and  $a_3$  along the principal directions 1, 2 and 3 respectively. In this case,  $a_i = s_i/p$  and the magnitude of the vector  $a$ , denoted by the scalar ( $a$ ), will be termed the "parameter of inherent anisotropy". The procedure to modify equations of isotropic yield curves to account for anisotropy is explained in Appendix 4B.

Note that in formulating results from different void ratios ( Figure 4-16 and Figure 4-18 ), the same value of  $a = 0.28$  was used regardless of void ratio. From the limited data shown in Figure 4-16 and Figure 4-18 , however, it was not possible to draw a definitive conclusion regarding the variability or otherwise of this parameter with void ratio. These figures also show that the same parameter was used for all values of  $\alpha_\sigma$ . It was noticed earlier ( Figure 4-8 and Figure 4-9 ) that a nearly constant difference ( $a_p$ ) existed between  $\tan\phi_p$  measured from TC and TE tests. A constant difference in  $\tan\phi_p$  regardless of void ratio is an indication of a constant degree of strength anisotropy regardless of void ratio. It is possible, therefore to use this difference between values of strength at peak in TC and TE as a measure of the soil's inherent anisotropy, and to compare the degree of inherent anisotropy of different soils by this parameter.

## 4.6 Effect of direction of loading

### 4.6.1 Representation of states of stress corresponding to different directions of loading

In the principal stress space, states of stress corresponding to the same set of principal stresses  $\sigma_1$ ,  $\sigma_2$  and  $\sigma_3$ , but for different directions of loading  $\alpha_\sigma$ , can not be distinguished from each other, since a fourth axis is required to account for the added degree of freedom produced by the variation of  $\alpha_\sigma$ . In true triaxial tests (TTT), in which the "magnitudes" of the three principal stresses can be changed arbitrarily and independently, directions of the principal stresses are fixed but their relative magnitudes, as represented by  $b$  or  $\theta$ , can vary. Such variations can, therefore, be easily represented in the  $O\sigma_1\sigma_2\sigma_3$  space by different  $\theta$  angles in the octahedral plane or the ROP, and any effect due to differences in  $\theta$  can be viewed and formulated (see e. g. Yamada and Ishihara, 1979). This, however, is not applicable to results of HC tests since in these tests, the value of  $\theta$  can be kept constant while applying loads along different directions  $\alpha_\sigma$ .

To represent stress states corresponding to different loading directions a stress configuration should be used in which the angle  $\alpha_\sigma$  appears as an independent variable. The Mohr circle of stresses will be used for this purpose as shown below.

Figure 4-19-a shows the Mohr circle diagram for a soil element with its depositional direction oriented along the z-axis and subjected to three different principal stresses  $\sigma_1, \sigma_2$  and  $\sigma_3$ . Consider planes with their normal lying in the zx plane. Points representing stress states on such planes will remain on the  $\sigma_1$ - $\sigma_3$  circle in the Mohr diagram shown. As long as magnitudes of the principal stresses remain constant, stress states on planes rotated by different angles  $\alpha_\sigma$  can be obtained using a Mohr diagram with only the biggest circle.

In the majority of practical applications both in field and in laboratory samples, soils exhibit anisotropy in one direction. In such cases, it will be sufficient to investigate directions of loading that are rotated only in the zx plane, and use the Mohr circle  $\sigma_1$ - $\sigma_3$  to represent states of stress during this rotation. A rotation in the zy plane will produce the same response, and a rotation in the xy plane will not have any effect, because the behavior in this plane is isotropic. It was noticed earlier that strength of soils, represented by friction angle, is affected by b. It is expected, therefore, that Mohr circles representing different friction angles be obtained for soils loaded with different b values. In plotting HC data using the Mohr diagram, we will therefore use a separate Mohr circle for data with the same value of b.

Since "magnitudes" of stresses at peak, obtained from different tests, are often not the same, a suitable strength parameter should be used that allows comparison of different test results with different stress magnitudes using a unique variable. To this end, the following procedure is followed.

In a HC test with constant b and  $\alpha_\sigma$ , the stresses are increased along a certain radius of the Mohr circle (i. e. constant  $\alpha_\sigma$  in Figure 4-19-a) and a certain direction in the

octahedral plane (i. e. constant  $\theta$  in the octahedral plane), until failure occurs for that condition. The radius of the Mohr circle at any stage of the test can be obtained from the following equation:

$$R_m = \frac{\sigma_1 - \sigma_3}{2} = \sqrt{\left(\frac{\sigma_z - \sigma_x}{2}\right)^2 + \sigma_{zx}^2} \quad 4-24$$

where  $\sigma_z$  and  $\sigma_x$  are the normal stresses acting on planes normal to the z and x directions respectively, and  $\sigma_{zx}$  is the shear stress on these planes. Dividing both sides by  $\sigma_m = (\sigma_1 + \sigma_3)/2$  and recalling Equation 4-20 yields:

$$R = \frac{\sigma_1 - \sigma_3}{\sigma_1 + \sigma_3} = \sqrt{\left(\frac{\sigma_z - \sigma_x}{\sigma_m}\right)^2 + \left(\frac{\sigma_{zx}}{\sigma_m}\right)^2} = \sin\phi \quad 4-25-a$$

where R is the radius of the "reference Mohr circle" (RMC) in the "reference Mohr diagram" (RMD) (Figure 4-22-b). The RMD is a diagram in which the abscissa and ordinate of the Mohr diagram are divided by  $\sigma_m$ . The center of the Mohr circle in this diagram has a coordinate (1,0) as shown in Figure 4-19 -b, and the radius of the circle equals  $\sin\phi$  regardless of the magnitudes of the principal stresses  $\sigma_1$  and  $\sigma_3$ . Results of tests with the same b but varying  $\alpha_\sigma$  can therefore be plotted on the same diagram, and values of friction angles can be compared, even when they are obtained from various magnitudes of stresses.

Principal stresses at peak can be obtained from values of p and q' at peak, and for a given value of b, using Equation 4-13. The following equation can then be used to calculate the radius of the RMC at peak,  $R_p$ , for tests with any loading direction  $\alpha_\sigma$ :

$$R_p = \left(\frac{\sigma_1 - \sigma_3}{\sigma_1 + \sigma_3}\right)_p = \sin\phi_p \quad 4-25-b$$

Values of  $R_p$  obtained from the above equation can then be plotted in a polar coordinate system with  $R_p$  being the radius and  $2\alpha_\sigma$  the angle, and starting from the center of the RMC. In this diagram, variations in the friction angle at peak with  $\alpha_\sigma$  are reflected in the variations of  $R_p$ .

Pradel et al. (1990) investigated yielding of sands during rotation of principal stresses by following complex stress paths in the HC apparatus (Fig 4-17-a). They obtained circular shaped yield surfaces in a stress space with its abscissa and ordinate defined as  $X = \frac{\sigma_z - \sigma_x}{2\sigma_m}$  and  $Y = \frac{\sigma_{zx}}{\sigma_m}$  respectively ( Figure 4-20 -b). The centers of these circles, however, did not coincide with the origin of their coordinate system, and they attributed the difference to anisotropy in the yield behavior. Gutierrez et al. (1993) plotted failure points using a similar procedure and observed similar indications of anisotropy ( Figure 4-20 -c). All tests in the above studies on yield-failure behavior, however, were conducted with a constant value of  $b = 0.5$ .

#### 4.6.2 Correlating experimental results

Figure 4-21 shows diagrams of RMCs for results of tests plotted previously in Figure 4-16 and Figure 4-18. The following observations can be made:

1. Data from tests with the same  $b$  exhibit friction angles at peak of the UESPs that are decreasing with  $\alpha_\sigma$ . This decrease is reflected in reductions in the radius of the RMC  $R_p = \sin\phi_p$  as  $\alpha_\sigma$  increases.
2. Variations of  $R_p$  with  $\alpha_\sigma$  can be approximated by a circle with its center displaced in the direction corresponding to  $\alpha_\sigma = 0$ . This is consistent with the results reported earlier (Pradel et. al., 1990) regarding yielding of sand during rotation of principal stresses in the HC apparatus. The amount of displacement is an indication of the soil's inherent anisotropy and is referred to here as  $a_p$ . The radius of the displaced

circle is denoted by  $R'_p$ , and the angle between a radius connecting the displaced center and a point on the circle is denoted by  $\alpha'_\sigma$  ( Figure 4-23).

3. The radius of the RMC  $R_p$  is a function of  $b$ . It can be seen that bigger  $R_p$  values are obtained for  $b$  values of about 0.5 and 0.25 compared to  $b$  values smaller or larger than these. This is consistent with the observation frequently made regarding higher friction angles at failure measured for  $b$  values in the order of 0.25 and 0.5. The current results show that the same is true for the strength at yielding obtained from the UESPs.

Figure 4-22 shows similar plots obtained from HC data on three other sands for which such data were available. It can be seen that although in some cases, more scatter in the data can be observed, data corresponding to a particular value of  $b$  can generally be approximated by a RMC with a displaced center. Data for Ham river sand were obtained using stress-controlled tests in which measurement of peak strength might have been difficult, since stress-controlled tests exhibits instability upon reaching the peak of the UESP. This may have caused the increased scatter observed in Figure 4-22-c.

Variation of  $R_p = \sin\phi_p$  with the intermediate principal stress (or  $b$ ) can be obtained through the function  $g(\theta_p)$  discussed in Appendix 4B. The variation with the direction of loading  $\alpha_\sigma$  is given in the following equation that can easily be obtained from the geometry shown in Figure 4-23:

$$R_p = \sin\phi_p = a'_p \cos 2\alpha_\sigma + [ R_p'^2 - (a'_p \sin 2\alpha_\sigma)^2 ]^{1/2} \quad 4-26$$

The average value of  $\sin\phi_p$  ( i. e.  $R'_p$  ) and may vary with the value of  $b$ , and appropriate values should therefore, be substituted in the above equation for a specific stress condition. The value of  $a'_p$  may also change with  $b$  in general. However, data presented in Figure 4-21 suggest that this value may be constant.

## 4.7 Approximating the combined effects of $b$ and $\alpha_\sigma$

### 4.7.1 Representation of states of stress

The procedures used in Figure 4-16 and Figure 4-21 can correlate the variations of strength at peak with  $b$  and  $\alpha_\sigma$  respectively. In both procedures, the anisotropic yield behavior of sands was revealed, and was determined in terms of a suitable stress quantity. It is preferable, however, to account for anisotropy that was exhibited in both procedures, with a unique variable. Two reasons for this preference are given below:

1. In an arbitrary loading condition, we may encounter different combinations of  $b$  and  $\alpha_\sigma$ , and we need to account for both effects at the same time using a unified measure of considering soil anisotropy on the yield behavior.
2. Commonly available testing equipment can produce results for only certain combinations of  $b$  and  $\alpha_\sigma$ , and we often cannot separate these two effects from such results. An example is the common availability of TC ( $b=0$ ,  $\alpha_\sigma=0$ ) and TE ( $b=1$ ,  $\alpha_\sigma=90$ ) test results that cannot be used to derive the effects of  $b$  and  $\alpha_\sigma$  separately. In such cases, degrees of anisotropy of soils should be derived from such results, by properly accounting for both effects using a unique variable. The possibility of such correlation is therefore explored in what follows.

Consider the stress states in the tests performed by Yamada and Ishihara (1979) in the true triaxial test (TTT) where  $p$  was kept constant and shear stresses were increased along different radii in the same octahedral plane (Figure 4-17). The position of each loading radius is determined by the angle  $\beta$ , that is measured clockwise from the ZC-direction. In this case,  $\beta = 0$  corresponds to ZC, and  $\beta = 180$  to ZE. The angle  $\beta$  can be calculated from the following equation:

$$\tan\beta = \frac{\sqrt{3}(\sigma_y - \sigma_x)}{2\sigma_z - \sigma_y - \sigma_x} \quad 4-27$$

In this test  $\sigma_z$  always remains a principal stress, and is the major principal stress when  $0 < \beta < 60$ , the intermediate principal stress when  $60 < \beta < 120$ , and the minor principal stress when  $120 < \beta < 180$ . The magnitude of  $\sigma_z$ , therefore, gradually decreases, as the angle  $\beta$  increases. Fig 4-14, also shows that the yield stresses (that were obtained from contours of constant  $\gamma$ -oct.) decrease monotonically as  $\beta$  increases.

Note that in Figure 4-17,  $\alpha_\sigma$  is equal to 0 when the load is applied along a radius with  $\beta$  slightly below 60 degrees, but jumps to 90 degrees when  $\beta$  increases slightly above 60 degrees. This is because for values of  $\beta$  below 60 degrees, the major principal stress is  $\sigma_z$ , but as  $\beta$  increases to values above 60 degrees,  $\sigma_y$  becomes the major principal stress. It can be seen from Figure 4-17, that this discontinuous change in  $\alpha_\sigma$ , has not caused a discontinuity in the yield strength. It is also noted that despite this discontinuity in  $\alpha_\sigma$ , the magnitude of  $\sigma_z$  changes continuously at this point, since it decreases monotonically from a value higher than  $\sigma_y$  to a value lower than that.

Referring to Figure 4-16 and Figure 4-18, we note that the stress ratio  $M_p$  measured from results of HC tests decreased as  $b$  increased from 0 to 1 (or  $\theta$  increased from 0 to 60 degrees). In HC tests in which the soil sample is deposited in the  $z$ -direction, stresses applied to the sample in the  $x$ ,  $y$  and  $z$  directions may not be the principal stresses, since a shear stress component  $\sigma_{zx}$  can act in the  $x$  and  $z$  planes. Magnitudes of  $\sigma_x$ ,  $\sigma_y$ ,  $\sigma_z$ , and  $\sigma_{zx}$  can be determined from the following equations:

$$\sigma_z = p - \frac{s}{\sqrt{6}} \left( \sin(\theta - 30) - \sqrt{3} \cos(\theta - 30) \cos 2\alpha_\sigma \right) \quad 4-28-a$$

$$\sigma_x = p - \frac{s}{\sqrt{6}} \left( \sin(\theta - 30) + \sqrt{3} \cos(\theta - 30) \cos 2\alpha_\sigma \right) \quad 4-28-b$$

$$\sigma_y = p + \frac{2s}{\sqrt{6}} \sin(\theta - 30) \quad 4-28-c$$



$$\sigma_{zx} = \frac{s}{\sqrt{2}} \cos(\theta - 30) \sin 2\alpha_\sigma \quad 4-28-d$$

in which  $p$ ,  $s$ , and  $\theta$  are as defined in Equations 4-23 to 4-26. The angle  $\theta$  can be obtained from  $b$  using the following equation:

$$\theta = 30 + \tan^{-1} \frac{(2b-1)}{\sqrt{3}} \quad 4-29$$

It can be shown from Equation 4-28 that as  $\alpha_\sigma$  increases, the magnitude of  $\sigma_z$  decreases, provided that all other variables remain constant. The normal stress  $\sigma_z$  will also decrease with the increase in  $\theta$  from 0 to 60 degrees (or in  $b$  from 0 to 1).

Figure 4-21 and Figure 4-22 show that in HC tests with fixed values of  $b$ , values of  $\sin\phi_p$  plotted in the RMC decrease monotonically with the increase in  $\alpha_\sigma$  from 0 to 90 degrees. For a given  $b$ , this is equivalent to a reduction in the stress ratio  $M_p$  with  $\alpha_\sigma$ . Variations of  $M_p$  obtained from tests with constant  $\alpha_\sigma$ , shown in Figure 4-16 and Figure 4-18, lead to the same conclusions regarding the effect of  $\alpha_\sigma$  on  $M_p$ . In both of these cases (i. e. tests with constant  $b$ , and with constant  $\alpha_\sigma$ ), as the magnitude of the normal stress  $\sigma_z$  decreases, the strength at peak as represented by  $M_p$  decreases.

From all the observations made above on results of HC and TTT, it is possible to conclude that changes in the yield strength due to anisotropy seem to be related to changes in the relative magnitude of  $\sigma_z$  compared to  $\sigma_x$  and  $\sigma_y$ . This was true both in the TTT where  $\sigma_z$  was always a principal stress, and in HC tests where it was not always so. In TTT, the relative magnitude of  $\sigma_z$  compared to  $\sigma_x$  and  $\sigma_y$  can be related to the angle  $\beta$  calculated from Equation 4-27 and shown in Figure 4-24. This angle is zero for ZC when  $\sigma_z$  (or  $s_z$ ) is largest, and 180 degrees for ZE when  $\sigma_z$  (or  $s_z$ ) is smallest (Figure 4-24). The angle  $\beta$  may therefore be related to the influence of anisotropy on the yield strength.

In the case of HC tests where  $\sigma_x$ ,  $\sigma_y$ ,  $\sigma_z$  are not always principal stresses, the angle  $\beta$  should be defined such that it determines the relative magnitude of  $\sigma_z$  compared to  $\sigma_x$  and  $\sigma_y$ . In this case, magnitudes of  $\sigma_x$ ,  $\sigma_y$ , and  $\sigma_z$  are affected by both  $b$  and  $\alpha_\sigma$  as shown in Equation 4-28, and the angle  $\beta$  should be related to them accordingly.

In principal stress space with principal directions oriented along the xyz axes, if the direction of application of the deviatoric stress  $s$  is determined by a unit vector  $u_s$ , and the projection of the direction of anisotropy (the z-direction here) on the octahedral plane is given by a unit vector  $u_a$ , the angle  $\beta$  can be obtained from the inner product of the two unit vectors as follows:

$$\cos\beta = u_s \cdot u_a. \quad 4-30$$

In general stress conditions, where stress states at peak are given in terms of non-principal stresses (as e. g. in HC tests), the inner product in Equation 4-30 will be replaced by a double contraction of two unit tensors  $u_s$  and  $u_a$ . The definition of these tensors and the determination of their components will be presented in Chapter 6 and used in modeling the effect of inherent anisotropy on the yielding behavior of sand.

In order to visualize and evaluate effects of  $b$  and  $\alpha_\sigma$  on  $M_p$  through an angle  $\beta$  that can account for both effects, an approximate method is adopted below to determine  $\beta$  from  $\theta$  (or  $b$ ) and  $\alpha_\sigma$  for cases in which the x, y, and z directions are not necessarily principal directions. This approximate method will also be used later to investigate the effect of direction of loading and mode of shearing on the susceptibility of sand to flow failures.

In determining  $\beta$  for any combination of  $b$  and  $\alpha_\sigma$ , it is possible to use the angle  $\theta$  obtained from Equation 4-27 for the given value of  $b$ , and to account for  $\alpha_\sigma$  approximately by converting it to an equivalent  $\beta$  angle using interpolation. It is noted

that in loading along ZC and XC (Figure 4-24), the value of  $b$  is the same, but  $\alpha_\sigma$  differs by 90 degrees. This 90 degrees difference in  $\alpha_\sigma$ , converts to 120 degrees difference in terms of  $\beta$  in Figure 4-24. The same applies for YE and ZE. For results of HC tests where values of  $0 < \theta < 60$  and  $0 < \alpha_\sigma < 90$  are given, the angle  $0 < \beta < 180$  will be approximated from the following equation:

$$\beta = \theta + \frac{4}{3}\alpha_\sigma \quad 4-31$$

Variations of  $M_p$  with the angle  $\beta$  defined above can be plotted in a polar coordinate with  $M_p$  the radius and  $\beta$  the angle measured from the ZC-direction. Note that such plots do not show stress states on the octahedral plane, but are simply ways of visualizing and evaluating the combined effects of  $b$  and  $\alpha_\sigma$  on the yield strength. These plots can also facilitate the evaluation of the susceptibility of loose sands to flow failures, as will be seen later.

Figure 4-25 shows results of HC tests shown in Figure 4-21-a to c, plotted in the way described above. It can be seen that for each density, the results can be approximated by circles with their centers shifted in the z-direction, and their radii being a function of void ratio. As void ratio decreases, the radius of the circle increases, indicating higher strength at peak for denser sands. Similar increase in strength was observed previously when the variations of strength at peak in TC and TE with void ratio was investigated. Figure 4-26 shows similar plots for the data obtained from tests on Syncrude sand, Fraser river sand and Ham River sand, shown previously in Figure 4-22.

## 4.7.2 Implications on stability analysis

### 4.7.2.1 *Stress ratios at which sand is collapsible*

A number of criteria for evaluating the susceptibility of soils to flow failures were reviewed in Chapter 2. These criteria mainly reduce to the determination of stress ratios

at which the soil starts softening, when loaded undrained. The majority of those criteria were obtained and investigated based on TC tests. In some cases, TE tests were also investigated (e. g. Vaid, 1985, Bopp and Lade, 1997) but the relationship between TC and TE results were not clarified or correlated. In a general practical problem, other modes of shearing like simple shear (SS), plane strain (PS) etc. may dominate the deformation process and therefore may need to be considered. Also, current studies often evaluate stability in a qualitative manner and a comprehensive formulation that accounts for various factors influencing  $M_p$ , including density, pressure, mode of shearing etc. has not been presented.

In the common case of cross-anisotropic materials, different modes of shearing differ from each other mainly due to differences in their corresponding values of  $b$  and  $\alpha_\sigma$ . Each shearing mode (e. g. TC, TE, SS, PS) reduces to a certain combination of  $b$  and  $\alpha_\sigma$ . Knowledge of values of  $M_p$  for different combinations of  $b$  and  $\alpha_\sigma$ , can be used to assess the degree of susceptibility of the soil subjected to different modes of shearing to flow liquefaction.

It was seen in Chapter 3 that in  $p$ - $q$  plane, the region where sand collapse and instability is possible is bounded by the stress ratios  $M_p$  and  $M_{PT}$  (i. e. the stress ratio at phase transformation, PT). It is the region between these two stress ratios where sand can undergo undrained softening and is, therefore, subject to collapse in a stress controlled loading. A sample of sand consolidated to a certain state has certain corresponding values of  $M_p$  and  $M_{PT}$ . The larger is the difference between these two stress ratios, the larger is the region of states at which the soil is collapsible.

The stress ratios at PT (i. e.  $M_{PT} = q_{PT}/p_{PT}$ ) are obtained from their corresponding friction angles ( $\phi_{PT}$ ), for any value of  $b$  from the following equation:

$$M_{PT} = \frac{6(1 - b + b^2)^{1/2} \sin \phi_{PT}}{3 + (2b - 1)\sin \phi_{PT}} \quad 4-32$$

A procedure similar to that used for plotting variations of  $M_p$  can be adopted to plot the variations of  $M_{PT}$ . In this procedure, the commonly used 60 degrees sector in the octahedral plane between the TC and TE stress states for isotropic sands is stretched to a 180 degrees sector for anisotropic sands. It was seen earlier that the variation of  $M_p$  when plotted in the ROP resembled 60 degrees sectors of rounded triangles. In the approximate method, 60 degrees sectors obtained from different values of  $\alpha_\sigma$ , are in fact averaged, so that values measured from TC ( $b=0$ ,  $\alpha_\sigma=0$ ) and TE ( $b=1$ ,  $\alpha_\sigma=90$ ) can be used as their two extremes. It was seen in the case of  $M_p$  that a circle gives a reasonable approximation of the variation.

The same applies to the variation of  $M_{PT}$  that is also expected to resemble a shape close to a rounded triangle in the ROP. Using the above method will expand the frequently observed 60 degrees sector of a rounded triangle between TC and TE, to a 180 degree sector in which the effects of both  $b$  and  $\alpha_\sigma$  are taken into account. It was noted earlier, that these plots of  $M_p$  and  $M_{PT}$ , are not the same as those of the ROP, but are simply plots to interpolate stress ratios from their commonly available TC and TE values.

Figure 4-27 shows plots of  $M_{PT}$  obtained from the tests on Toyoura sand from which values of  $M_p$  were measured and plotted previously. It can be seen that the variations can be approximated by circular shapes similar to those obtained for  $M_p$  but with the center of the circles less shifted from the pole. This reduction in the displacement of the center may have originated from a number of sources. It may be a result of the smaller effect of anisotropy on the stress ratio at PT compared to the stress ratio at yielding. It may also indicate that straining the soil up to the PT results in the elimination of most of the anisotropy that existed at the state where  $M_p$  was measured. Besides, differences in  $M_{PT}$  on the compression and extension side can also result from the frictional nature of the material. This is because if the same value of  $\phi_{PT}$  is mobilized in both TC ( $b=0$ ) and TE ( $b=1$ ), corresponding values of  $M_{PT}$  obtained from Equation 4-32, will be different for these two conditions. It can also be noticed that on average, values of  $M_{PT}$  measured from denser sand are somewhat smaller than those measured from looser sand. It will be

shown in Chapter 5 that this is consistent with Rowe's stress-dilatancy relationship, and can be derived from it.

We can use plots like Figure 4-25 and Figure 4-27 to obtain values of  $M_p$  and  $M_{PT}$  for different soil states and modes of shearing, by substituting their corresponding values of  $\theta$  and  $\alpha_\sigma$  (where they are known), in Equation 4-31 to calculate their relevant  $\beta$ . The value of  $\beta$  is given below for some common modes of shearing:

1. For TC:  $b=0 \Rightarrow \theta=0, \alpha_\sigma=0$  therefore  $\beta=0$
2. For TE:  $b=1 \Rightarrow \theta=60, \alpha_\sigma=90$  therefore  $\beta=180$
3. For PSC:  $b\cong 0.4 \Rightarrow \theta\cong 23, \alpha_\sigma=0$  therefore  $\beta\cong 23$
4. For PSE:  $b\cong 0.4 \Rightarrow \theta\cong 23, \alpha_\sigma=90$  therefore  $\beta\cong 143$
5. For SS:  $b\cong 0.25 \Rightarrow \theta\cong 18, \alpha_\sigma\cong 45$  therefore  $\beta\cong 78$

Note that in the case of simple shear (SS) loading, both  $b$  and  $\alpha_\sigma$  may change during loading. The constant values used above as equivalents of these variable quantities were based on experimental results obtained by Yoshimine (1996) from tests on Toyoura sand. Determination of values of  $M_p$  and  $M_{PT}$  for the above modes of shearing for a sample of Toyoura sand at a void ratio of  $e=0.82$  is shown in Figure 4-28. It is noted that such a plot can be obtained by only having UESP from TC and TE for the relevant density of the soil investigated. The increase in the susceptibility of the sample to collapse, as the shearing mode changes from TC to TE, is clearly evident from the plot. This increase is reflected in the increase in  $\beta$ , and consequently an increase in the difference between  $M_p$  and  $M_{PT}$ .

Figure 4-29-a to c show regions of collapsible states for the three ranges of void ratio of Toyoura sand investigated previously. It can be seen that for a certain soil state (certain void ratio here), samples sheared in TC are least subject to collapse, and those sheared in TE have the highest collapse potential. Other modes (eg PC, SS) are intermediate between these two. Figure 4-29-a shows that a sample of Toyoura sand with  $e=0.82$ , is completely stable when sheared in TC, but becomes increasingly

collapsible as the mode of shearing becomes closer to TE. As void ratio increases (Figure 4-29 b and c), the size of the region of collapsible states increases, since an increase in void ratio causes a reduction in stress ratios  $M_p$ , and a slight increase in  $M_{PT}$ .

Figure 4-27 and Figure 4-28 can also show the effect of rotation of principal stresses on the collapse potential. Consider a sample of soil that is subjected to a certain level of shear load (i. e. a constant stress ratio  $M$ ) in the direction of say TC. Assume that the level of the load (i. e. the value of  $M$ ) is such that the soil is in the region of stable states (i. e. inside the circle of stress ratios  $M_p$ ). If the principal stresses are rotated (i. e.  $\beta$  increased) without changing the magnitude of the shear load  $M$ , the region of collapsible states may be reached merely due to this rotation. Such plots are therefore useful in studying different aspects of collapse and instability of sands while being very simple and easy to construct.

It should be noted that if a sample of soil undergoes collapse in the region shown, it may experience increase in its strength upon reaching the stress state at PT. This will increase its stability and may eventually prevent the soil from collapse. During the period of experiencing instability, however, significant deformations may take place in the soil which may not be acceptable from a design point of view. If soil is sufficiently loose or is subjected to sufficiently high pressures such that it strain softens monotonically to the steady state, its stability will not improve upon further shearing and will remain unstable until the steady state is reached.

#### *4.7.2.2 Void ratios at which sand is collapsible: Practical implication of $e_\mu$*

Figure 4-30 shows the variation of  $M_p$  with the normalized (initial) void ratio as obtained from the investigation of the test results examined so far. Consider first the case of triaxial compression (TC) test. The maximum value of  $M_p$  that is measurable from undrained tests was denoted by  $M_\mu$ , and its corresponding (normalized) void ratio was termed  $e_\mu$  when Equation 4-2 or 4-7-b was used to formulate the variation. This

value of  $M_p$  is obtained from tests in which sand is consolidated to a state such that a peak just starts to appear in the UESP (points A and A' in Figure 4-30). If sand is consolidated to a state of slightly more dilative response, such peak will not appear in its UESP. Since instability and collapse is possible only in sand exhibiting undrained softening, such state represents a limit to the states at which sand is collapsible. Note that values of  $M_p$  higher than  $M_\mu$  can exist for sand, provided that sand is consolidated to states of more dilative response, but these higher values cannot be measured from UESPs since no peak appears in such stress paths. These values of  $M_p$  may be obtained by extrapolation using the relationships obtained before for the variation of  $M_p$  with void ratio and pressure. In the next two chapters such higher values of  $M_p$  obtained from these extrapolations will be used in modeling the behavior of dense sand.

Since the normalized void ratio corresponding to  $M_\mu$  is  $e_\mu$ , all states for which  $M_p=M_\mu$  lie on a normal consolidation line (NCL) that has  $e_\mu$  as its normalized (initial) void ratio. States at which softening just starts to appear in the UESP and consequently, sand begins to exhibit a potential for collapse can therefore, be defined by combinations of void ratios (or densities) and consolidation pressures lying on this NCL (see Figure 4-31-a). States below this line will not be subject to collapse (if sheared in TC). On the other hand, when sand is in its loosest possible state with  $e_{n,max}$  as its normalized (initial) void ratio, its corresponding value of  $M_p$  (i. e.  $M_{p,min}$  in Figure 4-30) will be a minimum below which no value of  $M_p$  can exist. Such minimum value is measured from tests in which sand experiences complete liquefaction with zero residual strength upon undrained loading (points B in Figure 4-30). The NCL starting from  $e_{n,max}$  will be the limit of states in the  $e$ - $p$  plane above which sand cannot exist. States between these two NCLs are those at which sand exhibits a drop in its undrained strength and is therefore, collapsible. For MT Toyoura sand sheared in TC, Figure 4-8-a (and also Figure 5-7-a in Chapter 5) gives values of  $e_\mu=0.88$  and  $e_{n,min}=1.0$ . Using these values as  $e_i$  in Equation 4-5, and a  $\beta=0.004$  obtained from compressibility data on Toyoura sand (see Figure 5-8-b in Chapter 5) combinations of void ratios and consolidation pressures at which sand is collapsible can be determined as shown in Figure 4-31-a.



It is interesting to note that Ishihara (1993) showed that there exists a line in the  $e$ - $\ln p$  plane that divides initial states leading to a temporary drop in the undrained shear stress, from those that do not produce such drop. He referred to this line as the "initial dividing line" (IDL) (see Figure 4-31-b). No analytical equation was given for this line but the form of the line that was obtained from results of a large number of undrained tests on Toyoura sand is very similar to the form of the NCL as can be noticed from Figure 4-31-a and b. This is consistent with the result of the current formulation explained above.

Note that the positions of the two NCLs obtained from the current formulation are slightly lower than the lines obtained by Ishihara (1993) from plotting test results. This is because the position of the two lines are determined by the void ratios  $e_{\mu}$  and  $e_{n,max}$  as discussed above. Both these void ratios were obtained by back calculation from results of undrained tests at higher pressures, and therefore, were influenced by the value of the parameter used to model sand compressibility. The smaller values of these two void ratios obtained from back-calculation can result from the choice of a small value for the compressibility parameter  $\beta$  (Equation 4-5) in the back calculation. In fact, it will be shown in Chapter 5 that if the value of  $\beta=0.004$  used for the wide range of pressures studied in this chapter is increased to  $\beta=0.006$ , better model predictions will be achieved for lower pressures.

It is important to note that the IDL obtained by Ishihara (1993) was based on results of TC tests on MT samples of Toyoura sand. It was shown previously in this chapter that the potential for collapse can increase substantially when sand is loaded in other directions or modes of shearing. Void ratios at which sand starts to exhibit collapsive behavior under different directions of loading or modes of shearing can be determined from plots such as those shown in Figure 4-28 and Figure 4-29. These figures indicate that the potential for collapse can increase substantially if sand is loaded in TE or PSE, for instance. The position of Ishihara's (1993) IDL will therefore, be lower in such cases compared to the position he derived from TC tests. Using Figure 4-8-a, it is possible to determine the void ratio at which Toyoura sand starts to exhibit a drop in its UESP

when sheared in TE (i. e. the void ratio corresponding to point A' in Figure 4-30). If the NCL starting with this void ratio is plotted (Figure 4-31-a, the dashed NCL), states between this line and the uppermost NCL (the one with  $e_i=e_{n,max}$ ) will be those at which sand may exhibit collapsive behavior, when all directions of loading and modes of shearing are considered. States below this line will be those at which sand cannot become collapsible regardless of the loading condition. Note that the size of the region of collapsible states can become substantially larger, when all possible loading conditions are considered. It will also be shown later in this chapter and in Chapter 5 that  $e_{\mu}$  can also be influenced by soil fabric. The value of  $e_{\mu}$  obtained from tests on appropriate specimens need to be used in determining void ratios beyond which sand becomes collapsible. Ishihara (1993) showed that the position of the uppermost NCL is strongly influenced by soil fabric. Therefore, both NCLs that determine the size of the region of collapsible states should be obtained from tests on samples having the appropriate fabric.

## 4.8 Effect of anisotropic consolidation

Figure 4-32-a to d show variations of  $M_p$  measured from results of TC and TE tests on sands studied previously. In each figure, some results are obtained from isotropically consolidated (IC) sands while others from anisotropically consolidated (AC) samples at different ratios ( $K_0$ ) of horizontal stress ( $\sigma_h$ ) to vertical stress ( $\sigma_v$ ):

$$K_0 = \frac{\sigma_h}{\sigma_v} \quad 4-33$$

All anisotropic consolidations were made in the compressional direction (i.e.  $\sigma_v > \sigma_h$ ) but shearing was applied in TC or TE. Stress ratios at consolidation  $\eta_c$  can be related to  $K_0$  by the following equation:

$$\eta_c = \frac{3(1 - K_0)}{(1 + 2K_0)} \quad 4-34$$

From Figure 4-32, it can be seen that in most cases, values of  $M_p$  do not seem to be affected by anisotropic consolidation, since values measured from IC and AC sands are close to each other. This, however, may not be so, if consolidation is made along a stress ratio  $\eta_c$  that is high, and is close to, or more than, the value of  $M_p$  corresponding to a sample of IC sand at the same state (i. e. if  $\eta_c > M_p$ ). In this case,  $M_p$  seems to increase and reach values greater than those of IC soil (see e. g. Figure 4-32-a). Di Prisco et al. (1995) also reported an increase in the stress ratio at peak,  $M_p$ , when samples were sheared along high stress ratios. From examination of the stress paths of their tests, it can be observed that in some cases, undrained softening started nearly immediately upon shearing, when  $\eta_c$  was sufficiently high.

As mentioned earlier, evidence presented in Appendix 4A suggest that the stress ratio  $M_p$  represents a shear stress level at which the deformation process changes from that due to small inter-particle slip to that governed by gross slippage at particle contact. In this case, consolidation along  $\eta_c > M_p$  is equivalent to applying shear stresses that cause large inter-particle slip during the consolidation phase because the limit of small strain behavior is exceeded during consolidation. This can cause the soil to become pre-stressed and somewhat stronger in the direction of consolidation while at the same time, close to experiencing significant reduction in strength upon further shearing, as observed by some researchers (see Section 3.4.5 in Chapter 3).

## **4.9 Effect of preparation method and soil fabric**

A number of studies (e. g. Ishihara, 1993; Vaid et al., 1996) have emphasized the importance of the method of sample preparation on the response of sands to shearing. Such an effect may not be easy to quantify, and it is useful to find parameters that can account for these effects, especially in the context of constitutive modeling of sands.

Effects of fabric are expected to be dominant in the low and medium range of strains, since they are eliminated when the soil experiences large strains. Since the parameter  $M_p$  is measured when the soil is just leaving the small strain and starting the medium strain level, it may provide the opportunity to quantify the effects of fabric, and to bring these effects into soil constitutive modeling.

Figure 4-33 shows variation of  $M_p$  for samples of Toyoura sand prepared by the Moist Tamping (MT) and Dry Deposition (DD) methods. Although adopted from three independent sources, it can be seen that results from samples prepared by the DD method plot close to each other, both on the compression and extension sides. Data from the MT method on the compression side plot higher than those of the DD method, implying higher  $e_n$  values (looser samples) needed to produce the same stress ratio  $M_p$ .

Figure 4-34-a and b show  $M_p$  data on Fraser River sand prepared by MT and WP, in addition to data from undisturbed samples that were frozen in situ, and then drilled and tested. Figure 4-34-a shows that different series of data exhibited somewhat different trends, each trend corresponding to a certain soil fabric. Results belonging to the same series, on the other hand, are generally consistent. The differences in the data belonging to different fabrics, however, decreased when the variations were plotted against void ratio in -b. Unlike Figure 4-34-b, values of  $e_n$  in Figure 4-34-a, were determined using the consolidation pressure and void ratio.

In Figure 4-34-c, variations of  $M_p$  for samples of Syncrude sand prepared by MT and WP are shown against void ratio after consolidation. Since consolidation pressures remained below 700 kPa and because no isotropic consolidation data were available, no normalization was done on the void ratio. It can be seen that unlike previous results, data from these two methods of preparation on the compression side fall close to each other.

From the above observation and other cases not shown here, it was concluded that variations of  $M_p$  were less sensitive to preparation method and fabric, when plotted in

terms of void ratio, but showed somewhat different trends, when plotted against  $e_n$  or  $\psi_n$ . This is because values of  $M_p$  were generally close to each other for a certain void ratio regardless of fabric, but the pressure at which the peak occurred, depended on the method of preparation. This caused different trends depending on fabric, when data were plotted in terms of  $e_n$  or  $\psi_n$  that are affected by pressure.

It is noted that since the stress ratio  $M_p$  is affected by soil fabric, it can change with the change in the procedure by which the sample is prepared, even if the same preparation method is used. Figure 4-35 shows UESPs of samples of Monterey No 0 sand prepared by MT. In Figure 4-35-a results of tests on samples prepared by using 6 lifts of soil during the tamping procedure, are shown. Figure 4-35-b shows results obtained from 12-lift samples. It can be seen that using 12 lifts (more compaction energy used) produces sharper peaks and higher stress ratios at peak. Considering the physical meaning of  $M_p$ , explained in Appendix 4A, the more gradual increase in shear stress observed in the 6 lift samples, can result from the larger small-strain deformation required to mobilize the inter-particle friction angle in these samples, because of their looser inter-particle contacts.

Sand type	Source	Mineralogy	Angularity	$e_{max}$	$e_{min}$	$M_{us}$	USL
Ottawa	Sasitharan (1994)	quartz	rounded to subrounded	0.82	0.50	1.19	$e = 0.864 - 0.0168 \ln p$
Toyoura	Ishihara (1993)	75 % quartz ; 25 % feldspar	subangular	0.977	0.597	1.24	$e = -0.006348p^3 + 0.0367p^2 - 0.1199p + 0.92548$ (p in Mpa) (obtained in present study)
Syncrude	(1) Wride & Robertson (1997a) (2) Sladen & Handford (1987)	95% quartz	angular to subangular	(1) 0.958 (2) 0.93	(1) 0.668 (2) 0.55	(2) 1.19	(1) $e = 0.919 - 0.0152 \ln p$ (for $e > 0.829$ ) (2) $e = 0.847 - 0.017 \ln p$
Fraser River	Wride & Robertson (1997b)	(*) 40 % quartz; 11% feldspar; 45% rock fragments etc.	(*) subangular to subrounded	1.056	0.677	(*) 1.4	$e = 1.071 - 0.0165 \ln p$ (for $e > 0.979$ )
Ham River	Symes et al. (1984)	Quartz with some Mica	subangular elongated	0.923	0.613		
Erksak	Been et al. (1991)	73% quartz; 22% feldspar	rounded to subrounded	0.753	0.527	1.24	$e = 0.82 - 0.0133 \ln p$ (for $p < 1000$ kPa)

(\*) Chillarige et al. (1997)

Table 4-1 Properties of sands investigated.

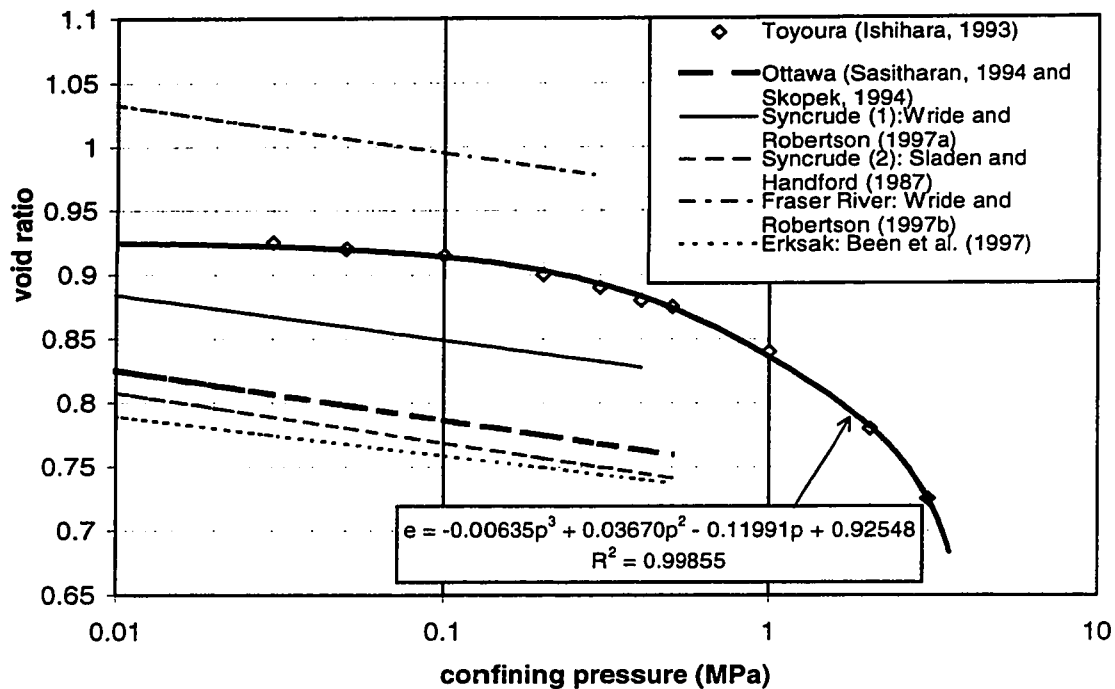


**Figure 4-1** Position of ultimate (steady) state lines (USL) of sands investigated in  $e$ - $\ln p$  plane. The USL of Toyoura sand is obtained by regression, using average test results reported by Ishihara (1993).

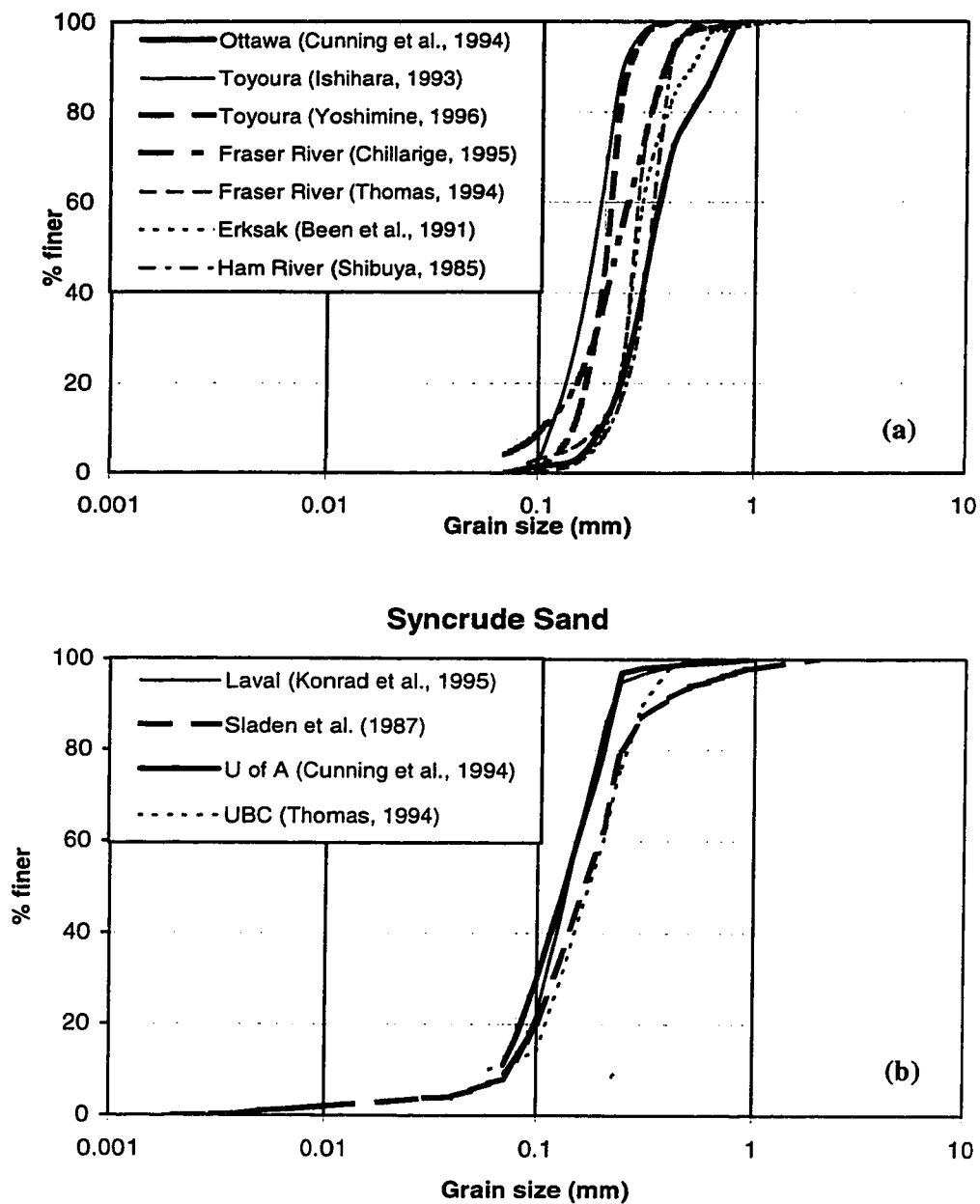


**Figure 4-2** Grain size distribution of sands investigated, as reported in different studies



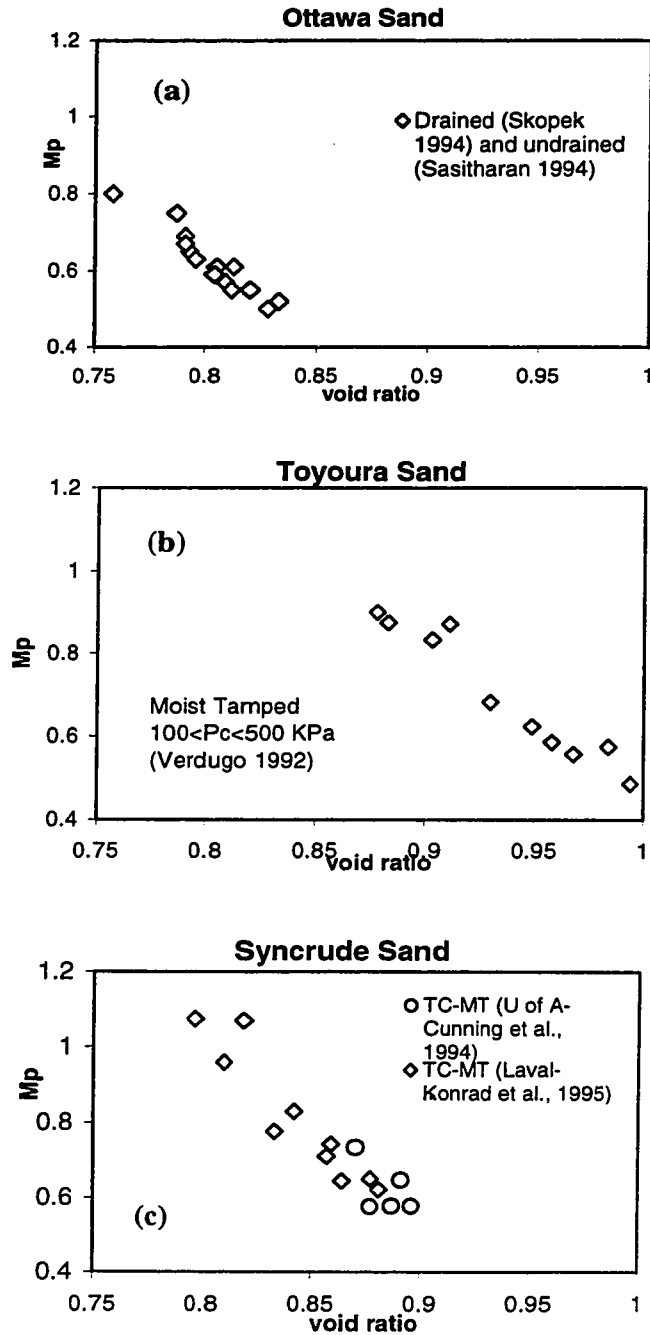
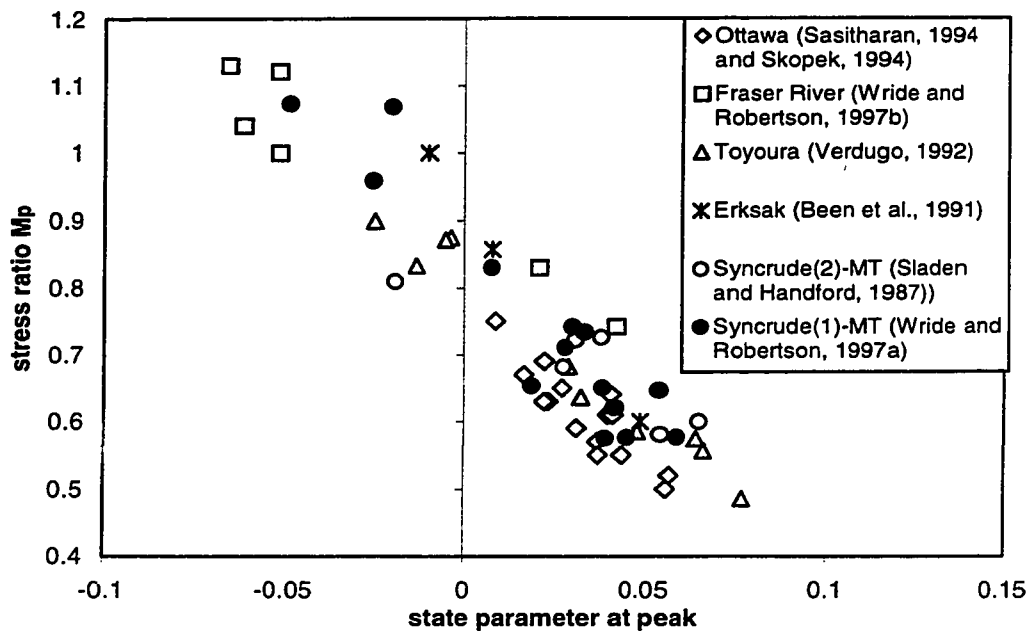


**Figure 4-3** Variation of  $M_p$  with void ratio at consolidation for three different sands consolidated to pressures up to 600 kPa.



	Ottawa	Toyourea	Syncrude		Fraser River	Erksak	all sands
			(1)	(2)			
Slope $k_{\psi}$	4.35	4.14	5.13	2.65	3.23	6.70	4.59
Regression coeff. $R^2$	0.786	0.960	0.890	0.818	0.916	0.996	0.865

**Figure 4-4** Variation of  $M_p$  with state parameter at peak in different sands, consolidated to pressures up to 600 kPa. Note that for some sands the available data covered a limited range of states (as e. g. in Syncrude(2)) or a limited number of data points (as e. g. in Erksak)

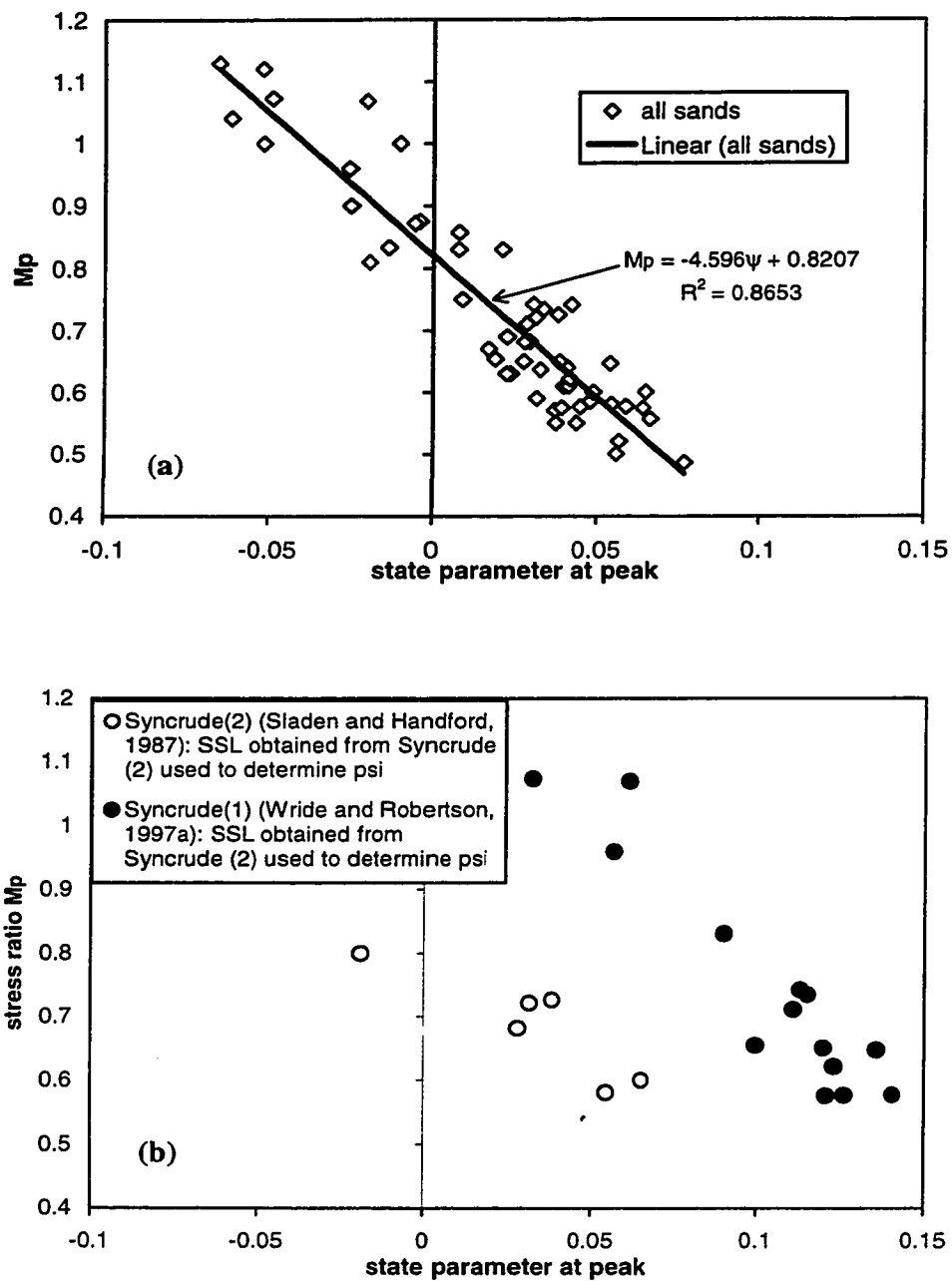


**Figure 4-5 (a)** Variation of  $M_p$  with state parameter at peak for all the sands investigated

**(b)** Effect of the choice of the USL on the variation of  $M_p$ .

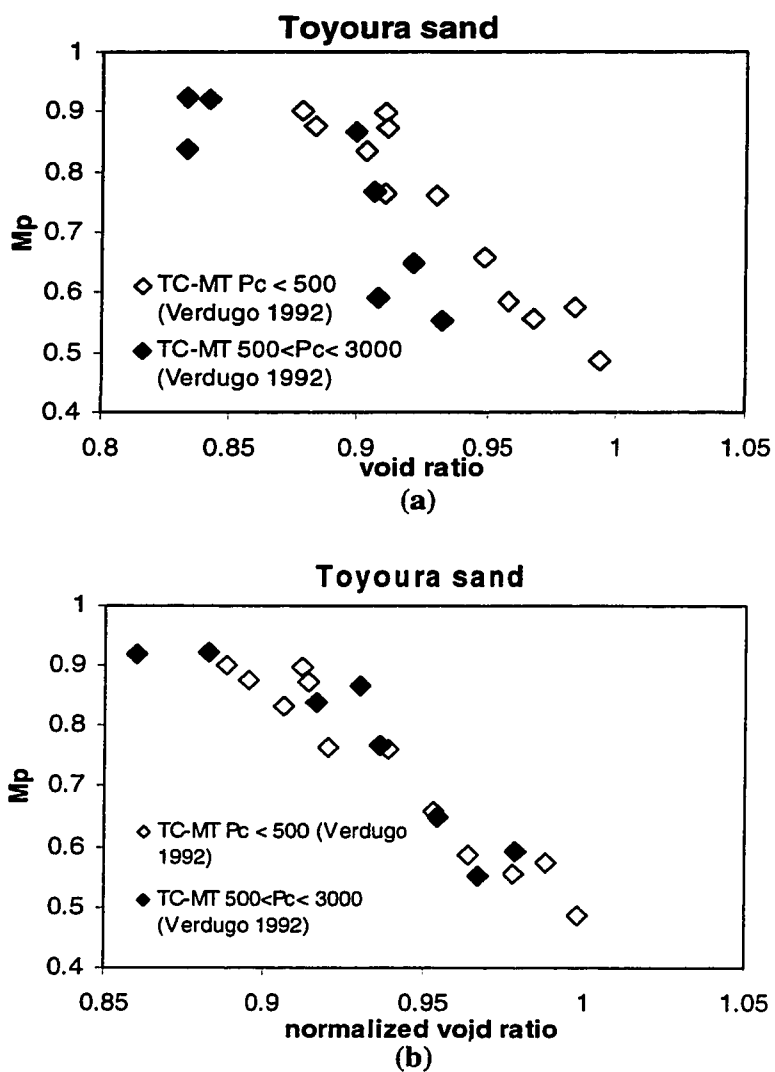


**Figure 4-6** Variation of  $M_p$  with void ratio and normalized void ratio in the low and high ranges of pressure. Samples were prepared by Moist Tamping (MT) and dry deposition (DD)

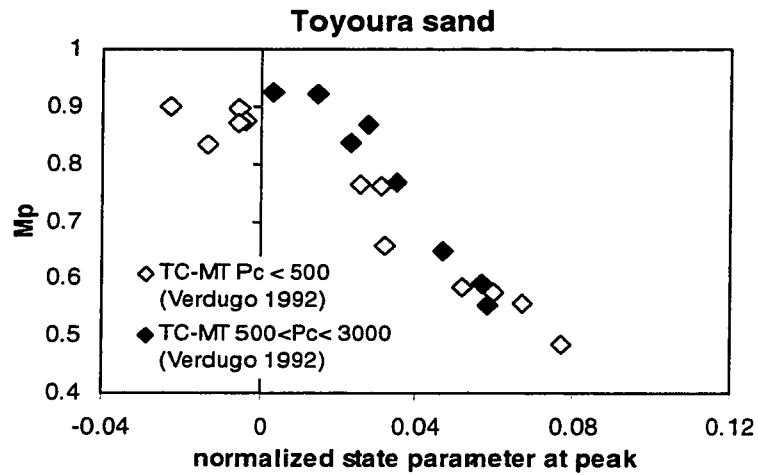
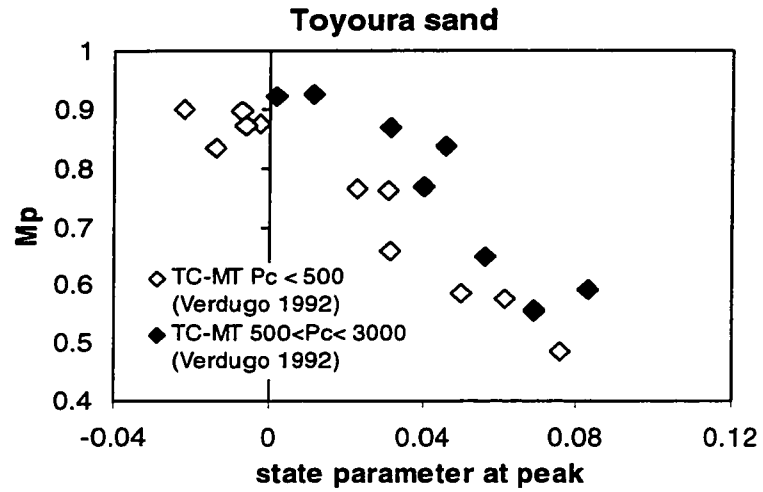


**Figure 4-7** Variation of  $M_p$  with state parameter and normalized state parameter for the low and high ranges of pressure. Samples were prepared by Moist Tamping (MT) and dry deposition (DD)

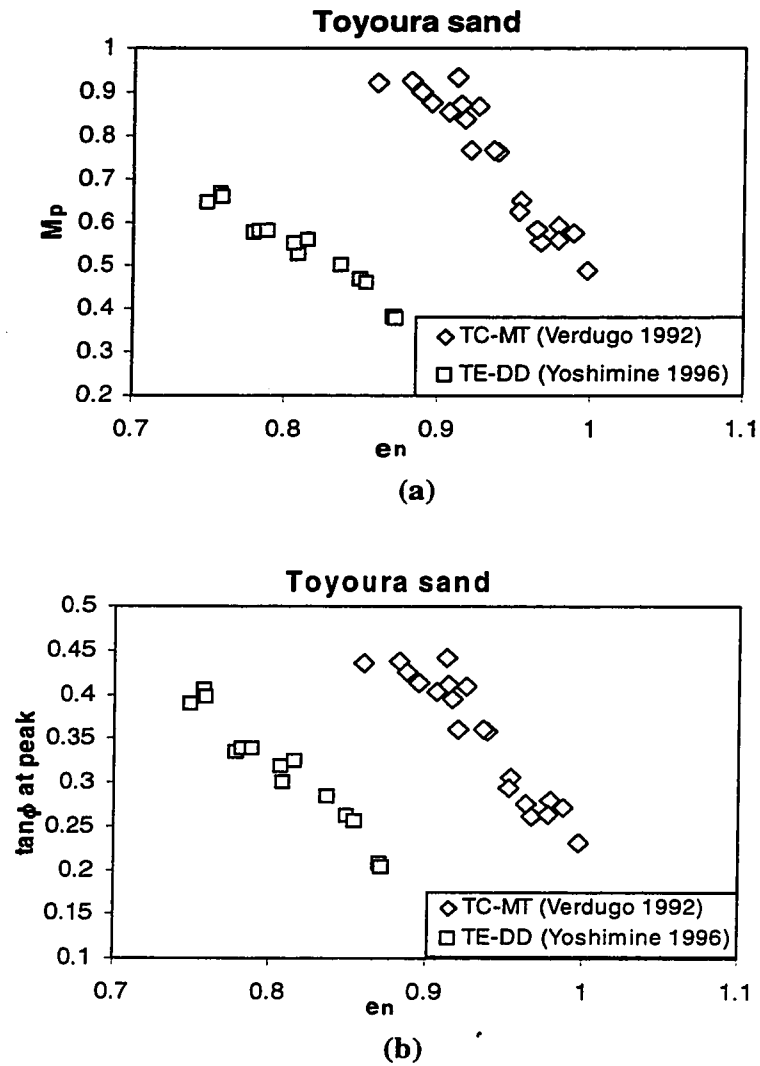


**Figure 4-8** Variation of  $M_p$  and  $\tan \phi_p$  with normalized void ratio ( $e_n$ ) in Triaxial Compression (TC) and Triaxial Extension (TE). Samples were prepared by Moist Tamping (MT) and dry deposition (DD)

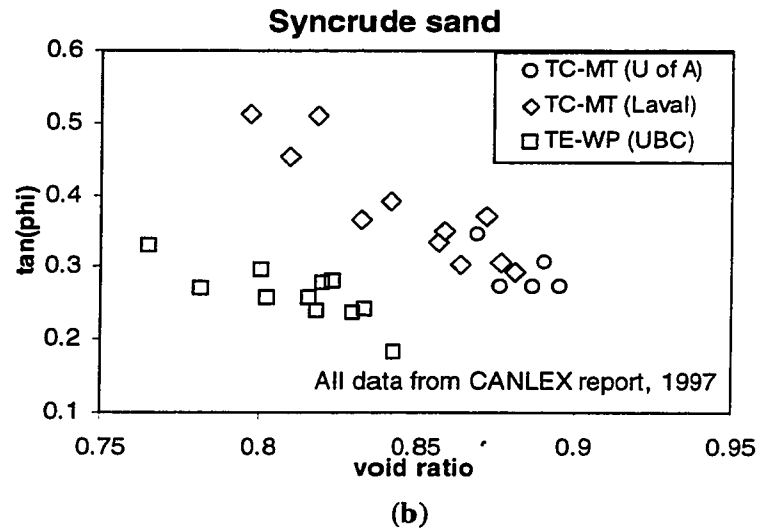
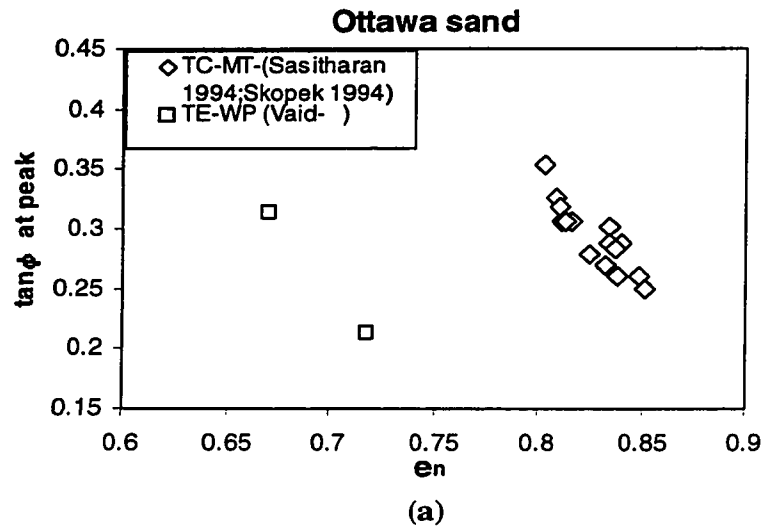


**Figure 4-9** Variation of friction angles at peak for Ottawa sand and Syncrude sand. Void ratios for Syncrude sand were not normalized because the range of pressures was small. Samples were prepared by moist tamping (MT) and water pluviation (WP)

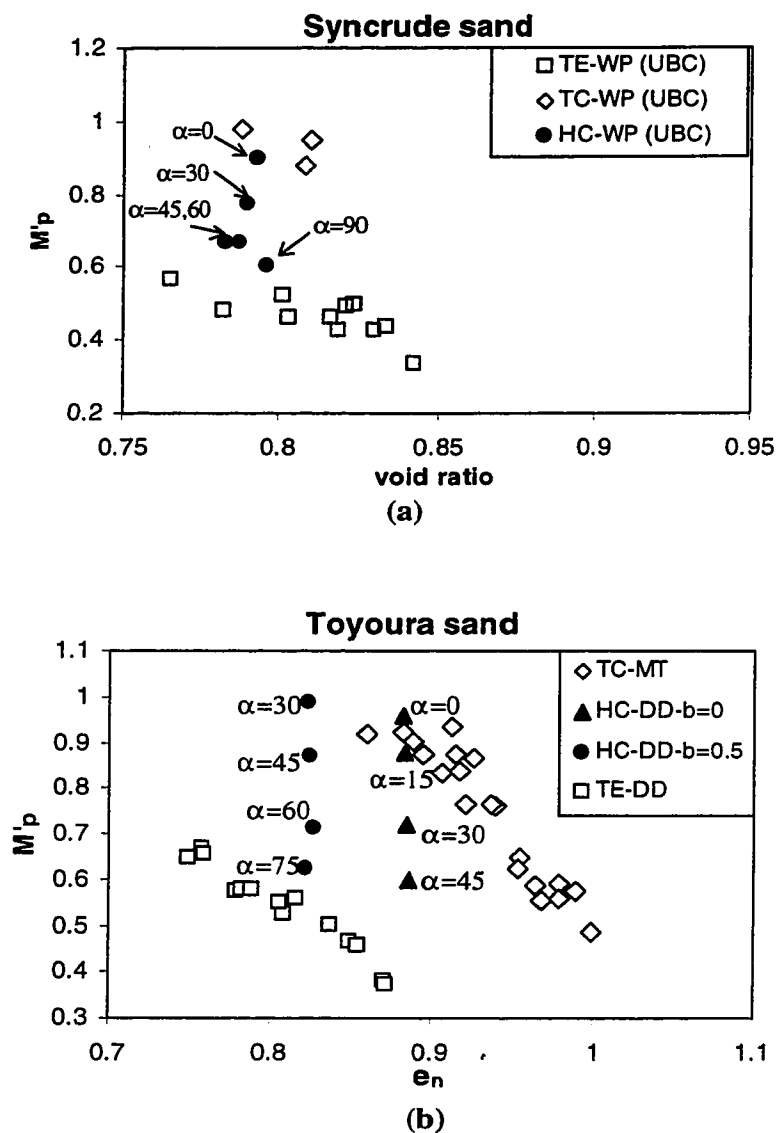


**Figure 4-10** Effect of direction of loading on  $M'_p$  for Syncrude sand (data from Wride and Robertson, 1997a), and Toyoura sand. (Data on moist tamped (MT) samples from Verdugo, 1992 and on dry deposited (DD) samples from Yoshimine, 1996).



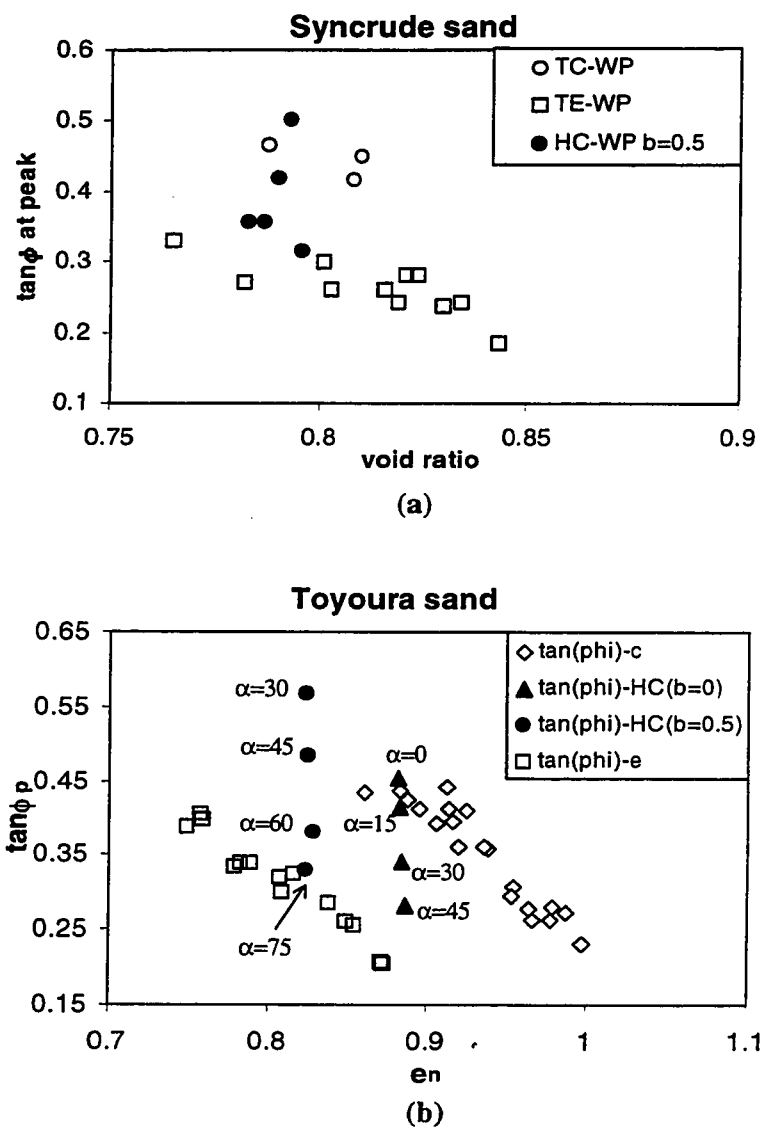


**Figure 4-11** Effect of direction of loading and intermediate principal stresses on  $\tan\phi_p$

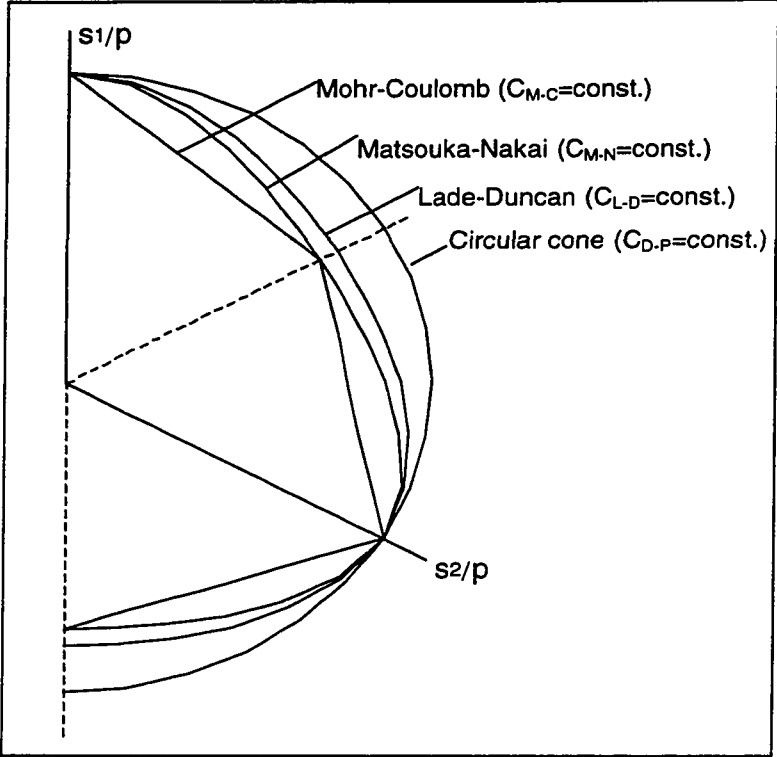
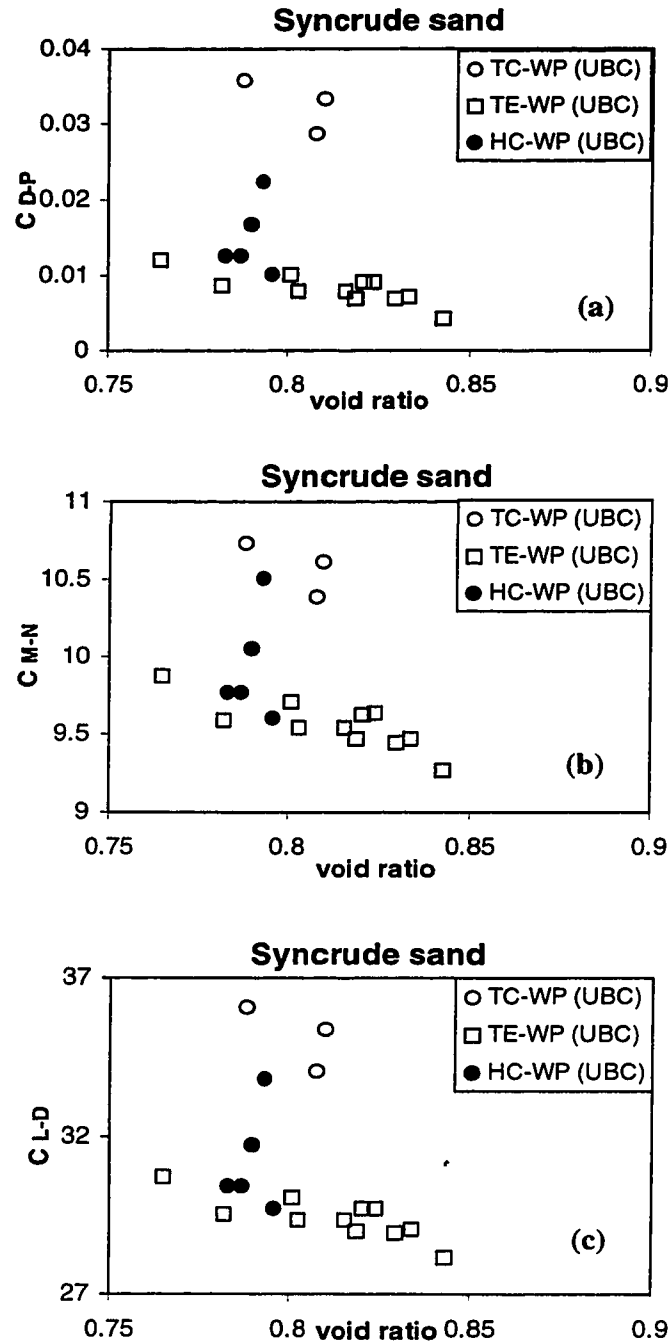
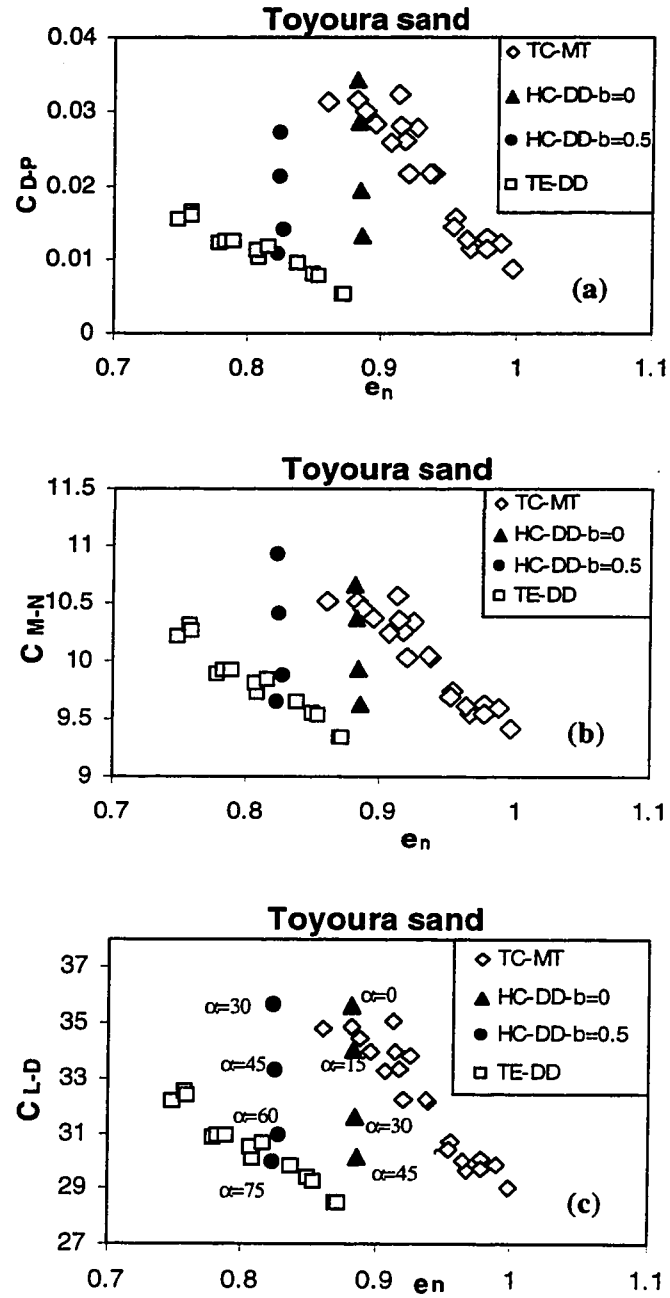


Figure 4-12 Representation of yield-failure criteria in the octahedral plane



**Figure 4-13** Different yield-failure criteria used to correlate stress states at peak for water pluviated (WP) Syncrude sand (data measured from Wride and Robertson, 1997a)



**Figure 4-14** Different yield-failure functions used to correlate stress states at peak (tests on Moist Tamped (MT) samples from Verdugo, 1992 and Dry Deposited (DD) samples from Yoshimine, 1996)

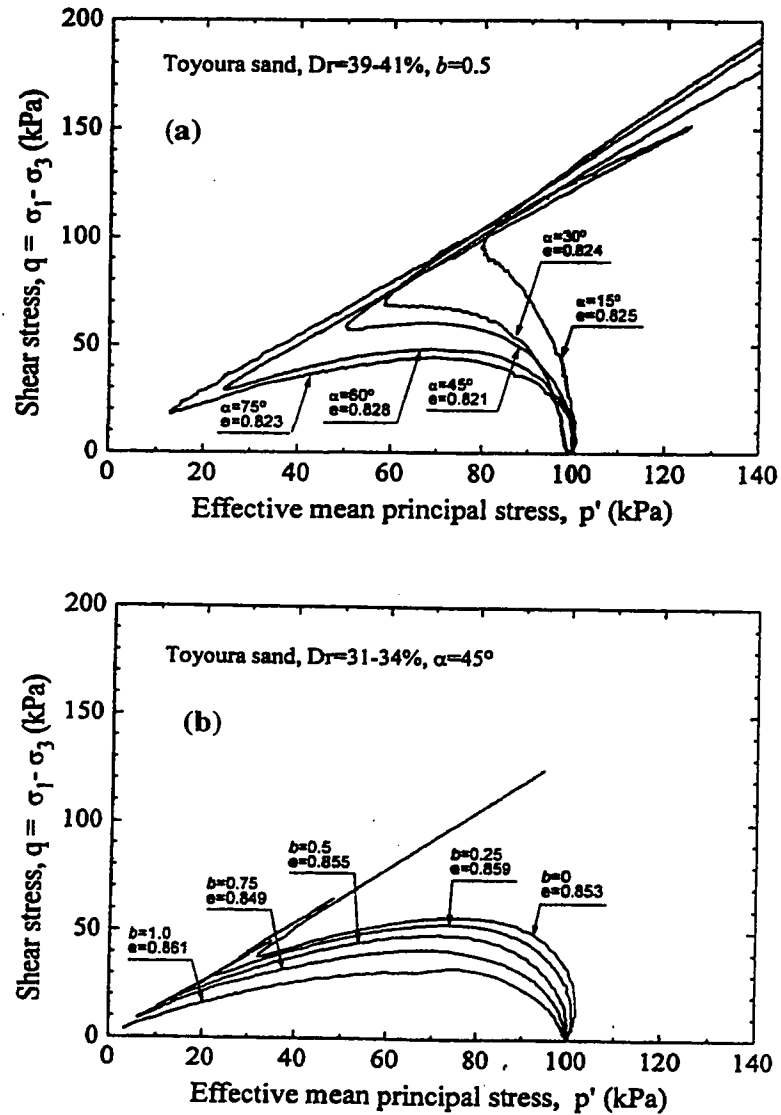


**Figure 4-15** Samples of undrained tests used to investigate the effects of  $\alpha_\sigma$  and  $b$  on  $M_p$  for Toyoura sand: (a) effect of  $\alpha_\sigma$  (b) effect of  $b$  (modified after Yoshimine, 1996)

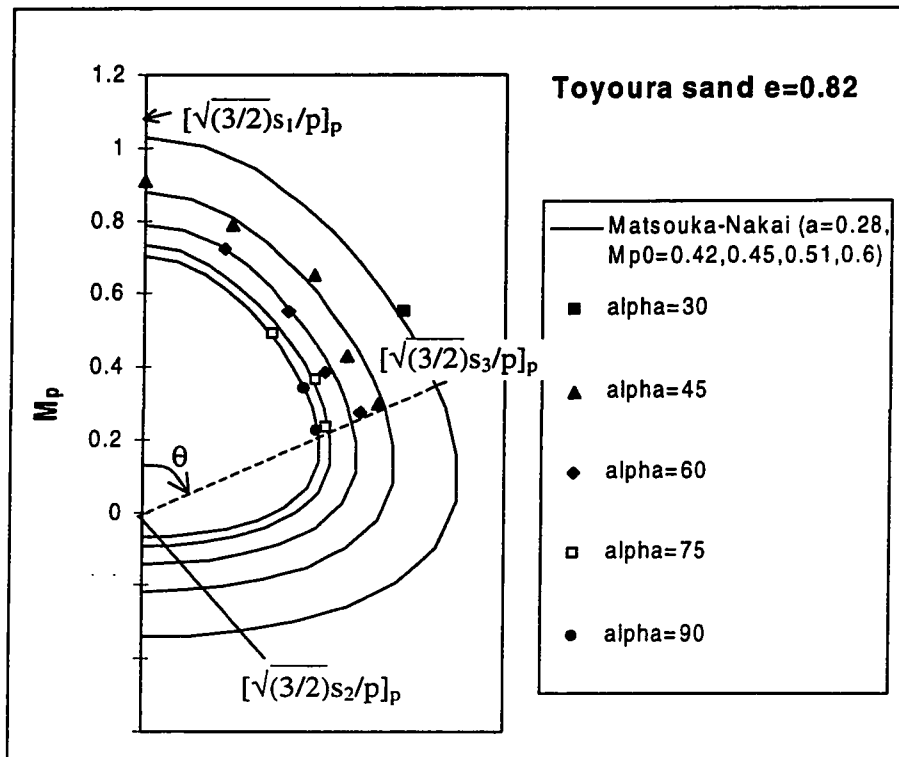


**Figure 4-16** Variation of  $M_p$  as represented in the reference octahedral plane (ROP). See Appendix 4B for the definition of variables and the analytical form of Matsouka-Nakai failure-yield criteria (data measured from Yoshimine, 1996)

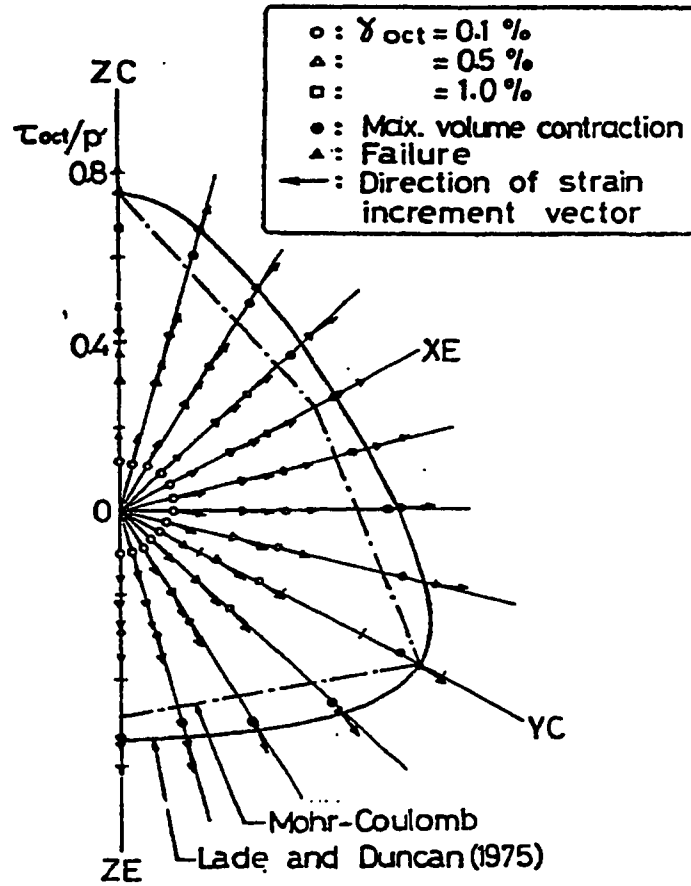
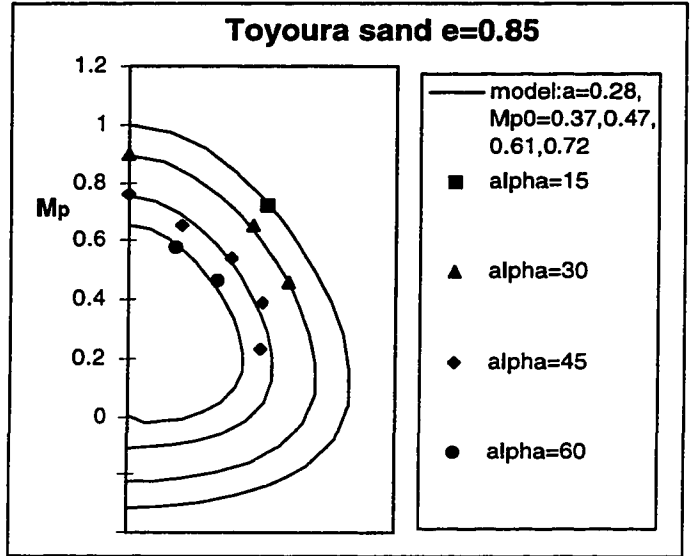
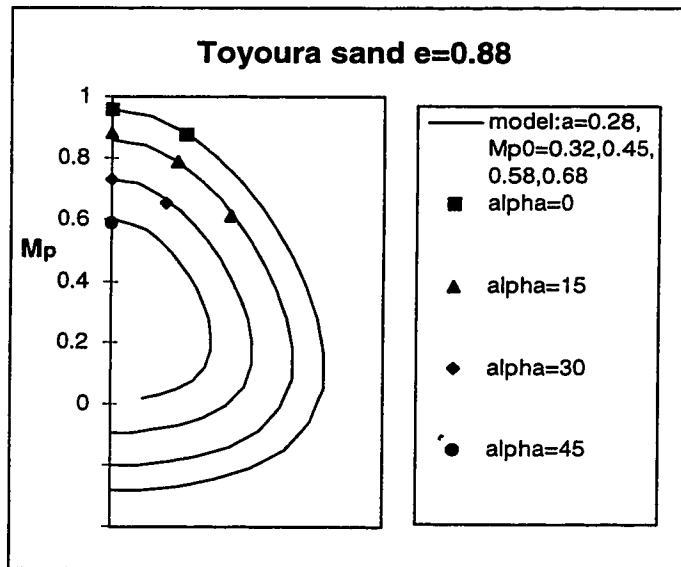


**Figure 4-17** Yield loci obtained from contours of equal shear stains in drained True Triaxial Tests (TTT). Stress states at Phase transformation (PT) and failure are also shown (modified after Yamada and Ishihara, 1979)



(a)



(b)

**Figure 4-18** Diagrams similar to Figure 4-16 but for Toyoura sand at two other void ratios. "Model" in the legends of the figures refers to the Matsouka-Nakai failure-yield criteria (Data measured from Yoshimine, 1996)



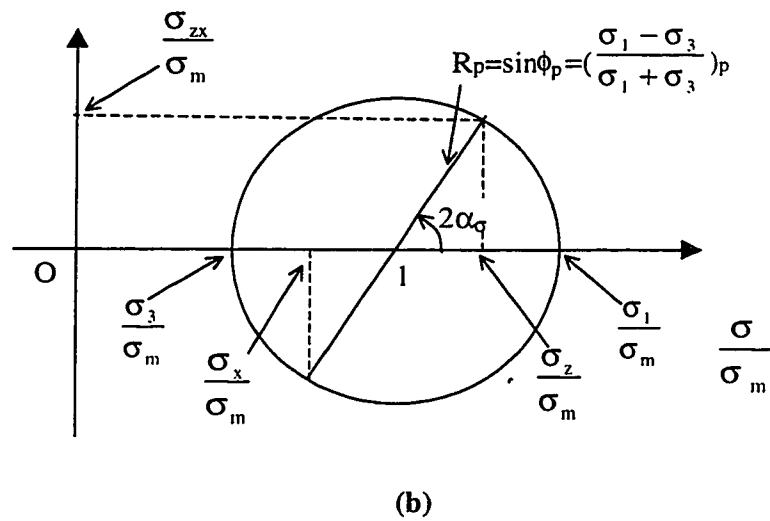
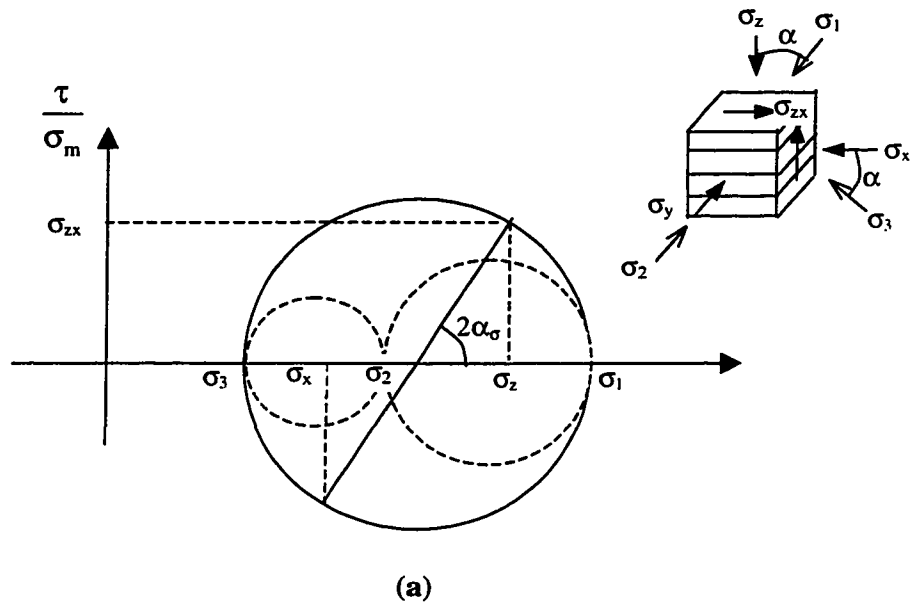


**Figure 4-19** (a) The Mohr diagram (b) the reference Mohr diagram and "Reference Mohr Circle" (RMC) used to represent stress states at peak with constant  $b$  and different directions of loading  $\alpha_\sigma$ .

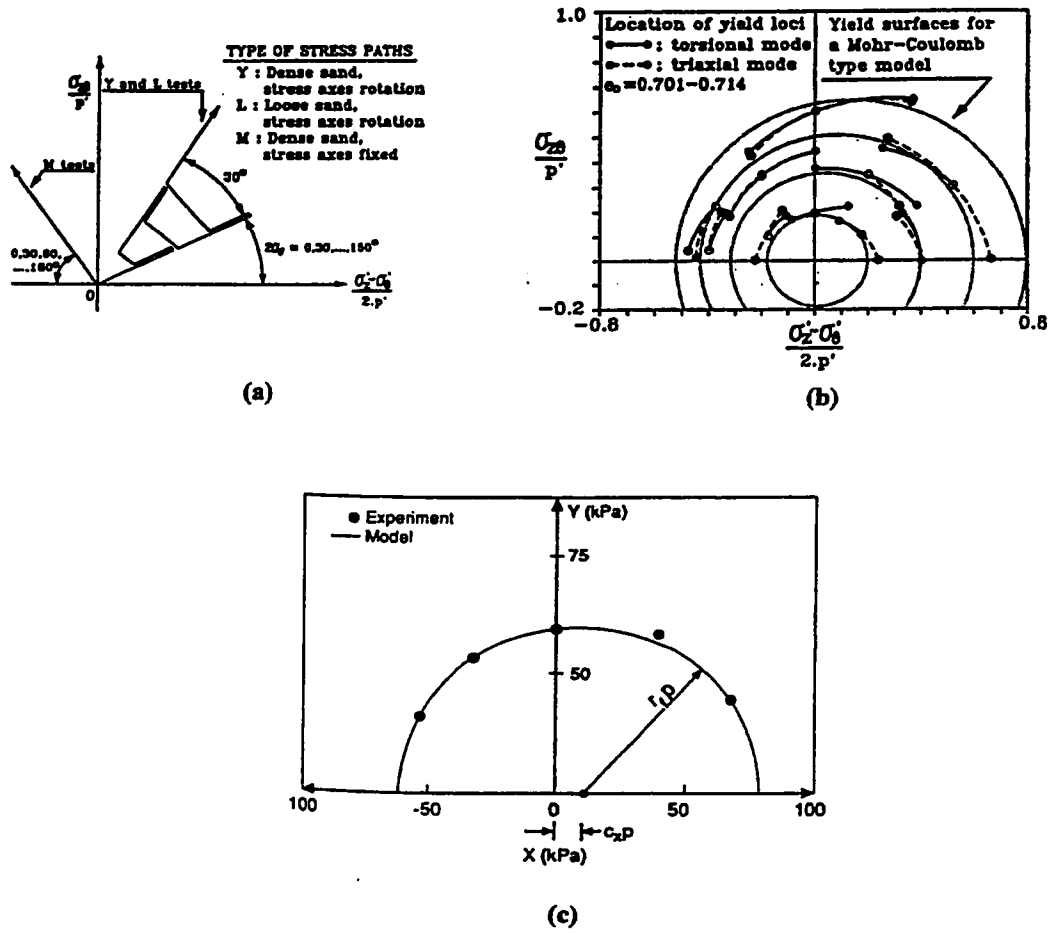


**Figure 4-20** Yield and failure surfaces obtained from torsional shear tests in the HC apparatus: (a) Stress paths followed to obtain yield stresses (b) Yield stresses (c) Failure stresses obtained by increasing shear stresses along fixed directions of loading  $\alpha_\sigma$  (a and b modified after Pradel et al., 1990 and c modified after Gutierrez et al., 1993)

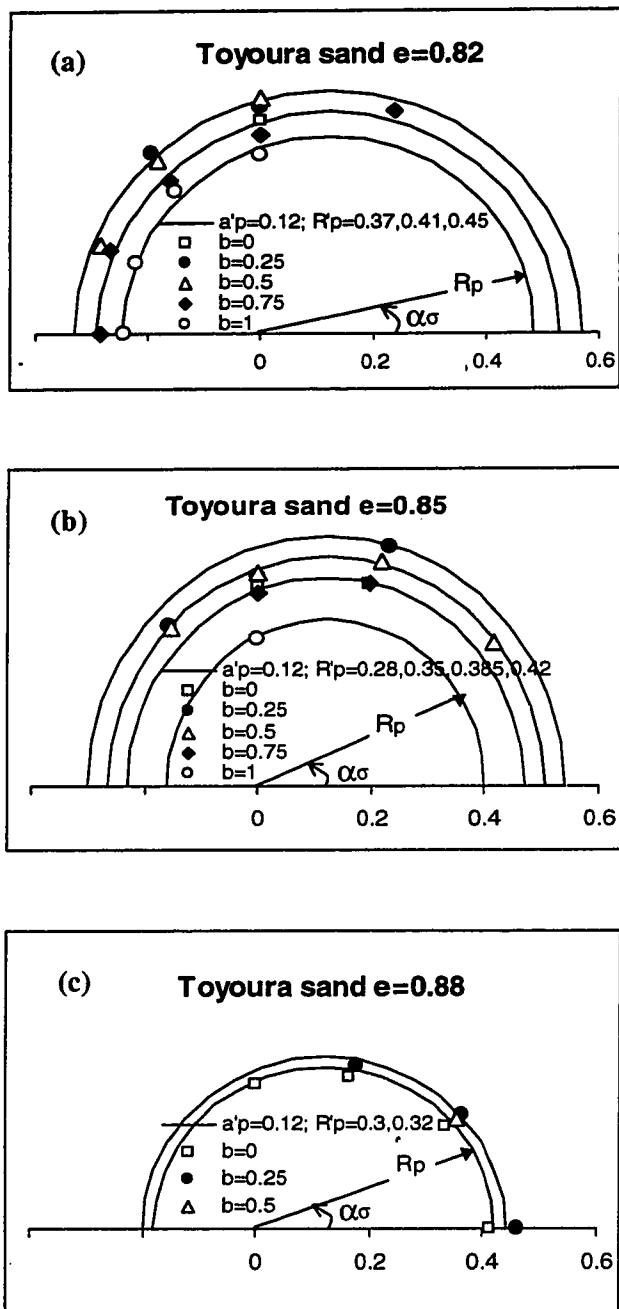
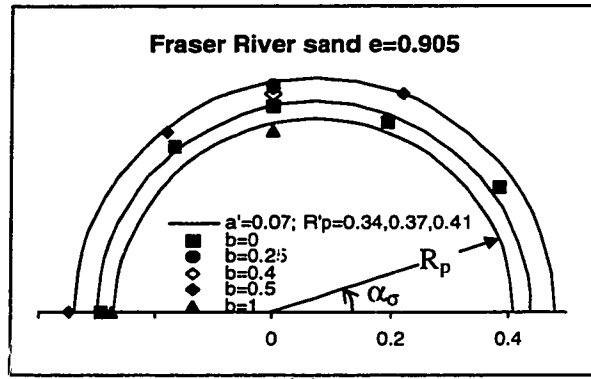
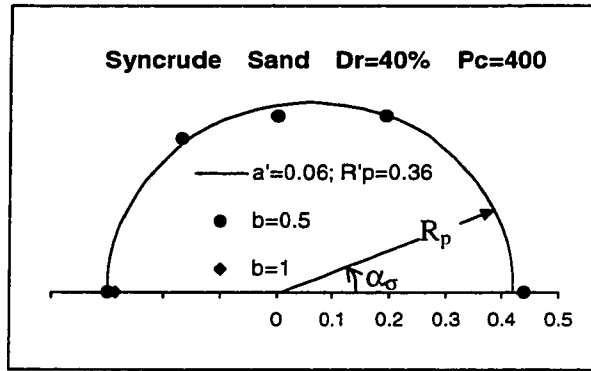


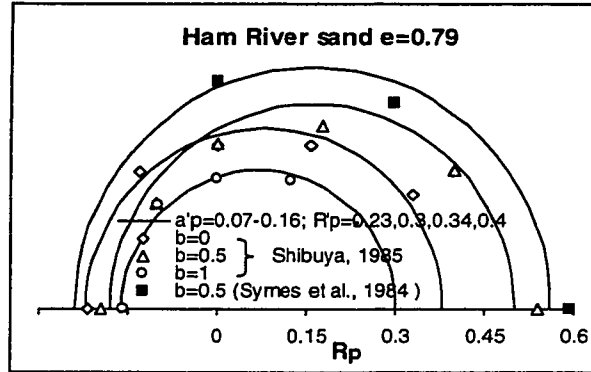
**Figure 4-21** Variations of  $R_p = \sin \phi_p$  with  $\alpha_\sigma$  for Toyoura sand. Void ratios were not normalized since pressures were small (below 100 kPa) (data measured from Yoshimine, 1996).



(a)



(b)



(c)

**Figure 4-22** Variations of  $R_p = \sin \phi_p$  with  $\alpha_\sigma$  for three different sands (Data for Syncrude sand and Fraser River sand measured from Wride and Robertson, 1997a and b)

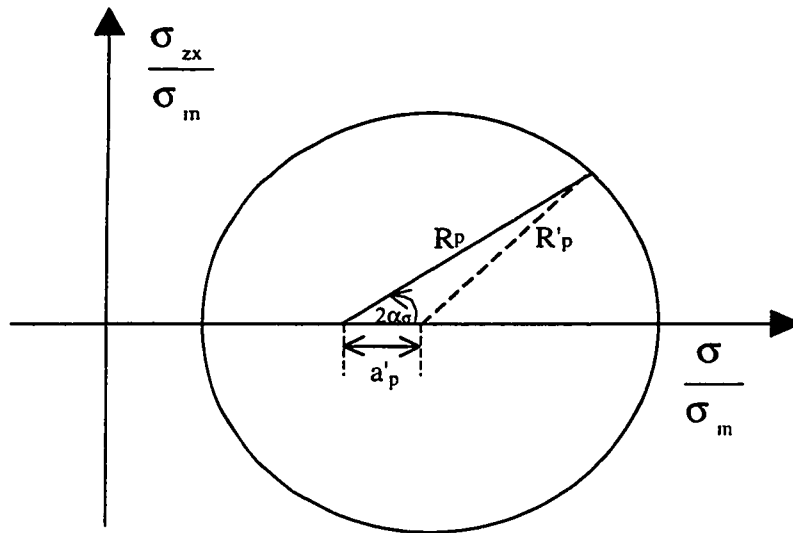


**Figure 4-23** Using the reference Mohr diagram to determine  $R_p$  from  $R'_p$  and  $a'_p$  for an arbitrary value of  $\alpha_\sigma$

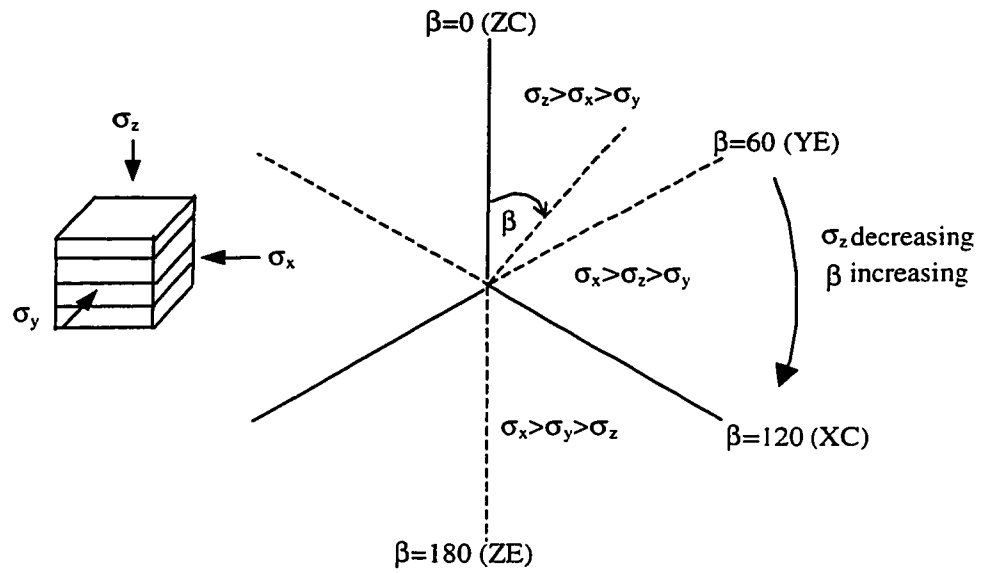


**Figure 4-24** Changes in the relative magnitudes of the three normal stresses with  $\beta$  in a true triaxial test (TTT)

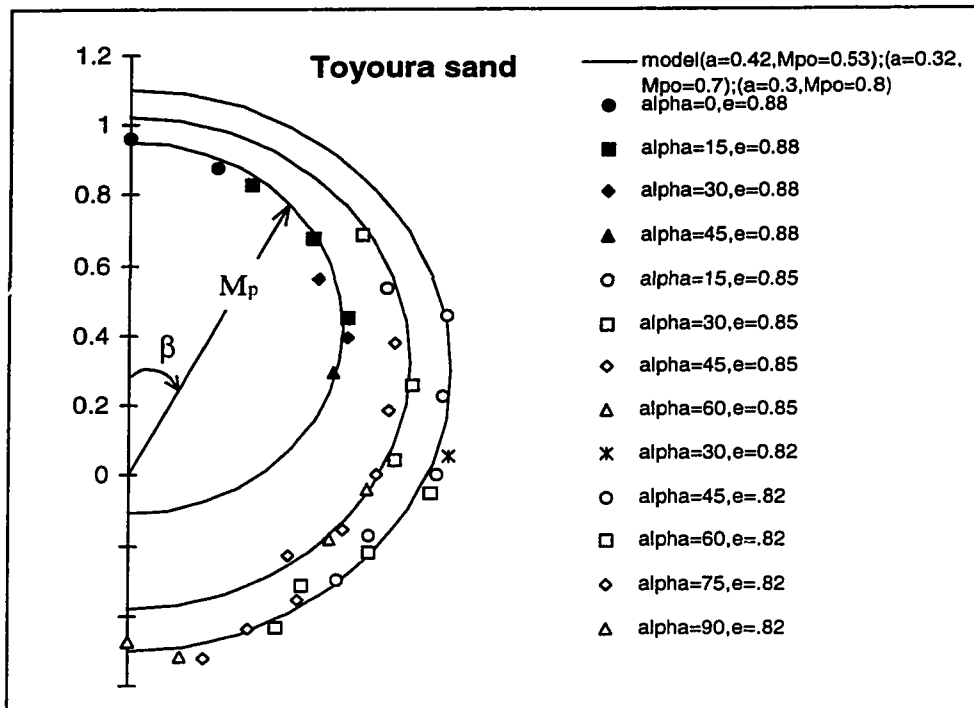
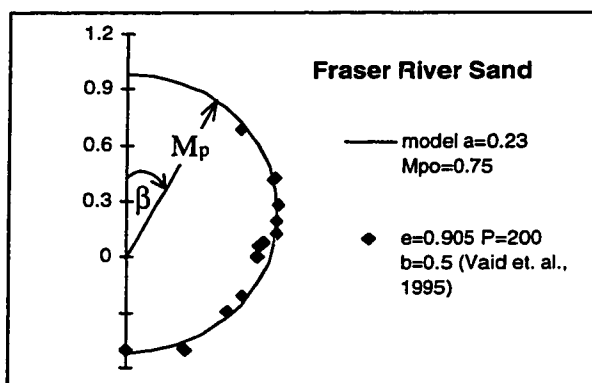
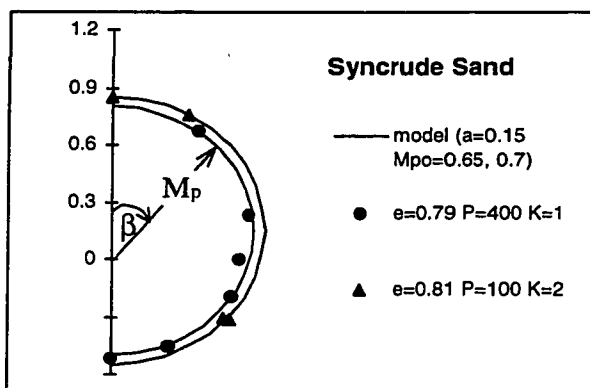


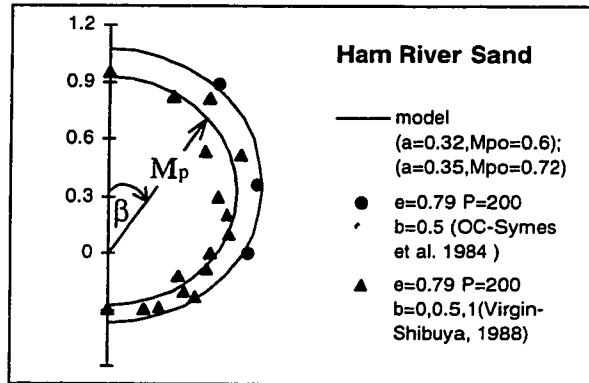
**Figure 4-25** Variation of  $M_p$  with  $\beta$  for three different densities of Toyoura sand plotted in a polar coordinate. Void ratios were those at consolidation and were not normalized because the confining stresses involved were small.



(a)



(b)



(c)

**Figure 4-26** Variation of  $M_p$  with  $\beta$  in polar coordinate for three different sands



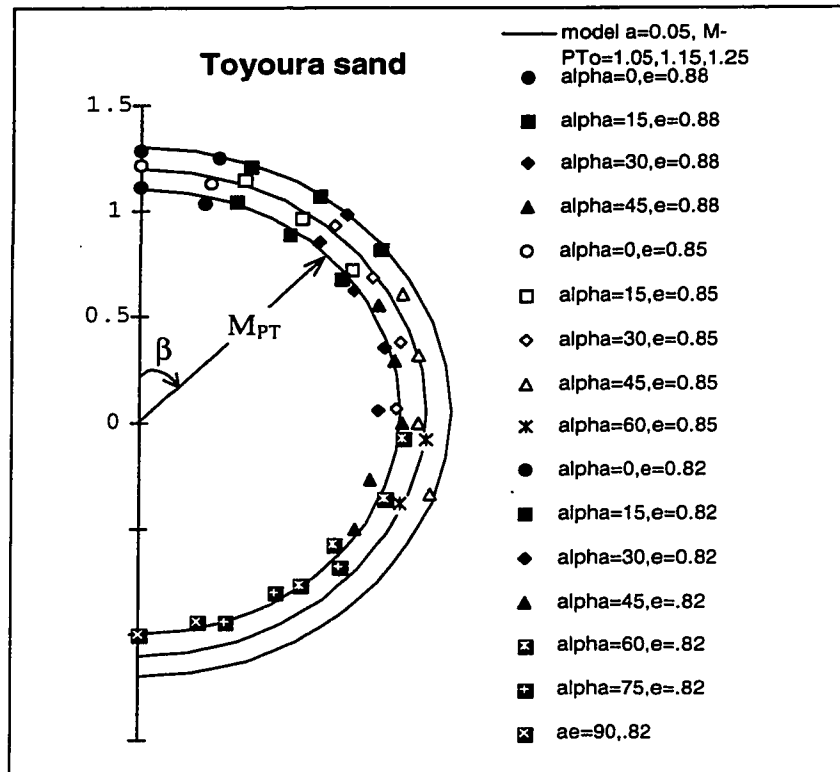


**Figure 4-27** Variation of stress ratio at Phase Transformation ( $M_{PT}$ ) with  $\beta$  (data measured from Yoshimine, 1996)

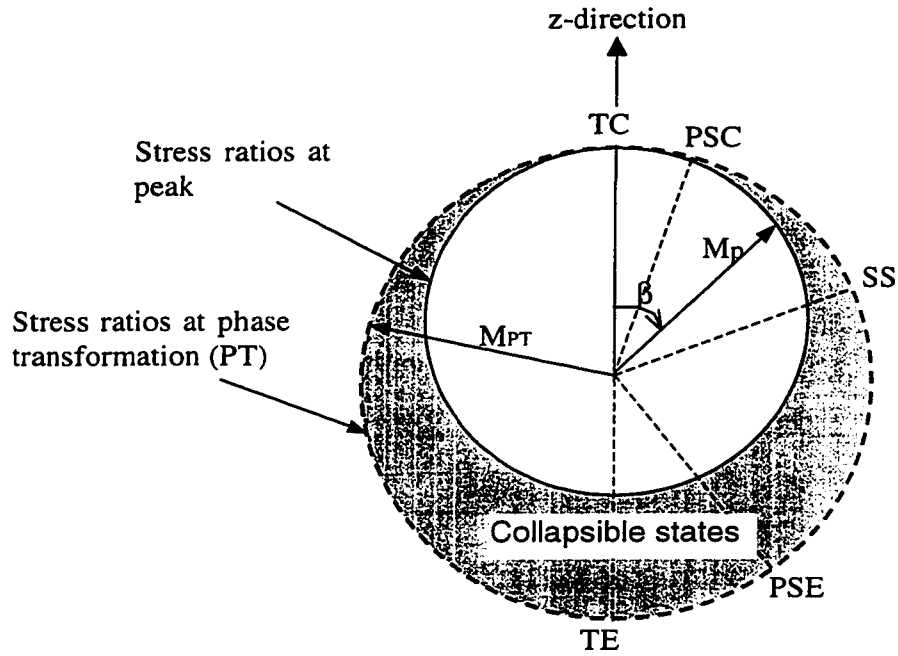
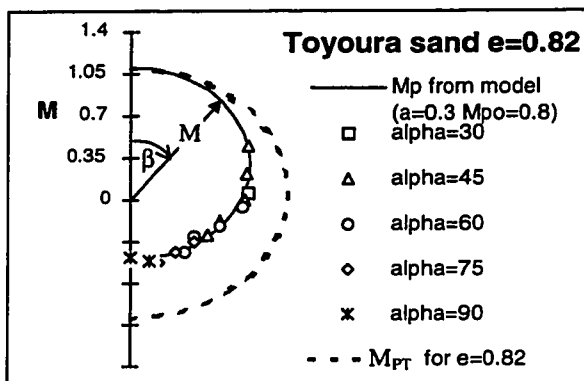
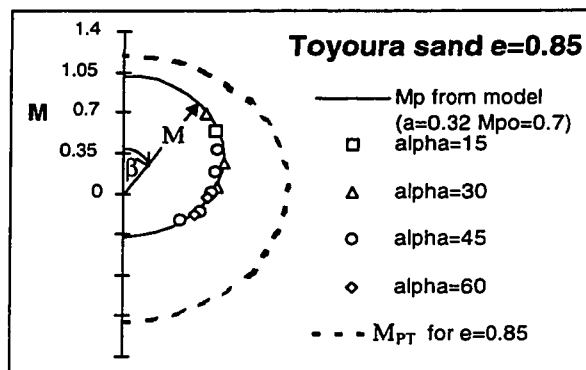


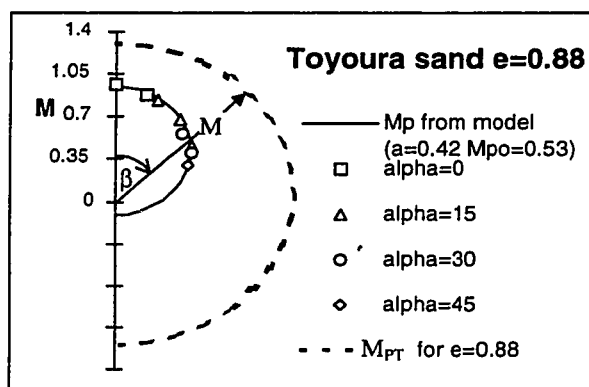
**Figure 4-28** Evaluation of the susceptibility of loose sand to collapse and flow failure when sheared in different modes



(a)



(b)



(c)

**Figure 4-29** Comparisons of regions of collapsible states for dry deposited Toyoura sand consolidated to 100 kPa and three different void ratios

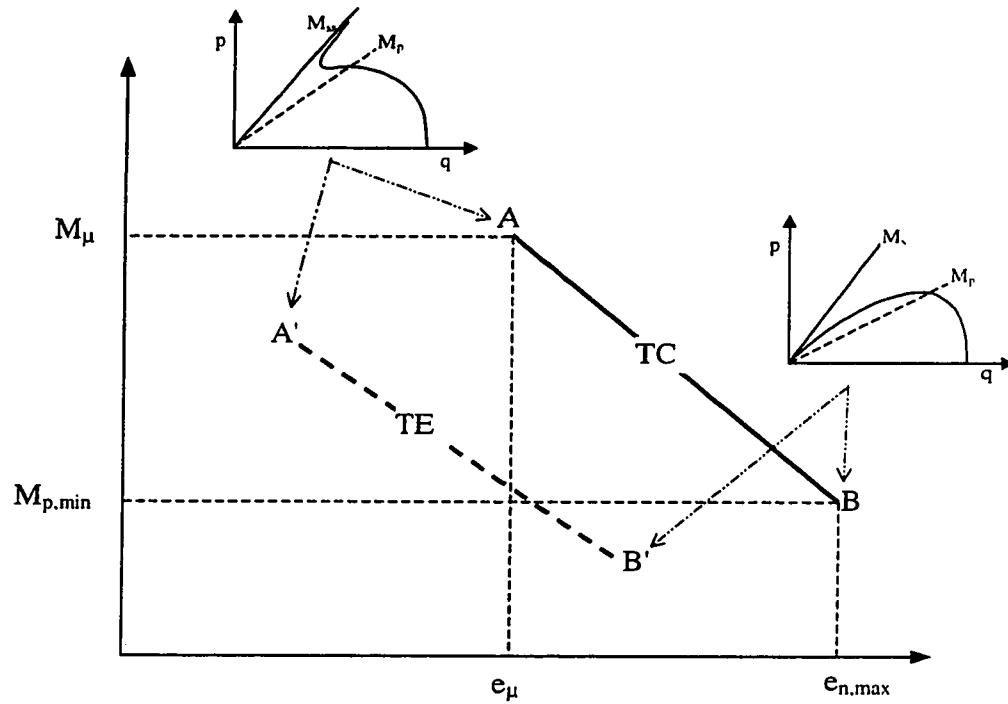


**Figure 4-30** Maximum and minimum values of  $M_p$  and undrained effective stress paths from which these values are measured. Normalized void ratios corresponding to these limiting values of  $M_p$  are also shown.

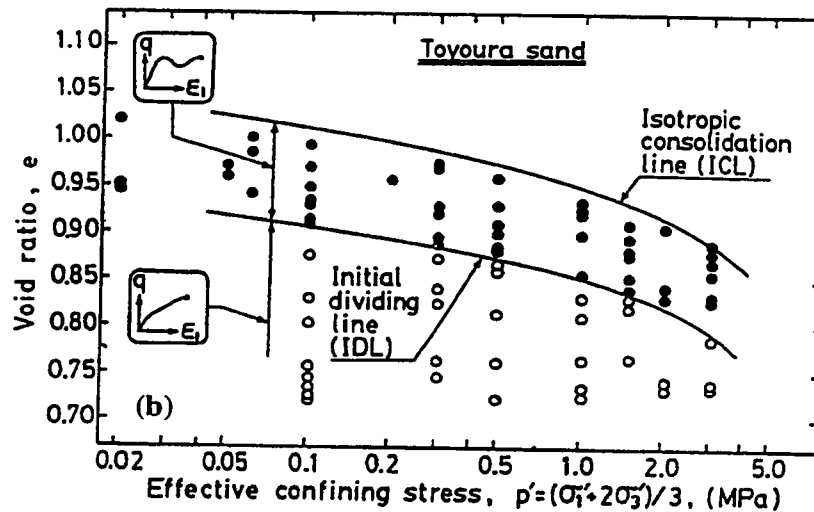
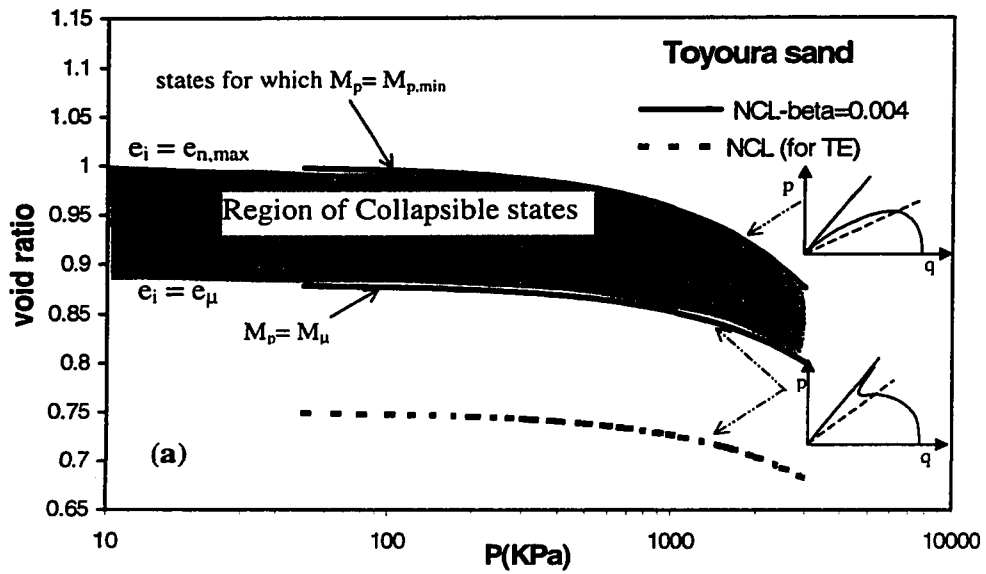


**Figure 4-31** Determination of combinations of void ratio and confining pressures at which sand is collapsible, from the variation of  $M_p$  with normalized void ratio. Note that the results shown above are obtained from triaxial compression tests on moist tamped samples (Figure (b) modified after Ishihara, 1993).

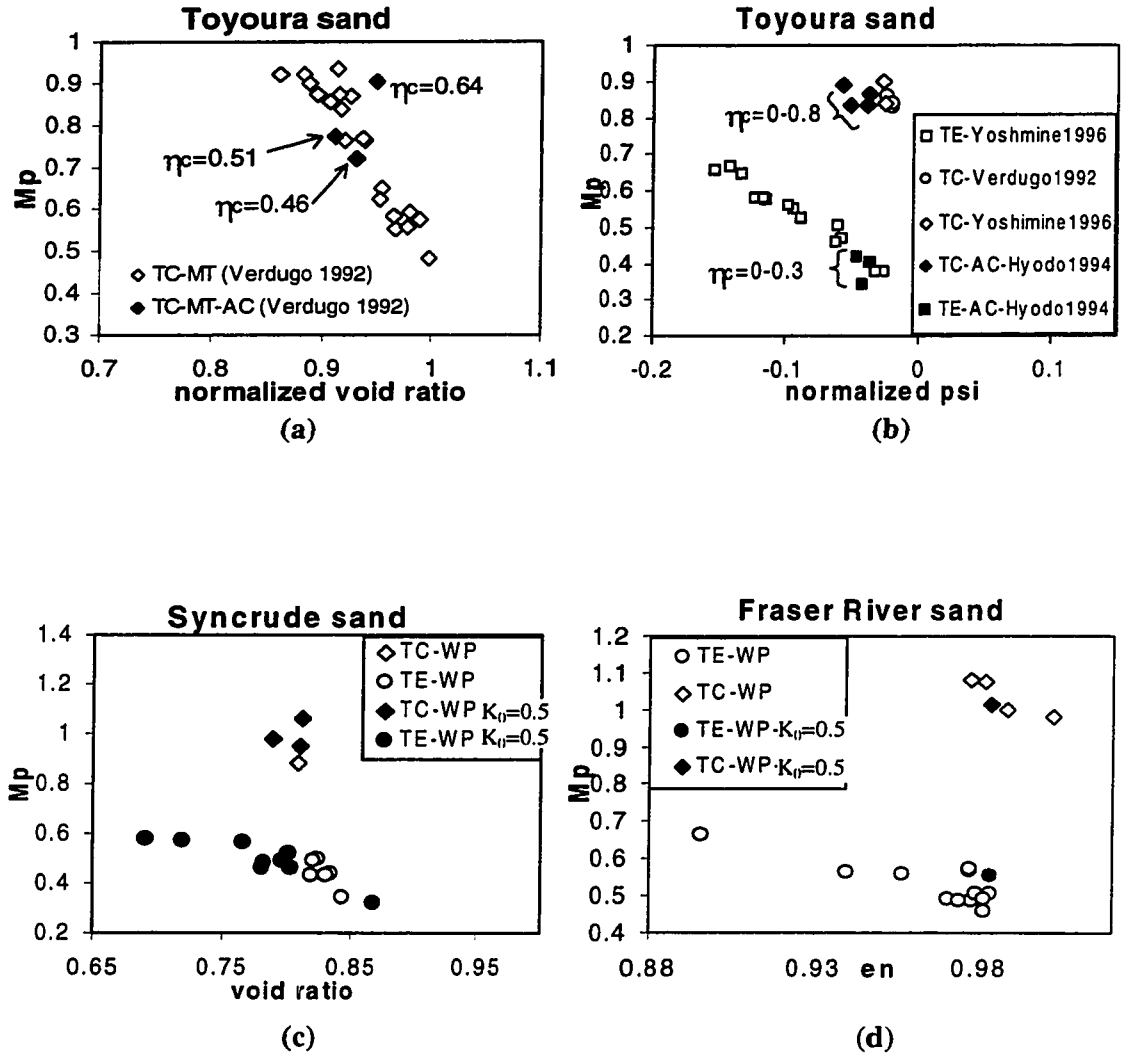


**Figure 4-32** Comparison between values of  $M_p$  measured from isotropically consolidated, and anisotropically consolidated sand (Syncrude sand data from Wride and Robertson, CANLEX report, 1997a; Fraser River sand data from Thomas, 1996)

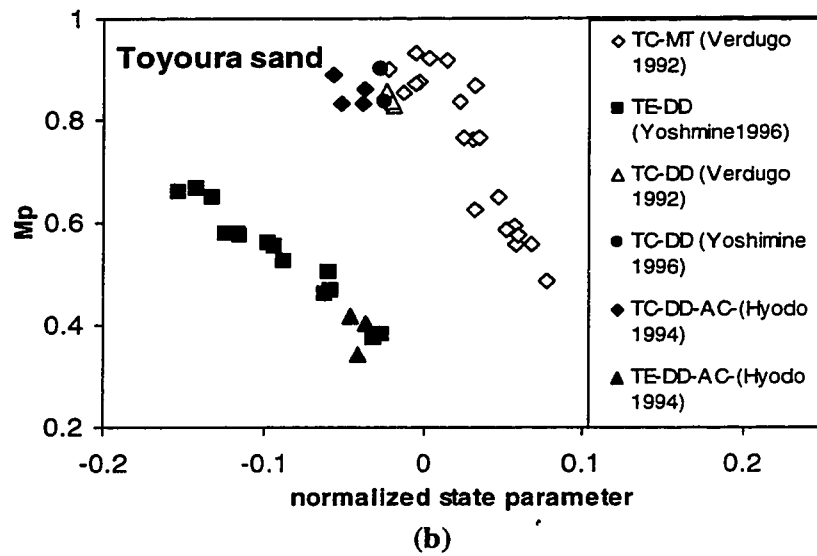
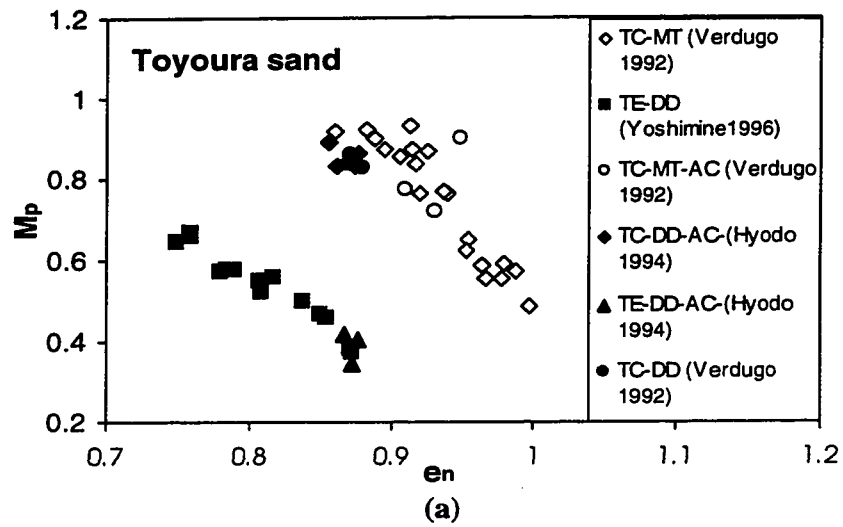
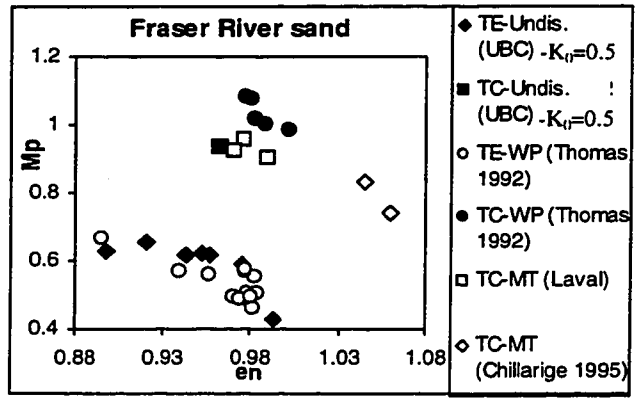
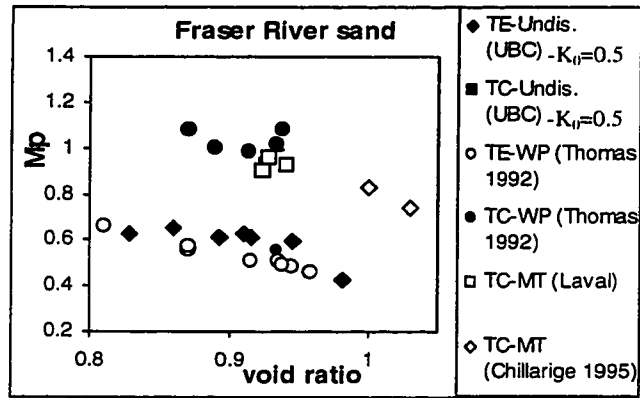


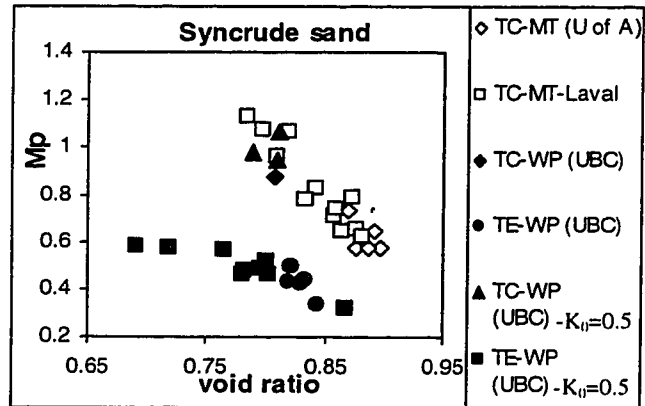
**Figure 4-33** Effect of soil fabric on the relationship between  $M_p$  and the normalized void ratio or normalized state parameter



(a)



(b)



(c)

Figure 4-34 Effect of soil fabric on the variation of  $M_p$  for two different sands



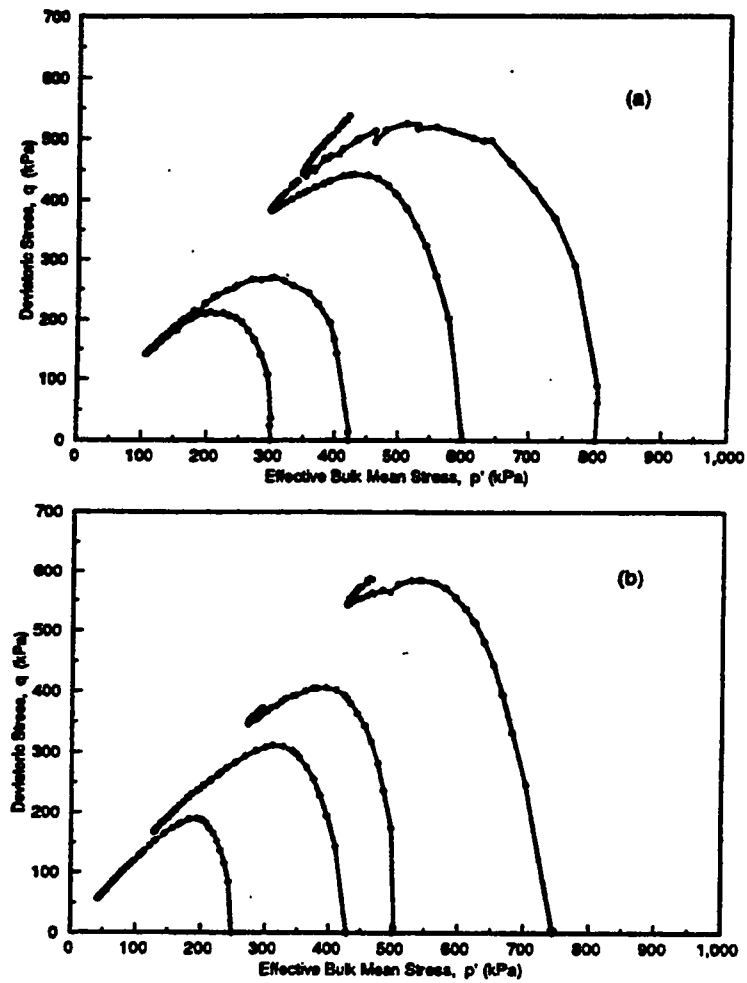


**Figure 4-35** Effect of preparation method on  $M_p$  measured from TC tests on moist tamped samples with different numbers of soil layers: (a) samples prepared using 6-lifts (b) samples prepared using 12-lifts (modified after Riemer, 1992)

## **Appendix 4A: Micromechanical phenomena involved in yielding**

### **4A-1 Shape of the yield surface and its relationship to the mechanisms involved in yielding**

Yielding of soils is the process of experiencing irrecoverable (plastic) deformations and a yield surface determines combinations of stresses that cause the material to be on the verge of experiencing such deformations. Any mechanism leading to such deformations should be taken into consideration once the yield surface is established. Different stress combinations may lead to different deformation mechanisms but all should be included once the yield surface is established for a material.

In explaining the origin of plastic deformation of sand, Rowe (1971) pointed out that yielding under low shear stress level is mainly due to crushing of grains at particle contacts. However, as shear stress increases, gross sliding at particle contact becomes the dominant process.

Experimentally derived yield surfaces for granular soils, some of which reviewed in Chapter 2 (see e. g. Nova and Wood, 1978; Yasufuko et al. 1991a), can be divided into two portions. One is an ascending cap-shaped portion corresponding to small stress ratios  $\eta$ , and starting from the consolidation pressure. The other is a descending portion corresponding to high stress ratios (i. e. high friction angles), and starting from the peak value of shear stress. We will refer to the former portion as the "cap" and to the latter as the front portion (FP). Many earlier constitutive models (e. g. Lade, 1977; Vermeer, 1978) have used different relationships to define the two portions, while recent models (see Chapter 2) have often used a single equation to define both portions. In the yield surface used in the current study, the stress ratio  $M_p$  determines the stress condition at which these two portions are separated from each other.

In the following sections, the shape of the yield surface and the variation of  $M_p$  obtained from experiments are examined with regard to the deformation mechanisms contributing to the yielding process of sand.

#### 4A-2 Small strain yielding at low shear stress levels

When the level of shear stress at a point of particle contact is small, gross slippage cannot occur between particles since the mobilized shear stresses are not sufficient to overcome the frictional resistance of the contact. However, small slip can occur at such contacts because of one or both of the reasons that are described below.

For the angle of inter-particle friction to be fully mobilized in a contact point, some relative slip is necessary in the contact region (Fig 4A-1-a). This has been seen both in single contacts (Billam, 1971) and in a mass of granular material (Matsuoka, 1974). In a particle contact that is on the verge of slippage under the applied stresses, any increase in stresses causes slippage in the contact. Therefore, if the shear stress is increased gradually from zero while the contact is kept on the verge of slip, the normal stress has to be reduced as the shear stress is increased, since the contact is not capable of mobilizing higher friction angles without experiencing further slip. This results in a semi-elliptical shape for the yield surface at shear stress levels at which this yielding mechanism is dominant.

On the other hand, it is generally noticed that the axial strain experienced by sand before the peak shear strength is reached under undrained loading increases with the increase in confining pressure, and the peak often occurs at relatively small strain (see e. g. Symes et al., 1984). The amount of strain to peak depends mainly on the confining pressure and the strength of the soil particles. In quartzic sand at normal ranges of pressures, this shear strain is a small fraction of a percent (Symes et al., 1984). In sand containing weak shale particles subjected to pressures as high as tens of Mega Pascals such strain can exceed one percentage of axial strain (see e. g. Lade et al., 1996). The

increase in strain with the decrease in soil strength and increase in confining pressure indicates the effect of breakage at particle contacts at such pressures. (Figure 4A-1-b). Nova and Wood (1978) showed that this mechanism also leads to a semi-elliptical form for the shape of the yield surface at small stress ratios.

Both mechanisms described above (i.e. the slippage required to mobilize the inter-particle friction and the breakage of grains at the contact region) result in a semi-elliptical shape for the yield surface in the  $p$ - $q$  plane at low shear stress levels. At lower pressures, the first mechanism is likely to be responsible for small strain yielding and as pressure increases, the effect of particle crushing becomes more dominant and the second mechanism is expected to govern the yielding process at small strain.

The semi-elliptical shape of yield surfaces obtained from experiment at stress ratios smaller than  $M_p$ , the small strains experienced before the peak is reached at stress ratio  $M_p$ , and the other observations reported above are all consistent with the notion that at stress ratios below  $M_p$ , sand experiences small strains caused by small inter-particle slip.

#### 4A-3 Large strain yielding at high shear stress levels

In a mass of granular soil, contact surfaces are inclined at different angles relative to the major principal stress, and states of stresses on these surfaces are different. At any instant, some contacts are subjected to smaller shear stress level while others experience gross inter-particle slip due to high shear stresses on the plane of slippage. As more and more contacts undergo gross slippage due to increased overall shear stress level, the behavior becomes increasingly governed by gross slippage and therefore, influenced by soil dilatancy. A transition zone therefore, exists where this change in the yielding mechanism occurs.

Experimentally derived yield surfaces, on the other hand, often start to bend as stress ratios increase until they reach a peak in the  $p$ - $q$  stress space (which occurs at stress

ratio  $M_p$  in the current formulation), after which they follow a descending trend that seems to be controlled by soil dilatancy.

The shear stress level required to initiate slippage at a frictional contact is a function of both the coefficient of friction between the contact surfaces (i. e. the inter-particle friction angle  $\varphi_\mu$  here), and the inclination of the slippage plane with respect to the applied stresses. Figure 4A-1-c shows that if the potential overall slippage is assumed to occur along the horizontal plane, the following relationship can be obtained from the equilibrium of forces at a single contact:

$$\frac{\tau}{\sigma_n} = \tan(\varphi_\mu + \theta) = \tan \varphi_m \quad 4A-1$$

in which  $\tau$  and  $\sigma_n$  are the shear and normal stresses acting along and normal to the potential slippage plane respectively,  $\varphi_\mu$  is the inter-particle friction angle, and  $\theta$  is the inclination of the inter-particle contact surface compared to the potential overall slippage plane. The value of  $\varphi_m = (\varphi_\mu + \theta)$  is the friction angle that should be mobilized along the potential slippage plane (here the horizontal plane) in order to initiate slippage. In a mass of granular material subjected to shear, the value of  $\theta$  is different for different contacts and only a small number of contacts are active and undergo slippage, others being in a condition less favourable for slippage and only transmit loads (Rowe, 1971; Oda, 1982). The effect of different  $\theta$  angles of the active contacts can be approximated by an equivalent angle of contact inclination  $\theta_e$  with respect to the potential plane of overall slippage. Therefore the overall friction angle that should be mobilized along the potential slippage plane will be  $\varphi_m = (\varphi_\mu + \theta_e)$ . In the case of a triaxial test, the stress ratio  $M_p$  required to mobilize this friction angle along the plane of overall slippage can be found from the following for TC:

$$M_{p,c} = \frac{6 \sin \varphi_m}{(3 - \sin \varphi_m)} = \frac{6 \sin(\varphi_\mu + \theta_e)}{3 - \sin(\varphi_\mu + \theta_e)} \quad 4A-2-a$$

If the same friction angle is mobilized in extension, the corresponding stress ratio for TE will be:

$$M_{p,e} = \frac{6 \sin \phi_m}{(3 + \sin \phi_m)} = \frac{6 \sin(\phi_\mu + \theta_e)}{3 + \sin(\phi_\mu + \theta_e)} \quad 4A-2-b$$

in which  $M_{p,c}$  and  $M_{p,e}$  are the stress ratios that should be mobilized in TC and TE respectively to initiate gross inter-particle slippage. In this case, a variation with state parameter such as that shown in Figure 4A-2-a is expected for  $M_{p,c}$  and  $M_{p,e}$  similar to that of soil strength (Figure 4A-2-b) observed from TC tests by Jefferies (1993). However, it was seen in Chapter 3 that in a real soil the friction angle at peak of the yield surface may not be the same in TC and TE, the difference being likely the result of the structural anisotropy of the soil. Differences in  $M_p$  in compression and extension were also observed in values measured from UESPs in Chapter 4.

#### 4A-4 Observed variation of $M_p$ and the micro-mechanical behavior of sand

The angle  $\theta_e$  in Equation 4A-2 is positive for sands with dilative tendencies and negative for contractive states. Dense sand or sand at negative  $\psi$  (i. e. dilative sand) is therefore expected to have positive values of  $\theta_e$  and loose sand consolidated to positive  $\psi$  will likely have negative values as shown in Figure 4A-1-c. Using Equation 4A-2 it may be concluded that the mobilized friction angle before the start of gross inter-particle slippage is smaller in loose sand (or sand consolidated to bigger  $\psi$ ) and larger in dense sand (or sand consolidated to smaller  $\psi$ ). All the data obtained from the different sands investigated in Chapter 4 (see e. g. Figure 4-3 and Figure 4-4) show such a trend.

From the above discussion, it is expected that at void ratios or states where no tendency for volume change exists (i. e. at  $\psi = 0$ ), the mobilized friction angle  $\phi_m$  should be close to  $\phi_\mu$  and the corresponding stress ratio be  $M_\mu$ .

Rowe (1962) measured values of  $\phi_\mu$  for Quartz sands and obtained friction angles in the range of 22-32 degrees depending on grain size with higher values for lower grain sizes. However, the majority of measurements reported elsewhere fall within a range of 23-26 degrees (Procter et al., 1974).

From Figure 4-4 it can be seen that values of  $M_p$  at  $\psi = 0$  obtained for the Quartz-based sands investigated lie between 0.85 and unity. Considering the values quoted above for  $\phi_\mu$  of Quartz, and using Equation 4A-2-a, a range of  $M_\mu$  between 0.9 and 1.03 for TC is obtained, which is close to the observed values of  $M_p$  at  $\psi = 0$ . It can also be seen from Figure 4-3 and Figure 4-4 that the variation is approximately linear for all the sands. This figure also shows that for very loose quartz sands,  $M_p$  may fall to values below 0.5 corresponding to a friction angle as low as 12 degrees that is significantly smaller than the values of  $\phi_\mu$  quoted earlier for quartzic sands.

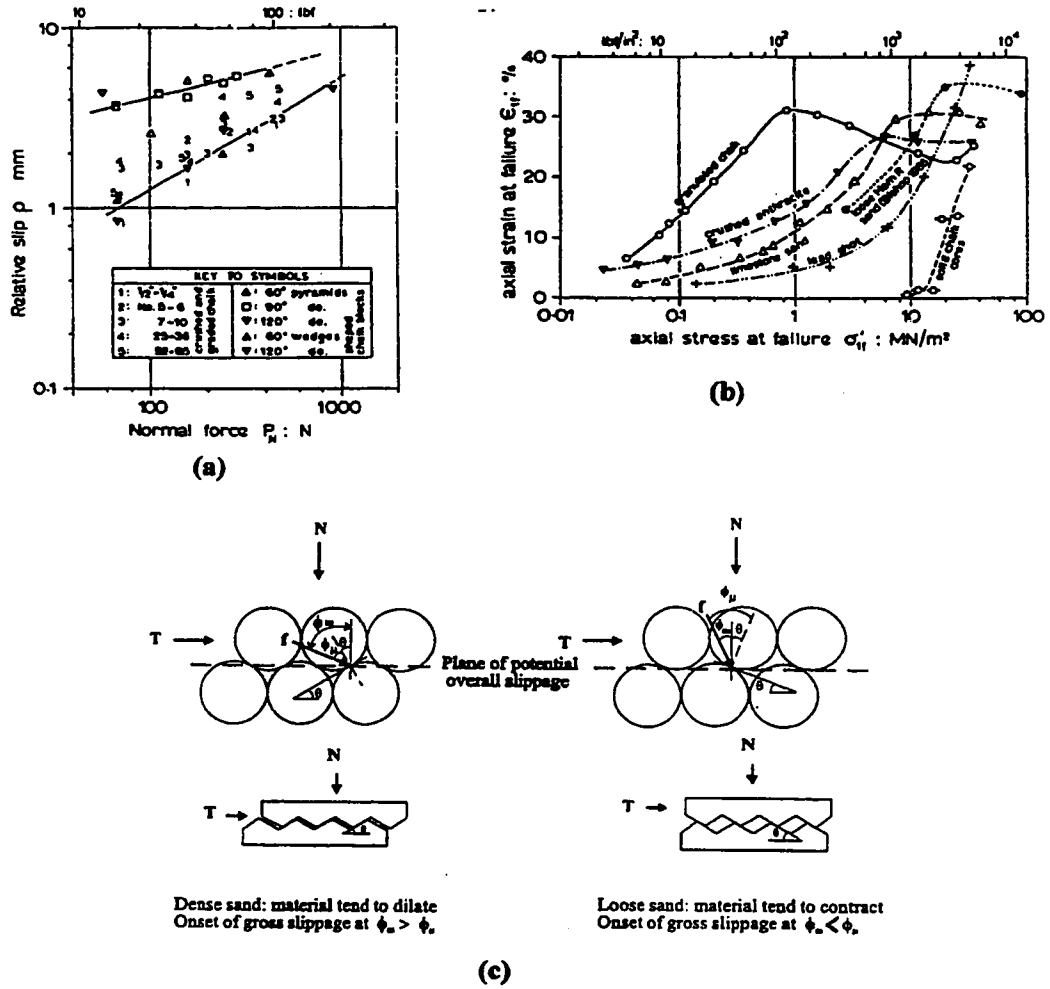


**Figure 4A-1** Aspects of the micro-mechanical behavior of granular materials in small strain: (a) Relative slip required to mobilize full inter-particle friction in chalk (b) Axial strain at failure as a function of axial stress at failure in drained TC tests for materials with different strength (c) Effect of density on the friction angle that should be mobilized ( $\phi_m$ ) along the plane of overall slippage, in order to initiate gross slippage at particle contacts ( $f$  is the inter-particle force and  $\theta$  is the angle of contact inclination) (a and b from Billam, 1971)



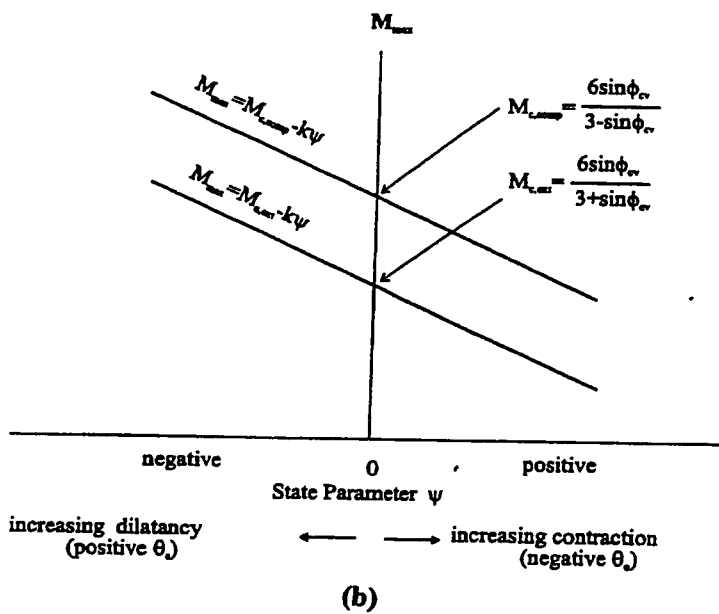
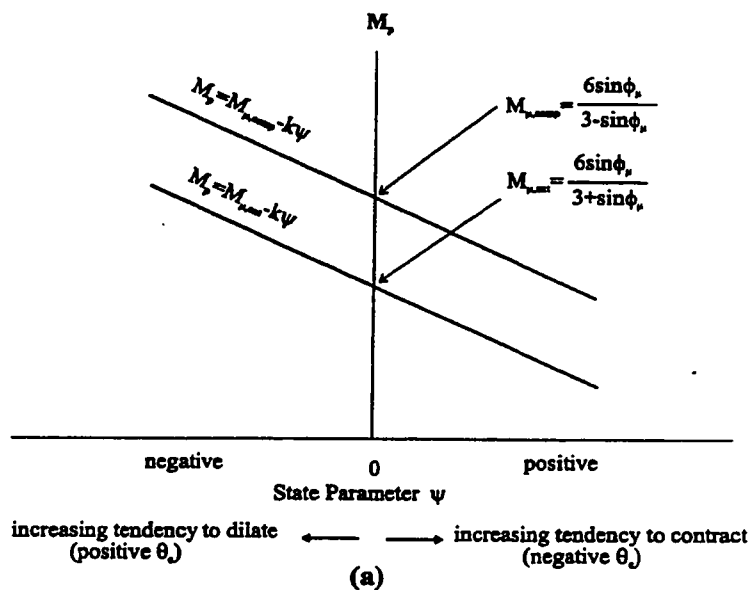


**Figure 4A-2** Variation of stress ratio at peak ( $M_p$ ) and at failure ( $M_{max}$ ) in triaxial compression (TC) and extension (TE) for an isotropic soil. Note that the slope  $k$  may not be the same in TC and TE.

## Appendix 4B Representation of the state of stress at peak in principal stress space

### 4B-1 Stress states in principal stress space

In principal stress space, a general state of stress represented by a vector  $OP = (\sigma_1, \sigma_2, \sigma_3)$  in Figure 4B-1-a can be decomposed into its hydrostatic part  $OB$  along the hydrostatic axis and deviatoric part  $BP$  in the octahedral plane:

$$OB = (p, p, p) \quad 4B-1$$

$$AP = (s_1, s_2, s_3) = (\sigma_1 - p, \sigma_2 - p, \sigma_3 - p) \quad 4B-2$$

in which  $s_1, s_2$  and  $s_3$  are components of the deviatoric stress along the three principal stress directions. Magnitude of these vectors and the direction of the deviatoric component in the octahedral plane can be calculated from the following equations:

$$|OB| = \sqrt{3} p = \sqrt{3} (\sigma_1 + \sigma_2 + \sigma_3) / 3 \quad 4B-3$$

$$|BP| = s = (2J_2)^{1/2} = \sqrt{3} [(\sigma_1 - \sigma_2)^2 + (\sigma_1 - \sigma_3)^2 + (\sigma_2 - \sigma_3)^2]^{1/2} \quad 4B-4$$

$$= [s_1^2 + s_2^2 + s_3^2]^{1/2} \quad 4B-5$$

$$\theta = \tan^{-1} \left[ \frac{\sqrt{3}(\sigma_2 - \sigma_3)}{2\sigma_1 - \sigma_2 - \sigma_3} \right] \quad 0 < \theta < 60 \quad 4B-6$$

in which  $| \quad |$  refers to magnitudes of vectors. The angle  $\theta$  is measured clockwise from the projection of the  $\sigma_1$  axis on the octahedral plane to the stress point in this plane. A value of  $\theta = 0$  corresponds to  $b = 0$  (as in TC) and  $\theta = 60$  degrees corresponds to  $b = 1$  (as in TE). The letter  $s$  (without subscript) is used here to refer to the magnitude of the vector of deviatoric stress. In general stress space, if components of deviatoric stresses are denoted by  $s_{ij}$ , the magnitude of the vector  $s$  can be obtained from:

$$s = (s_{ij}s_{ij})^{1/2} \quad 4B-7$$

States of stress in soil can be represented by either values of principal stresses  $\sigma_1$ ,  $\sigma_2$ ,  $\sigma_3$  or magnitudes of stress invariants  $p$ ,  $s$  and  $\theta$ . Test results are often expressed in terms of the first set (i. e. principal stresses), and yield-failure surfaces are usually formulated in terms of the second set (i. e. stress invariants). The second set can be obtained from the first set using Equations 4B-3 to 4B-6, and the first set are given in terms of the second set by the following equations:

$$\sigma_1 = \sqrt{\frac{2}{3}} s \cos \theta + p \quad 4B-8-a$$

$$\sigma_2 = \sqrt{\frac{2}{3}} s \cos (2\pi/3 - \theta) + p \quad 4B-9-b$$

$$\sigma_3 = \sqrt{\frac{2}{3}} s \cos (2\pi/3 + \theta) + p \quad 4B-10-c$$

In general stress space, stress ratio  $M_p$  can therefore be defined in terms of values of stress invariants at peak, in the following form:

$$M_p = \frac{q}{p} = \sqrt{\frac{3}{2}} \frac{s_p}{p_p} \quad 4B-11$$

Note that the generalized value of  $q$  (and not the stress difference  $q' = \sigma_1 - \sigma_3$ ) is used in the above definition. This generalized value is related to  $s$  in general stress space, and also to principal stresses, by the following equation:

$$q = \sqrt{\frac{3}{2}} s = \left[ \frac{1}{2} \left( (\sigma_1 - \sigma_2)^2 + (\sigma_1 - \sigma_3)^2 + (\sigma_2 - \sigma_3)^2 \right) \right]^{1/2} \quad 4B-12$$

All definitions presented here for  $M_p$  give a positive value for this stress ratio that is the magnitude of a generalized tensorial form of this quantity that will be defined in Chapter 6.

## 4B-2 Variation of strength on the octahedral plane

A "reference octahedral plane" (ROP) (Figure 4B-1-b). was defined in Chapter 4 to facilitate the representation of stress ratios  $M_p$  in principal stress space. Changes of  $M_p$  in this plane can be formulated in terms of a function  $g(\theta)$  that defines the variation of  $M_p$  with  $\theta$  (Equation 4B-6) such that:

$$M_p = M_{p,c} g(\theta_p) \quad 4B-13$$

in which  $M_{p,c}$  is the value of  $M_p$  at TC where  $b = 0$ , and the function  $g(\theta)$  defines the variation of stress ratio at peak with  $\theta$  (or  $b$ ). It was shown in Chapter 4, that this variation is similar to that of strength at failure. It is useful, therefore, to obtain the function  $g(\theta)$  that corresponds to the well-known failure criteria represented by Equations 4-20 and 4-21.

For the Mohr-Coulomb criteria, the following variation is obtained for  $g(\theta)$ , if the friction angle at failure is assumed to be  $\varphi$ :

$$g(\theta) = \frac{\sqrt{2} \sin \varphi}{\cos \theta \sin \varphi - \sqrt{3} \sin \theta} \quad 4B-14$$

For the L-D and M-N criteria defined by Equations 4-21-b and 4-21-c, a more elaborate procedure is required to obtain this function. Jiang and Pietrusczak (1988) showed that  $g(\theta)$  takes the following form in these two cases:

$$g(\theta) = \frac{\cos\left[60 - \frac{1}{3} \cos^{-1} A\right]}{\cos\left[60 - \frac{1}{3} \cos^{-1}(A \cos 3\theta)\right]} \quad \text{for } \cos 3\theta \geq 0 \quad 4B-15-a$$

$$= \frac{\cos\left[60 - \frac{1}{3} \cos^{-1} A\right]}{\cos\left[\frac{1}{3} \cos^{-1}(-A \cos 3\theta)\right]} \quad \text{for } \cos 3\theta \leq 0 \quad 4B-15-b$$

Parameter A in the above equations depends on the failure criteria chosen and can be obtained from the following relationships:

$$A_L = \sqrt{\frac{C_{L-D} - 27}{C_{L-D}}} \quad \text{and} \quad C_{L-D} \geq 27 \quad 4B-16-a$$

$$A_M = \sqrt{\frac{C_{M-N}^2 (C_{M-N} - 9)}{(C_{M-N} - 3)^3}} \quad \text{and} \quad C_{M-N} \geq 9 \quad 4B-16-b$$

The function  $g(\theta)$  has the following properties:

$$g(0) = 1 \quad 4B-17-a$$

$$g(60) = c = \frac{M_{p,e}}{M_{p,c}} \quad 4B-17-b$$

in which  $M_{p,c}$  and  $M_{p,e}$  are stress ratios at peak in TC and TE respectively. The ratio  $c$  can be calculated from the parameter A (or vice versa) as follows:

$$c = \frac{1}{2} + \frac{\sqrt{3}}{2} \tan\left(\frac{1}{3} \cos^{-1} A\right) \quad 1 \leq c \leq 1/2 \quad 4B-18$$

$$A = \cos \left[ 3 \tan^{-1} \left( \frac{2R-1}{\sqrt{3}} \right) \right] \quad 4B-19$$

Values of  $C_{L-D}$  or  $C_{M-N}$  can be obtained from the mobilized friction angle in TC,  $\varphi_c$ , as follow (Griffiths, 1990):

$$C_{L-D} = \frac{(3 - \sin \varphi_c)^3}{(1 + \sin \varphi_c)(1 - \sin \varphi_c)^2} \quad 4B-20-a$$

$$C_{M-N} = \frac{9 - \sin^2 \varphi_c}{1 - \sin^2 \varphi_c} \quad 4B-20-b$$

For a given friction angle in TC, the variation of strength with  $\theta$  or  $b$  can therefore be obtained from the L-D or M-N criteria from Equation 4B-15.

### 4B-3 Accounting for anisotropy of yield-failure strength

In anisotropic soils, the center of the yield curves in the octahedral plane may shift in the direction of anisotropy. Equations for the shifted yield curves can be obtained by substituting the shifted coordinates for the original coordinates in the yield-failure equations discussed previously. If the vector defining the amount of shift is  $a$  ( $a_1, a_2, a_3$ ) (refer to Chapter 4), we will have:

$$\bar{s}_i = s_i - a_i \quad \text{and} \quad i = 1-3 \quad 4B-21$$

$$\bar{s} = [\bar{s}_1^2 + \bar{s}_2^2 + \bar{s}_3^2]^{1/2} \quad 4B-22$$

$$\bar{M}_p = \sqrt{\frac{3}{2}} \frac{\bar{s}_p}{p_p} \quad 4B-23$$

in which variables with a bar refer to modified stress variables. The angle  $\theta_p$  used in Equation 4B-13, should be replaced by  $\bar{\theta}_p$ , which is calculated by using the modified values of the invariants of deviatoric stress:

$$\bar{\theta} = 30 - \frac{1}{3} \sin^{-1} \left( \frac{-3\sqrt{3}}{2} \frac{\bar{J}_3}{\bar{J}_2^{3/2}} \right) \quad 0 \leq \bar{\theta} \leq 60 \quad 4B-24$$

$$\bar{J}_3 = \bar{s}_1 \bar{s}_2 \bar{s}_3 \quad 4B-25$$

$$\bar{J}_2 = \frac{1}{2} (\bar{s}_1^2 + \bar{s}_2^2 + \bar{s}_3^2) \quad 4B-26$$

$$\bar{M}_p = M_{p0} g(\bar{\theta}_p) \quad 4B-27$$

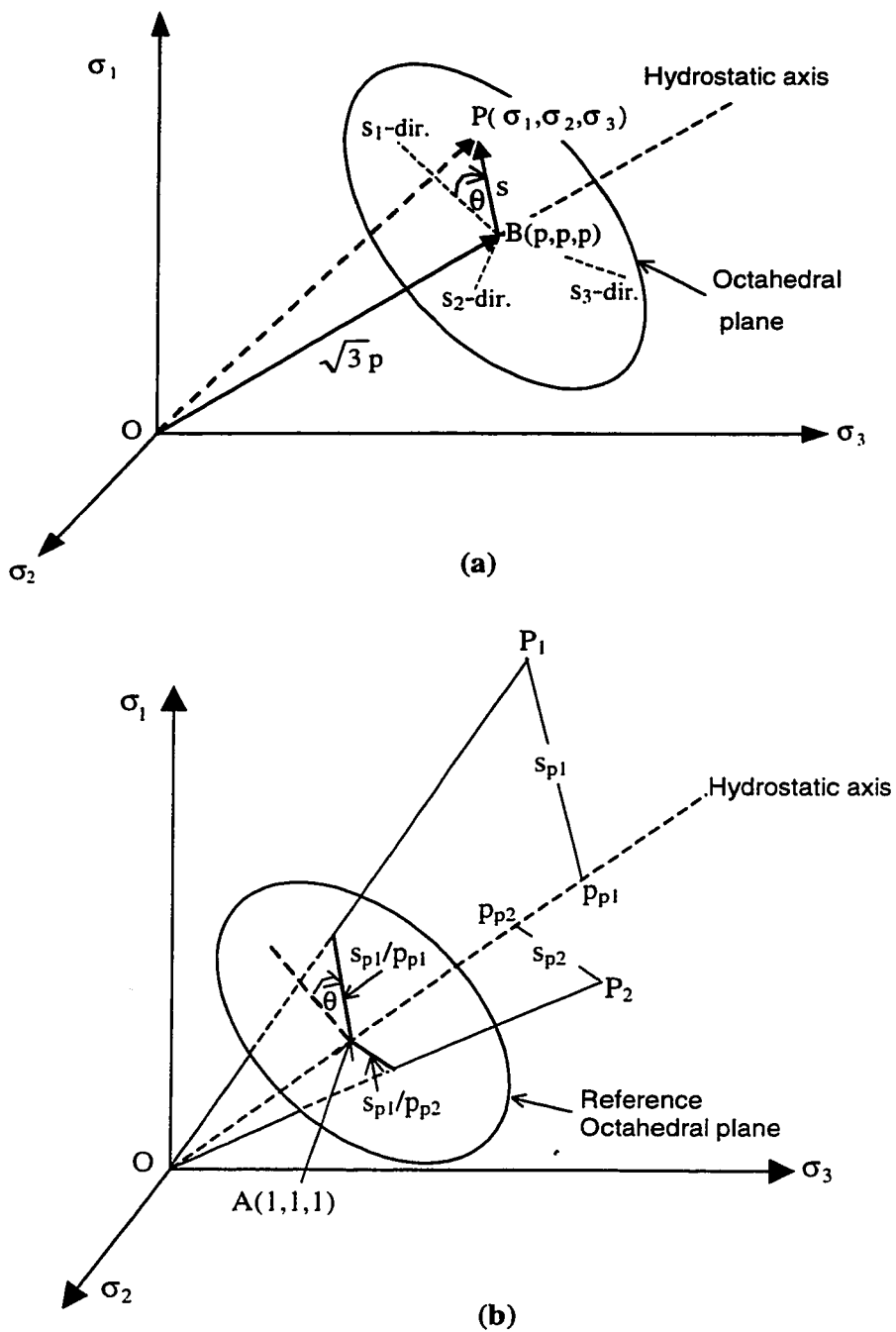


**Figure 4B-1** The "reference octahedral plane" (ROP) in principal stress space and representation of stress states at peak on this plane



## Chapter 5

# **5 A critical state constitutive model for sand**<sup>1,2</sup>

## **5.1 Introduction**

Some shortcomings of existing constitutive models for sands were discussed in Chapter 2. A constitutive model for sands has been developed in an attempt to overcome these shortcomings using a single formulation. The model is presented for monotonic loads in a triaxial stress framework in this chapter. Formulation of the model for general stress conditions will be presented in the next chapter.

The main characteristics of the model can be listed as follows:

1-A capped shape for the yield surface of sand is employed which is a function of void ratio, consolidation stresses and direction of loading. This shape was checked directly against the actual yield behavior of loose and dense sand consolidated isotropically and anisotropically. Yield parameters were related to the response of sand observed in conventional triaxial tests. The use of a precise shape for the yield surface

---

<sup>1</sup> Parts of this chapter were published: Imam, R., Robertson, P. K., Chan, D. H., and Morgenstern, N. R. 1998. "Constitutive modeling of loose collapsible soils" Proceedings of the 51st Canadian Geotechnical Conference, Edmonton, Alberta, Canada.

<sup>2</sup> Parts of this chapter were published: Imam, R., Chan D. H., Robertson, P. K., and Morgenstern, N. R. 1998. "Effect of loading direction on the constitutive behavior of sands". Proceedings of the 51st Canadian Geotechnical Conference, Edmonton, Alberta, Canada.

ensures accurate prediction of the behavior of sand at different densities, especially at their very loose states of packing, where they can exhibit collapsive behavior.

2-Differences in the yielding of sand resulting from loading them in different directions are captured through a stress ratio  $M_p$ . This stress ratio is measured directly from the undrained effective stress path (UESP) of sand, sheared while at a contractive state. The stress ratio is used to account for the effects of density, pressure and direction of loading on the yielding of sand. It was shown in Chapters 3 and 4 that the position and movement of the yield surface can be traced using this stress ratio.

3- A single set of model parameters is used to predict responses of sand at a wide range of densities and consolidation stresses, subjected to loading in different directions. A unique ultimate state line is used in the model regardless of the direction of loading. Model parameters are related to the fundamental and well-established concepts of soil strength and deformability. They can be measured readily from routine tests and have clear physical meanings. The variations and physical meaning of the parameter  $M_p$  introduced in this study were examined in Chapters 3 and 4, using a large database consisting of results of tests on different sands subjected to a variety of loading conditions, obtained from different laboratories.

4-It was noticed that the friction angle at phase transformation (PT) is not always equal to that at the ultimate state. It is shown in this study that this can also be derived from Rowe's (1962) stress-dilatancy relationship, in which a variable friction angle  $\phi_f$  was used to calculate the dilatancy coefficient  $K$  (Equation 5-5). In the current study, a simple linear dependency of  $\sin\phi_f$  (denoted here by  $\sin\phi_{PT}$ ), on the state parameter is adopted, and is shown to approximate experimental results reasonably. This allows for the comparison of the behavior in TC and TE with a single stress variable that is independent of the intermediate principal stress, and is preferred over the dependency of the stress ratio  $q/p$  on the state parameter.

5-The maximum friction angle attainable at failure is assumed to depend on the current state parameter (Been and Jefferies, 1985). This dependency was formulated by Wood et al. (1994) as a linear relationship between stress ratio  $q/p$  at failure and the state parameter. Different modeling configurations (e. g. Wood et al., 1994; Imam, 1996; Manzari et al., 1997) have used this relationship, sometimes with some modifications. Similar to other strength-related parameters, the value of  $\sin\phi$  at failure is related linearly to the state parameter, in the current formulation.

## 5.2 Model elements

In this section, each element of the constitutive model is discussed separately for triaxial conditions. Relationships given in Appendix 5A can be used together with the model elements given in this section to obtain the stress-strain relationship.

### 5.2.1 The yield surface

It was shown in Chapter 3 that the yield surface of isotropically consolidated sand can be written in the following form in  $p$ - $q$  stress plane:

$$\eta^2 - 5M_p^2(1-(p/p_c)^{1/2}) = 0 \quad 5-1$$

where  $\eta = q/p$  is the current ratio of the deviatoric stress  $q = (\sigma_1 - \sigma_3)$ , to the mean normal stress  $p = (\sigma_1 + \sigma_2 + \sigma_3)/3$ ;  $M_p$  is the ratio  $q/p$  at the point where the peak value of  $q$  occurs, and  $p_c$  is the consolidation pressure.

It was shown in Chapter 3 that for contractive sand, the stress ratio  $M_p$  in the above equation can be approximated by the stress ratio at the peak point of the UESP. The variation of  $M_p$  can be related linearly to void ratio when a limited range of pressures (e. g. between 100 to 500 kPa) is involved, and to the normalized void ratio ( $e_n$ ) when a wider range is considered. For a consolidation void ratio ( $e_c$ ) and consolidation pressure

( $p_c$ ), the normalized void ratio ( $e_n$ ) is obtained by moving along the current normal consolidation line to a reference pressure  $p_r$  (see Chapter 4). Determination of  $e_n$  from  $e_c$  and  $p_c$  using sand compressibility will be further explained later.

Variation of stress ratio  $M_p$  in TC can be obtained from the variation of the mobilized friction angle at peak ( $\phi_p$ ) in TC, that is related to  $e_n$  through the following equation:

$$\sin\phi_{p,c} = \sin\phi_\mu - k_p (e_n - e_\mu) \quad 5-2$$

where  $\phi_\mu$  and  $\phi_{p,c}$  are the inter-particle and the peak friction angles respectively, measured from TC tests;  $e_\mu$  is the normalized void ratio corresponding to  $\phi_\mu$ ;  $e_n$  is the current normalized void ratio, and  $k_p$  is a material parameter. Note that  $\sin\phi$  is used in this chapter instead of  $\tan\phi$  used in Chapter 4, since it can be related to stress ratios more conveniently.

On the extension side, values of  $\sin\phi_p$  were smaller for the same normalized void ratio, compared to those of TC, the difference being nearly constant regardless of values of  $e_n$ . Equation 5-2, therefore, can be written in the following form for TE:

$$\sin\phi_{p,e} = \sin\phi_\mu - a_p - k_p (e_n - e_\mu) \quad 5-3$$

where  $a_p$  is a material parameter related to the inherent anisotropy of the soil.

For anisotropically consolidated sand, it was shown in Chapter 3, that Equation 5-1 for the yield surface takes the following form:

$$f = (\eta - \alpha)^2 - M_\alpha^2 \left[ 1 - \left( \frac{P}{P_c} \right)^{\frac{1}{2}} \right] = 0 \quad 5-4-a$$

$$M_\alpha^2 = 5M_p^2 - 6\alpha M_p + \alpha^2 \quad 5-4-b$$

in which  $\alpha$  is the stress ratio  $q/p$  at consolidation and  $M_\alpha^2$  is the equivalent of  $5M_p^2$  in Equation 5-1 for an anisotropically consolidated sand. Figure 5-1 compares shapes of yield surfaces of samples of sand consolidated to the same mean normal stress  $p_c$ , and having the same void ratio, but subjected to different consolidation stress ratios  $\eta_c$ .

## 5.2.2 The plastic potential

### 5.2.2.1 Pressure and density dependence of stress-dilatancy derived from Rowe's relationship

Rowe's (1962) stress-dilatancy relationship can be written as:

$$R = KD \quad \text{in TC} \quad 5-5-a$$

$$R = K/D \quad \text{in TE} \quad 5-5-b$$

in which  $R = \frac{\sigma_1}{\sigma_3}$ ;  $K = \tan^2 ( 45 + \varphi_f/2 )$  is a material parameter with  $\varphi_\mu < \varphi_f < \varphi_{cv}$ ;  $\varphi_\mu$  and  $\varphi_{cv}$  are the inter-particle and constant volume friction angles respectively;  $D = ( 1 - \frac{d\varepsilon_v}{d\varepsilon_1} )$  is the dilatancy parameter with  $d\varepsilon_v$  and  $d\varepsilon_1$  being increments of volumetric and major principal strains respectively.

Based on the analysis of a large number of stress-dilatancy data, Rowe (1969) reported that  $\varphi_f$  varies as follows:

- i) In sand at its densest state, up to peak stress ratio (failure)  $\varphi_f = \varphi_\mu$
- ii) In sand at its loosest state, at peak strength (which is its critical state)  $\varphi_f = \varphi_{cv}$
- iii) In all cases in which  $\varphi_f < \varphi_{cv}$  at peak strength (i. e. in tests on sand at states other than at the loosest state)  $\varphi_f$  increases to  $\varphi_{cv}$  from peak to critical state

In the context of critical state soil mechanics, assuming a constant value for  $\varphi_f$ , equal to the critical state (or constant volume) friction angle  $\varphi_{cv}$ , Wood (1990) formulated Rowe's stress-dilatancy relationship for the case of TC as follows:

$$d = \frac{d\varepsilon_p}{d\varepsilon_q} = \frac{9(M_{c,c} - \eta)}{9 + 3M_{c,c} - 2M_{c,c}\eta} \quad \text{for TC} \quad 5-6-a$$

Following a procedure similar that of Wood (1990) leads to the following relationship for TE:

$$d = \frac{d\varepsilon_p}{d\varepsilon_q} = \frac{9(M_{c,e} - \eta)}{9 - 3M_{c,e} - 2M_{c,e}\eta} \quad \text{for TE} \quad 5-6-b$$

where  $d$  is the rate of sand dilatancy;  $d\varepsilon_p = d\varepsilon_1 + 2d\varepsilon_3$  and  $d\varepsilon_q = 2(d\varepsilon_1 - d\varepsilon_3) / 3$ , with  $d\varepsilon_1$  and  $d\varepsilon_3$  being the major and minor strain increments;  $M_{c,c}$  and  $M_{c,e}$  are stress ratios  $q/p$  at the critical state in TC and TE respectively, and  $\eta$  is the current stress ratio.

Numerous results reported by Rowe (1962, 1969) showed that a value of  $\varphi_f$  varying between  $\varphi_\mu$  and  $\varphi_{cv}$  gives a realistic soil stress-dilatancy relationship. This variation in  $\varphi_f$  usually involves a range of about 6 to 7 degrees (Horne, 1965; Rowe, 1969). Such a range can cause non-negligible differences in the predicted soil dilatancy, especially in the case of dense sand.

In constitutive modeling of sand, fixing the angle  $\varphi_f$  to a value equal to that of the steady state (constant volume) is more convenient, and may result in acceptable stress-dilatancy relationships for certain soil states. This is particularly true if calibration for other model parameters can compensate for possible changes in  $\varphi_f$ . This, in addition to the difficulty of determination of the variations of  $\varphi_f$  with soil state or density seem to be the reason for using a constant value for this angle by the majority of current models. However, when the behavior of sand over a wide range of states is modeled using a

unique set of parameters, it will not be possible to adjust model parameters according to soil state or density. In such cases, neglecting variations of  $\phi_f$  may result in significant deviations of the predicted behavior from the observed response. In the current model, therefore, a variable value will be used for  $\phi_f$ , and the difficulty of the determination of its variations with soil state or density will be resolved by relating it to the friction angle at phase transformation (PT) (Ishihara, 1975). The following paragraphs explain this procedure.

If a variable value is used for  $\phi_f$ , the constant stress ratios  $M_{c,c}$  and  $M_{c,e}$  that appear in Equation 5-6 will have to be replaced by the variable stress ratios  $M_{f,c}$  and  $M_{f,e}$  (following Rowe's terminology for  $\phi_f$ . Note that based on the discussion that will follow, the subscript "f" will be replaced by "PT", and "f" will be reserved to refer to the "failure" condition later). These stress ratios can be obtained from  $\phi_f$  as follows:

$$M_{f,c} = \frac{6 \sin \phi_f}{3 - \sin \phi_f} \quad \text{for TC} \quad 5-7-a$$

$$M_{f,e} = \frac{6 \sin \phi_f}{3 + \sin \phi_f} \quad \text{for TE} \quad 5-7-b$$

From the values quoted above from Rowe (1969) for  $\phi_f$ , it can be concluded that this angle depends on sand density, as well as the proximity of the state of the sand to its ultimate (critical) state condition. Also regardless of the state at which shearing starts, the value of this angle converges towards  $\phi_{cv}$  when the steady state is reached.

The stress ratios  $M_{f,c}$  and  $M_{f,e}$  can be estimated by noting that from Equation 5-6, the rate of dilation  $\frac{d\varepsilon_p}{d\varepsilon_q}$  vanishes when:

$$\eta = M_{f,c} \quad \text{in TC} \quad 5-8-a$$

$$\eta = M_{f,e} \quad \text{in TE} \quad 5-8-b$$

Except for states in which the sand remains contractive up to the steady state, the condition of zero dilatancy occurs twice in a normal shearing process: once temporarily at an earlier stage of shearing, when the condition of PT is reached, and the other at the ultimate (steady) state when the soil continues to shear at constant volume.

At the steady state we always have  $\phi_f = \phi_{cv}$ , according to Rowe (1962) and subsequent observations (e. g. Ishihara, 1993). To obtain the variation of  $\phi_f$ , therefore, the stress ratio  $\eta$  or the friction angle  $\phi$  should be measured when the condition of PT is reached. The stress ratio and friction angle at PT will be denoted here by  $M_{PT}$  and  $\phi_{PT}$  respectively. Note that for any friction angle  $\phi_{PT}$  corresponding to a certain soil state, the equivalent stress ratio  $M_{PT}$  depends on the intermediate principal stress as was shown in Equation 5-7 for TC and TE. Therefore, it was found preferable to relate variations of  $\phi_{PT}$  or  $\sin\phi_{PT}$  rather than  $M_{PT}$  to the void ratio or state of sand.

Figure 5-2 -a shows the variation of  $\sin\phi_{PT}$  with void ratio measured from undrained TC and TE tests on Toyora sand. Except for three data points that were measured from tests with a consolidation pressure of 3000 kPa, the rest of the data were from tests at consolidation pressures not more than 1000 kPa. It can be seen that as long as the consolidation pressure was within a certain limit (e. g. below 1000 kPa), there was a clear relationship between  $\sin\phi_{PT}$  (i. e.  $\sin\phi_f$ ), and void ratio. The corresponding friction angles varied from about 24 degrees ( $\cong \phi_{\mu}$  for quartz based sands) for the denser samples to about 31 degrees ( $\cong \phi_{cv}$  reported for Toyoura sand e. g. by Ishihara, 1993) for the looser samples. This is consistent with the observations reported by Rowe (1962) mentioned above. Evidence of such dependency has also been reported elsewhere (see e. g. Farouque et al., 1991). For the tests under higher consolidation stresses, the angles decreased and deviated from the above trend.

Figure 5-2-b shows the same data described above plotted against the state parameter (Been and Jefferies, 1985) at PT instead of the void ratio. It can be seen that the effect



of pressure was normalized, and all the data from TC tests followed nearly the same trend. Values of  $\sin\phi_{PT}$  were smaller for negative state parameters, but converged approximately to  $\sin\phi_{cv}$  at  $\psi = 0$ . It may be noticed, however, that values of  $\sin\phi_{cv}$  measured at  $\psi = 0$  from TC and TE tests, were not the same.

The variation of  $\sin\phi_{PT}$  with  $\psi$  shown in Figure 5-2-b for each of the TC and TE data series can be formulated as a linear dependency of  $\sin\phi_{PT}$  on  $\psi$  as follows:

$$\sin\phi_{PT} = \sin\phi_{cv} + k_{PT} \psi \quad 5-9$$

where  $k_{PT}$  is a material constant that may in general be different for TC and TE. Results shown in Figure 5-2-b suggest that nearly the same value of  $k_{PT}$  can be assumed for TC and TE conditions. It will be shown in Chapter 6 that examination of results of hollow cylinder tests with constant values of  $b$  (Bishop, 1971) leads to a similar conclusion. If the same value of  $k_{PT}$  is used for TC and TE, variations of  $\sin\phi_{PT}$  for TC and TE can be written in the following form:

$$\sin\phi_{PT,c} = \sin\phi_{cv} + k_{PT} \psi \quad \text{for TC} \quad 5-10-a$$

$$\sin\phi_{PT,e} = \sin\phi_{cv} + a_{PT} + k_{PT} \psi \quad \text{for TE} \quad 5-10-b$$

in which  $\phi_{cv}$  corresponds to the constant volume friction angle measured from TC tests (value of  $\sin\phi_{PT,c}$  measured at  $\psi = 0$ ), and  $a_{PT}$  is material parameter that accounts for the approximately constant difference between  $\sin\phi_{PT,c}$  and  $\sin\phi_{PT,e}$ . Once  $\sin\phi_{PT,c}$  and  $\sin\phi_{PT,e}$  are known for any state of the soil, they can be substituted in Equation 5-7 for  $\sin\phi_f$  for the TC and TE conditions respectively. The resulting stress ratios denoted here by  $M_{PT,c}$  and  $M_{PT,e}$  respectively can be substituted in Equation 5-6 for  $M_{c,c}$  and  $M_{c,e}$  to calculate the rate of dilatancy  $\frac{d\epsilon_p}{d\epsilon_q}$ . The stress-dilatancy relationship obtained using this procedure is sufficient to determine the direction of plastic flow of the soil at any state in triaxial conditions.

The data shown in Figure 5-2-b are plotted in Figure 5-2-c in terms of  $M_{PT}$  against  $\psi$  as suggested by Manzari and Dafalias (1997). While a linear relationship fits each of the TC and TE data series reasonably well, the relationship between the TC and TE data is not as clear. In the procedure mentioned previously, using  $\sin\phi_{PT}$  instead of the stress ratio  $M_{PT}$ , helped correlating values measured from TC and TE, using a nearly constant slope  $k_{PT}$ .

### 5.2.2.2 *Determination of the material parameter for Nova's simplified stress-dilatancy relationship*

Nova (1979) cast the stress-dilatancy relationship into an invariant form that has been used widely for sands because of its simplicity. This relationship can be written as:

$$\frac{d\epsilon_p}{d\epsilon_q} = A (M_c - \eta) \quad 5-13$$

where  $M_c$  is the stress ratio  $q/p$  at critical state,  $A$  is a material parameter which should be obtained experimentally and  $\eta$  is the current stress ratio. A value of  $A = 1$  yields the stress-dilatancy relationship of the original Cam-Clay (Roscoe et al., 1963). The determination of the parameter  $A$  requires measurement of incremental volume changes, or curve fitting against total volume changes, from results of drained tests. This should be done for both TC and TE conditions, since this parameter may be different for these two cases. A compilation of  $N = 1/(1-A)$  values for a variety of sands is presented by Jefferies (1993) using results of TC tests.

Since Rowe's (1962) stress-dilatancy relationship has matched an extensive body of experimental results, this relationship is used here to determine the parameter  $A$ . Comparing Equations 5-6 and 5-13 we obtain:

$$A_c = 9/(9 - 2M_c\eta + 3M_c) \quad \text{for TC} \quad 5-14-a$$

$$A_e = 9/(9 - 2M_e\eta - 3M_e) \quad \text{for TE} \quad 5-14-b$$

in which  $A_c$  and  $A_e$  are values of  $A$  for TC and TE respectively. It can be seen that values of  $A$  obtained for TC and TE are not the same, and are functions of both the current stress ratio and the stress ratio at zero dilatancy. Considering Equation 5-6, the same argument regarding the variation of  $M_f$  discussed in the previous section can be made for the stress ratio  $M_c$ . Parameters  $A_c$  and  $A_e$  in Equation 5-14 are not affected by these variations significantly, and constant values can be used for them as will be seen in the next section. The difference  $(M_c - \eta)$  in Equation 5-13, however, can have a substantial effect on the predicted sand dilatancy, as discussed earlier, therefore, stress ratios  $M_c$  and  $M_e$  should be replaced by  $M_{PT,c}$  and  $M_{PT,e}$  respectively. Values of  $M_{PT,c}$  and  $M_{PT,e}$  obtained from Equations 5-7 and 5-9 can be substituted in Equation 5-13 to account for the effect of density and pressure on the stress-dilatancy relationship of sand.

### 5.2.2.3 *The shape and movement of the plastic potential*

Although not necessary from a computational point of view, many models have used a plastic potential function to define the direction of plastic flow. It is useful to examine shapes of plastic potentials defined by the above two stress-dilatancy relationships in order to visualize their differences, and correlate their parameters.

Equation 5-13 can be used to obtain a plastic potential by setting:

$$\frac{d\varepsilon_p}{d\varepsilon_q} = A (M_{PT} - \eta) = -\frac{dq}{dp} \quad 5-15$$

Integrating in the p-q stress plane leads to the following equation:

$$q = p M_{PT} \left( \frac{A}{A-1} \right) \left[ 1 - \left( \frac{p}{p_0} \right)^{A-1} \right] \quad 5-16$$

in which  $p_0$  is a scaling parameter corresponding to the value of  $p$  at  $q = 0$  and  $p$  is the current mean normal stress.

Wood (1990) converted Rowe's stress-dilatancy relationship to the following plastic potential function, assuming strains given by Rowe's relationship are all plastic:

$$p = 3p_0 \left[ \frac{3 - \eta}{(2\eta + 3)^K} \right]^{1/(K-1)} \quad \text{for TC} \quad 5-17-a$$

$$p = 3p_0 \left[ \frac{3 + 2\eta}{(3 - \eta)^K} \right]^{1/(K-1)} \quad \text{for TE} \quad 5-17-b$$

$$K = \tan^2 ( 45 + \phi_{PT} / 2 ) \quad 5-17-c$$

in which  $p_0$  is as defined previously,  $\eta$  is the current stress ratio (negative in extension) and  $K$  is Rowe's dilatancy constant defined in terms of  $\phi_{PT}$  here.

Equations 5-16 and 5-17 represent plastic potential functions corresponding to the stress dilatancy relationships suggested by Rowe (1962) and Nova (1979). Both these equations define curves in the  $p$ - $q$  plane that intersect the  $p$ -axis at  $p = p_0$ , and have their peaks at a stress ratio  $\eta = M_{PT}$  (Figure 5-3). The curve represented by Equation 5-16, however, is a function of the parameter  $A$ , which was defined as a material constant by Nova (1979), and should be obtained from experiment. From Rowe's (1962) relationship, however, a variable value for  $A$  is obtained as shown in Equation 5-14. It is useful, therefore, to determine if  $A$  can be approximated by a constant as suggested by Nova (1979), to examine the numerical value of such a constant, and to identify if the same value of  $A$  can be used for TC and TE conditions (i.e. if  $A_c = A_e$ ). Note that the

above stress-dilatancy relationships may not produce good fit to measured strains at the beginning of loading where strains are elastic. They are used here to model soil dilatancy when only plastic strains are considered.

Equations 5-16 and 5-17 are plotted in Figure 5-3 for the typical value of  $\phi_{PT} = 30$  degrees that corresponds to  $M_{PT,c} = 1.2$  and  $M_{PT,e} = 0.857$ , and for a common steady state pressure of  $p_{ss} = 100$ . Figure 5-3-a shows that using values of  $A_c = 0.8$  and  $A_e = 1.6$  in Equation 5-16 provides a very close fit to Rowe's relationship, if stress ratios in the contractive region (i. e.  $|\eta| < |M_{cv}|$ ) are considered. In Figure 5-3-b, the curves are fitted to Rowe's equation in the region of higher stress ratios (i. e.  $|\eta| > |M_{cv}|$ ), where the soil is dilative. In this case, the larger values of  $A_c = 1.2$  and  $A_e = 2$  are obtained. Use of average values of  $A_c = 1$  and  $A_e = 1.8$  (Figure 5-3-c) is, therefore, possible, in this case, in the absence of measured stress-dilatancy data. Use of  $A_c = 1$  leads to the relationship used in the original Cam-Clay (Roscoe et al., 1963). The above analysis showed that a somewhat larger value for "A" may need to be used for sand at contractive states, compared to dilative states, and that "A" should be increased (almost doubled) for TE conditions.

Differences between inclinations of normals to the plastic potential in TC and TE in the contractive region in Figure 5-3-c, indicate that significantly higher volume contractions can take place on the extension side. This increased contraction in TE can cause significant differences in the undrained response of loose sand to loading in TC and TE. These differences will be examined in Section 5-4 when TC and TE test results are simulated.

Figure 5-4 shows the movement of the plastic potential and the change in stress ratio  $M_{PT}$  during a typical drained TC test on dense sand. The stress ratio  $M_{PT,c}$  has a value close to  $M_{\mu,c}$  (corresponding to the inter-particle friction angle) at an early stage in which the PT and then the peak strength are reached, but increases to  $M_{cv}$  when the steady state is ultimately achieved.

### 5.2.3 Sand compressibility

Modeling the compressibility of sand is not as straightforward as that of clay. Some researchers (e. g. Terzaghi and Peck, 1948; Nova and Wood, 1979; Matsouka and Sakakibra, 1987), have adopted a formulation similar to that of clays (i. e. a linear  $e - \ln p$  relationship), while others (e. g. Hardin, 1987) have defined bulk moduli  $K$  which are related to pressure by a power law. An important difference between the compressibility of sand to that of clay is that unlike clay, samples of normally consolidated sand can exist at different void ratios under the same consolidation pressure.

A comprehensive compression model for sands and clays was suggested by Pestana and Whittle (1995). The model requires 4 parameters to fully define the load-unload behavior of a certain sand in compression. The model in its most general form covers the full range of densities and pressures, including pressures as high as those at which particle crushing is the dominant mode of development of plastic volumetric strain. For the current constitutive model, however, a simplified version of the model, which can be used for the range of pressures that are encountered in most practical applications, will be sufficient. For the case in which only "plastic" volumetric strains are to be obtained, the simplified version requires only one parameter, which can be determined from results of compressibility tests on sand at different initial densities. Since the current constitutive model employs the conventional power law to predict elastic volumetric strains, this simplified relationship which determines only plastic volumetric strains is sufficient.

The simplified version can be written in terms of the variation of the plastic volumetric strain  $\epsilon_p^P$ , or current void ratio "e", with the current pressure "p" as follows:

$$\epsilon_p^P \approx \beta \frac{e_0^{3.5} p}{(1 + e_0) p_a} \quad 5-18a$$

$$\ln (e/e_0) \approx -e_0^{2.5} \beta (p/p_a) \quad 5-19$$

in which  $e_0$  is the formation void ratio,  $p_a$  is the atmospheric pressure and  $\beta$  is a material parameter that can be obtained by fitting test data on sand compressibility at different initial void ratios. Determination of this parameter based on "total" volumetric strains resulting from compression loading data is not expected to lead to significant lack of precision.

## 5.2.4 The hardening rule

During hardening or softening, the size and/or the shape of the yield surface may change. Size hardening occurs when the value of  $p_c$  in Equation 5-1 or 5-4 changes, and shape hardening may occur due to changes in  $M_p$ .

### 5.2.4.1 *Size hardening*

During shearing, changes in the size of the yield surface occur such that  $p_c$  approaches a value of  $p_f$  that corresponds to the size of the yield surface at soil failure. The size of the yield surface at failure  $p_f$  is determined from the stress ratio of the soil at failure  $M_f$ , which is a function of the current state parameter of the soil. Been et al. (1985) showed that the maximum attainable stress ratio or friction angle at failure is related to the state parameter of the soil  $\psi$  at failure. Wood et al. (1994) used this observation to formulate a relationship between the maximum attainable stress ratio of the soil  $M_{\max}$  and the current state parameter  $\psi$  in the following form:

$$M_{\max} = M_c - k \psi \quad 5-20$$

in which  $M_c$  is the stress ratio at steady state (i. e. at  $\psi = 0$ ) and  $k$  is a material parameter.

As with other strength-related parameters, the above relationship is modified in the following form and used to obtain stress ratios at failure at various soil states:

$$\sin\phi_f = \sin\phi_{cv} - k_f \psi_{curr} \quad 5-20$$

in which  $\phi_f$  and  $\phi_{cv}$  are the failure and constant volume (steady state) friction angles respectively, and  $k_f$  is a material parameter determining the slope of the variations. For a given value of  $\phi_f$  at a specific soil state, the stress ratio  $M_f$  at failure can be calculated using Equation 5-7. Note that because of the changes in the current state parameter, this stress ratio changes during loading.

To determine  $p_f$  at any stage of loading, the stress ratio  $M_f$  is substituted in the yield function (Equation 5-1 or 5-4) for  $\eta$ , and the corresponding size of the yield surface  $p_c$  is obtained. The stress ratio at peak  $M_p$  (or  $M_\alpha^2$  for anisotropically consolidated sand) is assumed to be the same as that of the current state. This leads to the following value for  $p_f$ :

$$p_f = \frac{p}{\left[1 - \frac{(M_f - \alpha)^2}{M_\alpha^2}\right]^2} \quad 5-21$$

It can be shown that, for the yield function used in this study, all yield surfaces that have the same value of  $M_p$ , have a common maximum possible yield stress ratio. This limiting stress ratio is the common tangent to all the yield surfaces, at the origin of the p-q plane. Therefore, values of  $M_p$  and  $M_f$  can not change arbitrarily, and the following condition should always be met:

$$(M_f - \alpha)^2 < M_\alpha^2$$

For isotropically consolidated soils, the above condition is equivalent to:



$$|M_f| < \sqrt{5} |M_p|$$

For sand in the most contractive state, the stress ratio at failure  $M_f$  is not expected to decrease to values below  $M_{cv}$ . A minimum value for the stress ratio  $M_p$  will, therefore, exist which is equal to  $M_{cv}/\sqrt{5}$ . For Toyoura sand with  $M_{cv} = 1.24$ , this corresponds to an equivalent friction angle at peak of about 13 degrees. It is interesting to notice that minimum strengths at peak obtained from results of both TC and TE tests shown in Figure 5-7-a correspond to friction angles close to this value. These minimum values were measured from UESPs of samples that experienced complete collapse with zero minimum strength.

At any soil state, the increment of hardening caused by an increment of plastic shear strain is a function of the difference between the current size of the yield surface  $p_c$ , and the size of the yield surface at failure  $p_f$ . The following hardening rule, therefore, will be used which is similar in its form to that used in the original Nor-sand model (Jefferies, 1993):

$$\frac{\partial p_c}{\partial \epsilon_q^p} = h(p_f - p_c) \quad 5-22$$

where  $\epsilon_q^p$  is the plastic shear strain and  $h$  is a material parameter which is related to the stiffness of the soil in shear. The physical meaning and the method of approximation of this parameter will be discussed later.

It should be realized that Equation 5-22 accounts for hardening that result from the application of shear stresses, which produce both shear and volumetric plastic strains because of the dilatancy characteristics of the material. Hardening at zero shear stress (i. e. at  $\eta = 0$ ) results in only volume changes and is governed by the isotropic consolidation law. Equation 5-18 can be used to derive the hardening rule in such cases:

$$\frac{\partial p_c}{\partial \epsilon_p^p} = \frac{(1 + e_0)p_a}{\beta e^{3.5}} \quad 5-18b$$

The nature of the volumetric strains induced by shearing and isotropic consolidation is different. Therefore, different hardening laws govern the two processes. Note that the plastic potential or stress-dilatancy relationship given by Equation 5-15 will lead to two different values for soil dilatancy at  $\eta = 0$ , obtained from TC and TE conditions. In this case, soil dilatancy resulting from the stress-dilatancy relationship should be equated to zero, and soil compressibility defined by the above equation should be used to determine the stress-strain relationship.

It is useful to examine the physical meaning of the parameter  $h$  for the simple case of an isotropically consolidated sand subjected to constant  $p$  shearing. The “plastic shear modulus” of the soil can be defined as follows for triaxial conditions:

$$3G^p = \frac{\partial q}{\partial \epsilon_q^p} \quad 5-23$$

For an isotropically consolidated sand, the yield function (Equation 5-1) can be solved for the deviatoric stress  $q$  as:

$$q = q(p, p_c, M_p) \quad 5-24$$

For shearing under constant  $p$ , the following can be obtained from the above relationship for the stiffness of the soil with respect to plastic shear strains ( $G^p$ ):

$$3G^p = \frac{\partial q}{\partial \epsilon_q^p} = \frac{\partial q}{\partial p_c} \frac{\partial p_c}{\partial \epsilon_q} + \frac{\partial q}{\partial M_p} \frac{\partial M_p}{\partial \epsilon_q} \quad 5-25$$

Substituting from Equation (5-1) in the above relationship:

$$3G^P = \frac{\sqrt{5}}{4} \frac{(p/p_c)^{3/2} M_p}{\sqrt{1-(p/p_c)^{1/2}}} \frac{\partial p_c}{\partial \epsilon_q} + \sqrt{5} p (1-(p/p_c)^{1/2})^{1/2} \frac{\partial M_p}{\partial \epsilon_q} \quad 5-26$$

which can be written in the following form:

$$G^P = f(p/p_c) M_p \frac{\partial p_c}{\partial \epsilon_q} + \frac{q}{3M_p} \frac{\partial M_p}{\partial \epsilon_q} \quad 5-27$$

in which the function  $f$  with the argument  $p/p_c$  is defined by:

$$f(p/p_c) = \frac{\sqrt{5}}{12} \frac{(p/p_c)^{3/2}}{\sqrt{1-(p/p_c)^{1/2}}} \quad 5-28$$

The variation of the function  $f$  with the ratio  $p/p_c$  is shown in Figure 5-5. It can be seen that at  $p/p_c$  equal to unity (i. e. after consolidation and prior to shearing), the function has a value equal to infinity, but as  $p/p_c$  decreases (upon shearing), it decreases rapidly.

The term  $\frac{\partial p_c}{\partial \epsilon_q}$  in Equation 5-27 defines the shear hardening of the material (Equation 5-22). This term also decreases upon shearing, and vanishes at the ultimate state at which unlimited shear strain can develop without changes in shear stress.

At an early stage of shearing, the second term in Equation 5-27 is small compared to the first term, since  $M_p$  generally varies slightly with shear strains, and the value of  $q$  is small at the start of shearing. Neglecting the second term in Equation 5-27 and substituting for  $\frac{\partial p_c}{\partial \epsilon_q}$  from Equation 5-22 leads to the following approximation for the plastic shear modulus  $G^P$ :

$$G^p \cong h ( p_f - p_c ) M_p f ( p / p_c )$$

5-29

The above equation determines the degradation of the plastic shear modulus during the shearing process. At the start of shearing when  $p = p_c$ , the function  $f ( p/p_c )$  (and accordingly, the value of  $G_p$  ) equals infinity, and this is consistent with the physical notion that at the start of shearing, all shear strains are elastic. However, this situation quickly changes to the condition at which the elastic and plastic strains become comparable, and then the plastic strains become dominant in controlling the deformation process.

#### 5.2.4.2 *Shape of the yield surface*

The stress ratio  $M_p$  which appears in the equation of the yield surface determines the shape (i. e. the width) of the surface. The stress ratio  $M_p$  is a function of  $e_n$  and its initial value can be obtained from Equation 5-2 using values of void ratio and pressure at consolidation. Small changes in  $M_p$  may occur subsequently during shearing but these changes are neglected here to retain the simplicity of the formulation. Satisfactory model predictions were obtained as will be seen in this chapter and in the next chapter, despite this simplification.

#### 5.2.5 Elasticity

Two parameters are needed to characterize the behavior of an isotropic linear elastic material, namely, the elastic bulk modulus  $K$  and the elastic shear modulus  $G$ . Alternatively, one of these two parameters can be used together with Poisson's ratio such that the other one can be calculated from the following relationship:

$$G = \frac{3(1 - 2\nu)}{2(1 + \nu)} K \quad 5-30$$

where  $\nu$  is Poisson's ratio. Elastic moduli with power dependency on the mean normal stress "p" are used frequently. The moduli are often defined as:

$$G = G_r (p / p_r)^n \quad 5-31$$

$$K = K_r (p / p_r)^n \quad 5-32$$

where  $G_r$  and  $K_r$  are reference values of  $G$  and  $K$  respectively for a reference pressure equal to  $p_r$ . The exponent  $n$  can be obtained by fitting experimental data and is often close to 0.5. For an assembly of ideal elastic spheres, Duffy and Mindlin (1957) derived a value of 1/3 for  $n$ . Actual soils, however, exhibit higher values that can range in the order of 0.5-0.7. The increase in  $n$  is attributed to the increase in the number of particle contacts in real soils, compared to ideal spheres (Jovicic and Coop, 1997).

It is noted that in this model, as in many other sand models (e. g. Prevost, 1985; Manzari and Dafalias, 1997), a constant value was assumed for Poisson's ratio, and elastic stiffness parameters were used that were functions of the mean normal stress only. In modeling unload-reload behavior, these assumptions may lead to non-conservative response and the prediction of unrealistic values for  $K_0$ . The above assumptions were made, however, to preserve model simplicity, especially because the current formulation was primarily intended for predicting the response of sand to monotonic loading.

In the above formulation of  $G$  and  $K$ , only the effect of mean normal stress on the elastic moduli was considered and sand density was not accounted for. These equations can be used when model calibration is made to predict the behavior of sand within a relatively small range of densities. If the variation of the moduli with both pressure and density is examined, some difficulty is encountered, since the effect of density on the stiffness of granular soils may vary in different soils. Jovicic and Coop (1997) showed that the effect of density may be more significant in carbonate sand, compared to silica sand. In constitutive modeling of sand over a wide range of densities, it is necessary to

account for the effect of density on the elastic moduli, since in some cases, this effect may not be negligible.

The widely used relationship obtained by Hardin and Richart (1963) for  $G$  accounts for both pressure and void ratio. Results of laboratory tests presented by Hardin and Black (1963), and in situ tests presented by Bellotti et al. (1997) and Yamashita et al. (1997) suggested that this relationship gives realistic predictions of the elastic shear modulus. For many clean sands and normally consolidated clays, Hardin and Black (1969) showed that the following relationship can be used to approximate the initial shear modulus  $G_{\max}$ :

$$G_{\max} = 1230 \frac{(2.973 - e)^2}{1 + e} p^{1/2} \quad 5-33$$

where  $G_{\max}$  and  $p$  are both in psi. If  $G_{\max}$  and  $p$  are substituted in terms of kPa, the above relationship can be used with the coefficient 476 instead of 1230. In this relationship, the effect of void ratio has been accounted for, by the following function:

$$F(e) = \frac{(2.973 - e)^2}{(1 + e)} \quad 5-34$$

Since the exponent in Equation 5-33 may change for different sands as mentioned earlier, the following form will be used in the current model:

$$G = G_r \frac{(2.973 - e)^2}{1 + e} (p)^n \quad 5-35$$

which is similar to equation 5-32 multiplied by the function  $F(e)$  to account for the effect of void ratio. The bulk modulus can also be defined in a similar fashion:

$$K = K_r \frac{(2.973 - e)^2}{1 + e} (p)^n \quad 5-36$$

Alternatively, Equation 5-30 may be used to calculate K if G and Poisson's ratio are known.

### 5.3 Model Calibration

If model predictions are to be made for the response of sand to loading in both TC and TE, the following parameters need to be determined in the calibration of the model:

- a) -Shape hardening parameters:  $a_p$ ,  $k_p$ ,  $e_\mu$
- b) -Stress-dilatancy parameters:  $\phi_{cv}$ ,  $a_{pT}$ ,  $k_{pT}$
- c) Failure:  $k_f$
- d) -Sand compressibility parameter:  $\beta$
- e) -Elastic parameters:  $n$ ,  $G_r$ ,  $K_r$  ( or  $\nu$  )
- f) -Steady (ultimate) state line

If model predictions are to be made only for TC conditions, 9 parameters will be needed, and if both TC and TE are considered, a total of 11 parameters will be required. The position of the ultimate state obtained from TC tests will also be needed in both cases. Methods of determination of model parameters will be described in the following. It is noted that these methods may not be unique and alternate procedures may also be used to obtain the parameters.

Shape hardening parameters: Parameters  $a_p$ ,  $k_p$  and  $e_\mu$  can be obtained from results of undrained TC and TE tests in which the UESP exhibits undrained softening after reaching a peak. The void ratio  $e_\mu$  is the value of the normalized void ratio  $e_n$ , corresponding to  $\sin\phi_\mu$  in a  $\sin\phi_p$  vs.  $e_n$  plot Figure 5-6-a. The actual value of the inter-particle friction angle  $\phi_\mu$  is of less importance since it is, in fact, an arbitrary reference

point on the  $\sin\phi_p$  vs.  $e_n$  line that helps determine the position of line along with the slope  $k_p$ . A value of 7 degrees smaller than  $\phi_{cv}$  is assumed here for  $\phi_\mu$ . It was shown in Section 4.7.2.2 (Chapter 4) that the maximum and minimum values of stress ratios at peak that can be measured from undrained tests correspond respectively to cases in which sand just starts to exhibit a peak in its UESP, and when it is in its loosest possible state and experiences complete liquefaction upon undrained shearing. It is preferable to determine these values and use them in the determination of the constants related to peak state. Otherwise, strengths at peak obtained from tests on samples exhibiting a peak in their UESPs, and having states as farther apart as possible, can be used for this purpose. Such two undrained tests are the minimum required, but results of more tests can help in further refining the parameters. If predictions are to be made for TE tests as well as TC, results of at least one undrained TE test, in which a peak in its UESP appears is required. Figure 5-7 shows the determination of peak parameters for moist tamped and dry deposited Toyoura sand.

Stress-dilatancy parameters: Parameters  $k_{PT}$  and  $a_{PT}$  can be obtained by plotting variations of  $\sin\phi_{PT}$  vs.  $\psi$  obtained from TC and TE tests (Figure 5-6-b). A minimum of two TC tests and one TE test are required to determine  $\phi_{cv}$ ,  $k_{PT}$  and  $a_{PT}$ . If the behavior for a wide range of states is to be predicted, it is preferable that tests at states as farther apart as possible be used. Either drained or undrained test results can be used. The angle  $\phi_{cv}$  is the steady state friction angle reached when the material is sheared to sufficiently large strains such that no volume changes occur upon further shearing. This angle can either be measured directly from tests in which the ultimate state is reached, or from plots of  $\sin\phi_{PT}$  vs.  $\psi$  discussed above. The value of  $\phi_{PT}$  corresponding to  $\psi = 0$  is taken to be  $\phi_{cv}$ . Figure 5-2-b shows the determination of parameters  $\phi_{cv}$ ,  $k_{PT}$  and  $a_{PT}$  for Toyoura sand from results of a large number of undrained tests. In a typical model calibration, however, such a large number of tests will not be needed.

Failure: Parameter  $k_f$  determines the variation of the maximum friction angle (or stress ratio) that can be attained at failure, with the current state parameter. This parameter can be determined from friction angles at failure, measured from drained tests at different



soil states. In addition to maximum strength, changes in shear strength with strain are also controlled by this parameter. A larger value for  $k_f$  results in larger peak strength, and more rapid reduction in shear strength after peak. Some investigations (e. g. Chu et al., 1993) suggested that such changes in strength observed in results of conventional drained tests, may be affected by boundary conditions and end restraints. To match results of such tests, therefore, it may be necessary to vary  $k_f$  in order to obtain a best fit to the observed response. In such cases, it may be difficult to assess the degree of validity of test results in representing real sand behavior.

**The compressibility parameter  $\beta$ :** The parameter  $\beta$  can be determined through the use of Equation 5-18-b to fit results of isotropic compression tests on samples with different initial void ratios  $e_0$ . Since the rather complicated compression behavior of sand (compared to that of clay) is formulated by a single parameter  $\beta$ , it is necessary to choose a value for this parameter that gives reasonable predictions for the range of pressures under consideration. Figure 5-8 shows the experimental isotropic compression data used in obtaining parameter  $\beta$  for Ottawa and Toyoura sands. Use of a single value for  $\beta$  produced satisfactory match to the majority of experimental results obtained from tests conducted over a range of pressures encountered in most practical applications.

**Elastic parameters:** Elastic parameters  $n$ ,  $G_r$ ,  $\nu$  (or  $K_r$ ) can be determined from results of either unloading or seismic tests. Alternatively, the tangent to the  $q$  vs  $\epsilon_q$  plot from a drained shear test at the origin can be used to obtain the elastic shear modulus, and undrained test results can be used to obtain the elastic bulk modulus by fitting it against observed UESPs. A typical value of Poisson's ratio can also be used together with measured shear modulus. These latter procedures however, often give substantially smaller values for the elastic moduli compared to values obtained from unloading or seismic tests. This may be due to the development of some plastic strain at points where the slope of the tangent is measured, since identifying the tangent at the origin of the  $q$  vs.  $\epsilon_q$  curve is often difficult.

The coefficient  $h$  that appeared in the size hardening relationship given by Equation 5-22 was not taken as a new material parameter, because it may be approximated from other model parameters and variables as explained below. This method was used in all model predictions presented in this chapter and in Chapter 6.

It was shown in Section 5-2-4-1 that  $h$  is directly proportional to the shear stiffness of the soil. The elastoplastic shear stiffness varies smoothly from its initial value  $G_{\max}$  (that is often taken as the elastic shear modulus) at very small strain to values that are predominantly controlled by plastic deformations. The degradation of the plastic shear modulus during shearing is controlled by changes in  $(p_f - p_c)$  and the function  $f(p/p_c)$  (see Equation 5-29). If the variations of the elastic and plastic stiffnesses with the mean normal stress and void ratio are assumed to be similar (as suggested e. g. by Prevost, 1985),  $G^p$  at initial stages of shearing will be related to  $G_{\max}$  measured from the initial slope of the shear stress-strain curve. Experience with model predictions showed that the parameter  $h$  can be approximated from  $G_{\max}$  and the initial value of  $(P_f - P_c)$  according to the following relationship:

$$h \cong G_{\max} / (P_f - P_c)_{\text{ini}} \quad 5-37$$

in which  $(P_f - P_c)_{\text{ini}}$  is the initial value of  $(P_f - P_c)$  that corresponds to the state of the soil after consolidation and prior to shearing. The approximate value obtained for  $h$  from Equation 5-37 may need to be refined to match the behavior for a certain range of states. Since  $h$  is now directly related to the elastic shear stiffness, which is in turn controlled by  $G_r$ , it was possible to refine  $G_r$  such that the best fit to test results is obtained. Experience showed that this procedure can lead to good match between model predictions and experimental data for a wide range of soil states.

Steady state parameters: Determination of the position of the ultimate (steady) state line (USL) is probably one of the most difficult parts of the calibration procedure of all critical state models for sands. Castro (1969) recommended that the position of the USL be determined using data from undrained tests on loose samples. In the current model,

however, the exact position of this line may not affect the predicted response at the small and medium ranges of strain significantly. This is because in the current model, the USL characterizes the behavior at large strain, and other model parameters account for the earlier stages of shearing. A linear  $e - \ln p$  relationship is often used for sand similar to what has long been used for clay. Experimental evidence, however, indicate that the line representing this relationship becomes curved at higher pressures (Jefferies, 1985; Ishihara, 1993). In these cases, a suitable function or a curve fitting procedure should be used if modeling is to be made over a wide range of pressures. When pressures involved are smaller, the USL can be approximated by a straight line with the following equation:

$$e_{ss} = \Gamma - \lambda \ln p_{ss} \quad 5-38$$

where  $\Gamma$  is the void ratio for a pressure equal to unity,  $\lambda$  is the slope of the USL in the  $e - \ln p$  plot, and  $p_{ss}$  is the mean normal stress at steady state. The determination of the USL for Toyoura sand by fitting a polynomial to the test results is shown in Figure 4-1.

It is noted that in the determination of model parameters using individual test results, some adjustments often need to be made in order to achieve the best fit to a range of experimental results. This is because experimental results often show some scatter, and model parameters should be selected such that predictions conform to an overall average behavior.

## 5.4 Model performance

In this section, the response of very loose saturated and dry Ottawa sand to undrained and drained loading along a number of stress paths in the triaxial apparatus is predicted and compared with test results reported by Sasitharan et al. (1994) and Skopek (1994). All model predictions were made using a unique set of model parameters that are given in Table 1. The drained and undrained behavior of Toyoura sand in TC and TE is also

predicted and compared with test results in this section. A wide range of void ratios and consolidation stresses was considered. Model predictions were compared with results of tests reported by Ishihara (1993), Verdugo (1996) and Yoshimine (1996). All tests reported from the first two authors were performed on samples prepared by moist tamping (MT) and those reported from the third author were on samples prepared using dry deposition (DD). Table 5-1 lists model parameters used in all these predictions. Model predictions for TE tests on Ottawa sand were not made because of the unavailability of suitable data therefore, relevant parameters were not determined. Parameters used for the peak state were fabric-dependent, and were given in the table for the two types of preparation methods mentioned above. Figure 5-7 shows variations of stress ratio at peak obtained from tests on MT and DD samples. Very loose samples cannot be prepared using the dry deposition method therefore, peak friction angles measured from TC results on DD samples do not cover a wide range of void ratios.

It is noted that although the parameters for peak state are affected by soil fabric, the effect of differences in parameters obtained for different fabrics on the predicted response of sand was not significant in the cases studied here. This can be noticed from Figures 6-20 to 6-22 in the next chapter. In cases where the effect is significant, parameters should be determined from tests on samples that have a fabric similar to that of the soil in situ. Alternatively, results of tests on undisturbed samples may be used for the determination of parameters. Note, however, that Figure 4-4 shows that values of  $M_p$  obtained from undisturbed samples prepared by ground freezing were not substantially different from those obtained from tests on reconstituted samples, when appropriated methods are used in sample preparation.

#### 5.4.1 Modeling the collapse behavior of very loose Ottawa sand

A number of drained and undrained triaxial tests were performed by Sasitharan (1993) and Skopek (1994) on very loose Ottawa sand (relative densities of about zero), by subjecting them to different stress paths in the p-q plane. Ottawa sand is a uniform,

medium sand comprised primarily of rounded to subrounded quartz grains. Maximum and minimum void ratios determined using the ASTM D2049 standard are 0.82 and 0.50 respectively (Sasitharan, 1993).

Details of test setups and relevant information can be found in the above two references. All samples were prepared using the moist tamping (MT) method to produce states as loose as possible in order to investigate the collapse and instability behavior of very loose granular materials. Of more interest were states at which the soil was on the post-peak portion of the undrained effective stress path (UESP), where it experienced reduction in strength upon undrained shearing. This is because collapse and instability were seen to occur when such states are achieved (Sasitharan et al., 1993, Lade 1993).

Figure 5-9 and Figure 5-10 show results of drained and undrained triaxial compression (TC) tests performed on such sand along with model predictions. These tests were used for model calibration. In Figure 5-10, in addition to the simulation of the undrained response of samples with a void ratio of 0.804 under consolidation pressures of 350 and 550 kPa, the response of a sample with the same void ratio, consolidated to a pressure of 100 kPa is also predicted. It is seen that although the predicted response is completely different from the other two samples, all samples finally reach the same state of stress at large strain.

Figure 5-11 shows results of a two-stage test, in which the sample was first sheared undrained until a state after the peak was reached. The back pressure was then set equal to the current pore pressure, and a drained stage of shearing under a constant mean normal stress ( $p$ ) was initiated, and continued until the steady state condition was reached. It can be seen from Figure 5-11-b that very small axial strain was developed before the peak was reached, after which the rate of development of the axial strain somewhat increased, until drained shear was applied. Although the shear stress in the drained stage increased by less than 50 kPa before reaching the steady state, substantial axial strain and volume contraction developed consequently. It can be seen from Figure 5-11-a to d that the proposed model predicted the observed response very well. In

simulating this test, values of the hardening parameters ( $p_c$  and  $M_p$ ) at the point where the drained stage was initiated, were set equal to those at the end of the undrained stage.

Figure 5-12 shows results and simulations for a test similar to that of Figure 5-11 but with a stress path along the TC in the drained post-peak shearing stage. A behavior similar to that shown in Figure 5-11 is observed, in which the axial strain developed in the undrained stage, which continued slightly beyond the peak in this test, was very small. In the stage of drained loading, however substantial axial strain developed accompanied by significant volume contraction. The volume contraction was measured up to about 2.5%, when the test was terminated at an axial strain of about 16%. The simulations, however, indicate that contraction might have continued if further axial strain had been applied.

Another series of tests were performed on "dry" Ottawa sand by Skopek (1994). Samples were sheared in drained TC up to a certain shear stress level, then a stage of drained shearing with a constant deviatoric stress (CDS) was initiated, and continued until the steady state was reached. During the CDS stage, the mean normal stress ( $p$ ) was being reduced by decreasing the confining pressure, while a constant deviatoric stress ( $q$ ) was applied using a hanger that exerted a constant load on the sample, and allowed free development of strains, without any interference of the hydraulic system.

Figure 5-13 shows test results and model predictions for one of these tests. It can be seen that the void ratio experienced a small increase during part of the CDS stress path because of unloading. The axial strain developed during this stage was also very small. A certain point was then reached at which substantial contraction, associated with large axial strain was initiated.

Proper modeling of such behavior is important, since as was discussed in Chapter 3, this behavior is likely to be responsible for failures that have been observed in loose granular materials, when a stress path similar to that of the CDS test was followed prior to failure.

Figure 5-14 shows the effect of density on the response of Ottawa sand to CDS loading. Since the same stress path was imposed on samples with different initial void ratios, the same value of  $p$ ,  $q$  and  $e$  was reached at steady state by all samples, as predicted in Figure 5-14-b and c. It can be seen that as the initial void ratio decreased from 0.84 to 0.8, the predicted volume contraction before the steady state was reached, and also the mean normal stress ( $p$ ) at which contraction started, decreased. Reduction in void ratio, in fact, has resulted in less contraction prior to steady state. This contraction started at a later stage, and continued for a smaller range of stresses, as the sample became denser. For samples with higher densities, therefore, the possibility of such pre-failure contraction will be eliminated. Experimental evidence of such effect of density on collapse potential has been shown by Anderson and Riemer (1995).

#### 5.4.2 Modeling the behavior of Toyoura sand in triaxial compression and extension

Ishihara (1993) reported results of undrained triaxial compression tests on Toyoura sand that covered a wide range of void ratios and involved pressures up to 3000 kPa. Figure 5-15 to Figure 5-19 compare observed and predicted responses of samples of Toyoura sand prepared by the moist tamping (MT) technique presented in the above reference. All these predictions were made using a single set of model parameters that are listed in Table 5-1 for Toyoura sand.

Figure 5-15 compares predicted and observed responses of samples consolidated to a void ratio of 0.833 ( $D_r = 38\%$ ) and pressures between 100 and 2000 kPa. The behavior changes from fully dilative at a confining pressure of 100 kPa to fully contractive with a slight tendency for dilation towards the steady state at a confining pressure of 2000 kPa. It can be seen that although the consolidation pressure for the high pressure test was 20 times larger than that of the low pressure test, the response was predicted well using a unique set of model parameters. In Figure 5-16, the response of samples at void ratios of

0.735 subjected to the same range of pressures is compared with model predictions. All samples exhibit purely dilative behavior under these pressures. The response is again predicted by the model with good accuracy.

Test data on the response of Toyoura sand at the two void ratios discussed above but for a consolidated pressure of 3000 kPa were also available. Model predictions made for these test results were not as successful as those made for lower pressures. It was noticed, however, that use of a somewhat modified value for the parameter  $\beta$  used in the simplified version of the compressibility model suggested by Pestana and Whittle (1995) could improve the predictions. Figure 5-17 compares measured and predicted responses of Toyoura sand at void ratios of 0.735 and 0.833 consolidated to 3000 kPa. In this figure, predictions are shown using  $\beta=0.006$  that was used for all the predictions made for Toyoura in this thesis. To obtain a better match to the observed responses, other predictions were made using a reduced value of  $\beta=0.0048$  for the  $e=0.833$  test and an increased value of  $\beta=0.008$  for the  $e=0.735$  test. It can be seen that very good match to the measured response is obtained. Referring to Figure 5-8-b, it may be noticed that at higher pressures, predicted compression of loose samples of Toyoura sand is over-estimated, and that of dense sand is under-estimated by the simplified one-parameter model. In fact, the  $\beta=0.006$  used for all model predictions of Toyoura sand is somewhat larger than the  $\beta=0.004$  used in Figure 5-8-b to fit the compression data over the range of pressures shown in the figure. The  $\beta=0.006$  was found more suitable for the range of pressures relevant to most practical applications. It may be possible, therefore, to use the simplified single parameter for the range of pressures relevant to most practical applications. However, a more comprehensive model has to be adopted if higher pressures are involved.

Model predictions and observed responses are compared for samples of Toyoura sand at  $e=0.907$  in Figure 5-18. Both observed and predicted responses indicate that for this void ratio, an increase in consolidation pressure from 100 to 1000 kPa is sufficient to change the behavior from fully dilative to fully contractive.



It has been reported (e. g. by Ishihara, 1993) that if sand is consolidated to a void ratio higher than a certain value, it will experience complete liquefaction with zero residual strength upon undrained shearing. This limiting void ratio is about 0.93 for Toyoura sand sheared in TC (Ishihara, 1993). Figure 5-19 shows test results and model predictions for samples at such void ratios consolidated to pressures from 100 to 1000 kPa. Test data for the stress paths followed were not available, but stress-strain predictions show a generally good match to the measured response.

Figure 5-20 shows results of a series of tests performed by Yoshimine (1996) for which measured data were available up to a limited strain level. The model was used to predict the response for these tests. It can be seen that model predictions are in very good agreement with the observed response for the range of strains for which experimental data were available. The model also provided the possibility to extend the predictions to higher levels of strain up to the ultimate state.

The model was used to simulate results of two series of drained TC tests on moist tamped samples of Toyoura sand, reported by Verdugo (1996). In one series, samples with consolidated void ratios of 0.831, 0.917 and 0.96 were sheared under a confining pressure of 500 kPa. Comparison between model predictions and test results for this series is made in Figure 5-21. In the other series shown in Figure 5-22, consolidated void ratios were 0.831, 0.917 and 0.996, corresponding to relative densities of 38.4%, 15.8% and -5% (very loose sand) respectively, and the confining pressure was 100 kPa. It can be seen that for both series, the agreement between model predictions and test results is very good. Parameters used in all these predictions were the same as those used for predicting the undrained response.

In what follows, model predictions are compared with the measured response of Toyoura sand to undrained triaxial extension (TE). The tests simulated were reported by Yoshimine (1996) and involved consolidation pressures ranging from 50 to 500 kPa.

In Figure 5-23, the behavior of samples with void ratios from 0.802 to 0.817, corresponding to relative densities of about 43%, consolidated to pressures from 50 to 400 kPa is predicted and compared with test results. It can be seen that at such density, the behavior is contractive in TE at an early stage, but becomes dilative after the state of phase transformation is reached. The observed response derived from measurements on sample boundaries diverges from model predictions at higher shear strain. This may be attributed to the possible non-uniformity of the sample that has been often experienced in TE tests. Studies comparing local strain distribution with global strains measured from displacements of sample boundaries (see e. g. Ayoubian and Robertson, 1998) have often shown differences in these strains.

It was seen previously that undrained TC loading of samples of Toyoura sand at void ratios of more than about 0.93 leads to complete liquefaction of the samples and the achievement of zero residual strength. Figure 5-24 shows results of undrained TE tests on samples at void ratios ranging from 0.86 to 0.876, and consolidation pressures from 100 to 500 kPa. All samples have liquefied to zero strength. The state of the soil when zero strength is achieved, however, is different in this case than that of the samples subjected to TC loading shown in Figure 5-19. In TE tests zero strength is reached at or before the state of PT, while in TC tests this condition is reached at the ultimate state. This has resulted from the fact that samples subjected to TE loading experience larger contractions before the state of PT is reached, compared to those loaded in TC as will be shown in Figure 5-25. This contraction can lead to complete liquefaction of the sample before PT is reached, where hardening can start and continue until the steady state. Further discussion regarding this behavior is made when the effect of direction of loading on sand response is simulated in Chapter 6. Note that the void ratio at which zero minimum strength is reached is substantially lower ( $e = 0.86$ ) for TE than that in TC ( $e = 0.93$ ). Although the model uses the same set of parameters including a unique ultimate steady state line for TC and TE tests, these differences in behavior in TC and TE at smaller levels of strain are modeled accurately.

Test results and model predictions discussed previously indicated that significant differences could exist between sand behavior obtained from TC and TE tests. Comparison between model predictions and experimental data, on the other hand, suggested that the proposed constitutive model can account for these differences. It is useful, therefore, to use the model to compare the behavior of samples at the same state, sheared in TC and TE tests, in order to gain some insight into the causes of these differences. In the following paragraphs, both drained and undrained responses of Toyoura sand will be investigated for this purpose.

Figure 5-25 shows the same test results and model predictions that were shown in Figure 5-21 regarding drained behavior in TC tests, along with prediction of the response of samples consolidated to the same states, but loaded in TE. It can be seen that the looser samples ( $e = 0.96$ ,  $e = 0.886$ ) contract throughout the shearing process in both loading directions until the ultimate state is reached. The sample with  $e = 0.81$  that exhibited limited contraction followed by a strong dilation in the TC test, experienced substantial contraction before reaching the state of PT. At PT, dilation initiated and continued until the ultimate (steady) state was reached, as shown in Figure 5-25-b. It is interesting to note that the predicted shear strain required to reach the ultimate state in TE is substantially more than that required in TC, due to the significantly more contraction that takes place prior to the PT. This volume reduction should first be compensated for, before net volume increase starts, which brings the sample to the ultimate state in extension. The achievement of such level of shear strain using common laboratory equipment may be difficult, and modeling techniques can be used in such instances to extend the behavior derived from laboratory tests.

Similar observation is made in Figure 5-26, in which the same test results and model predictions regarding undrained TE behavior of Toyoura sand shown in Figure 5-23 are shown, along with model predictions for TC conditions. The response in TC is predicted for samples at states the same as those of the TE samples. Figure 5-26 shows that while on the extension side, the soil contracts to a small minimum shear strength at PT, the behavior in compression is substantially stronger, with a highly dilative tendency.

Figure 5-27 shows the same predictions shown in Figure 5-26 extended until the ultimate state reached. This figure indicates that while all samples sheared in TC and TE finally reach their ultimate states, substantially more shear strain is required to bring the TE samples to their ultimate states. Similar differences were observed in the drained response of Toyoura sand to TC and TE loading shown Figure 5-25. The exact shear strain needed to achieve the ultimate (steady) state in extension, however, is masked by the lack of sufficient experimental evidence regarding the possible evolution of soil anisotropy (and subsequently the possible change or elimination of the anisotropy parameter  $a_p$  in Equation 5-3) during the shearing process. A gradual elimination of ( $a_p$ ) will result in a higher rate of hardening, and a smaller shear strain required to reach the ultimate state. Another source of uncertainty is related to the position of the ultimate state line when subjecting sand to different directions of loading or modes of shearing. A higher position for the USL in the void ratio vs. mean normal stress plane is expected to necessitate larger shear strains before the ultimate state condition is reached.

Another comparison between the response to undrained loading in TC and TE is made in Figure 5-28. This figure shows the predicted behavior of samples of Toyoura sand at a void ratio of 0.86 and consolidation pressures between 100 and 500 kPa subjected to undrained TC and TE. It can be seen that while on the extension side, all samples experience complete liquefaction with zero minimum strength, samples subjected to TC loading exhibit strongly dilative behavior with an ultimate strength equal to 880 kPa (the steady state strength in compression for this void ratio). For complete liquefaction with zero residual strength to occur in compression, the void ratio has to be as large as about 0.93 as was shown in Figure 5-19.

## 5.5 Summary and conclusions

A constitutive model for sand based on the concept of critical state soil mechanics was presented in this chapter for triaxial stress conditions. Selection of model elements, strength and deformability parameters was made such that well-established and widely

comprehended concepts related to the behavior of sand be used where possible. Results obtained from previous chapters regarding yielding of sand were used in the formulation of the yield surface. Effects of void ratio, consolidation pressure and direction of loading on yielding stresses of sand were accounted for, through the dependency of the stress ratio at the peak of the yield surface, on these factors.

Unlike the common simplification of using a constant stress ratio at zero dilatancy in the stress-dilatancy relationship of sand, variable stress ratio was used in the current formulation, which was related to mean normal stress and void ratio. This relationship was obtained from measuring the variation of the stress ratio at phase transformation at different soil states. It was shown that this dependency could be derived directly from Rowe's (1962) stress-dilatancy relationship.

Comparison of model predictions and observed behavior of Ottawa and Toyoura sands in triaxial compression (TC) and triaxial extension (TE) tests showed that the model is able to predict drained and undrained behavior of sands over a wide range of pressures and void ratios using a single set of parameters. A unique ultimate state line was also used for all model predictions. Differences in the response of sand to loading in TC and TE were accounted for by the model, and possible causes of these differences were discussed using model predictions.

It is noted that while differences in the behavior of sand in TC and TE have been modeled using a unique set of model parameters including a unique ultimate state line, it is not the intention of this study to draw any conclusion regarding the uniqueness or otherwise of the USL, when subjecting sand to different modes of shearing. It is in fact difficult to speculate on the outcome of tests in which the sand is actually sheared until the steady (ultimate) state condition, as defined e. g. by Poulos (1981) is reached in different modes of shearing. The achievement of such a state in the laboratory is often hampered by the limitations of the available testing equipment. The current model however, demonstrates that many of the differences in the response of sand to shearing in different modes can result from differences in the behavior at smaller levels of strain.

Parameter type	Parameter name	Ottawa sand	Toyoura sand
Peak state	$k_p$	1.6	1.5 (1.3 for DD)
	$e_\mu$	0.76	0.88 (0.82 for DD)
	$a_p$		(0.15 for DD)
Stress-dilatancy	$\varphi_{cv}$	28.5	31
	$k_{pT}$	1	1.25
	$a_{pT}$		0.15
Failure	$k_f$	0.75	0.75
Compression	$\beta$	0.012	0.006
Elastic	$G_r$	500	500
	$K_r$	1500	850
	$n$	0.55	0.55
Ultimate State Line	$e_{ss} =$	$0.867 - 0.0167 \ln p_{ss}$	$-0.0063477p^3 + 0.0367p^2 - 0.11991p + 0.92548$ (p in MPa)

**Table 5-1** Model parameters used in response predictions for Ottawa and Toyoura sands. For Toyoura sand, parameters for peak state are given for moist tamped (MT) samples, and values in parenthesis are for dry deposited (DD) samples. All unit-dependent parameters are given assuming that (p) is substituted in the equations in terms of kPa, except where stated otherwise.

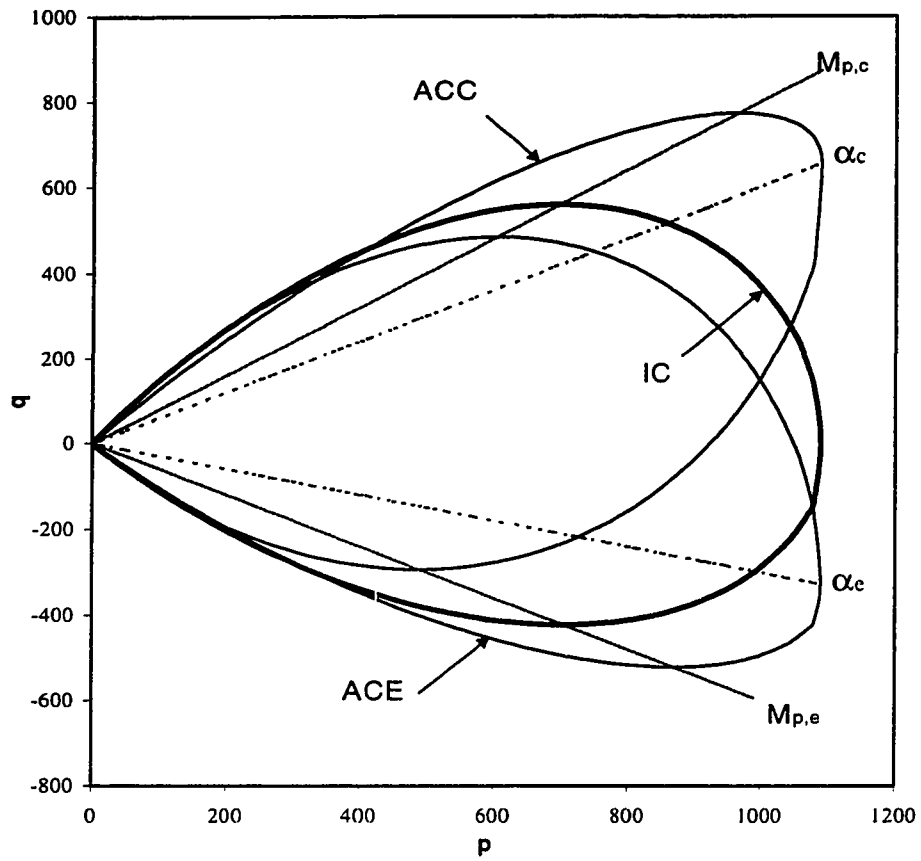
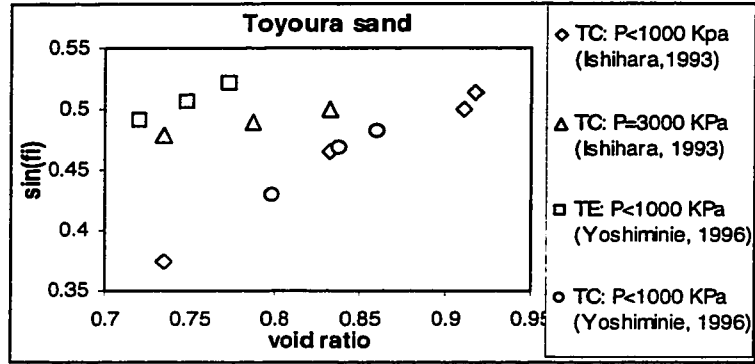
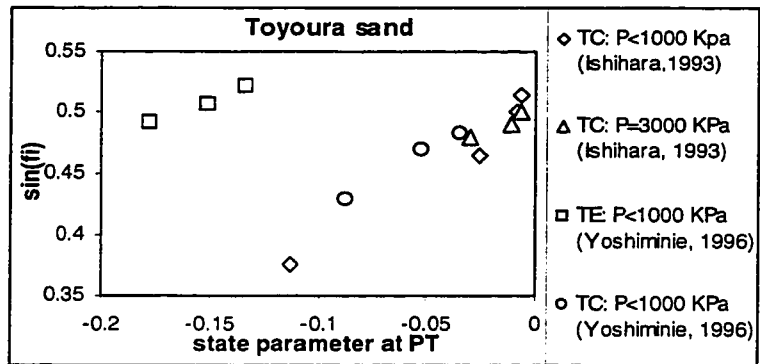


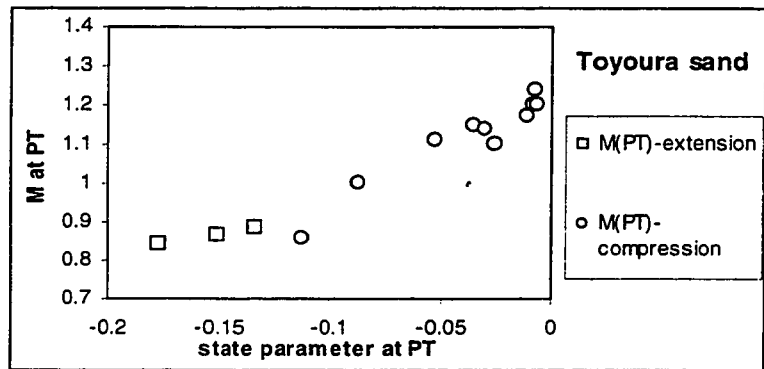
**Figure 5-1** Shape of the yield surface for isotropically consolidated (IC) sand, Anisotropically consolidated sand in compression (ACC) and Anisotropically consolidated sand in extension (ACE).



(a)



(b)



(c)

**Figure 5-2** Correlation of the friction angle at phase transformation (PT) with void ratio and state parameter



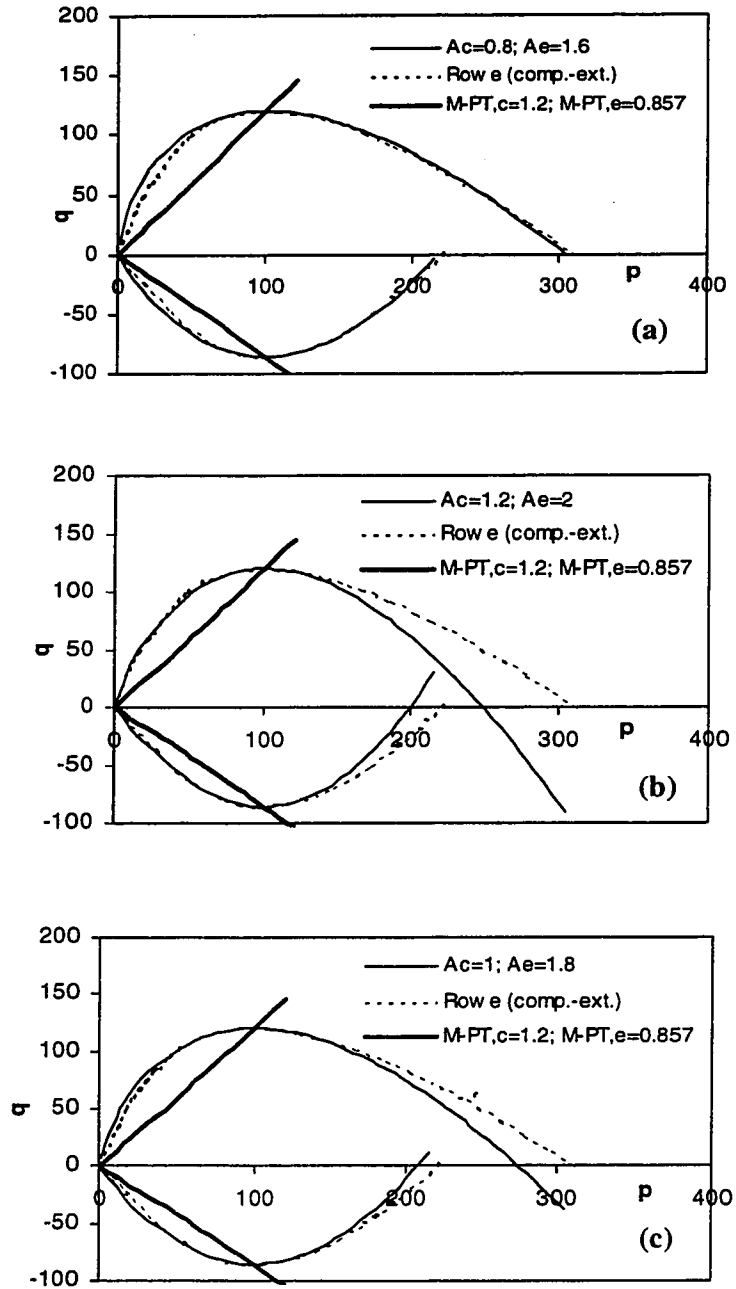


**Figure 5-3**-Determination of parameter A in Equation 5-14, using Rowe's (1962) stress-dilatancy relationship

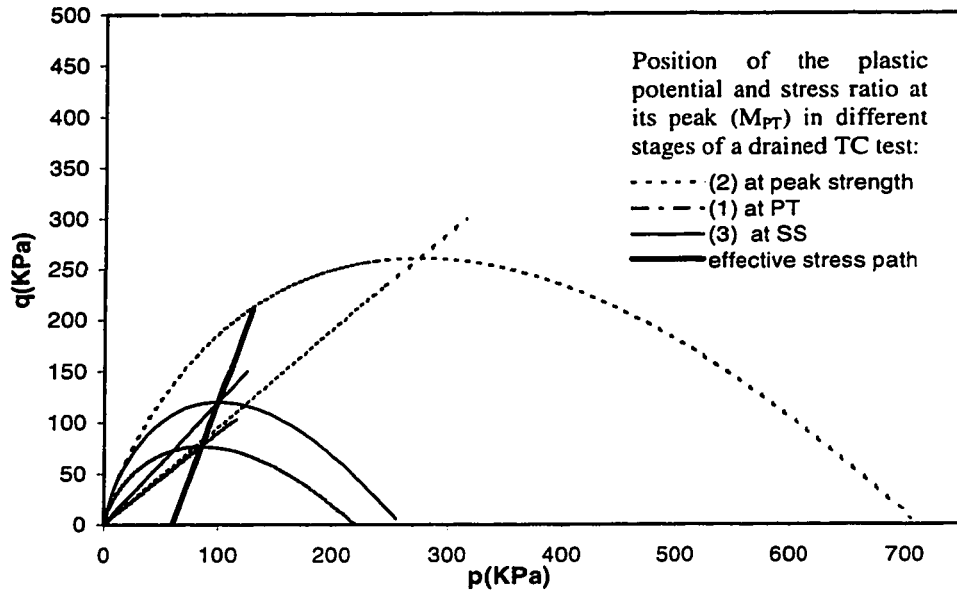


**Figure 5-4** Evolution of the plastic potential (PP) and the stress ratio at its peak  $M_{PT}$  in a drained triaxial compression (TC) test: (1) at phase transformation (PT) ; (2) at peak strength (failure); (3) at ultimate (steady) state (SS) where  $M_{PT} = M_{cv}$ .

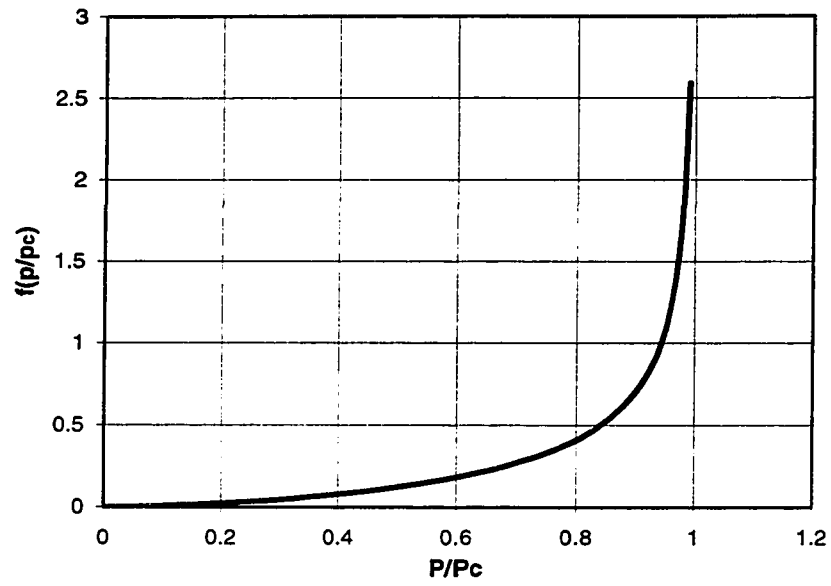
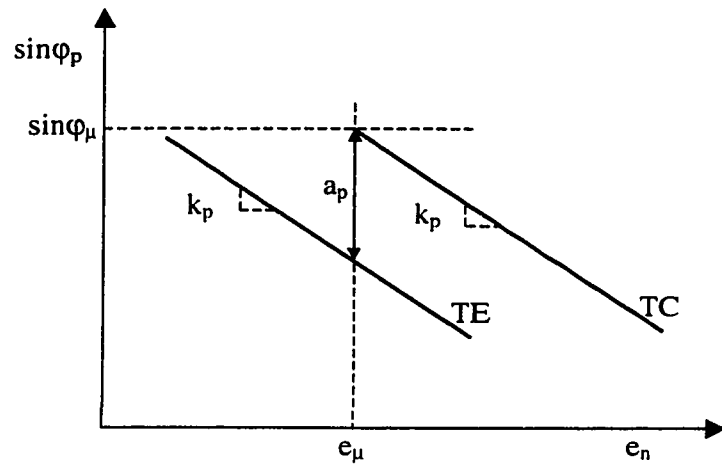
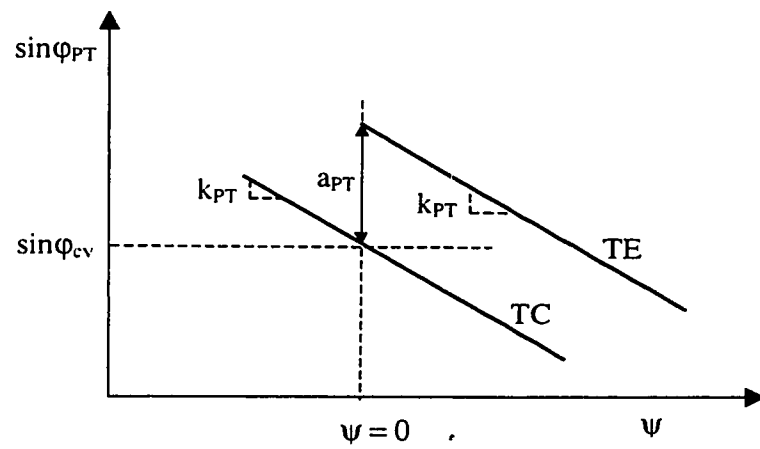


**Figure 5-5** Variation of the function  $f(p/p_c)$  (Equation 5-28) with the ratio  $p/p_c$



(a)



(b)

**Figure 5-6** Definition of model parameters used to determine friction angles of sand: (a) at the peak of the yield surface (b) at phase transformation (PT)

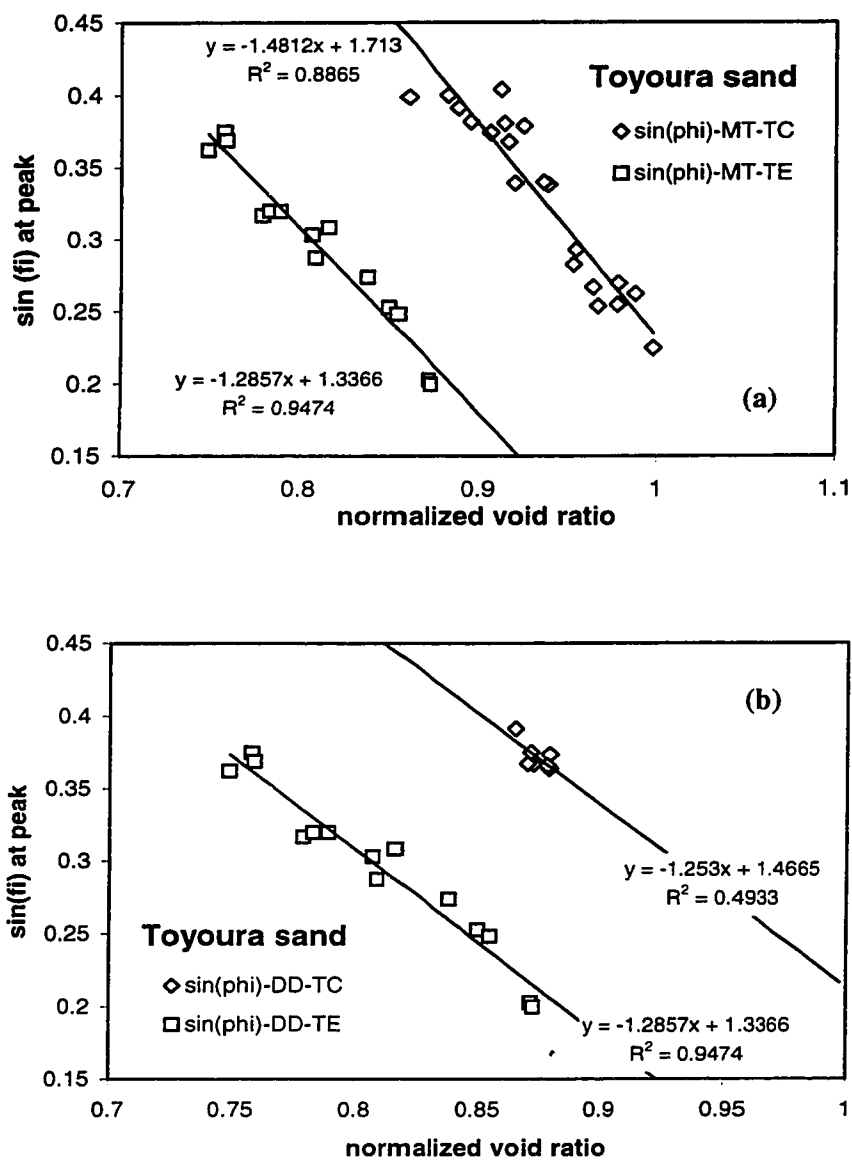


**Figure 5-7** Determination of parameters for peak state for moist tamped (MT) and dry deposited (DD) samples of Toyoura sand.

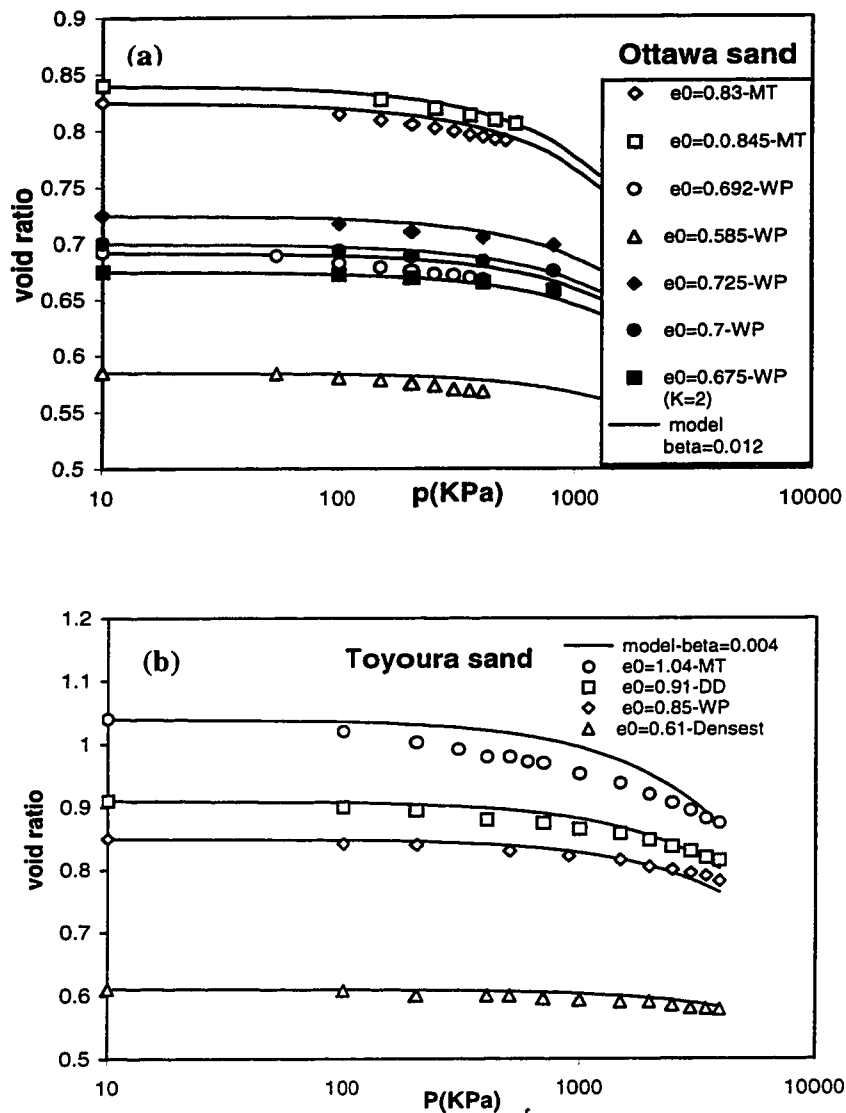


**Figure 5-8** Determination of the compressibility parameter  $\beta$  (Pestana and Whittle, 1995) using compression data on Ottawa and Toyoura sands. Ottawa sand data shown with hollow markers are from Sasitharan (1993) and those with solid marker from Vaid et al. (1985). Toyoura sand data from Ishihara (1993). Samples were prepared using moist tamping (MT), water pluviation (WP) and dry deposition (DD) methods.

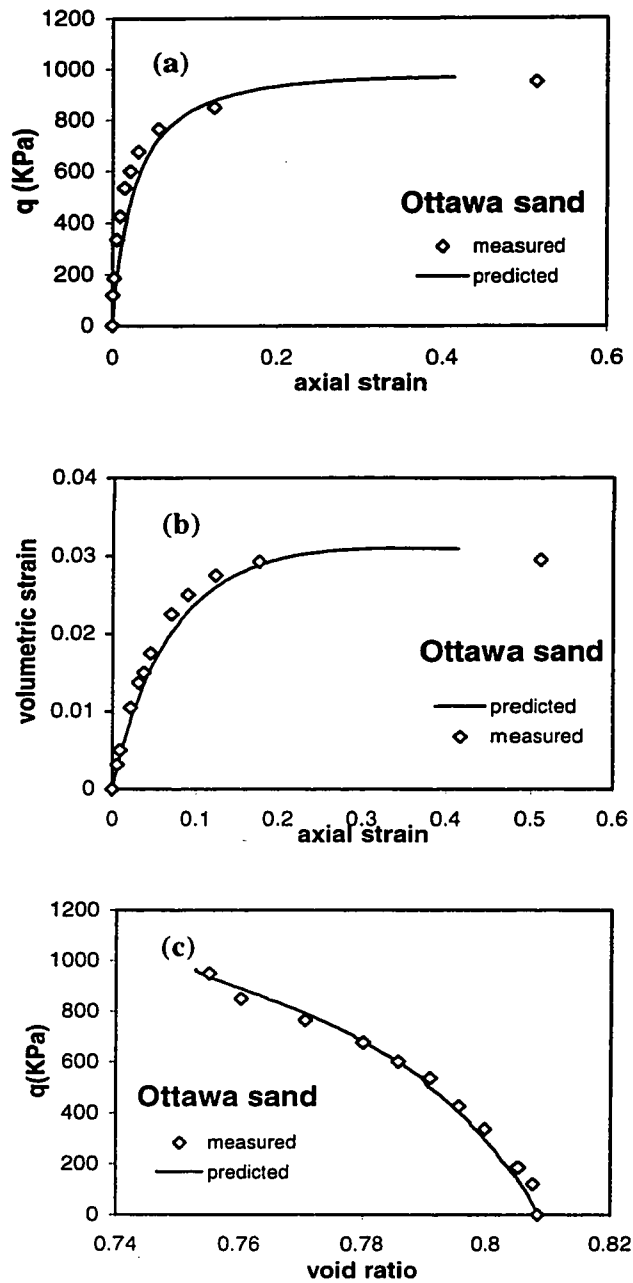
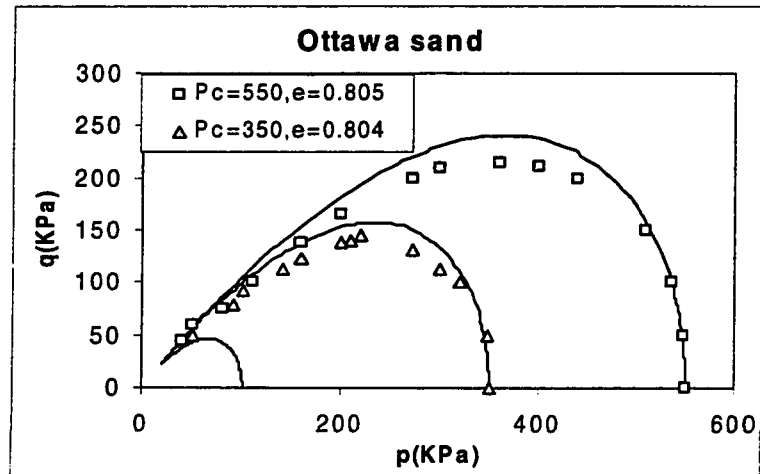
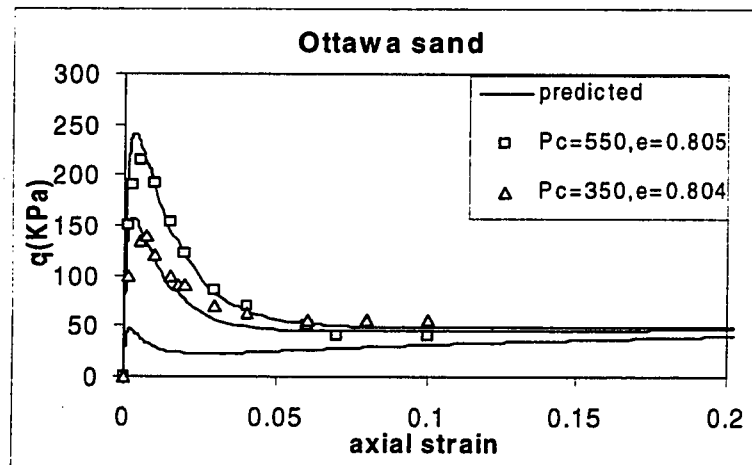


**Figure 5-9** Predicted vs. measured response of very loose Ottawa sand ( $e=0.808$ ,  $D_r=4\%$ ) consolidated isotropically to 515 KPa in drained triaxial compression test (Note: Different horizontal and vertical scales used in (b) for clarity).



(a)



(b)

**Figure 5-10** Predicted and Measured responses of very loose Ottawa sand ( $D_r = 4\%$ ) in undrained triaxial compression tests. The two tests with  $p_c = 550$  kPa and  $p_c = 350$  kPa were used for general model calibration. The test with  $p_c=100$  kPa was predicted, and no experimental data were available for comparison.



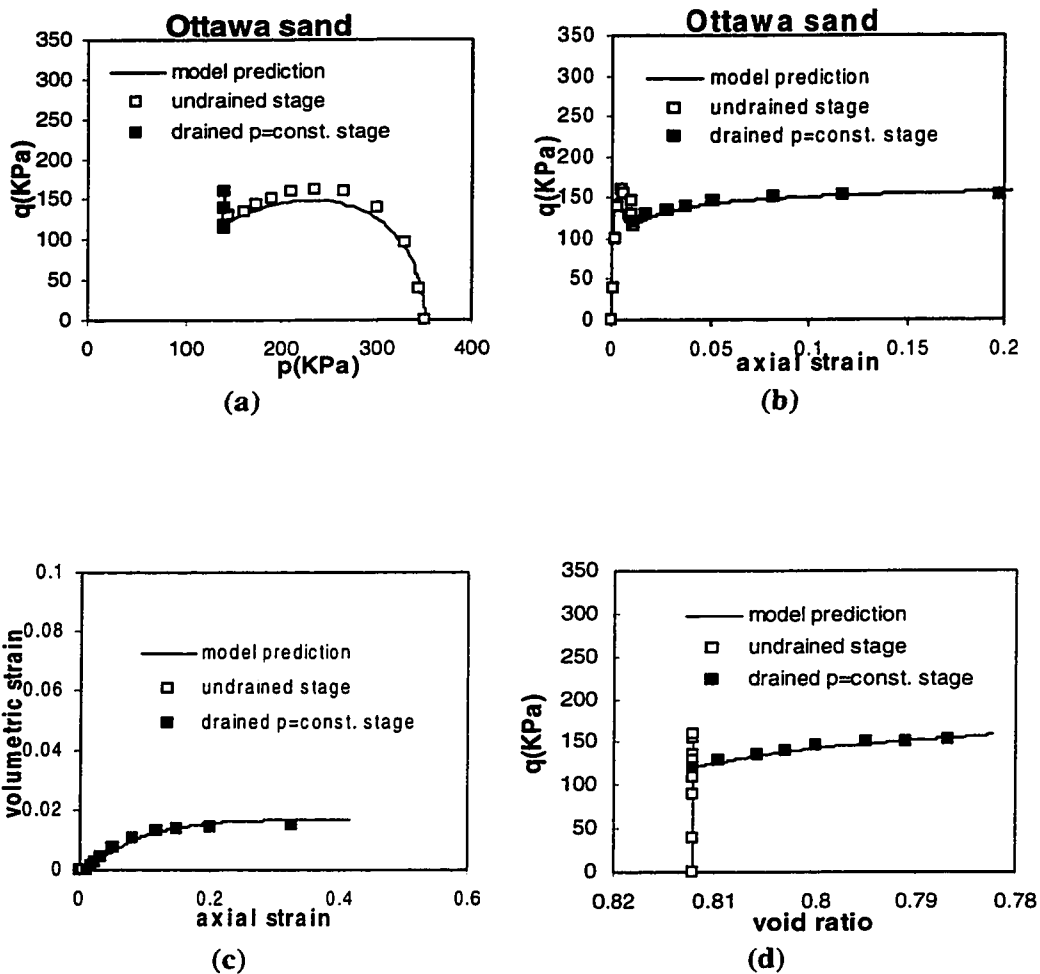


**Figure 5-11** Predicted vs. measured responses of very loose Ottawa sand ( $D_r = 2\%$ ) in a drained  $p = \text{const.}$  test starting from a state on the post-peak portion of the undrained effective stress path

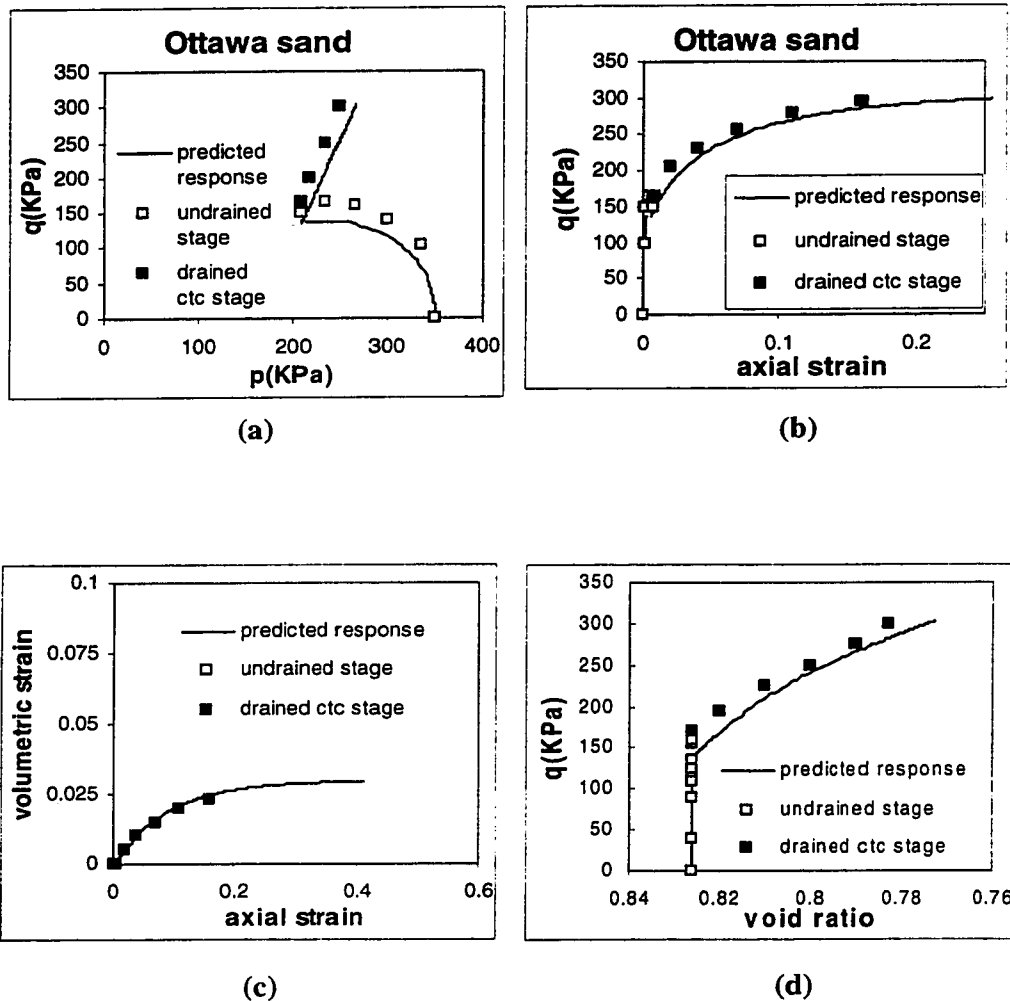


**Figure 5-12** Predicted vs. measured responses of very loose Ottawa sand ( $D_r = -2\%$ ) in a drained triaxial compression test starting from a state on the post-peak portion of the undrained effective stress path (Note: (c) not to scale).

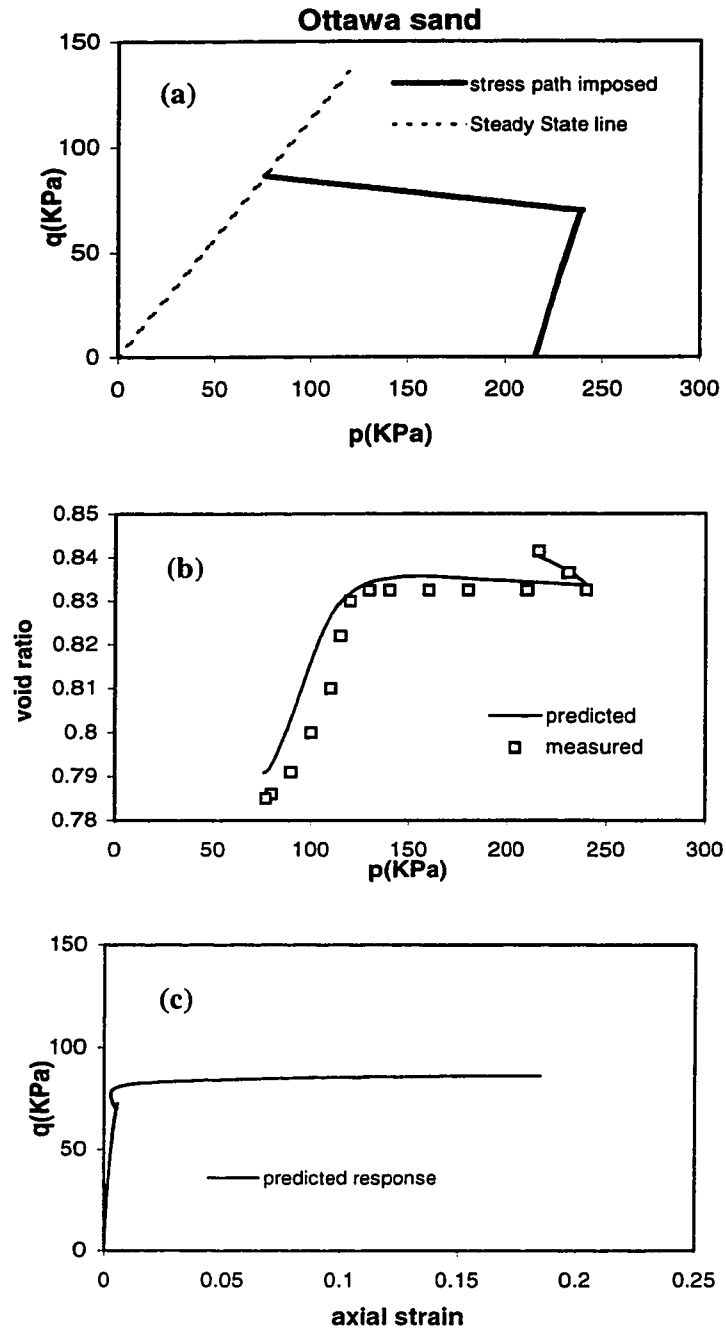


**Figure 5-13** Predicted and measured responses of very loose dry Ottawa sand ( $D_r = 8\%$ ) in a CDS test. Note that the deviatoric stress was not strictly constant during this test because of the loading method used, as explained in Chapter 3.

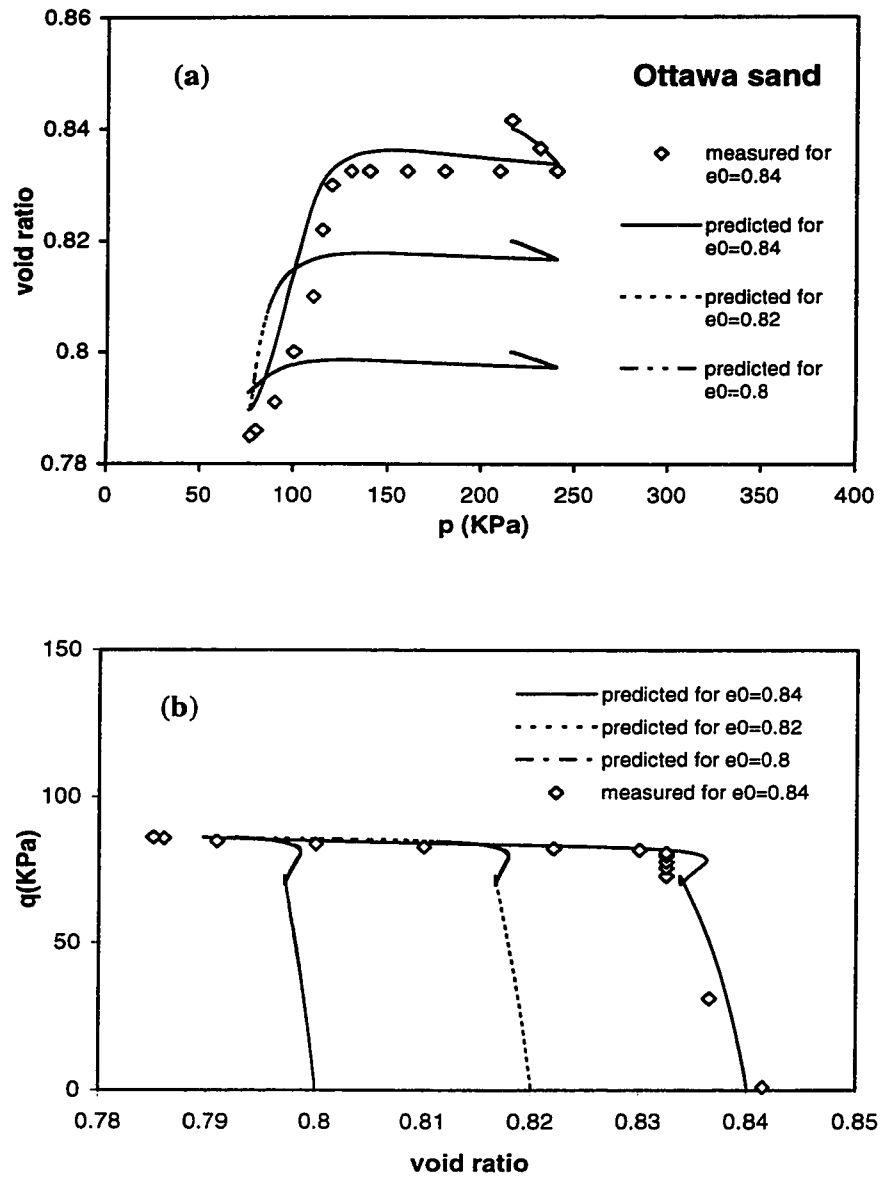


**Figure 5-14** Model predictions illustrating the effect of void ratio on the susceptibility of sands to collapse in CDS tests

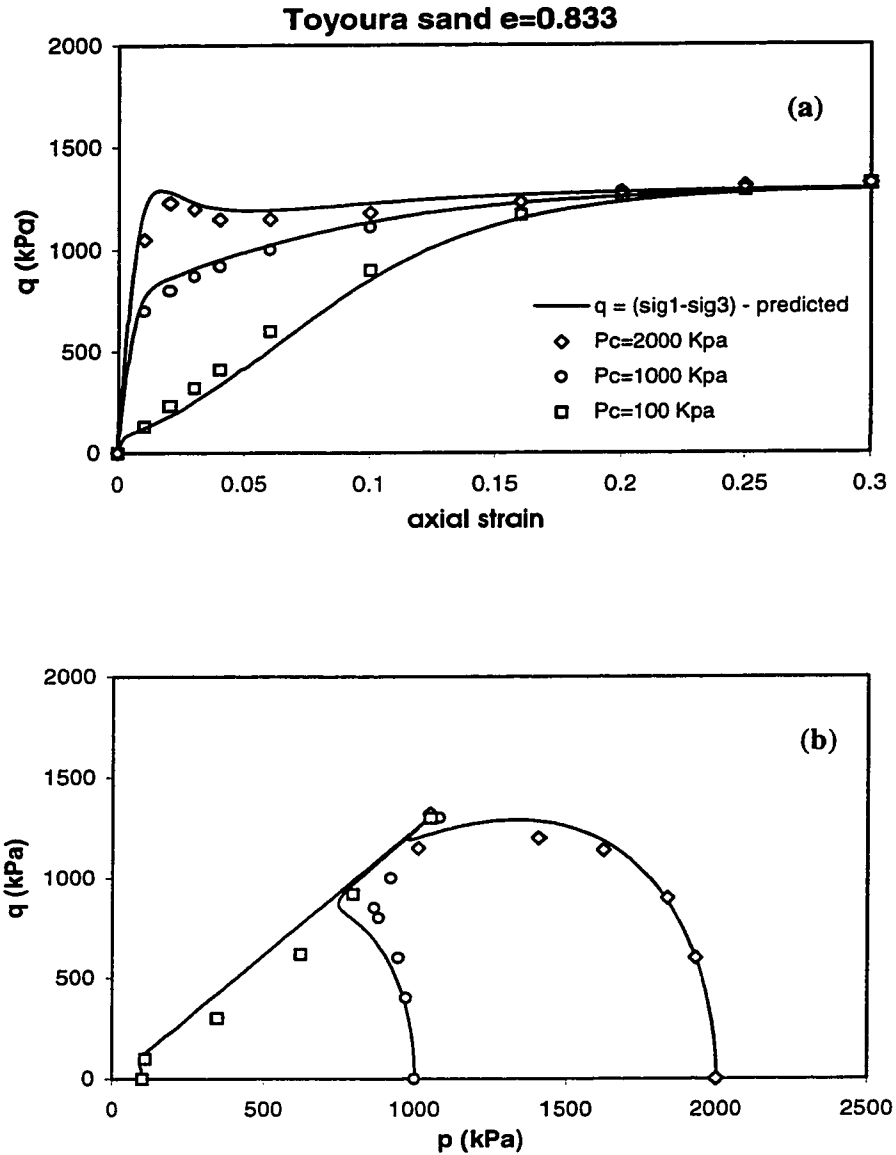


**Figure 5-15** Predicted vs. measured response of Toyoura sand with a void ratio of 0.833 and consolidation pressure of 100 to 2000 kPa in undrained triaxial compression (Note: **(b)** not to scale)

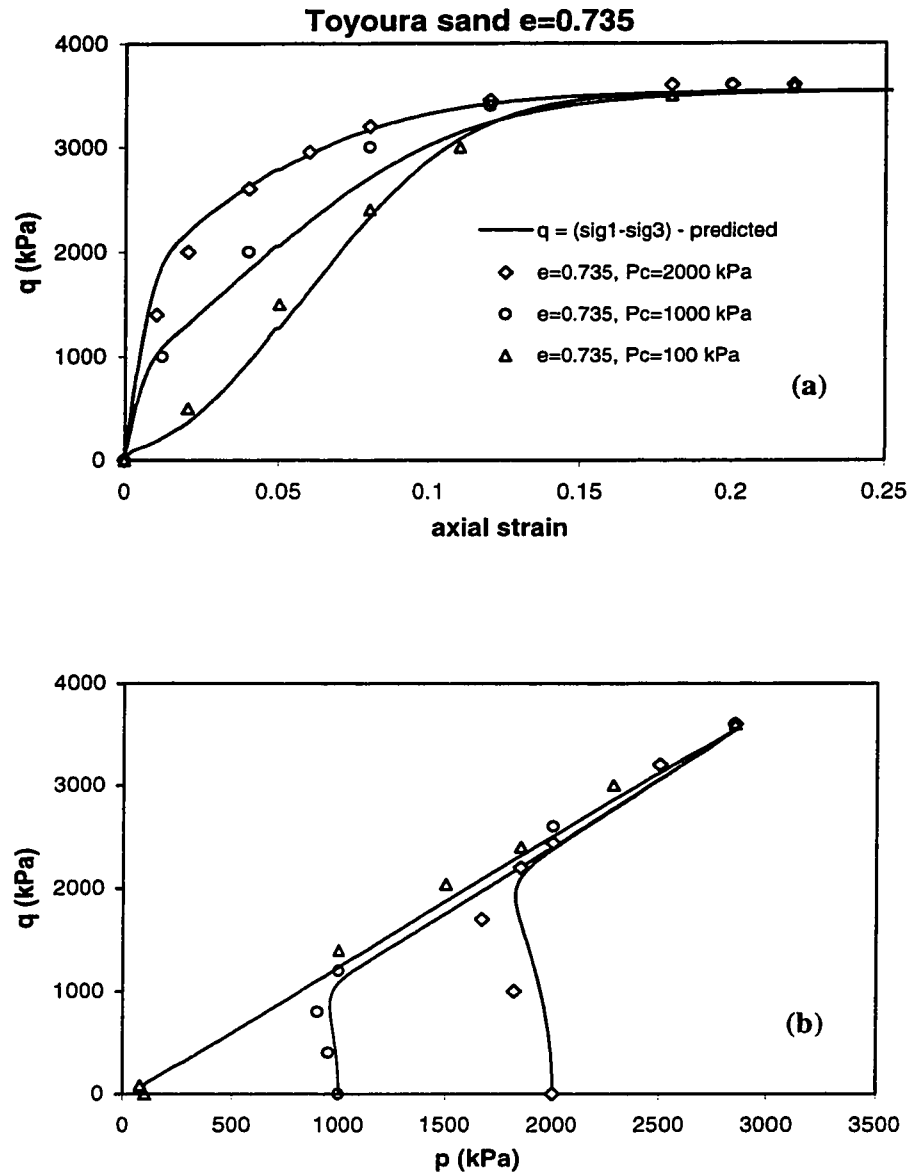


**Figure 5-16** Predicted vs. measured response of Toyoura sand with a void ratio of 0.735 and consolidation pressures of 100 to 2000 kPa in undrained triaxial compression (Note: (b) not to scale).

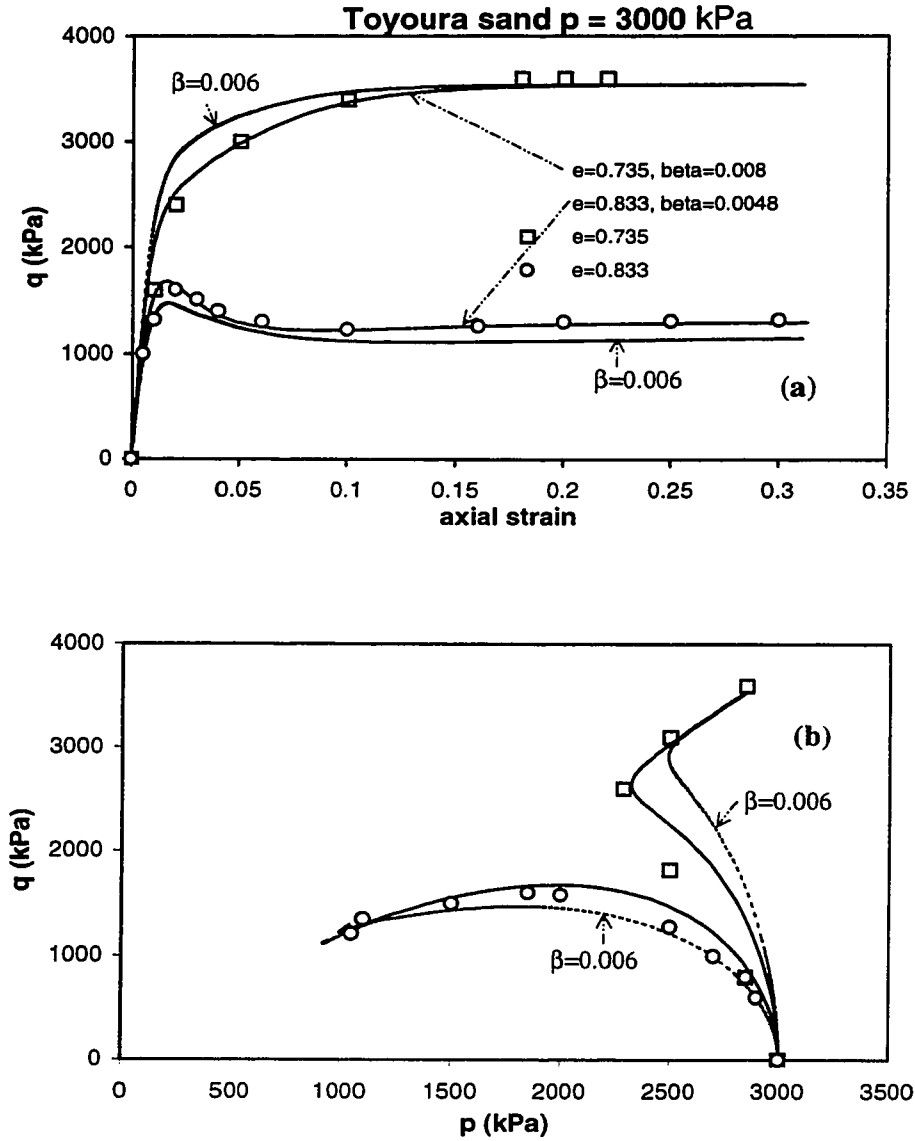


**Figure 5-17** Effect of compressibility parameter  $\beta$  (Pestana and Whittle, 1995) on the predicted response of Toyoura sand at different void ratios consolidated to  $p = 3000$  kPa loaded in undrained triaxial compression.

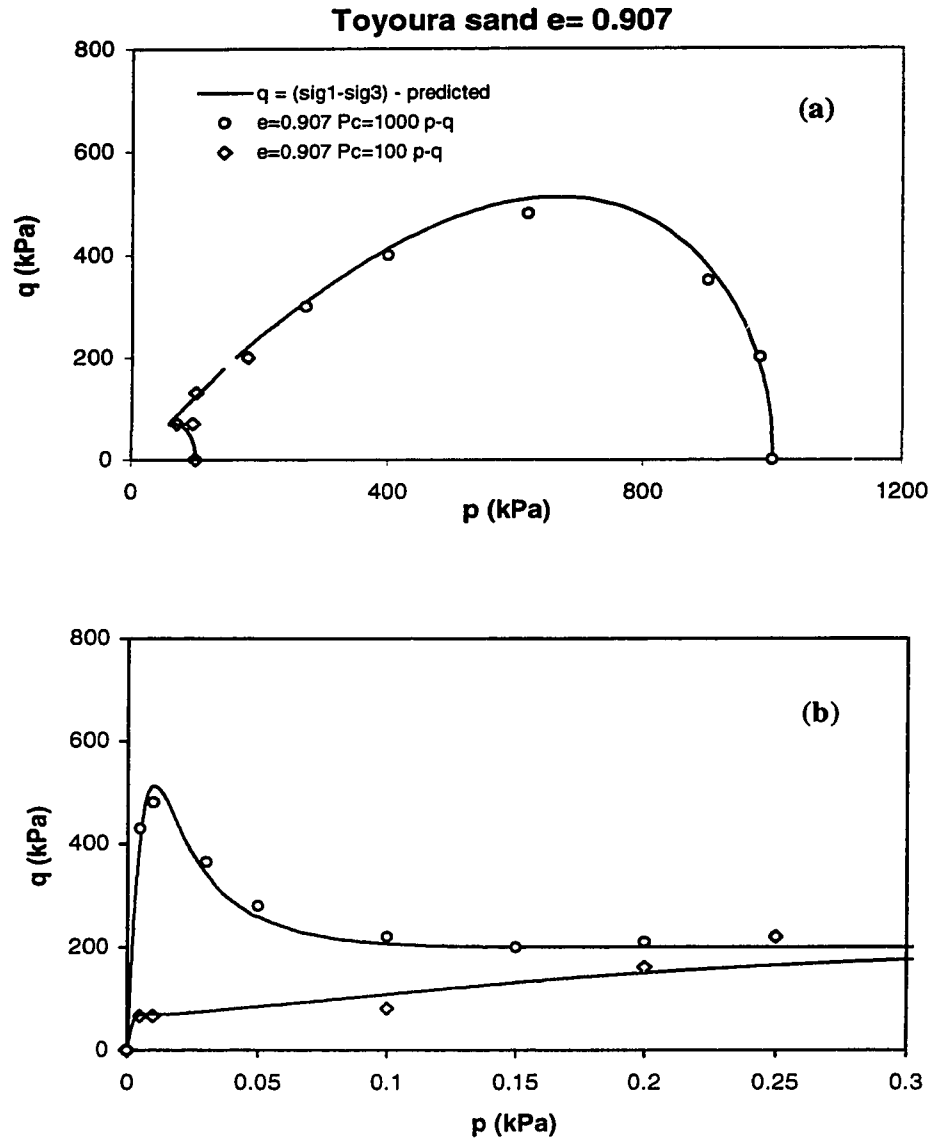


**Figure 5-18** Predicted and observed behavior of loose Toyoura sand consolidated to 100 and 1000 kPa and subjected to undrained triaxial compression loading.



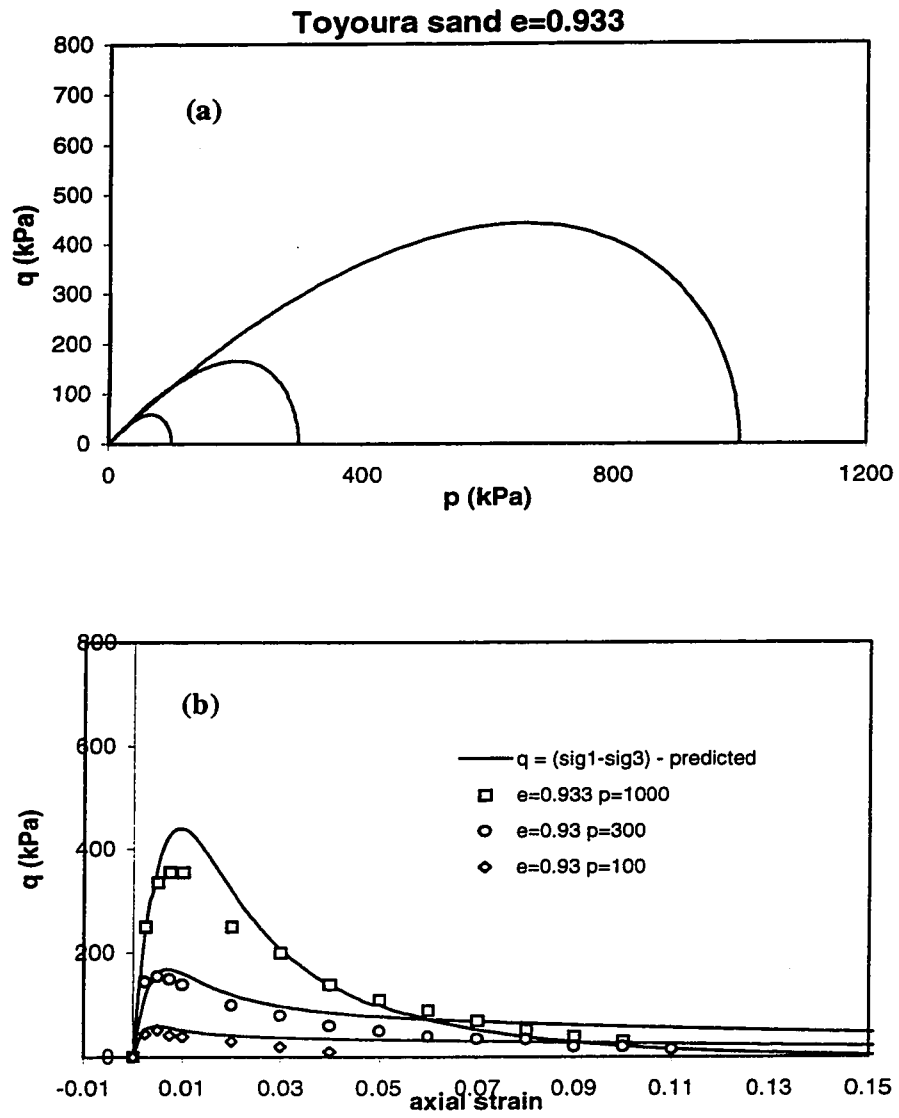


**Figure 5-19** Complete liquefaction of very loose Toyoura sand with zero minimum strength in undrained triaxial compression.

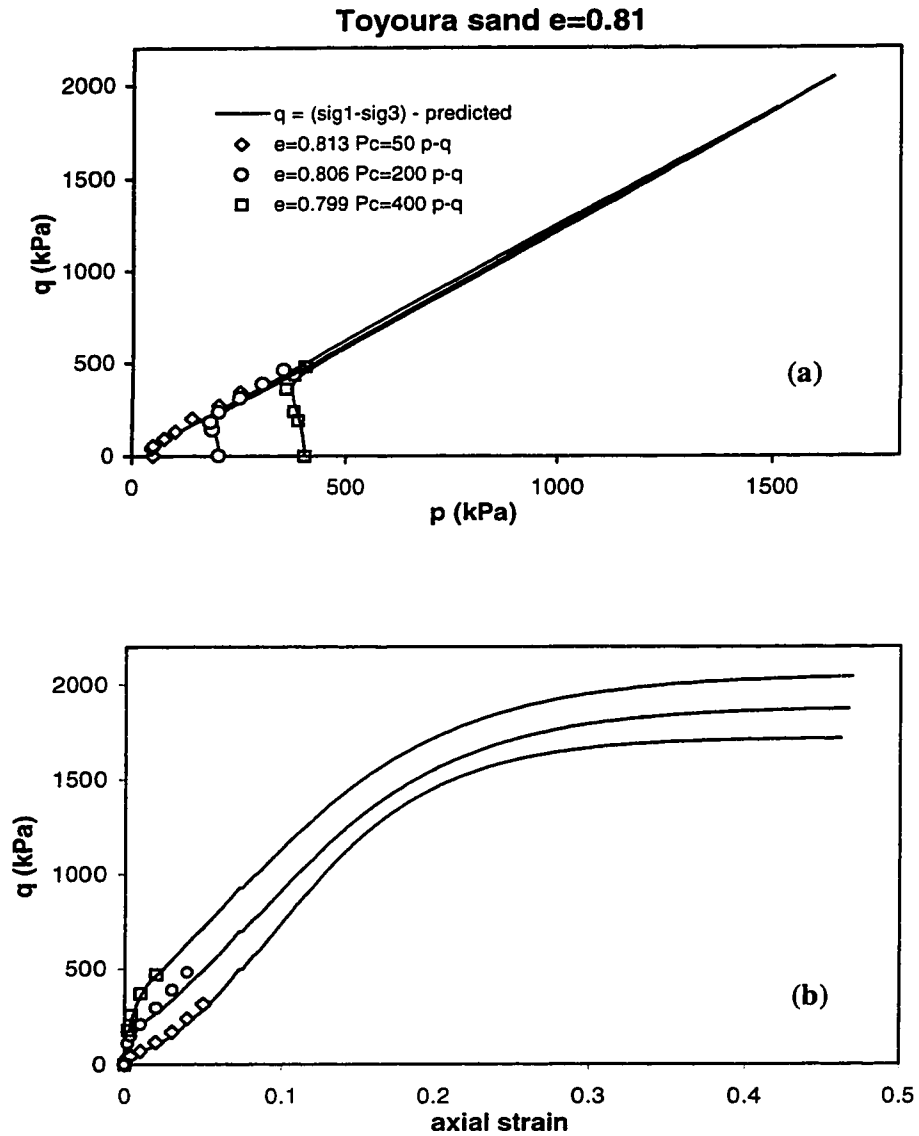


**Figure 5-20** Model predictions including and beyond measured data for Toyoura sand in undrained triaxial compression (test data from Yoshimine, 1996) ((a) not to scale).

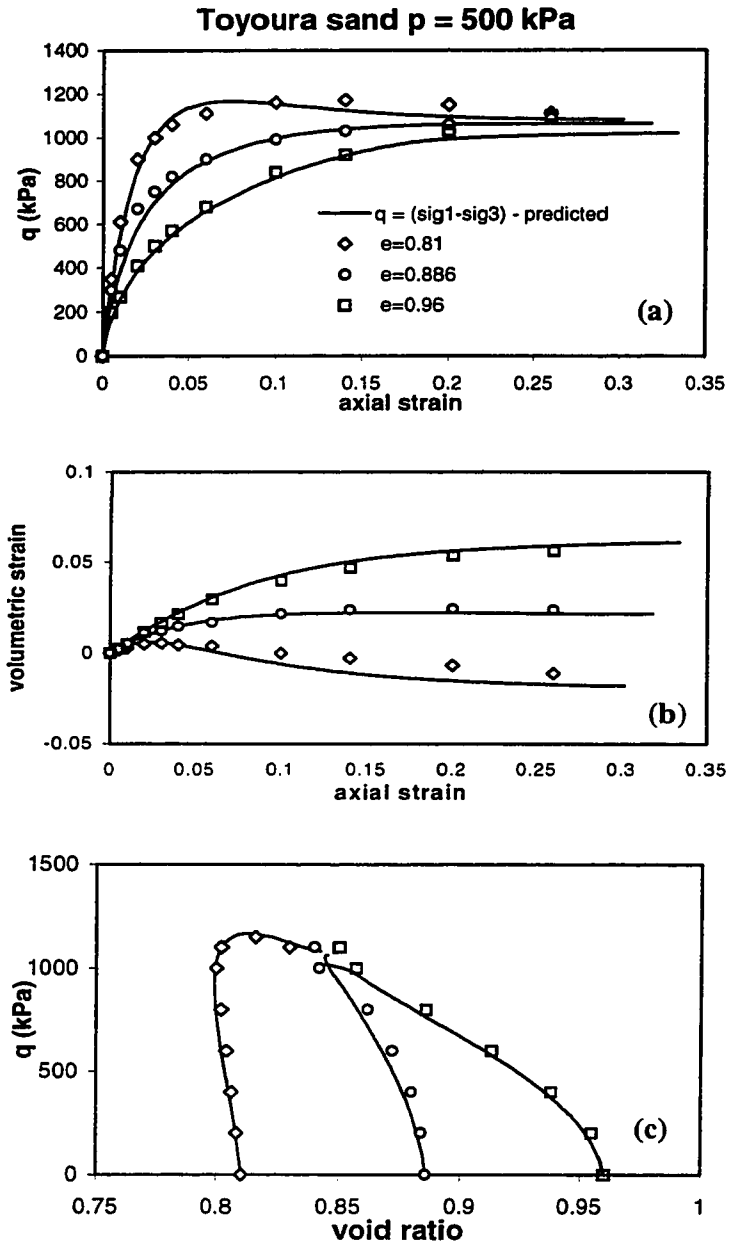


**Figure 5-21** Measured vs. predicted response of samples of Toyoura sand with different initial densities consolidated to 500 KPa and sheared in drained triaxial compression (Data from Verdugo et al., 1996).

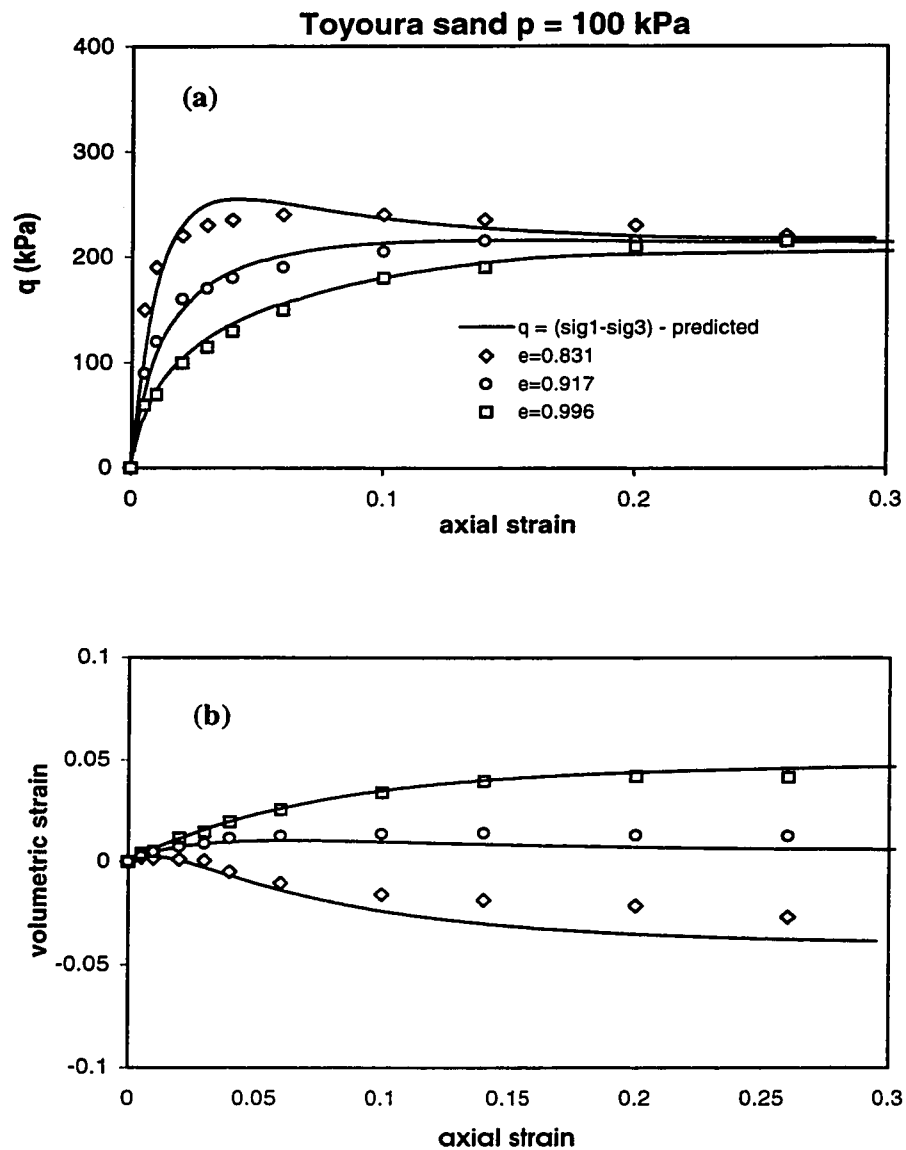


**Figure 5-22** Measured vs. predicted response of samples of Toyoura sand with different initial void ratios, consolidated to 100 kPa and sheared in drained triaxial compression (Data from Verdugo et al., 1996)

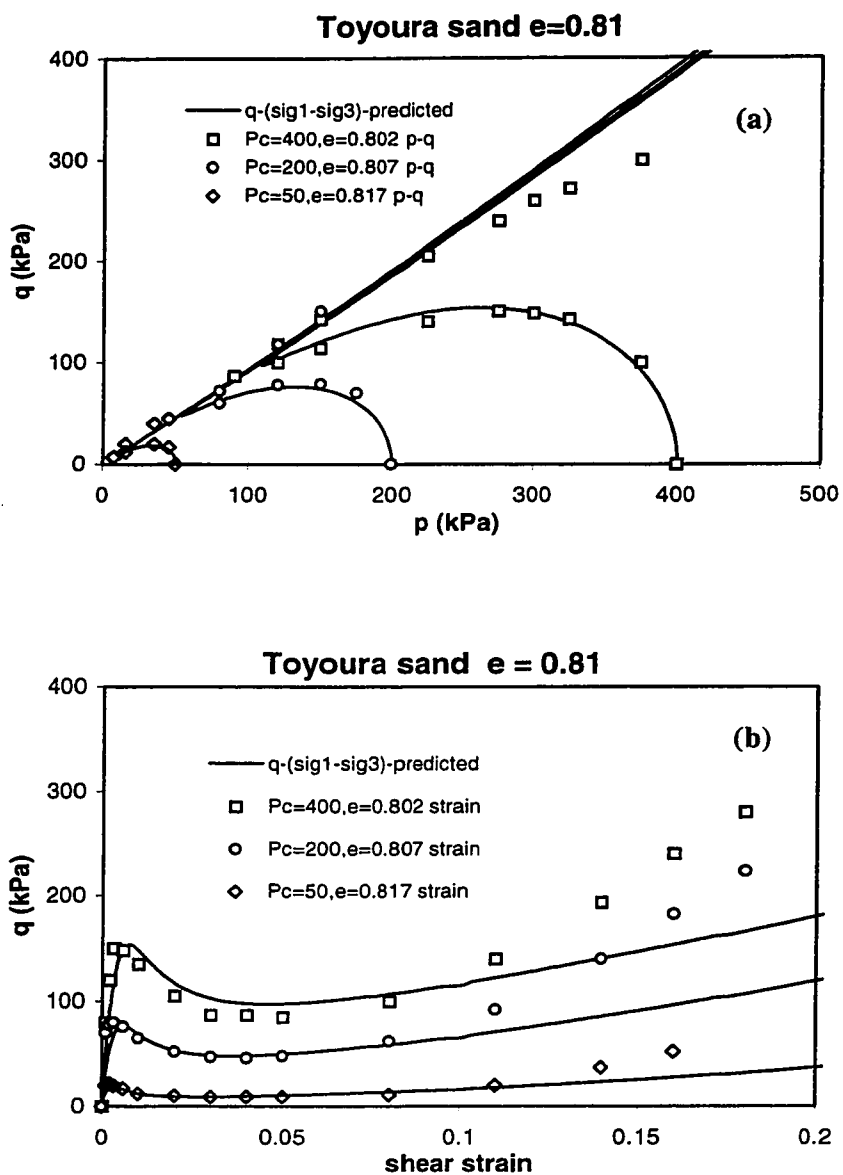


**Figure 5-23** Model predictions and measured data for undrained triaxial extension tests on Toyoura sand. Notice the difference between measured and predicted responses at larger strain levels (Data from Yoshimine, 1996)

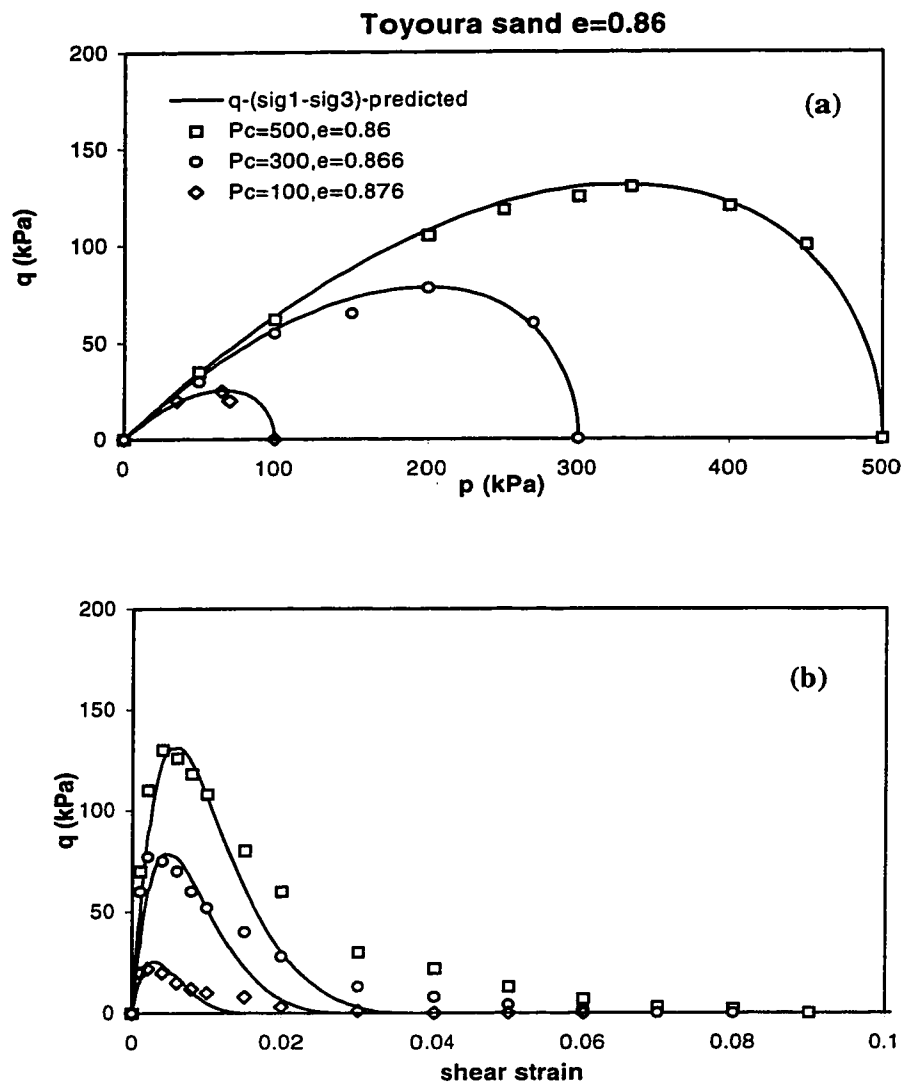


**Figure 5-24** Model predictions and test data on the complete liquefaction of Toyoura sand at void ratios of 0.86 or more ( $D_r=30\%$  or less) in undrained triaxial extension (Data from Yoshiminie, 1996)

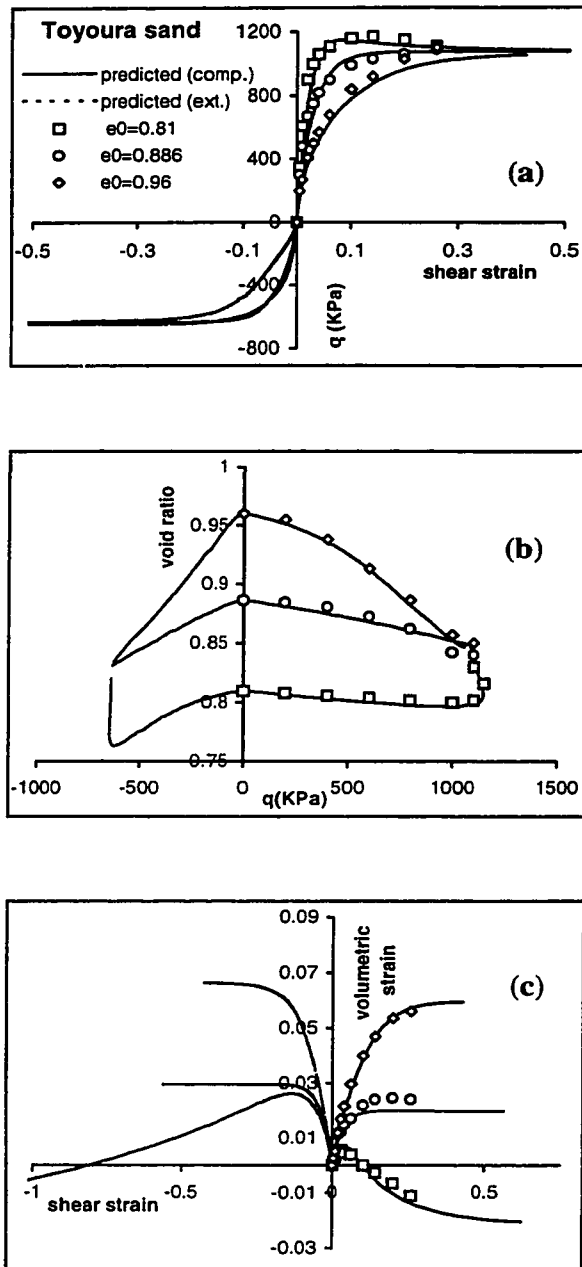


**Figure 5-25** Differences between drained behavior of Toyoura sand consolidated to 500 kPa and sheared in triaxial compression and extension (Note: (c) not to scale).

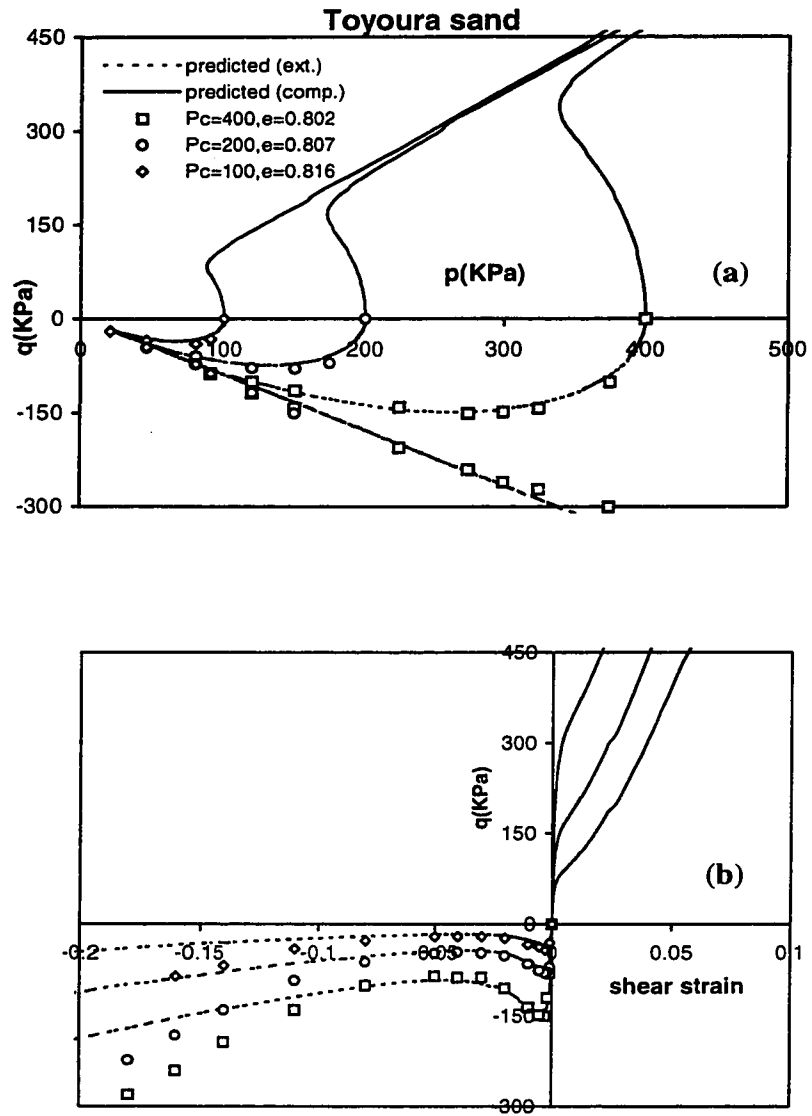


**Figure 5-26** Differences between undrained behavior of samples of Toyoura sand having the same state, but sheared in triaxial compression and extension (Data from Yoshimine, 1996).



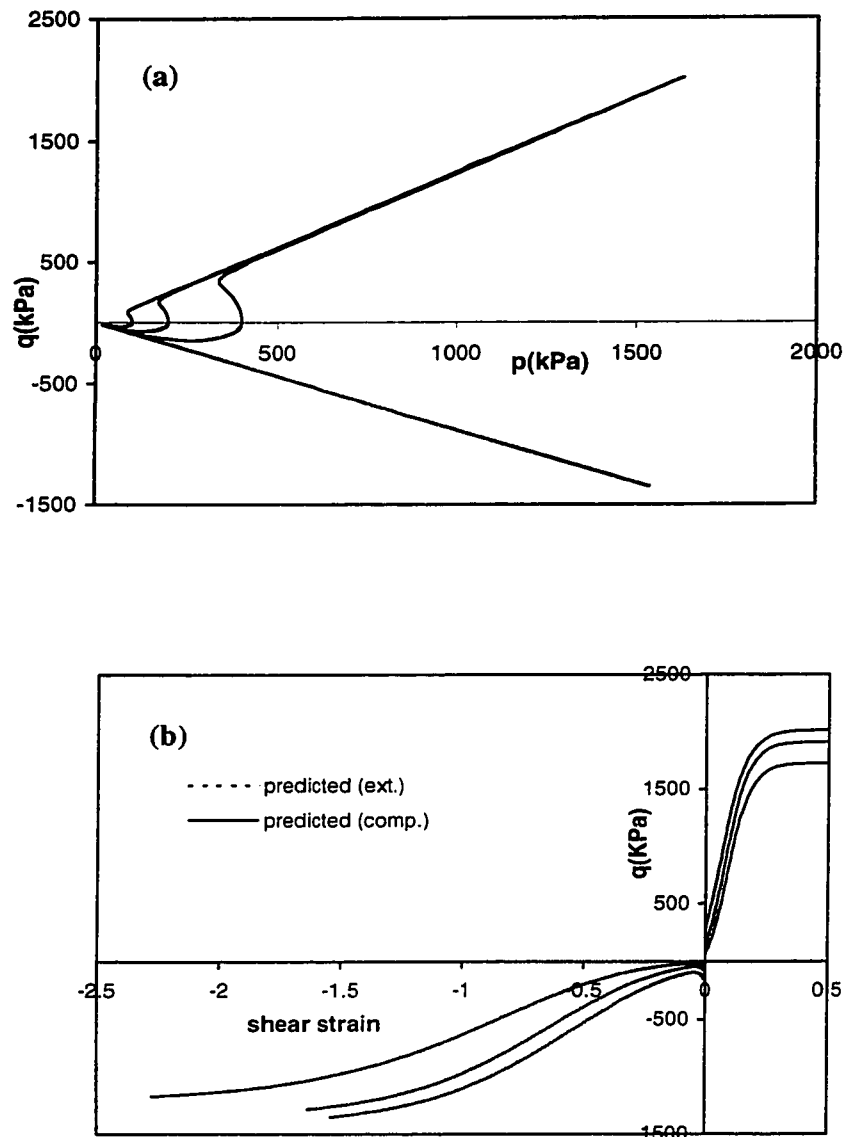


**Figure 5-27** Differences between the stress-strain response, and the amount of strain required to reach the ultimate state in undrained triaxial compression and extension

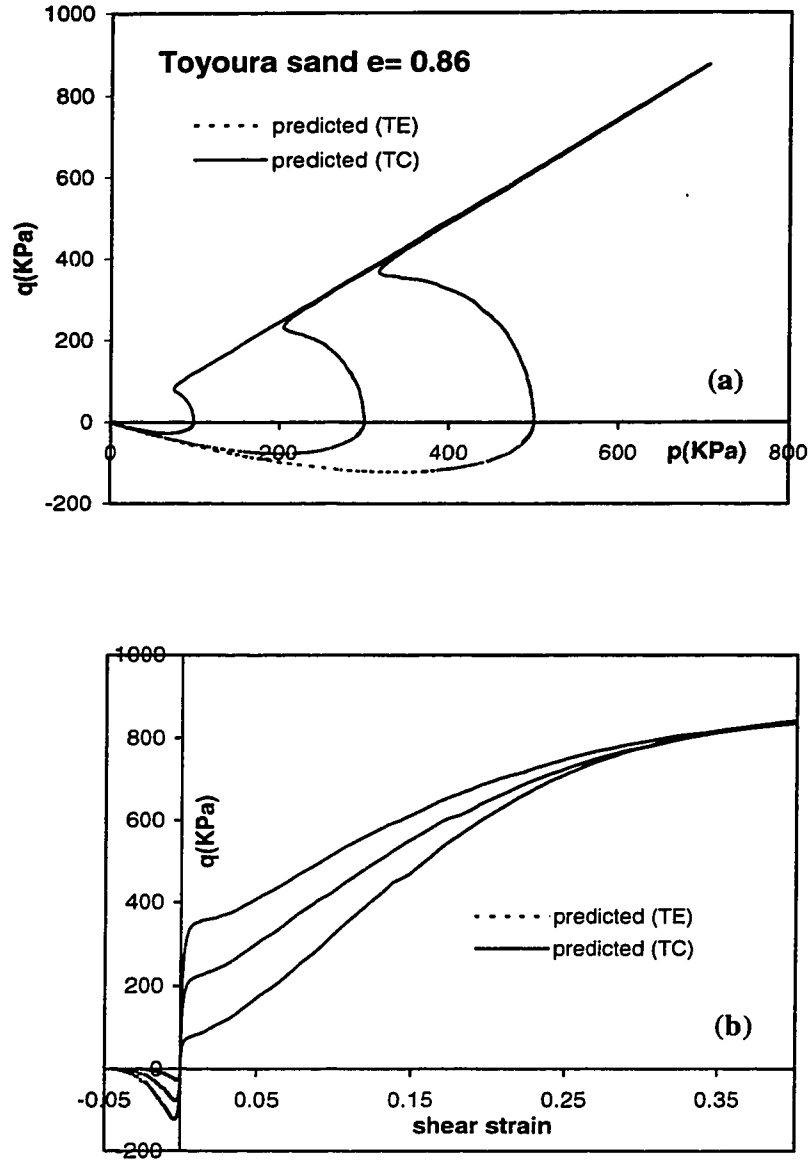


**Figure 5-28** Predicted differences between undrained response of Toyoura sand at a void ratio of 0.86 to loading in triaxial compression and extension: strong dilatancy in compression and complete liquefaction in extension

## Appendix 5A: General formulation of the stress-strain relationship for triaxial conditions

In an elastoplastic material, total strains are assumed to be the summation of the elastic and plastic components:

$$d\epsilon_p = d\epsilon_p^e + d\epsilon_p^p \quad 5A-1-a$$

$$d\epsilon_q = d\epsilon_q^e + d\epsilon_q^p \quad 5A-1-b$$

where  $d\epsilon_p = d\epsilon_1 + 2d\epsilon_3$  is the increment of volumetric strain and  $d\epsilon_q = 2 ( d\epsilon_1 - d\epsilon_3 ) / 3$  is the increment of shear strain, and  $d\epsilon_1$  and  $d\epsilon_3$  are increments of the major and minor principal strain. The superscripts e and p refer to the elastic and plastic portions respectively. For an isotropic linear elastic material, elastic strains are related to increments of stress as follows:

$$d\epsilon_q^e = \frac{dq}{3G} \quad 5A-2-a$$

$$d\epsilon_p^e = \frac{dp}{K} \quad 5A-2-b$$

in which  $q = (\sigma_1 - \sigma_3)$  is the deviatoric stress,  $p = (\sigma_1 + \sigma_2 + \sigma_3)/3$  is the mean normal stress, and  $G$  and  $K$  are the elastic shear and bulk moduli respectively. Increments of plastic strain can be obtained from:

$$d\epsilon_p^p = \Lambda \frac{\partial g}{\partial p} \quad 5A-3-a$$

$$d\epsilon_q^p = \Lambda \frac{\partial g}{\partial q} \quad 5A-3-b$$

in which  $g$  is the plastic potential function and  $\Lambda$  is the positive "plastic index". The yield function defined by  $f = 0$  may in general depends on a series of  $n$  hardening parameters  $N_i$ , which depend in turn on the plastic volumetric and shear strains:

$$f = f ( p, q, \psi_i ) \quad 5A-4$$

$$N_i = N_i (\epsilon_p^p, \epsilon_q^p)$$

5A-5

During plastic deformation, the state of stress stays on the yield surface. This requires the consistency condition to be satisfied:

$$\dot{f} = \frac{\partial f}{\partial p} \dot{p} + \frac{\partial f}{\partial q} \dot{q} + \sum_1^n \frac{\partial f}{\partial N_i} \dot{N}_i \quad 5A-6$$

and we have :

$$\dot{N}_i = \frac{\partial N_i}{\partial \epsilon_p^p} \dot{\epsilon}_p^p + \frac{\partial N_i}{\partial \epsilon_q^p} \dot{\epsilon}_q^p \quad 5A-7$$

Substituting Equation 5A-7 in 5A-6 and using Equation 5A-3 leads to the following relationship for the plastic index  $\Lambda$ :

$$\Lambda = - \frac{\frac{\partial f}{\partial p} \dot{p} + \frac{\partial f}{\partial q} \dot{q}}{\sum_1^n \frac{\partial f}{\partial N_i} \left( \frac{\partial N_i}{\partial \epsilon_p^p} \frac{\partial g}{\partial p} + \frac{\partial N_i}{\partial \epsilon_q^p} \frac{\partial g}{\partial q} \right)} \quad 5A-8$$

Or equivalently:

$$\Lambda = \frac{1}{H} \left( \frac{\partial f}{\partial p} \dot{p} + \frac{\partial f}{\partial q} \dot{q} \right) \quad 5A-9$$

in which the plastic modulus  $H$  is defined by the following equation:

$$H = \sum_1^n \frac{\partial f}{\partial N_i} \left( \frac{\partial N_i}{\partial \epsilon_p^p} \frac{\partial g}{\partial p} + \frac{\partial N_i}{\partial \epsilon_q^p} \frac{\partial g}{\partial q} \right) \quad 5A-10$$

For a given yield function  $f$  and plastic potential function  $g$ , Equation 5A-3 can be used together with Equation 5A-8 to obtain increments of plastic strain resulting from an increment of stress.

## *Chapter 6*

# **6 Formulation of the constitutive model in general stress space**

## **6.1 Introduction**

The constitutive model presented in Chapter 5 will be generalized in this chapter to include cases in which the state of stress does not correspond to that of the triaxial condition. The model will then be used to simulate effects of a number of factors such as the consolidation stress history, direction of loading, soil fabric and mode of shearing on the behavior of sands.

Some characteristics of the model related to its formulation for triaxial conditions were explained previously in Section 5.1. In what follows, some features of the model pertaining to the generalized formulation are listed:

1-While the model can be used to predict the behavior of sands over a wide range of densities and pressures, it also specifically addresses issues that can be of particular importance in modeling the response of loose collapsible soils. Taking these factors into account can be important in analysing the behavior of soil masses subjected to static liquefaction. These factors include effects of direction of loading, anisotropic consolidation, mode of shearing and soil fabric.

2-The parameter  $M_p$ , which is measured directly from experiment, introduces some small to medium-strain characteristics of the soil into the model, and enables it to capture most of the effects mentioned previously. Many of these effects seem to result from the small to medium-strain anisotropy or the initial fabric of the soil, and might disappear at larger levels of strain. In contrast, most of the recent constitutive models for sand use isotropic elastic parameters to model small strain and ultimate state or failure parameters to model large strain behavior. Another series of parameters are often needed to model the behavior between these two extremes. Determination of these parameters often requires curve fitting against the response of the soil obtained from specific tests.

3-To the author's knowledge, except for one case (i. e. the model by Pestana, 1994), other recently presented constitutive models for sands (e. g. Jefferies, 1993; Crouch et al., 1994; Manzari and Dafalias, 1997) that attempt to predict the behavior over a wide range of states with a unique set of parameters, use the ultimate state line (USL) as a reference to which different states of the soil are compared. A major predicament in this approach, however, is the difficulty in the determination of the position of the USL. More problematic is the uncertainty of its position, when sand is loaded in different directions or modes of shearing. Inaccuracies in the determination of the USL in such models can cause significant errors in the predicted response. The current model still relies on the position of the USL in determining the state of the soil at "large strain". However, effects of uncertainties in the position of the USL on soil properties at smaller levels of strain are offset by measuring key elements of these properties from experiment, and correlating them to the USL. In these correlations, effects of mode of shearing, soil fabric or anisotropy are accounted for. Consequently, the model is able to predict differences in soil response that result from these effects, through using a unique USL.

4-The model clearly distinguishes between directional properties of sand produced by stresses from those due to initial sand structure. Separate and independent measures are used for each of them. Changes in the yielding behavior caused by stress-induced

anisotropy are represented by a tensor  $\alpha$  and those due structural anisotropy by a tensor  $a$ . A material parameter ( $a$ ) that can be measured readily from undrained triaxial tests is used to determine the degree of structural anisotropy and facilitates the comparison of anisotropies of different sands. Many current models for sand either account only for the first type of anisotropy or treat both forms of anisotropy within the same variable. Experimental evidence, however, suggest that these two types of directional properties are governed by different physical phenomena, the first being readily altered by changes in stress state and the second being less affected by the stress history.

5-A particular difficulty in modeling effects of void ratio, direction of loading, soil fabric, etc. lies in the determination of the variation of the plastic modulus with these factors. The hardening rule used in the current model is such that the effects of these factors on the plastic modulus considered through the shape of the yield surface, without the need for additional considerations.

6- In most current models, the amount of strain experienced by the soil from the start of shearing, or the work done during this period is related to the hardening of the soil. This requires knowledge of the amount of such strains or such work at any step during loading, if prediction of the response to the next loading step is to be made. However, the current model is based on a "state hardening" concept rather than the above-mentioned "strain hardening" or "work hardening" formulations. In this model, knowledge of the current "state" relative to the ultimate state is used to obtain the current hardening modulus. This characteristic of the model helped simulate the behavior of Ottawa sand in the two-stage undrained to drained tests described in Chapter 5.

7-Considering the wide range of physical phenomena and soil responses that can be predicted by the model, the model is believed to be particularly simple in its formulation and parameter determination. Model parameters are determined in terms of strength and deformation concepts that are well established in geotechnical practice. They generally

have clear physical meaning and can be determined directly without trial and error or curve fitting.

## 6.2 General formulation of the stress-strain relationship

General formulation of the stress-strain relationship and the definition of the variables used in the formulation of the generalized model are briefly reviewed in this section. Model elements needed to obtain the required relationships will be given in the next section. In this chapter, slightly larger italicized notations will be used to refer to second order tensor, or vector quantities, and normal letters will refer to scalar quantities.

### 6.2.1 General formulation

An increment of total strain ( $\dot{\boldsymbol{\epsilon}}$ ) in an elastoplastic material is assumed to be composed of an elastic reversible part ( $\dot{\boldsymbol{\epsilon}}^e$ ) and a plastic irreversible part ( $\dot{\boldsymbol{\epsilon}}^p$ ) such that:

$$\dot{\boldsymbol{\epsilon}} = \dot{\boldsymbol{\epsilon}}^e + \dot{\boldsymbol{\epsilon}}^p \quad (6-1)$$

The increment of total strain and each one of its two parts can be decomposed into a volumetric ( $v$ ) and a deviatoric or shear ( $e$ ) component such that

$$(a) \quad \dot{v} = \dot{\boldsymbol{\epsilon}}_{ii} \quad (b) \quad \dot{e} = \dot{\boldsymbol{\epsilon}} - \frac{1}{3} \dot{v} \boldsymbol{\delta} \quad (6-2)$$

where  $\boldsymbol{\delta}$  is the Kroneker delta. Increments of elastic volumetric strain ( $\dot{v}^e$ ) and elastic shear strain ( $\dot{e}^e$ ) are related to the elastic bulk modulus ( $K$ ) and elastic shear modulus ( $G$ ) by the following equations:



$$(a) \dot{\nu}^e = \frac{\dot{p}}{K} \quad (b) \dot{\epsilon}^e = \frac{\dot{s}}{2G} \quad (6-3)$$

where  $s$  is the deviatoric stress and  $p$  is the mean normal stress defined by:

$$(a) s = \sigma - p \delta \quad (b) p = \frac{1}{3} \sigma_{ii} \quad (6-4)$$

Increments of plastic strain  $\dot{\epsilon}^p$  can be obtained from:

$$\dot{\epsilon}^p = \langle \Lambda \rangle P \quad (6-5)$$

The scalar  $\Lambda$  is the plastic (loading) index and  $P$  is a second order tensor determining the “direction” of the plastic strain rate. The symbol  $\langle \ \rangle$  represents the MacCaulay brackets that is defined by:  $\langle a \rangle = a$  if  $a > 0$ , and  $\langle a \rangle = 0$  otherwise.

Though not necessary, it is possible to postulate the existence of a plastic potential function  $g$  such that:

$$P = \frac{\partial g}{\partial \sigma} \quad (6-6)$$

The tensor  $P$  can be decomposed into its deviatoric ( $P'$ ) and spherical ( $p''$ ) components:

$$(a) P = P' + p'' \delta \quad (b) p'' = \frac{1}{3} (\text{tr} P) \quad (6-7)$$

such that:

$$(a) \dot{\epsilon}^p = \langle \Lambda \rangle P' \quad (b) \dot{\nu}^p = \langle \Lambda \rangle (3 p'') \quad (6-8)$$

Increments of stresses can now be related to increments of total strains according to the following equations:

$$(a) \dot{p} = K [\dot{\nu} - \langle \Lambda \rangle (3p'')] \quad (b) \dot{s} = 2G [\dot{\epsilon} - \langle \Lambda \rangle P'] \quad (6-9)$$

The tensor  $Q$  defining the direction normal to the yield (loading) surface  $f$  can also be decomposed into its deviatoric component  $Q'$  and spherical component  $Q''$ :

$$Q = Q' + Q'' \delta \quad (6-10)$$

$$(a) Q' = \frac{\partial f}{\partial \sigma} \quad (b) Q'' = \frac{1}{3} (\text{tr} Q) \quad (6-11)$$

These components can be determined by differentiating the yield function with respect to the shear stress tensor  $s$  and mean normal stress  $p$ :

$$(a) Q' = \frac{\partial f}{\partial s} \quad (b) 3Q'' = \frac{\partial f}{\partial p} \quad (6-12)$$

An important part of the establishment of the stress-strain relationship is the determination of the plastic index  $\Lambda$  by applying the consistency condition. For a total of  $n$  hardening parameters  $N_i$  ( $i = 1, n$ ) that change with strain, imposition of the consistency condition following the application of a stress increment ( $\dot{\sigma}$ ) leads to:

$$\dot{f} = \frac{\partial f}{\partial \sigma} \dot{\sigma} + \sum_{i=1}^n \frac{\partial f}{\partial N_i} \dot{N}_i = 0 \quad (6-13)$$

If increments of the hardening parameters  $N_i$  are functions of the increments of plastic volumetric strains  $\dot{\nu}''$  and the plastic shear strain tensor  $\dot{\epsilon}''$  we have:

$$\dot{N}_i = \frac{\partial N_i}{\partial v^p} \dot{v}^p + \frac{\partial N_i}{\partial e^p} \dot{e}^p \quad (6-14)$$

Substituting from Equations 6-8 and 6-14 into 6-13 leads to the determination of the plastic index  $\Lambda$  for a given stress increment (i. e. in “stress controlled” conditions):

$$\Lambda = \frac{1}{H} [Q' \dot{s} + 3Q'' \dot{p}] \quad (6-15)$$

where the plastic modulus  $H$  is defined according to the following:

$$H = -\frac{\partial f}{\partial N_i} \left( \sum_{i=1}^n \frac{\partial N_i}{\partial v^p} (3P'') + \sum_{i=1}^n \frac{\partial N_i}{\partial e^p} P' \right) \quad (6-16)$$

In “strain controlled” conditions, Equation 6-9 can be used to substitute for the stress increment and the following expression will result for  $\Lambda$  after some rearrangements:

$$\Lambda = \frac{K(3Q'')\dot{v} + 2GQ'\dot{e}}{H + K(3Q'')(3P'') + 2GQ'P'} \quad (6-17)$$

The constitutive relationships are now complete and can be used to determine the stress-strain relationship. For cases of mixed stress and strain-controlled conditions, the appropriate relationship can be obtained by proper substitutions in the consistency condition.

## 6.2.2 Determination of the constitutive relationships using unit tensors

In many cases, it is more convenient to use unit normals to define directions of loading and plastic strain, because it is sometimes difficult to explicitly define suitable functions for the yield surface and plastic potential. Sub-surfaces or relative directions are therefore given in some cases such that the complete directions of loading and plastic strain are defined by them. The use of unit tensors can also lead to simpler forms for the stress-strain relationships. The stress-strain relationships given previously will therefore be determined in terms of such tensors.

Referring to the tensor  $P$  that defines the direction of plastic strain, Equation 6-7 can be written in the following form:

$$n_p = u_p + \frac{1}{3} D \delta \quad (6-18)$$

$$D = \frac{\text{tr}P}{|P|} = \frac{\dot{v}^p}{|e|} \quad (6-19)$$

where the symbol  $| |$  refers to the norm of the tensor, or the length of the vector quantities. The tensor  $n_p$  defines the direction normal to the plastic potential function and  $u_p$  is a unit tensor normal to the deviatoric subsurface such that:  $u_p u_p = 1$ . The "dilatancy parameter"  $D$  determines the volumetric strains associated with shear strains and can be obtained from a suitable stress-dilatancy relationship.

The loading direction defined by the tensor  $Q$  can now be obtained from the following relationships derived from Equation 6-10:

$$n_Q = u_Q + \frac{1}{3} R \delta \quad (6-20)$$

$$R = 3 \frac{Q^r}{|Q|} = \frac{\frac{\partial f}{\partial p}}{\left| \frac{\partial f}{\partial s} \right|} \quad (6-21)$$

where  $n_Q$  is the tensor normal to the loading surface and  $u_Q$  is the unit tensor normal to the deviatoric subsurface and we have:

$$u_Q u_Q = 1 \quad (6-22)$$

The constitutive equations, therefore, can be written in terms of the unit normals and the scalar ratios defined above. Equation 6-15 can now be written as:

$$L = \frac{1}{H_n} [u_Q \dot{s} + R \dot{p}] \quad (6-23)$$

where  $L = \Lambda |P'|$  is the normalized loading index and

$$H_n = \frac{H}{|P'| |Q'|} = \frac{1}{|Q'|} \frac{\partial f}{\partial N_i} \left( - \sum_{i=1}^n \frac{\partial N_i}{\partial v^p} D - \sum_{i=1}^n \frac{\partial N_i}{\partial e^p} u_p \right) \quad (6-24)$$

is the “normalized plastic modulus”.

Following the same procedure used to obtain Equation 6-17 leads to:

$$L = \frac{KR\dot{v} + 2Gu_Q\dot{e}}{H_n + KR D + 2Gu_Q u_p} \quad (6-25)$$

In cases in which an associated flow rule for the deviatoric parts is postulated, we will have  $u_p = u_Q$ , and consequently  $u_p u_Q = 1$  should be substituted in the above equation.

Strain increments can now be obtained from the following equations by substituting for  $\Lambda$  in Equations 6-8:

$$(a) \dot{e}^p = \langle L \rangle u_p \quad (b) \dot{v}^p = \langle L \rangle D \quad (6-26)$$

and stress increments will be:

$$(a) \dot{p} = K [\dot{v} - \langle L \rangle D] \quad (b) \dot{s} = 2G [\dot{e} - \langle L \rangle u_p] \quad (6-27)$$

## 6.3 Model elements

Model elements presented in Chapter 5 for triaxial stress conditions will be extended here to the general stress space. The generalization will be based on the physical evidence presented in Chapters 3 and 4 and other published works.

### 6.3.1 The yield function

The yield function used in Chapter 5 for triaxial stress conditions takes the following form in general stress space:

$$f = (\eta - \alpha)(\eta - \alpha) - M_\alpha^2 \left[ 1 - \left( \frac{p}{p_\alpha} \right)^{1/2} \right] = 0 \quad (6-28)$$

in which  $\eta = \sqrt{\frac{3}{2}} \frac{s}{p}$  is the stress ratio tensor and  $\alpha = \sqrt{\frac{3}{2}} \frac{s_\alpha}{p_\alpha}$  is the tensor that accounts for the effect of stress-induced anisotropy on the yielding behavior of the material. The coefficient  $\sqrt{\frac{3}{2}}$  is introduced in the above definitions in order to make stress ratio quantities directly comparable with those commonly used in triaxial tests. In 3D

principal stress space, this function is represented by a drop-shaped surface with its tip at the origin of the stress space (Figure 6-1).

The stress ratio  $\alpha$  and the pressure  $p_\alpha$  correspond to the stress state at which the normal to the yield surface becomes parallel to the hydrostatic axis in principal stress space. The scalar  $M_\alpha^2$  can be determined from the stress ratio tensors  $\alpha$  and  $M_p$ , as follows:

$$M_\alpha^2 = 5 M_p M_p - 6\alpha M_p + \alpha\alpha \quad (6-29)$$

in which  $M_p = \sqrt{\frac{3}{2}} \frac{s}{p_p}$  is the stress ratio at points where the normal to the yield surface

in principal stress space is perpendicular to the hydrostatic axis. In a meridian section (i. e. the section containing the hydrostatic axis) of the yield surface, this stress ratio corresponds to the point of peak shear stress on the yield surface. The locus of all stress ratios  $M_p$  will be referred to as the “shape hardening surface”. In principal stress space, the shape-hardening surface can be illustrated as shown in Figure 6-1. The physical meaning and method of determination of the quantities that appear in the equations of the yield surface are explained in the following sections.

### 6.3.1.1 *Stress-induced anisotropy*

The stress ratio  $\alpha$  in the equation of the yield surface is a measure of the stress-induced anisotropy of the soil. Since the current formulation primarily addresses soil response to monotonic loading, and provided that the number and/or size of the stress reversals imposed on the soil is limited, it is assumed that  $\alpha$  remains unchanged during shearing. In the octahedral plane, anisotropic consolidation leads to a shift in the yield surface in the direction of consolidation (Figure 6-2), which is represented by the stress ratio  $\alpha$ .

It was noted in Chapter 3 that for a soil consolidated anisotropically along a stress ratio  $\eta_c$  and to a pressure  $p_c$ , the pressure  $p_\alpha$  and the stress ratio  $\alpha$  may not be equal to  $p_c$  and  $\eta_c$  respectively. A procedure to determine the former stresses from the latter was suggested in Chapter 3. In the current formulation, however, these stresses will be taken to be equal in order to preserve the simplicity of the formulation. We will therefore have:

$$p_\alpha = p_c \quad (6-30)$$

$$\alpha = \eta_c \quad (6-31)$$

Model simulations did not seem to deviate from the actual behavior significantly as a result of this simplification.

Measurements of  $M_p$  from undrained tests reported in Section 4.8 and elsewhere (e.g. in Vaid et al., 1985) suggested that the stress ratio  $M_p$  seemed to be not affected by anisotropic consolidation. It was shown in the previous chapters variations in  $M_p$  could reflect the effect of inherent anisotropy on the yielding behavior. The independence of  $M_p$  from anisotropic consolidation stresses, therefore, may be interpreted as being the result of the independence of the effects of inherent anisotropy from those of the stress-induced anisotropy. Use of values for  $M_p$  independent of  $\alpha$  led to accurate model predictions of the behavior of anisotropically consolidated sand, as will be shown in Section 6.4.2. However, if anisotropic consolidation is made along a stress ratio that is higher than  $M_p$ , the material will in fact experience shear stresses that are outside the region of small strain behavior. Therefore,  $M_p$  will increase accordingly. This increase in  $M_p$  due to high consolidation stress ratios was observed in Section 4.8 and reported in a recently published work (di Prisco et al., 1994). The stress ratio  $M_p$ , therefore, will not be changed as long as  $\alpha$  remains inside the shape hardening surface, otherwise it will increase to a value slightly larger than  $\alpha$ . In this case, the shape-hardening surface will move along  $\alpha$ . Rules governing the movement of the shape hardening surface with  $\alpha$



will not be discussed here, as they are more relevant to modeling the behavior in cyclic loading.

### 6.3.1.2 Structural (inherent) anisotropy

For an anisotropic material, full description of the behavior requires knowledge of the six components of the stress tensor, or the principal stresses and the directions of anisotropy relative to the principal directions. However, in the majority of practical applications both in soils in-situ and in samples made in the laboratory, the soil exhibits a cross-anisotropic behavior, being strongest in the direction of deposition and weakest in directions perpendicular to it. Accounting for anisotropy in cross-anisotropic materials is significantly more straightforward than in materials with general anisotropic behavior. In such materials, description of the behavior is possible through knowledge of the three principal stresses (or a suitable combination of three stress invariants) in addition to an indication of the direction of application of the stresses relative to the direction of cross-anisotropy. The formulation presented here is aimed at modeling such anisotropies.

The effect of structural (inherent) anisotropy on the yielding behavior is considered through the variable  $M_\alpha^2$  that is defined in Equation 6-29. The stress ratio  $M_p$  in this equation can be obtained from the following relationships:

$$M_p = M_p u_{\bar{s}} \quad (6-32)$$

$$M_p = |M_p M_p|^{1/2} \quad (6-33)$$

where

$$u_{\bar{s}} = \frac{\bar{s}}{|\bar{s}|} \quad (6-34)$$

such that we have  $u_{\bar{s}} u_{\bar{s}} = 1$  and  $\bar{s} = s - p\alpha$ . The scalar  $M_p$  is determined from the following relationships:

$$M_p = a u_{\bar{s}} + [(a u_{\bar{s}})^2 + r^2 - a^2]^{1/2} \quad (6-35)$$

$$a = a u_a \quad (6-36)$$

$$a = |aa|^{1/2} \quad (6-37)$$

and  $u_a$  is a unit tensor such that  $u_a u_a = 1$ . The scalar values  $a$  and  $r$  in the above equations can be determined from the following relationships:

$$a = (M_{p,c} - M_{p,e}) / 2 \quad (6-38)$$

$$r = (M_{p,c} + M_{p,e}) / 2 \quad (6-39)$$

$$(a) M_{p,c} = \frac{6 \sin \varphi_{p,c}}{(3 - \sin \varphi_{p,c})} \quad (b) M_{p,e} = \frac{6 \sin \varphi_{p,e}}{(3 + \sin \varphi_{p,e})} \quad (6-40)$$

The friction angles at peak in TC and TE are denoted by  $\varphi_{p,c}$  and  $\varphi_{p,e}$  respectively and are functions of void ratio and pressure as will be seen in the next section. A description of the notations used above is given in what follows:

$a$  : stress ratio tensor indicating the degree of inherent anisotropy in the yielding behavior and its principal directions are oriented along the principal directions of anisotropy

$u_s$  : unit tensor of deviatoric stress

$r$  : material parameter corresponding to the average stress ratio at peak

$M_{p,c}$  ,  $M_{p,e}$ : stress ratios at the peak of the yield surface measured from triaxial compression and extension tests respectively

The above relationships were written for general stress conditions. However, it is useful to examine results of the above relationships for the special cases that correspond to the stress states in the common testing equipment.

If a sample of soil is deposited along the z-direction such that its strongest response is exhibited when loaded in this direction, and if the x-y-z directions remain principal directions during shearing (as e. g. in most triaxial or true triaxial tests), then changes in the stress ratio  $M_p$  as represented by Equation 6-35 can be illustrated by Figure 6-3. In this case, the unit tensor of deviatoric stress  $u_s$  will have three non-zero components that can be obtained from the following equations:

$$(a) \quad u_{s,zz} = \sqrt{\frac{2}{3}} \cos \beta \quad (6-41)$$

$$(b) \quad u_{s,xx} = \sqrt{\frac{2}{3}} \cos (2\pi/3 - \beta)$$

$$(c) \quad u_{s,yy} = \sqrt{\frac{2}{3}} \cos (2\pi/3 + \beta)$$

in which  $\beta$  is the angle from the z-direction to the point representing the stress state, measured clockwise in the octahedral plane. This angle is related to the magnitudes of the three principal stresses (that are applied in the xyz directions in this case) by the following equation:

$$\tan \beta = \frac{\sqrt{3}(\sigma_y - \sigma_x)}{2\sigma_z - \sigma_y - \sigma_x} \quad (6-42)$$

However, for an anisotropic material, states of stress for tests conducted in the hollow cylinder (HS) apparatus can not be fully described in principal stress space (or the octahedral plane). Therefore, it is common in these tests to represent loading conditions in terms of the parameter  $b$  (or the modified Lode angle  $\theta$ ) and the angle  $\alpha_\sigma$  between the

direction of application of the major principal stress and the direction of soil deposition (the latter direction taken to be the z-direction here). In this case, the four non-zero, non-principal stresses can be determined in terms of the two stress invariants  $p$  and  $s$ , plus the two angles  $\theta$  and  $\alpha_\sigma$  as was given in Equation 4-58 in Chapter 4. From this equation, it is possible to derive the four non-zero components of the unit tensor of deviatoric stress  $u_s$ :

$$(a) \quad u_{s,zz} = \frac{1}{\sqrt{6}} [ \sqrt{3} \cos(\theta - \pi/6) \cos 2\alpha_\sigma - \sin(\theta - \pi/6) ] \quad (6-43)$$

$$(b) \quad u_{s,xx} = \frac{1}{\sqrt{6}} [ -\sqrt{3} \cos(\theta - \pi/6) \cos 2\alpha_\sigma - \sin(\theta - \pi/6) ]$$

$$(c) \quad u_{s,yy} = \frac{2}{\sqrt{6}} \sin(\theta - \pi/6)$$

$$(d) \quad u_{s,zx} = \frac{1}{\sqrt{2}} \cos(\theta - \pi/6) \sin 2\alpha_\sigma$$

In HC tests, one direction usually remains principal direction. In the above equations, this is assumed to be the y-direction, and the angle  $\alpha_\sigma$  is measured in the zx plane. The modified Lode angle  $\theta$  is limited between 0 and  $\pi/3$ , and  $\alpha_\sigma$  can change from 0 to  $\pi/2$ .

The unit tensor of anisotropy  $u_a$  determines the effect of the direction of loading relative to the direction of anisotropy, on the yield strength. In a coordinate system directed along the principal directions of material anisotropy, this tensor is represented by a vector in the octahedral plane that is oriented in the direction of maximum yield strength (that normally coincides with the direction of soil deposition). If this direction is taken to be the z-direction, then the three components of this vector can be obtained by substituting for  $\beta = 0$  in Equation 6-41.

Note that the double contraction in the term  $u_a u_s$  of Equation 6-35 implies that in HC tests, the component  $u_{s,zx}$  of the unit tensor of deviatoric stress has no effect on the value of  $M_p$  calculated from this equation, since its corresponding component in  $u_a$  is zero. This means that the anisotropy in yield strength is primarily a function of the relative

magnitudes of the normal stresses applied in the principal directions of anisotropy rather than the in-plane shear stresses. Variations of  $M_p$  obtained from HC tests studied in Chapter 4 and yield loci obtained from results of TTT reported by Yamada and Ishihara (1979) were interpreted in Chapter 4 as implying such dependency.

From Figure 6-3 and from Equation 6-35 it can be concluded that the maximum yield strength as represented by the norm of the stress ratio tensor  $M_p$  (i. e. the scalar value  $M_p$ ) is obtained when loading is applied in the same direction as the direction of  $u_a$  (i. e. the direction of deposition that corresponds to TC). The minimum occurs when  $u_s$  and  $u_a$  are in opposite directions (as in the TE).

Peak strengths corresponding to TC and TE tests in the above equations are assumed to be measured from triaxial tests in which during loading, the major principal stress is oriented along the direction of deposition (strongest response) in the TC test, and normal to this direction (weakest response) in the TE test. Therefore in tests in which the sample is rotated after its deposition and prior to its placement in the triaxial apparatus, the TC and TE tests will not provide the parameters required for the above relationships directly. In this case, the scalar values  $a$  and  $r$  should be determined from results of such tests using the actual directions of  $u_s$  and  $u_a$  that are now rotated relative to each other.

### 6.3.1.3 *Effect of void ratio and pressure on the yielding behavior*

The effect of void ratio and mean normal stress on the yielding behavior is accounted for, through the variations in the friction angle at peak in TC and TE (used in Equation 6-40) with the normalized void ratio  $e_n$  :

$$\begin{aligned} \text{(a)} \quad & \sin \varphi_{p,c} = \sin \varphi_{\mu} - k_p (e_n - e_{\mu}) \\ \text{(b)} \quad & \sin \varphi_{p,e} = \sin \varphi_{\mu} - a_p - k_p (e_n - e_{\mu}) \end{aligned} \quad (6-44)$$

The angle  $\varphi_\mu$  is close to the inter-particle friction angle of the material. Since the linear variation of  $\sin \varphi_{p,c}$  can be defined by the slope  $k_p$  and the position of any data point on the line, the friction angle  $\varphi_\mu$  actually serves as a reference value for which the corresponding  $e_\mu$  should be obtained from test results. The actual value of  $\varphi_\mu$  therefore, is of less importance and it will be taken to be 7 degrees less than  $\varphi_{cv}$  here (i. e.  $\varphi_\mu = \varphi_{cv} - 7$ , friction angles in degrees). The constants  $k_p$  and  $a_p$  are material parameters determining the slope of variation of  $\sin \varphi_p$ , and the degree of inherent anisotropy in terms of  $\sin \varphi_p$  respectively. Note that the scalar “a” defined in Equation 6-37 is also affected by the degree of anisotropy, but is determined in terms of the stress ratio  $M_p$ . Unlike  $a_p$ , “a” is not constant.

For any consolidation pressure  $p_c$  and its corresponding void ratio  $e_c$ , the normalized void ratio  $e_n$  can be obtained from the following equation:

$$\ln (e_c / e_n) = -\beta e_n^{2.5} (p_c/p_a) \quad (6-45)$$

in which  $\beta$  is a material constant related to the compressibility of the soil as was explained in Chapter 5.

Results reported in Chapter 5 suggested that slopes  $k_p$  measured from TC and TE tests are close to each other. Results measured from the hollow cylinder tests reported by Yoshimine (1996) lead to a similar conclusion, although show some scatter (see Figure 6-4). Note that since  $\sin \varphi_p$  was affected by both the direction of loading (represented by  $\alpha_\sigma$ ) and the intermediate principal stress (represented by  $b$ ), results of tests at the same values of  $b$  and  $\alpha_\sigma$ , but measured at different void ratios were used to obtain this slope in Figure 6-4. It can be noticed that values measured for all combinations of  $b$  and  $\alpha_\sigma$  lie between those measured from tests with  $b = 0$  and  $\alpha_\sigma = 0$  (that correspond to TC) and  $b = 1$  and  $\alpha_\sigma = 90$  (that correspond to TE). An exception is the value measured for  $b = 0.25$  and  $\alpha_\sigma = 0$  that showed strength slightly higher than that of TC. A similar trend was seen in results of tests on Syncrude sand reported in Chapter 4.

All the parameters needed above to calculate the stress state at peak in general stress space can be obtained from undrained TC and TE tests. In cases where predictions are to be made for high pressures, the compressibility parameter  $\beta$  will also be needed. For ordinary ranges of pressure, however, normalization for  $e_c$  will not be needed and the actual (non-normalized) values of  $e_c$  can be used in Equation 6-44.

### 6.3.2 The “direction” of strain increments

#### 6.3.2.1 *The stress-dilatancy relationship*

The following relationship (Equation 5-13 in Chapter 5) was suggested by Nova (1979) to relate volumetric strains to shear strains in triaxial stress conditions :

$$d = \frac{d\varepsilon_p}{d\varepsilon_q} = A ( M_{cv} - \eta )$$

where  $\varepsilon_p = v_p = \varepsilon_1 + 2\varepsilon_3$  is the volumetric strain and  $\varepsilon_q = 2(\varepsilon_1 - \varepsilon_3)/3$  is the shear strain with  $\varepsilon_1$  and  $\varepsilon_3$  being the major and minor principal strains. The stress ratios  $M_c$  and  $\eta$  are values of  $q/p$  ( $q = \sigma_1 - \sigma_3$ ) at the critical state and current stress state respectively and  $A$  is a material parameter that should be obtained from experiment. This relationship was used in Chapter 5 with  $M_{cv}$  replaced by  $M_{PT}$  (the stress ratio at phase transformation, PT), and “A” derived from Rowe’s (1962) stress-dilatancy relationship in TC and TE as was given in Equation 5-14:

$$A_c = 9 / (9 - 2M_{PT,c}\eta + 3M_{PT,c}) \quad \text{for TC}$$

$$A_e = 9 / (9 - 2M_{PT,c}\eta - 3M_{PT,e}) \quad \text{for TE}$$

In the above equations,  $A_c$  and  $A_e$  are values of  $A$  for the TC and TE respectively, and  $M_{PT,c}$  and  $M_{PT,e}$  are values of the corresponding stress ratios. These stress ratios can

be obtained from the friction angles at PT in TC and TE denoted by  $\phi_{PT,c}$  and  $\phi_{PT,e}$  respectively. These friction angles are related to the state parameter at phase transformation  $\psi$ , according to the following equations:

$$(a) \quad \sin\phi_{PT,c} = \sin\phi_{cv} + k_{PT} \psi \quad (6-46)$$

$$(b) \quad \sin\phi_{PT,e} = \sin\phi_{cv} + a_{PT} + k_{PT} \psi$$

where  $\phi_{PT,c}$  and  $\phi_{PT,e}$  are friction angles at PT;  $\phi_{cv}$  is the constant volume friction angle measured from TC; and  $k_{PT}$  is the slope of variation of  $\sin\phi_{PT}$  with  $\psi$ . The parameter  $a_{PT}$  is the difference between  $\sin\phi_{PT,c}$  and  $\sin\phi_{PT,e}$ . Experimental evidence presented in Chapter 4 suggested that the slope  $k_{PT}$  is nearly the same in TC and TE. Measurements made from the HC tests reported by Yoshimine (1996) led to a similar conclusion, although as with the case of triaxial tests, the slope seemed to slightly decrease as  $b$  increased (see Figure 6-5).

The above relationships give stress ratios at PT only for TC and TE conditions. In order to generalize the above equations, the variation of the stress ratio  $M_{PT}$  and the coefficient  $A$  should be determined for general stress conditions. This will be attempted in the following sections.

### 6.3.2.2 *Stress ratio at phase transformation*

The variation of stress state at PT can be obtained using the failure-yield criteria suggested by Lade-Duncan (1975) (L-D) or Matsouka-Nakai (1974) (M-N) explained in Chapter 4.

Figure 6-6 shows variations of this stress ratio in principal stress space, measured from results of HC tests used in Figure 6-5. These results suggest that  $M_{PT}$  is not



affected by the direction of loading  $\alpha_\sigma$  significantly, while other results (e. g. those presented by Symes et al., 1985) show otherwise.

Use of the L-D and M-N criteria, however, often introduces algebraic complexity in soil constitutive modeling. Also, there is no general agreement among researchers on the variation of strength with the intermediate principal stress, and contradictory test results have been presented by different workers that correspond to either or none of these criteria. An alternative form that was suggested by Gudehus (1973) is widely used in soil constitutive modeling and will therefore be used here. This relationship is simpler but produces shapes that are similar to the L-D and M-N criteria in principal stress space, with more adaptability to measured soil behavior. Using this relationship for the stress ratio at PT leads to the following form:

$$M_{PT} = M_{PT,c} g(\theta) \quad (6-47)$$

$$g(\theta) = \frac{2c}{(1+c) - (1-c)\cos 3\theta} \quad (6-48)$$

$$c = \frac{M_{PT,e}}{M_{PT,c}} \quad (6-49)$$

such that  $M = \sqrt{\frac{3}{2}} \frac{|s|}{p}$  and  $\theta$  is the modified Lode angle defined previously. The coefficient  $c$  in the above equation can be determined using  $M_{PT,c}$  and  $M_{PT,e}$  obtained from  $\sin\phi_{PT,c}$  and  $\sin\phi_{PT,e}$  respectively:

$$c = \frac{\sin \phi_{PT,e} (3 - \sin \phi_{PT,c})}{\sin \phi_{PT,c} (3 + \sin \phi_{PT,e})} \quad (6-50)$$

Substituting from Equation 6-46 into 6-50 leads to:

$$c = \frac{(\sin \varphi_{cv} + a_{PT} + k_{PT}\psi)(3 - \sin \varphi_{cv} - k_{PT}\psi)}{(\sin \varphi_{cv} + k_{PT}\psi)(3 + \sin \varphi_{cv} + a_{PT} + k_{PT}\psi)} \quad (6-51)$$

It is possible now to calculate the variation of the stress ratio at PT with  $\psi$  for given values of  $\theta$  during a shearing process. For any state parameter  $\psi$ , the variation of  $M_{PT}$  with  $\theta$  in the octahedral plane represents a rounded triangle similar to the L-D or M-N strength criteria. The size of this triangle is represented here by the stress ratio  $M_{PT,c}$  which varies with  $\psi$ . The value of  $M_{PT}$  will be equal to  $M_{cv}$  at the ultimate state (i. e. when  $\psi = 0$ ). In this case, the coefficient  $c$  is:

$$c = \frac{(\sin \varphi_{cv} + a_{PT})(3 - \sin \varphi_{cv})}{\sin \varphi_{cv}(3 + \sin \varphi_{cv} + a_{PT})} \quad (6-52)$$

Note that since  $\varphi_{cv}$  and  $a_{PT}$  are assumed to be constant material parameters, the value of  $c$  at ultimate state will be constant according to the above equation. A  $c = 1$  produces a circular cross-section in the octahedral plane and smaller values of "c" produce rounded triangles that become less rounded as "c" decreases. Jiang and Pietrusczak (1988) indicated that to ensure convexity of the yield-failure surface, the value of  $c$  should not be smaller than  $\frac{7}{9}$ .

### 6.3.2.3 Determination of the dilatancy parameter $D$

Using the generalized forms for the current stress ratio and the stress ratio at PT, and replacing  $M_{cv}$  with  $M_{PT}$ , Equation 5-13 can be written in the following form:

$$d = \frac{\dot{v}_p}{\dot{\epsilon}_q} = A (M_{PT} - \eta) \quad (6-53)$$

where  $\eta = |\eta\eta|^{1/2} = \sqrt{\frac{3}{2}} \frac{|s|}{p}$  is the norm of the current stress ratio tensor and

$$\varepsilon_q = \left| \frac{2}{3} e e \right|^{1/2} = \sqrt{\frac{2}{3}} |e| \quad (6-54)$$

Values of "A" in Equation 6-53 were derived from Rowe's (1962) stress dilatancy relationship for TC and TE conditions. It will be assumed here that "A" varies with  $\theta$  between the values corresponding to TC and TE given by Equation 5-14. The following relationship is suggested here to determine the variations between TC ( $\theta = 0$ ) and TE ( $\theta = 60$  degrees):

$$A = \frac{9}{(9 - 2\eta M_{PT}) + 3M_{PT} \cos 3\theta} \quad (6-55)$$

The dilatancy coefficient D (Equation 6-19) that is required in the formulation of the constitutive equations can now be obtained from:

$$D = \frac{\dot{v}^p}{|\dot{e}^p|} = \sqrt{\frac{2}{3}} A [ M_{PT,c} g(\theta) - \eta ] \quad (6-56)$$

### 6.3.3 The hardening rule

Two parameters define the yield surface in general stress space, namely the pressure  $p_\alpha$  that controls the size (i. e. the length) of the drop-shaped yield surface and the stress ratio  $M_p$  that determines its shape (i. e. its width). The value of these parameters after consolidation depends on the state (i. e. the stress state and void ratio) of the soil at consolidation. Subsequent changes of the parameters during shearing will be termed "size hardening" and "shape hardening" respectively. However, use of the model in predicting sand behavior both in this chapter and in Chapter 5 showed that use of the value of  $M_p$  corresponding to the state of the soil at consolidation is sufficient to obtain

good model predictions, and the subsequent shape hardening could be neglected for simplicity of the formulation.

### 6.3.3.1 Size hardening

Changes in the pressure  $p_\alpha$  can take place due to shear or volumetric strains. In the case of shear strains, at any instant,  $p_\alpha$  changes such that it approaches a maximum value  $p_f$  corresponding to the failure of the soil. At any stage during shearing, the maximum size of the yield surface  $p_f$  can be obtained from the stress ratio at failure  $M_f$ , which in turn is a function of the current state parameter. The maximum size  $p_f$  is obtained by assuming that if the soil was at failure under the current pressure  $p$ , the current stress ratio  $\eta$  had to be equal to the stress ratio of the soil at failure  $M_f$ . Therefore, at any stage of shearing, the pressure  $p_f$  can be calculated by substituting the stress ratio at failure  $M_f$  into the yield function (Equation 6-28) as follows:

$$p_f = \frac{p}{\left[ 1 - \frac{(M_f - \alpha)(M_f - \alpha)}{M_\alpha^2} \right]^2} \quad (6-57)$$

Current values of  $M_\alpha^2$  and  $p$  should be substituted in the above equation.

Note that the equation used here for the yield surface dictates that the stress ratio at failure cannot become larger than the maximum possible stress ratio at yielding that occurs at the origin, where  $p = 0$ . Otherwise the yield surface will not intersect with the failure line and  $p_f$  cannot be obtained from Equation 6-57. An  $M_f$  equal to the maximum stress ratio at yield causes the denominator of the above equation to become zero. Therefore, the following condition should always be met:

$$(M_f - \alpha)(M_f - \alpha) < M_\alpha^2 \quad (6-58)$$

For any  $\alpha$ , the RHS of the above inequality is a function of  $M_p$  and the LHS is a function of  $M_f$ .  $M_p$  changes with the (normalized) void ratio at consolidation and  $M_f$  with the current state parameter. In applying the model, it was noticed that the above condition was generally satisfied except in the case of very loose sand where  $M_p$  becomes very small. To satisfy the condition for all cases, an upper limit to the stress ratio  $M_f$  was therefore placed and was taken to be such that the condition given in the above inequality is always satisfied.

The stress ratio  $M_f$  is related to the current state parameter in the same way as the stress ratio at PT discussed in the previous section. Similar to the PT, the friction angle at failure in TC ( $\phi_{f,c}$ ) can be related to the current state parameter  $\psi$  according to the following :

$$\sin\phi_{f,c} = \sin\phi_{cv} - k_f \psi \quad (6-59)$$

$$M_{f,c} = \frac{6 \sin \phi_{f,c}}{3 - \sin \phi_{f,c}} \quad (6-60)$$

$$M_f = M_{f,c} g(\theta) \quad (6-61)$$

$$M_f = |M_f M_f|^{1/2} \quad (6-62)$$

The function  $g(\theta)$  and the parameter  $c$  required for its calculation are the same as those used for calculating the stress ratios at PT. Note that at any stage during shearing, the same value of  $g(\theta)$  used to calculate  $M_{PT}$  will be used to calculate  $M_f$ .

The pressure  $p_f$  corresponds to the size of the yield surface that the sand should have, if it was currently at failure. The current size of the yield surface, however, is not generally equal to  $p_f$ . The size of the surface will therefore change during shearing such that it tends to eventually become equal to the size  $p_f$  corresponding to the current state. Note that although  $p_\alpha$  always changes towards  $p_f$ , it becomes equal to it only at the

ultimate state, since as  $p_\alpha$  changes, the state parameter changes, causing a change in  $M_f$  and  $p_f$ . Following this concept, the size-hardening resulting from shear strain can be obtained from the following equation:

$$\frac{\partial p_\alpha}{\partial |e^p|} = h (p_f - p_\alpha) \quad (6-63)$$

in which  $|e^p| = |e^p e^p|^{1/2}$  and  $h$  is a material parameter related to the plastic shear modulus of the soil. It was shown in Chapter 5 that considering the simple case of  $p = \text{const.}$  loading of an isotropically consolidated sand, and ignoring the small effect of shape hardening, using the above hardening rule, implies assuming the following value for the plastic shear modulus as given in Equation 5-29:

$$G^p = h (p_f - p_\alpha) M_p f(p/p_\alpha)$$

and  $h$  was approximated from the initial shear modulus  $G_{\max}$  and  $(p_f - p_\alpha)_{\text{ini}}$  (see Equation 5-37) as follows:

$$h = G_{\max} / (p_f - p_\alpha)_{\text{ini}}$$

The terms  $f(p/p_\alpha)$  and  $(p_f - p_\alpha)$  control the degradation of the plastic shear modulus with shearing. The function  $f(p/p_\alpha)$  is equal to infinity at the start of shearing (i. e. at  $p = p_c$ ) where the elastic shear modulus governs the response (see Figure 5-5 in Chapter 5) but decreases afterwards. The initial shear modulus  $G_{\max}$  is often taken to be equal to the elastic shear modulus, which is assumed to be isotropic. The form of the plastic shear modulus given by Equation 5-29, which results from the form of the hardening rule and the equation of the yield surface, suggests that  $G^p$  is directly related to  $M_p$ . Factors that affect  $M_p$  will therefore, influence  $G^p$  accordingly. The stress ratio  $M_p$  is a function of the state of the soil and more importantly, the direction of loading. It is smaller for soil states and loading directions at which the response of the soil is weaker,

and larger when the response is stronger. Therefore, changes in the plastic modulus due to changes in the loading direction are embedded in the way the hardening rule is written (i.e. Equation 6-63). As will be seen in the next section, this quality of the hardening rule enables the model to take into account effects such as direction of loading, soil fabric, etc., through changes only in the stress ratio  $M_p$ , without the need to account for these effects through other model variables or parameters.

It may also be noted that the amount of strains experienced by the soil since the start of shearing does not appear in Equation 6-63 for the hardening rule. Hardening rules that relate hardening to plastic strains or plastic work will generally need the amount of these strains at any stage of shearing in order to predict the next increment of hardening. Unlike such “strain hardening” or “work hardening” formulations, the “state hardening” relationship used in Equation 6-63 determines the increment of shear hardening by comparing the current size of the yield surface with its maximum size, without the need for knowledge of the strains. The maximum size of the yield surface is a function of the current state parameter.

The size of the yield surface can also change due to volumetric strains caused by isotropic compression. Unlike volumetric strains caused by dilatancy that are governed by the stress-dilatancy relationship, these volume changes are controlled by compressibility. From the compressibility relationship defined in Equation 5-19, the following relationship can be derived:

$$\frac{\partial p_c}{\partial v^p} = \frac{(1+e)}{\beta e^{3.5}} \quad (6-65)$$

where  $\beta$  is a compressibility parameter as defined earlier, and  $e$  is the current void ratio. Equation 6-65 will be used whenever loading is applied at  $\eta=0$ , where volume changes occur exclusively due to isotropic consolidation. In this condition, stress-dilatancy relationships or plastic potentials obtained from different directions of loading (e. g. TC and TE) result in different dilatancies and no unique value is obtained from such

relationships (see slopes of plastic potentials for TC and TE conditions at  $q=0$  shown in Figure 5-3). Equation 6-65 will therefore, replace the stress-dilatancy relationship in such instances.

### 6.3.3.2 *Shape hardening*

As stated earlier, shape hardening may occur due to changes in the shape-hardening surface that defines the stress ratio  $M_p$ . Changes in this surface can result from changes in the normalized void ratio  $e_n$ , which is, in turn, related to the void ratio and consolidation pressure. However, using the model to simulate the tests presented in this thesis showed that once the shape hardening surface is determined from the equations given in Section 6.3.1.2 based on the state of the soil at consolidation, the possible shape hardening during shearing could be neglected.

## 6.3.4 Other model elements

Other model elements including compressibility and elasticity are the same as those used in the formulation of the model for triaxial conditions, and will not be repeated here.

## 6.4 Model performance

### 6.4.1 Sands modeled and parameters used

The performance of the model will be demonstrated by modeling the behavior of Toyoura sand observed in hollow cylinder (HC) and triaxial tests, and also the behavior of Ham River sand observed in HC tests. Physical properties of Toyoura sand and Ham River sand were given in Chapter 4. Model parameters used in the simulations for the



two sands are given in Table 6-1. The calibration procedure was explained in Section 5.3 in Chapter 5.

The tests on Ham River sand simulated here were conducted on samples at a void ratio of 0.786 that can be considered as medium loose ( $D_r = 44\%$ ). The samples were prepared by pluviation through water that produced strong horizontal bias in particle orientation (Symes et al., 1984).

Results of undrained and drained tests on Ham River sand were reported by Symes et al. (1984) and Symes et al. (1988) respectively. All tests were done in the HC apparatus on samples at a void ratio of 0.786 and under a constant consolidation pressure of 200 kPa and  $b=0.5$ , but an  $\alpha_\sigma$  that varied between 0 and 45 degrees. Some of the parameters that enable the model to predict the behavior over a wide range of soil states are not given in Table 6-1 since they could not be obtained from these tests at constant state. The high value of  $\phi_{cv}$  given in Table 6-1 resulted from the  $b=0.5$  condition of the HC tests that produced higher friction angles compared to those obtained from the triaxial  $b=0$  or  $b=1$  tests. A value of  $k_p$  equal to that of Toyoura sand was assumed and  $e_\mu$  was obtained based on this assumption. Model parameters were obtained from the undrained tests and used to predict the behavior of the drained tests.

Model parameters for Toyoura sand obtained from results of TC and TE tests on moist tamped (MT) and dry deposited (DD) samples were given in Table 5-1 of Chapter 5. The same parameters were used to predict results of triaxial tests where necessary. The parameters for stress-dilatancy and peak given in Table 6-1 are slightly different from those given in Chapter 5. This is because these parameters were obtained from results of HC tests on DD samples reported by Yoshimine (1996) rather than the triaxial tests on MT samples reported by Ishihara (1993) and Verdugo (1992) in Chapter 5. It is noted that in this chapter, all HC tests on Toyoura sand were conducted on DD samples and were reported by Yoshimine (1996), and all TC tests for any preparation method are reported from Verdugo (1992), except where stated otherwise. It is also noted that in

many cases in this chapter, different horizontal and vertical scales were used in plotting the results.

#### 6.4.2 Anisotropically consolidated sand and the effect of direction of consolidation

The response of a sample of Toyoura sand at a void ratio of 0.9 consolidated anisotropically in compression and loaded in triaxial compression is shown in Figure 6-7. Both predicted and observed responses show that the sample remained contractive until the ultimate state was reached. Figure 6-8 shows the same simulation along with the predicted response of samples with the same void ratio but consolidated to 800, 400 and 4 kPa. It can be seen that as with the sand consolidated isotropically discussed in Chapter 5, the behavior becomes increasingly dilative as pressure decreases. Such a loose sample can become completely dilative at a pressure as low as 4 kPa that is 300 times smaller than the pressure that led to the fully contractive response. Note that performing a test under a pressure of 4 kPa can be very difficult practically. The model, however, predicted the response expected from such a test. Also, in spite of the exceptional difference in the consolidation pressures, a unique ultimate state is predicted as expected.

A comparison between the observed and predicted responses of a sample of very dense Toyoura sand consolidated anisotropically to a pressure of 1500 kPa is made in Figure 6-9. A very good match exists. This sample was subjected to a high shear stress during consolidation, which corresponded to a value of  $K_0$  as low as 0.37.

The behavior on the extension side is shown in Figure 6-10. Predicted and observed responses of a sample of Toyoura sand consolidated isotropically and sheared in extension is shown in this figure, along with those of a sample consolidated anisotropically on the compression side, but sheared on the extension side. Predicted and observed response show that both samples have completely liquefied when sheared in extension. This is expected from samples of Toyoura sand at void ratios higher than

0.86 sheared in triaxial extension, as was shown in Chapter 5. It is also seen that the sample that was first consolidated anisotropically in compression, exhibited smaller peak strength when sheared on the extension side. This behavior was also observed by di Prisco et al. (1993) that reported significantly weaker response for samples that were sheared in one direction, and then loaded in the opposite direction, compared to samples that were consolidated isotropically.

The effect of density on the behavior of anisotropically consolidated sand can be seen in Figure 6-11. Differences in responses are similar to those of the isotropically consolidated samples. However, the sample with a void ratio of 0.85, consolidated anisotropically in compression and sheared in extension exhibits very small peak strength. This effect is similar to that observed previously and will be noticed further in the following simulations.

The predicted effect of the direction of consolidation is shown in Figure 6-12. It can be seen that samples initially consolidated in one direction and then loaded in the same direction exhibit higher peak strength compared to those initially consolidated in one direction and sheared in the opposite direction. As can be seen in the samples sheared on the extension side, the difference can be very significant, since the sample consolidated in compression exhibited very small peak strength compared to that consolidated in extension.

Note that the predictions made above for the behavior of anisotropically consolidated sand were made using the same values for the stress ratio at peak  $M_p$  regardless of consolidation stress history (i. e. the shape hardening surface was not affected by the consolidation stress history). The predicted effects of anisotropic consolidation (i. e. the stress-induced anisotropy) were therefore results of the stress history on the geometry of the yield surface. The shape hardening surface that mainly represents inherent anisotropy is generally independent of these effects.

### 6.4.3 Effect of direction of loading

The predicted and observed responses of samples of Toyoura sand at a void ratio of 0.86 consolidated to a common pressure of 100 kPa and sheared undrained in the HC apparatus is shown in Figure 6-13. The parameter  $b$  was equal to 0.25 for all the tests but  $\alpha_\sigma$  was varied from 0 to 60 degrees. At this void ratio, the response changed from dilative at  $\alpha_\sigma = 0$  to complete liquefaction for  $\alpha_\sigma = 60$  degrees. Model predictions are generally in good agreement with the observed behavior and the increase in the tendency of the samples to contract as  $\alpha_\sigma$  increases, is modeled very well. It is interesting to notice that the remarkable change in the undrained response with  $\alpha_\sigma$ , and the associated differences in the plastic modulus were modeled only through the dependency of the yield behavior on  $\alpha_\sigma$ . This dependency was introduced into the yield surface through the shape hardening surface (i. e. the stress ratio  $M_p$ ). The form of the hardening rule employed in the model leads to the implicit dependency of the plastic modulus on  $\alpha_\sigma$  as discussed in Section 6.3.3.1. Note, however, that differences can be seen between the measured and predicted initial stiffnesses. This results from the fact that the initial stiffness is governed by the elastic behavior that is assumed to be isotropic. However, as shearing proceeds, the  $\alpha_\sigma$ -dependent plastic response dominates the deformation process.

The response of samples at void ratio and loading conditions the same as those of the above tests, but loaded in drained shear was predicted as shown in Figure 6-14. It can be seen that the same increase in the tendency of the soil to contract as  $\alpha_\sigma$  increases, can be seen in the drained response. It is noted that the predictions are made for loading at  $b = 0.25$  (close to plane strain) to make it comparable with the undrained response. Such values of  $b$  can lead to larger dependency of the response on  $\alpha_\sigma$  as was shown by some researchers (see e. g. Lam and Tatsuoka, 1988).

The effect of direction of loading on the drained behavior of Ham River sand was studied at Imperial College by Symes et al. (1984, 1988) using the HC apparatus. Figure

6-15 shows results of such tests along with model predictions. These load-controlled tests were conducted on samples that were subjected initially to a cycle of compressional load-unload up to a certain stress ratio, before being sheared again in the HC apparatus. All samples were prepared at the same void ratio and loaded under  $b = 0.5$ , but the direction of loading  $\alpha_\sigma$  was varied from 0 to 45 degrees. Changes in the deviatoric stress with the octahedral shear strain are predicted well by the model. Predicted and measured volume changes are in very good agreement for the case of  $\alpha_\sigma = 45$ , but differ from each other as  $\alpha_\sigma$  decreases. The increase in strength of sand in the direction of preshearing is a well-studied subject and was also mentioned in the previous section. Experimental evidence suggest that as the direction of loading deviates from the direction of preshearing, the effect of preshearing decreases (see e. g. Cambu and Lanier, 1993). The lower volumetric strain in the direction of the cycle of preshearing ( $\alpha_\sigma = 0$ ) compared to the predicted value might have therefore resulted from such effect.

It was noted in Chapter 5 that the void ratio of Toyoura sand at which complete liquefaction occurs is different in TC and TE loadings. This difference suggests that the void ratio leading to complete liquefaction might be a function of the direction of loading. Figure 6-16 shows the predicted response of Toyoura sand at void ratios that just lead to complete liquefaction (i. e. void ratios slightly higher than those shown in the figure, will not lead complete liquefaction). The void ratios are functions of the direction of the applied load  $\alpha_\sigma$ . It can be seen that samples at substantially higher void ratios can remain unliquefied, if loading is applied along the stronger direction. These results are slightly different from those measured in TC and TE tests on Toyoura sand, since they were obtained from calibrations based on results of the HC tests.

#### 6.4.4 Effect of mode of shearing

Differences in the responses of a cross-anisotropic material to various modes of shearing can be attributed to the combined effects of differences in their corresponding

values of intermediate principal stress ( $b$ ), and direction of loading ( $\alpha_\sigma$ ). During shearing, values of  $b$  and  $\alpha_\sigma$  may either remain constant (as in TC, TE and TTT), or change with the applied loads (as in SS and PS tests). Differences in the behavior resulting from differences in the mode of shearing of cross-anisotropic materials can often be accounted for through using appropriate combinations of " $b$ " and " $\alpha_\sigma$ " as shown in Section 4.7.2 in Chapter 4. The effect of  $\alpha_\sigma$  was investigated in the previous section. The combined effects of  $b$  and  $\alpha_\sigma$ , as observed in tests at various modes of shearing are discussed in this section.

Figure 6-17 shows the undrained response of Toyoura sand at different void ratios consolidated to a pressure of 100 kPa and sheared in simple shear using the hollow cylinder apparatus. The tests were performed by Yoshimine (1996). It can be seen that both model predictions and observed behavior indicate an increasing tendency for contraction and a weaker response, as void ratio increases. The same trend was observed in both TC and TE tests discussed in Chapter 5. At a void ratio of 0.888, the soil experiences complete liquefaction and zero residual strength. It was noted in Chapter 5 that this void ratio was about 0.93 in TC and 0.86 in TE tests. The void ratio leading to complete collapse in simple shear, therefore, was between those of TC and TE tests.

The predicted effect of mode of shearing on the behavior of a sample of Toyoura sand at a void ratio of 0.85 and consolidation pressure of 100 kPa is shown in Figure 6-18. Tests data for all modes of shearing were not available for comparison with model predictions. It can be seen that the responses to loading in TC and plane strain compression (PSC) are close to each other and they both show a strong dilative behavior. The response in TE loading was very contractive and led to complete liquefaction as expected from samples of Toyoura sand at such void ratios. Although not shown here, the predicted response to plane strain extension (PSE) was close to TE, with slightly stronger behavior. The response to loading in SS was between those of TC and TE, exhibiting a postpeak softening followed by hardening after reaching the minimum strength.

To investigate the effects of mode of shearing on the response of samples at different densities, the predictions made in Figure 6-18 were repeated in Figure 6-19 but for samples at a void ratio of 0.75. It can be seen that while the “relative” differences between the responses to the shearing modes investigated were similar to those of the void ratio 0.85, the “amount” of the differences were substantially smaller. The remarkable effect of mode of shearing on the behavior of the looser samples can result from the fact that in loading at any mode of shearing, the soil will first contract before experiencing any subsequent dilation. The amount of this initial contraction depends heavily on the density of the material and the mode of its shearing, being more at higher void ratios and angles  $\alpha_{\sigma}$ . In an undrained test, this initial contraction results in the movement of the stress path towards the origin of the stress space. If this contraction is large enough, as is the case in looser sand and higher values of  $\alpha_{\sigma}$ , the sample may completely collapse (i. e. reach the origin of the stress space) before having any chance to start its subsequent dilation.

#### 6.4.5 Effect of soil fabric

Differences in soil fabric are those observed in samples or deposits having the same characteristics such as grain size distribution, mineralogy, etc., except that they are formed in different environments and circumstances. These differences can result from differences in the arrangement of the soil particles, which result from differences in the way the soil samples or the soil deposits are formed.

The effects of soil fabric on the response of sand to loading have been emphasized by a number of researchers (see e. g. DeGregorio, 1990; Ishihara, 1993; Vaid et al., 1996). While the effect of soil fabric on the small to medium strain behavior of sand is clearly demonstrated in these studies, the possible effect on the large strain and ultimate state condition is not agreed upon.

Because of the uncertain and complex physics involved, effects of soil fabric can be very difficult to quantify, and as a result, difficult to model. This is because most material characteristics remain unaffected by changes in soil fabric. The current model, however, can reproduce predictions that differ from each other in the same way as the responses of sand with different fabric. These predictions are made by merely changing one model variable, namely, the shape hardening parameter  $M_p$ . Other model parameters and variables remained the same for sands with different fabric.

Figure 6-20 compares predicted and observed responses of samples of Toyoura sand prepared by the moist (wet) tamping (MT) and dry deposition (DD) methods. The latter method produced a more contractive response compared to the former method. Differences in the predicted responses were reproduced by using a smaller value of  $M_p$  for the DD sample, compared to the MT sample. This reduction in  $M_p$  is obtained by using smaller values for  $e_\mu$  for the DD sample as shown in Table 5-1 in Chapter 5. since  $\phi_\mu$  is the same for both MT and DD samples. A value of  $e_\mu = 0.82$  was used for all dry deposited samples, compared to the  $e_\mu = 0.88$  used for the MT samples. A similar difference was assumed in modeling the behavior of all MT and DD samples of Toyoura sand sheared in triaxial tests. Other model parameters were unchanged in modeling these differences.

Figure 6-21 shows the observed and predicted stress paths of samples of Toyoura sand prepared by moist tamping and water pluviation. The stress-strain behavior is shown in Figure 6-22. It can be seen that the water-sedimented samples exhibited a weaker response compared to the moist tamped samples. These differences were also modeled by using a smaller value of  $M_p$  for the WS sample compared to the moist tamped sample.

Note that the way the behavior changes with the method of deposition is not reported similarly by various researchers and seems to be a function of the details of the preparation procedure. A soil sample in the field may have been subjected to a range of physical changes and its fabric may have changed accordingly. Therefore it may not be



easy to reach a definitive conclusion regarding the way soil fabric changes with preparation method. The current model, however, shows a potential for quantifying and modeling such differences regardless of how they might have been produced. The stress ratio  $M_p$  that accounts for these differences is measured directly from undrained tests. No volume change occurs in such tests, and very small shear strain often occurs before the peak is reached. The fabric of the soil may therefore remain largely unaltered by undrained shearing, and the fabric of the soil may be reflected in differences in the stress ratio  $M_p$ .

Parameter type	name of parameter	Toyoura sand	Ham River sand ( for b=0.5 )
peak	$k_p$	1.3	1.3
	$e_\mu$	0.82	0.7
	$a_p$	0.2	0.28
Stress-dilatancy	$\phi_{cv}$	34	42
	$k_{pT}$	1.25	
	$a_{pT}$	0.15	0.11
Failure	$k_f$	0.75	0.75
Compression	$\beta$	0.006	
Elastic	$G_r$	500	500
	$K_r$	850	1500
	$n$	0.55	0.5
Ultimate state line	$e_{ss} =$	$-0.0063477p^3 + 0.0367p^2 - 0.11991p + 0.92548$ (p in MPa)	

**Table 6-1** Model parameters used in response predictions for Toyoura sand and Ham River sand. Parameters are obtained from results of hollow cylinder (HC) tests. Peak parameters for Toyoura sand were obtained from dry deposited (DD) samples. Values of  $a_p$  and  $\phi_{cv}$  obtained for Toyoura sand from results of HC tests were somewhat different from those obtained from triaxial tests (Table 5-1). Parameters for Ham River sand were obtained from results of tests at  $b=0.5$  and therefore, indicate larger strengths in terms of friction angle. Data to determine other parameters for Ham River sand were not available.

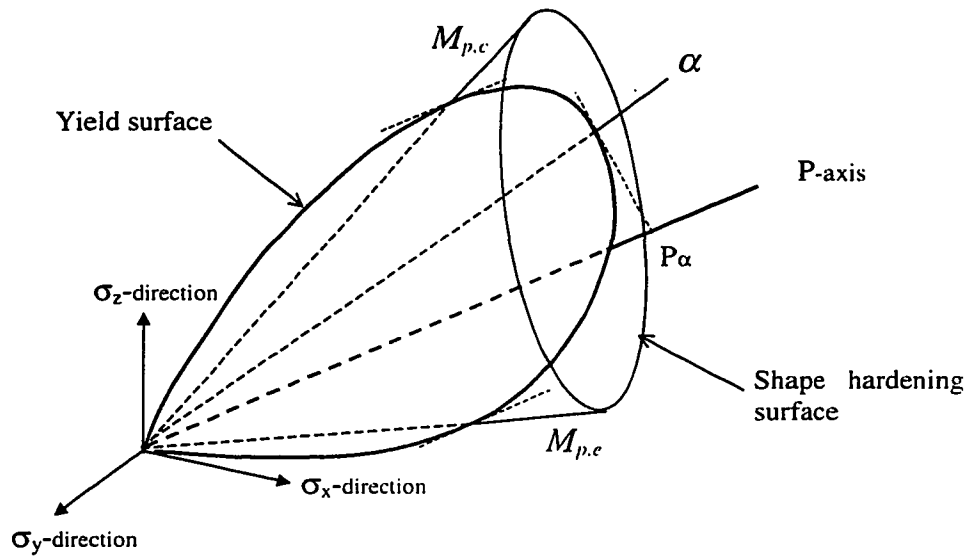


**Figure 6-1** Shape of the yield surface in principal stress space when principal directions of stress and anisotropy coincide.

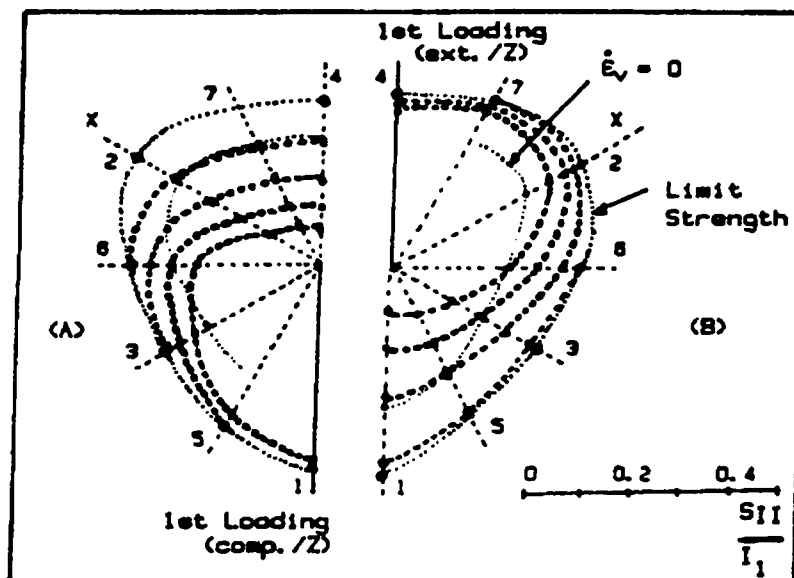
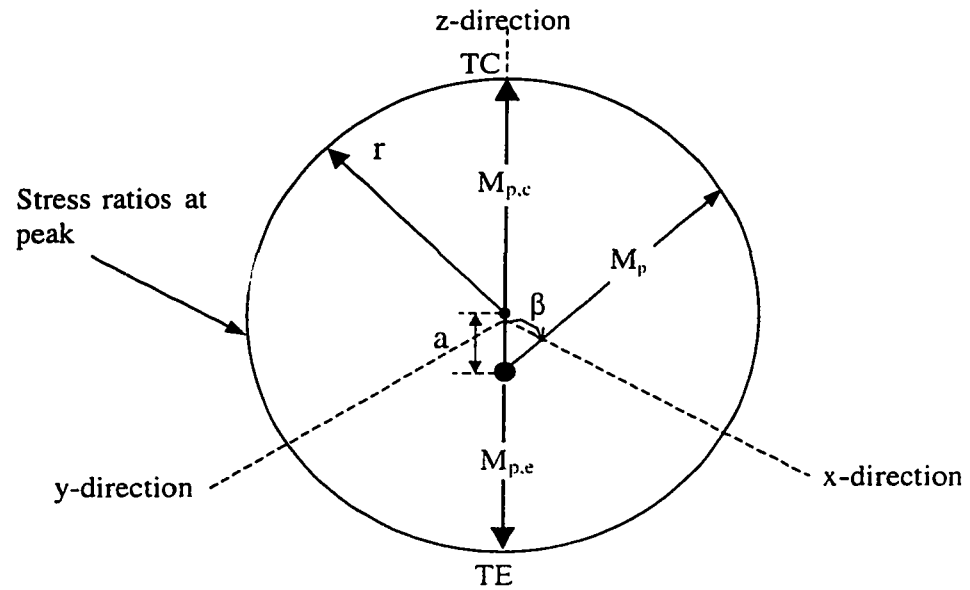
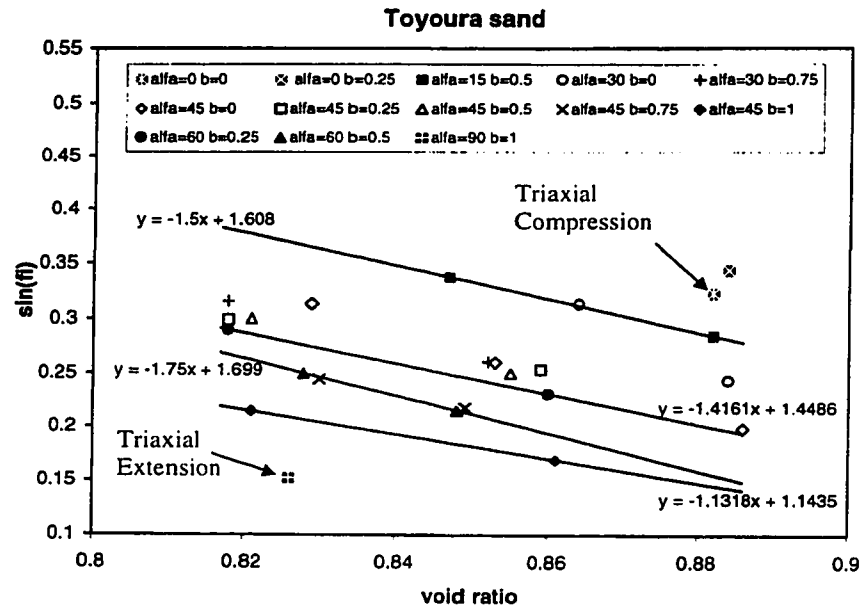


FIGURE 7. Lines of iso-deviatoric deformations in II-stress plane  
 $(E_{II} = 1, 2, 4, 8 \%)$   
 (A) after a compression on the Z-direction  
 (B) after an extension on the Z-direction.

**Figure 6-2** Effect of stress induced anisotropy on the position of the yield surface of sands. Note that the stress state at phase transformation (PT) is not affected by changes in the stress ratio at anisotropic consolidation (modified after Cambu and Lanier, 1988).



**Figure 6-3** Definition of parameters used to model the effect of inherent anisotropy on the yield behavior



**Figure 6-4** Effect of  $b$  and  $\alpha_\sigma$  on the variation of friction angle at peak with void ratio, as measured from hollow cylinder tests

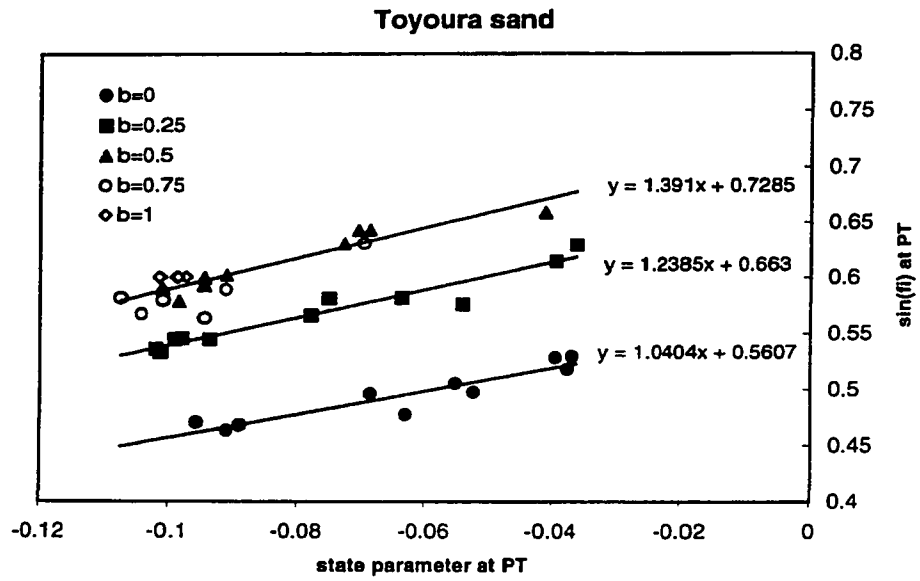


**Figure 6-5** Effect of intermediate principal stress (*b*) on the variation of friction angle at phase transformation (PT) with state parameter as measured from hollow cylinder test

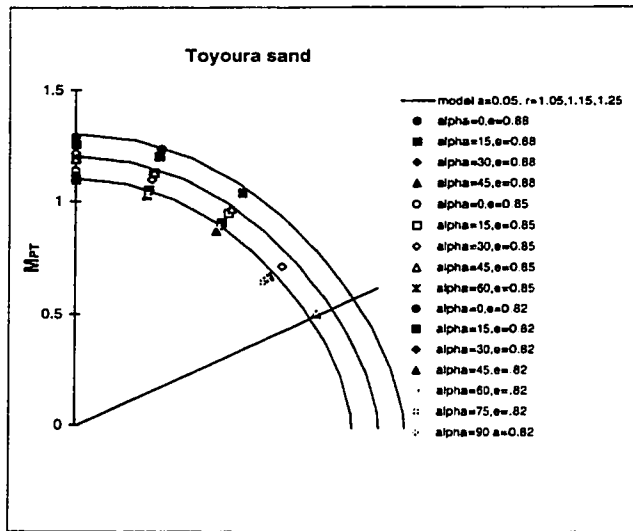


**Figure 6-6** Effect of stress state on the variation of stress ratio at phase transformation ( $M_{PT}$ ) with void ratio, as represented in the octahedral plane

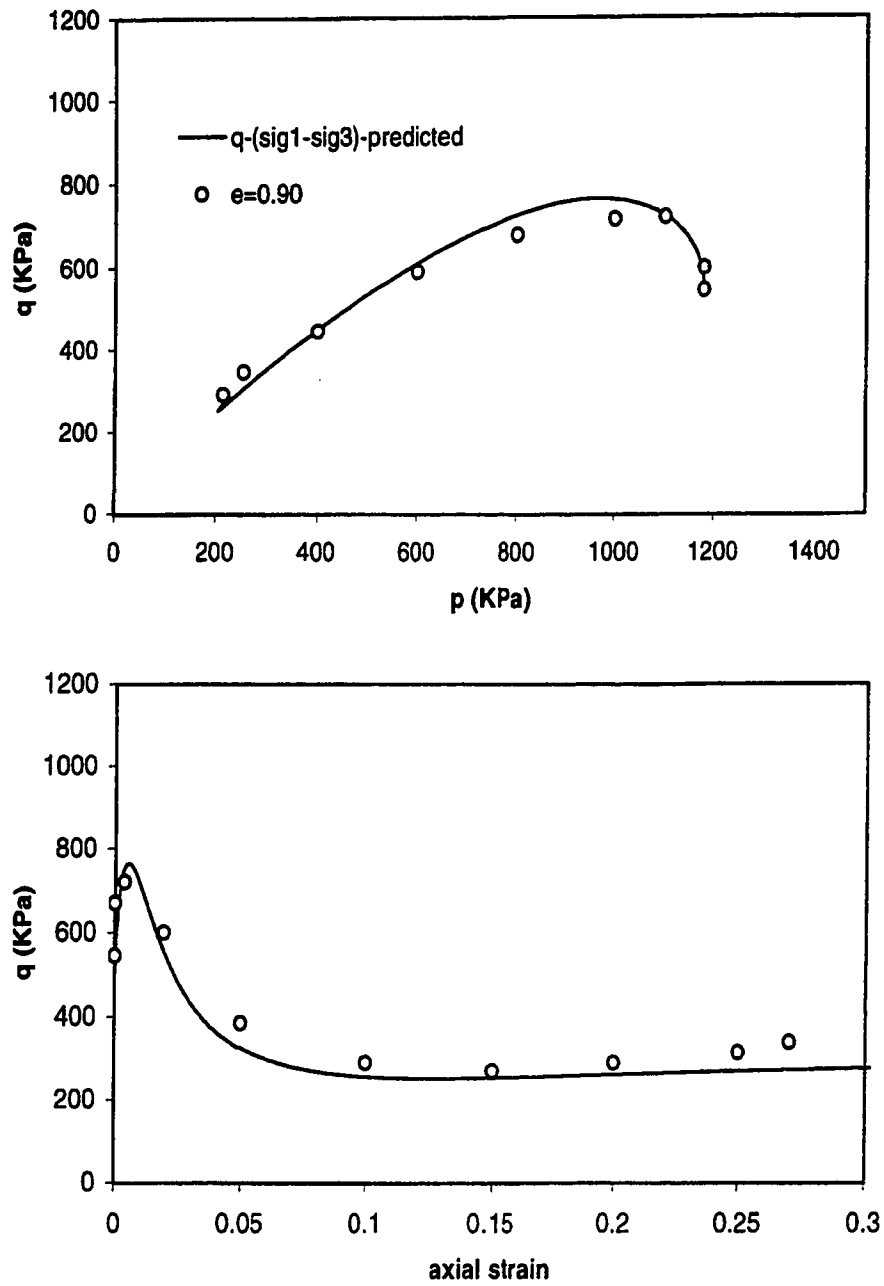


**Figure 6-7** Undrained response of anisotropically consolidated loose Toyoura sand to shearing in triaxial compression



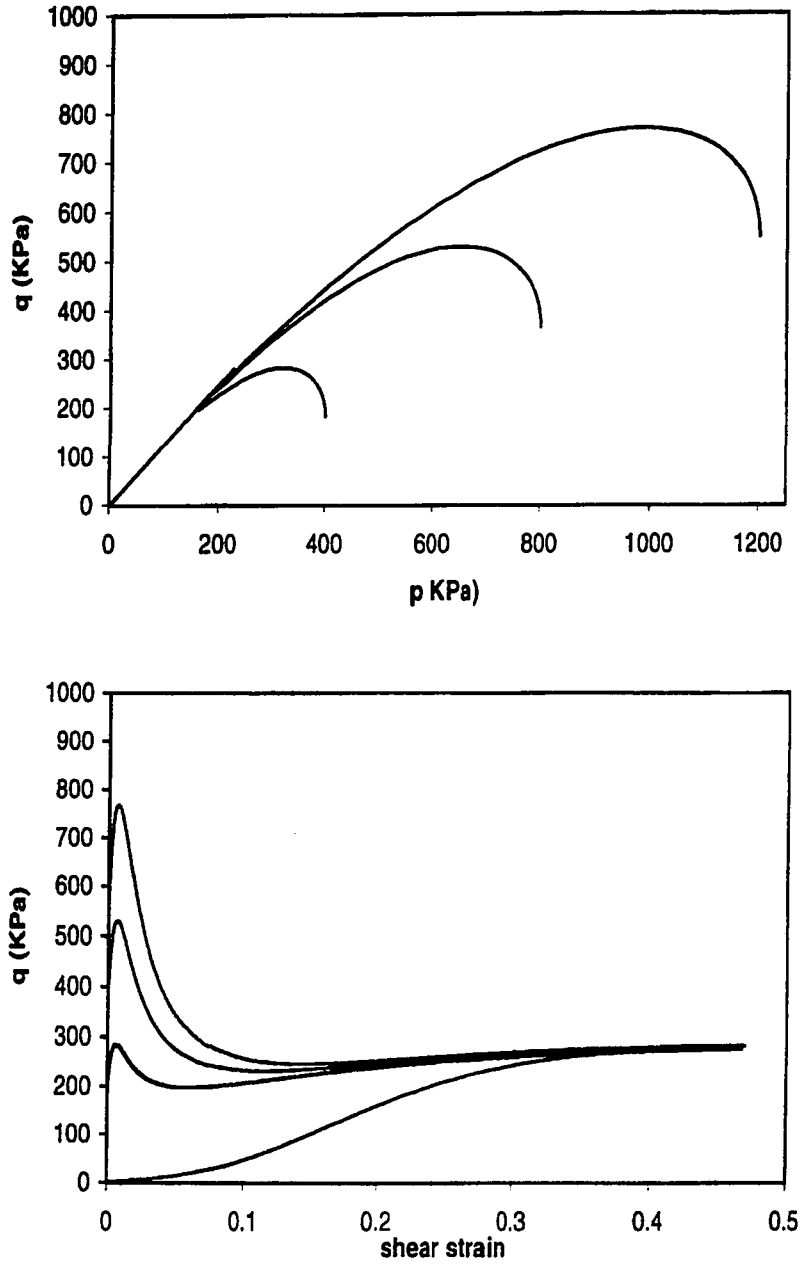


**Figure 6-8** Effect of consolidation pressure on the behavior of anisotropically consolidated loose Toyoura sand

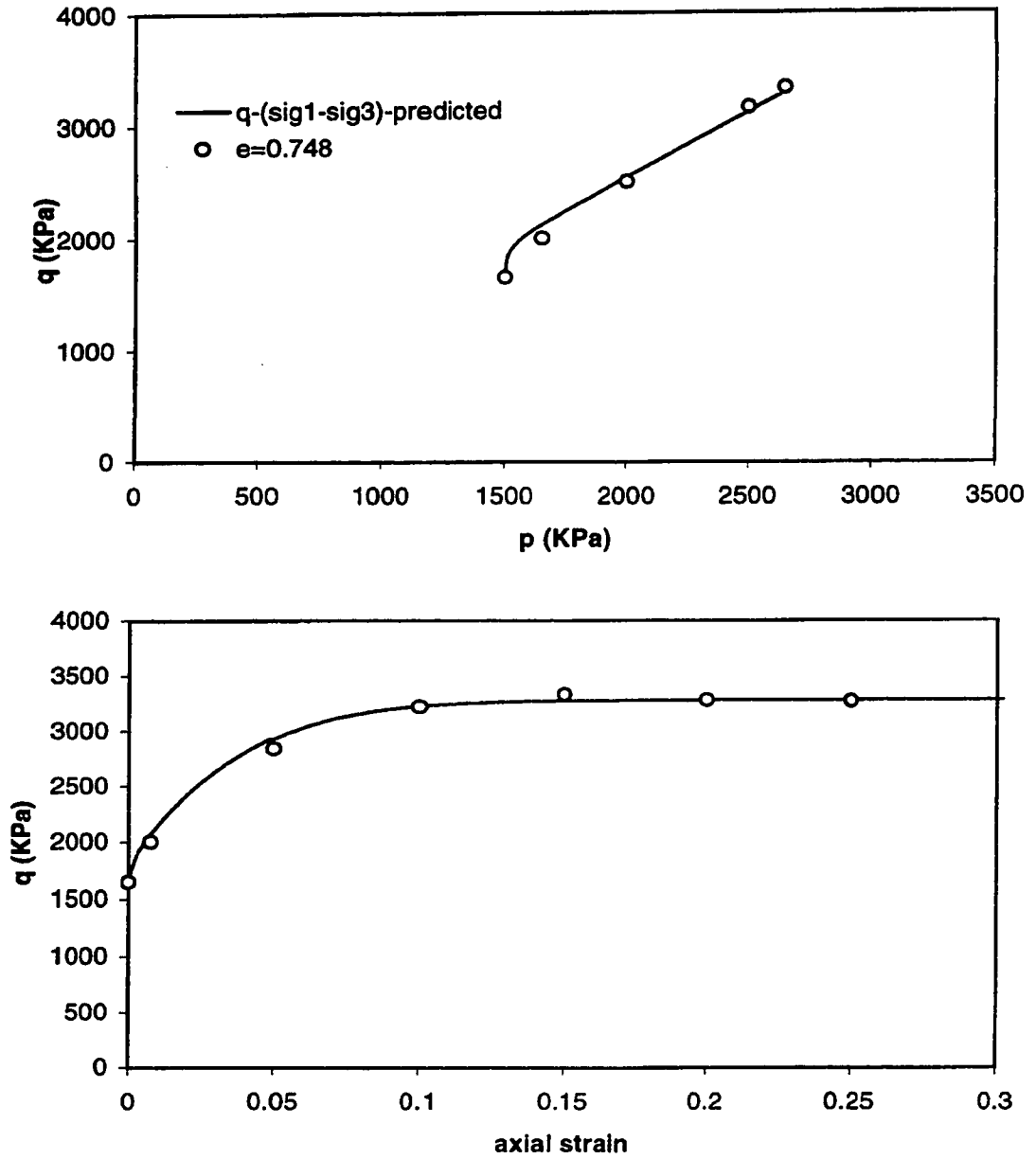


**Figure 6-9** Predicted and observed behavior of a sample of very dense Toyoura sand consolidated anisotropically at  $K_0 = 0.37$ .

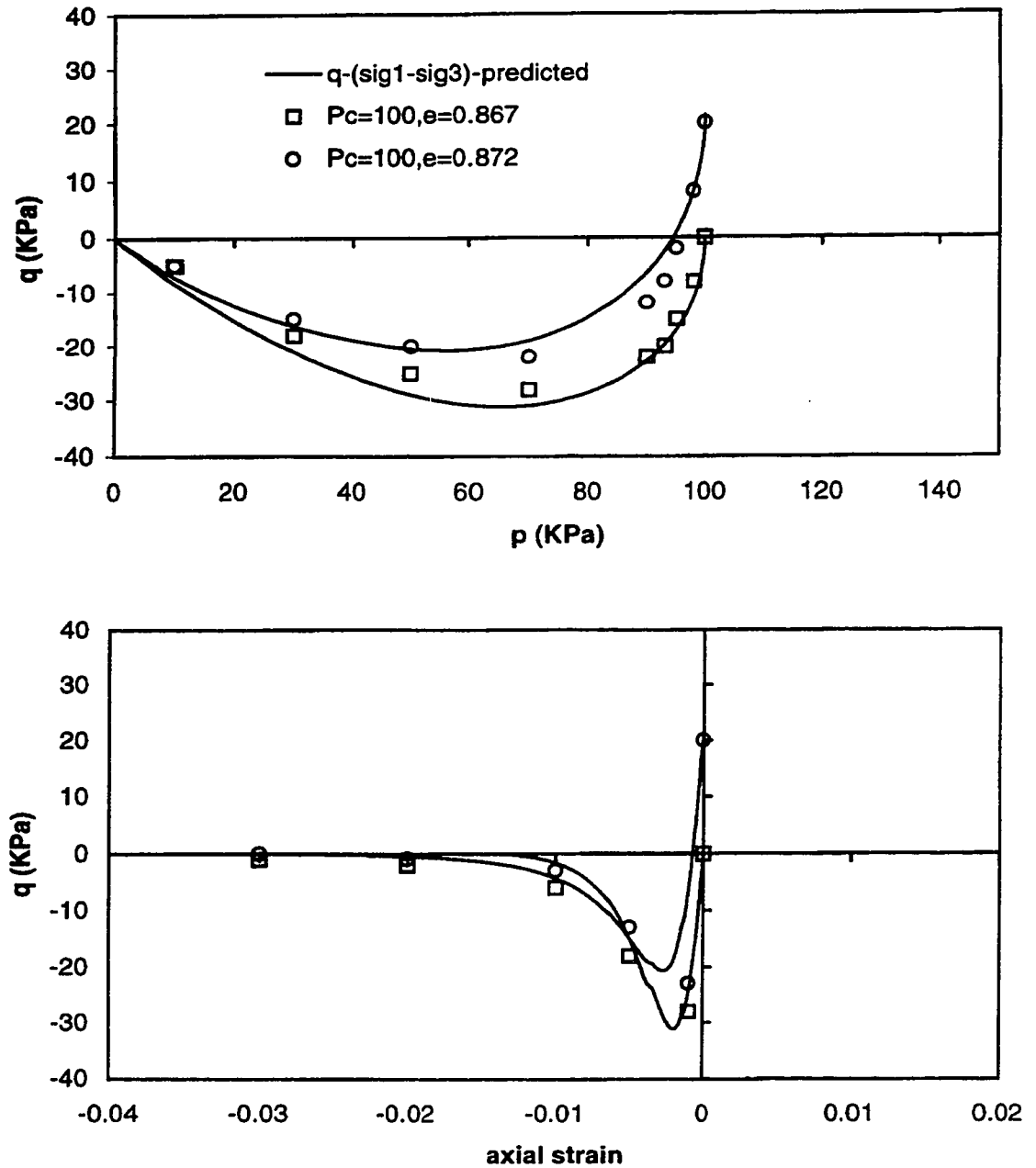


**Figure 6-10** Behavior of Toyoura sand consolidated in compression and sheared in extension (Data from Hyodo et al., 1994)

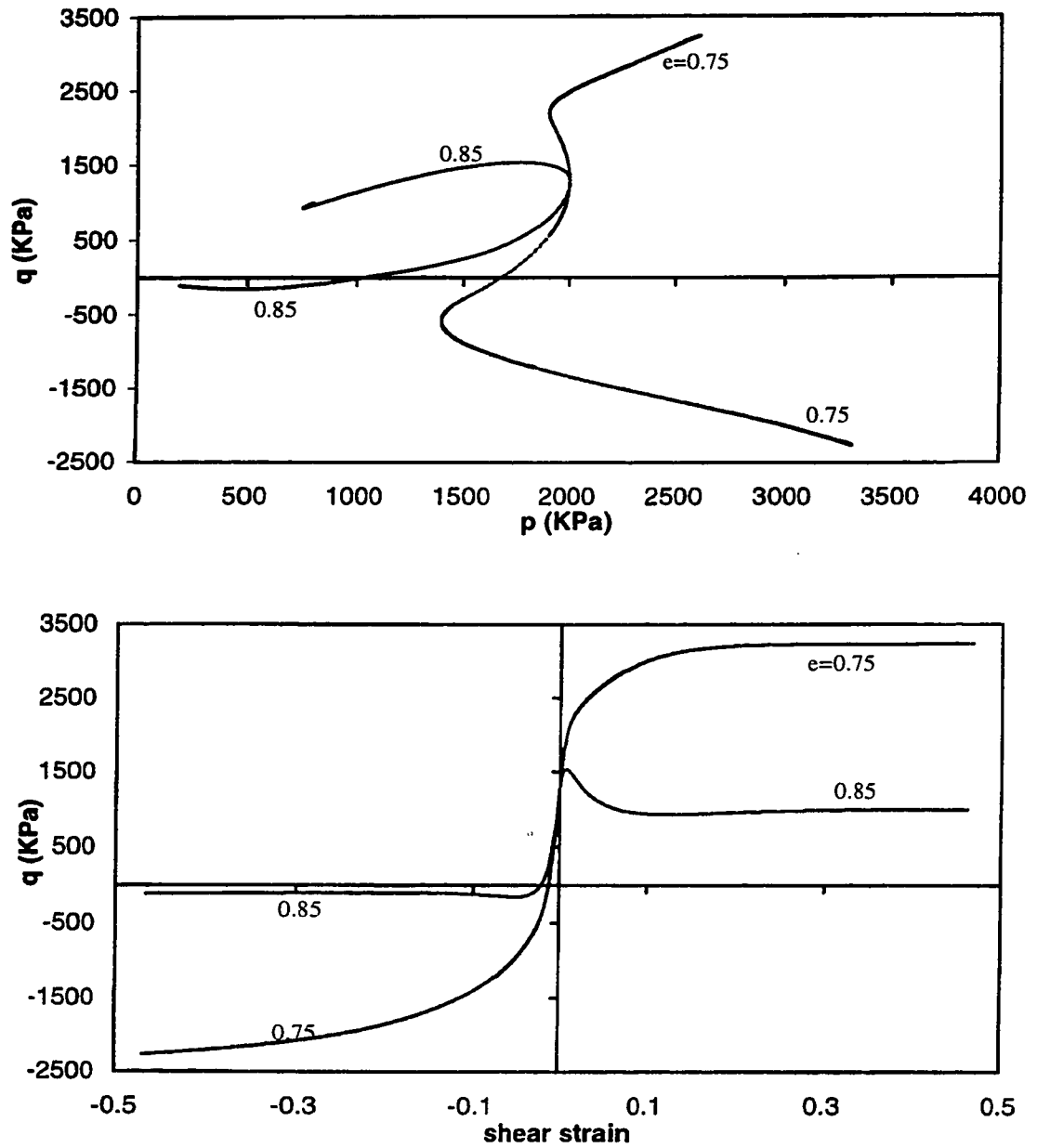


**Figure 6-11** Effect of direction of loading on the undrained response of anisotropically consolidated Toyoura sand consolidated to different densities.

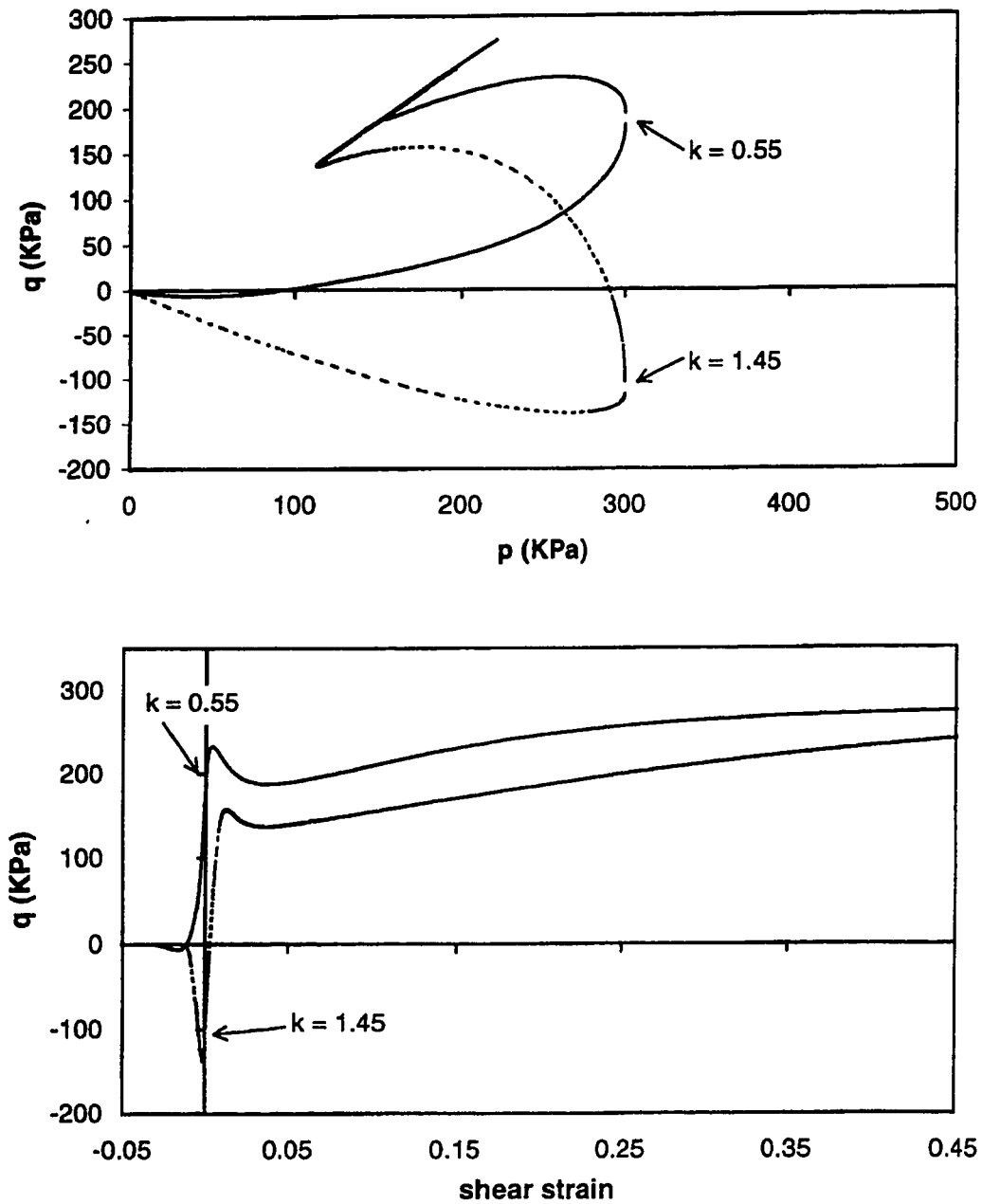


**Figure 6-12** Effect of direction of consolidation on the response of loose Toyoura sand to undrained shear in triaxial compression and triaxial extension.

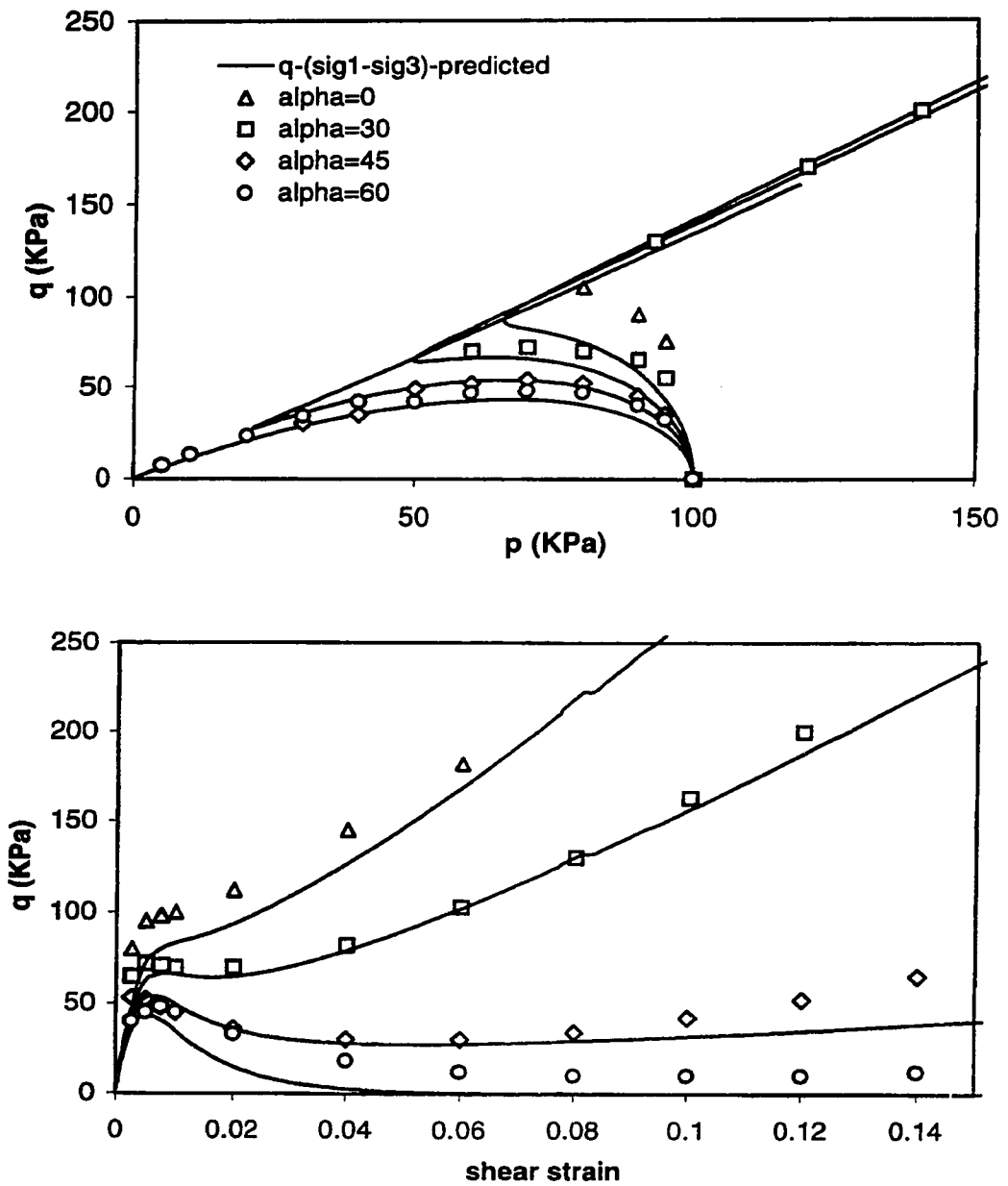


**Figure 6-13** Effect of direction of loading on the undrained behavior of Toyoura sand with  $e=0.86$  sheared under  $b=0.25$  in the hollow cylinder apparatus

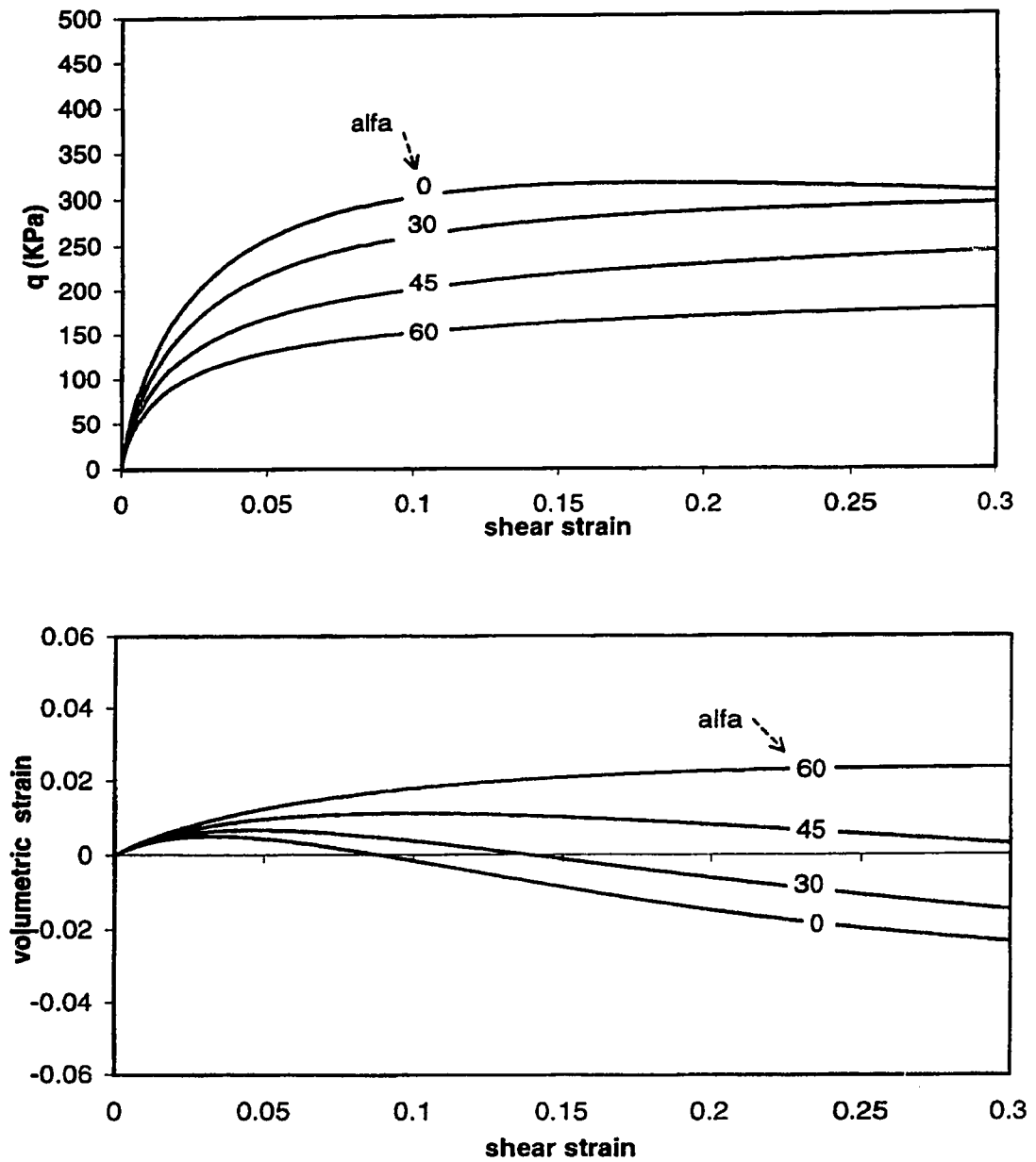


**Figure 6-14** Predicted drained response of Toyoura sand with  $e=0.86$  and  $b=0.25$  sheared under different values of  $\alpha$  in the hollow cylinder apparatus

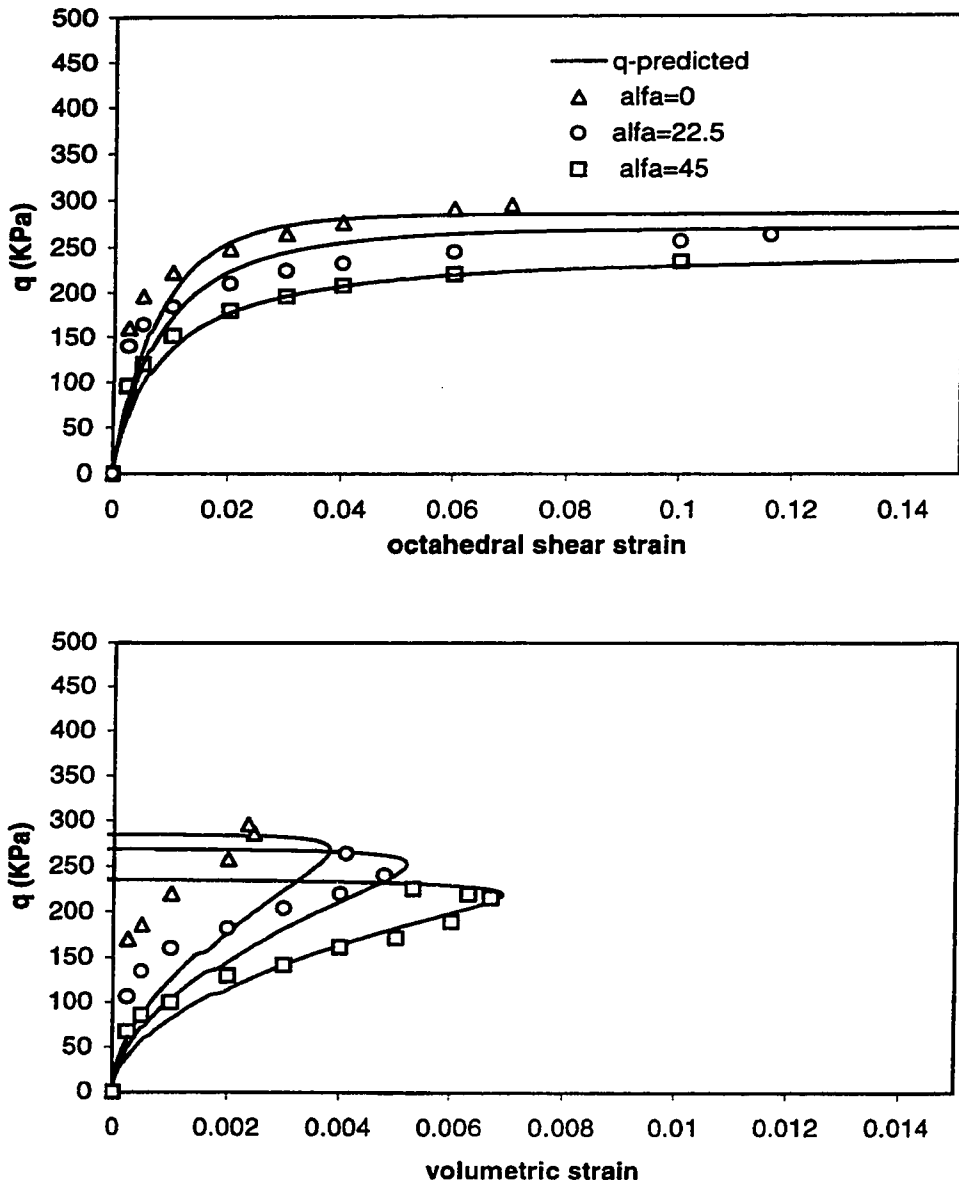


**Figure 6-15** Measured and predicted response of loose Ham River sand to drained shear with  $b=0.5$  in the hollow cylinder apparatus



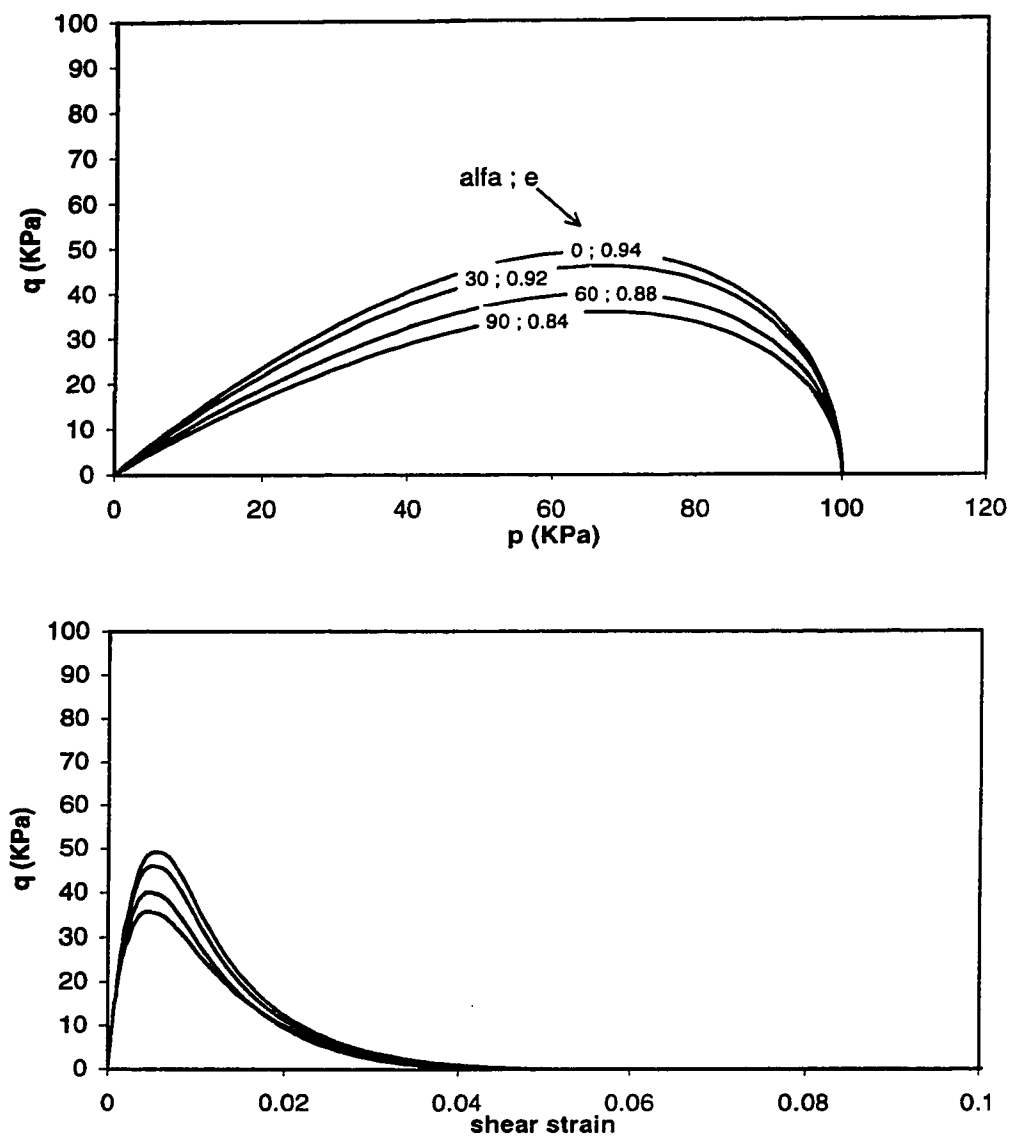


**Figure 6-16** Effect of direction of loading on the void ratio of Toyoura sand that leads to complete undrained collapse

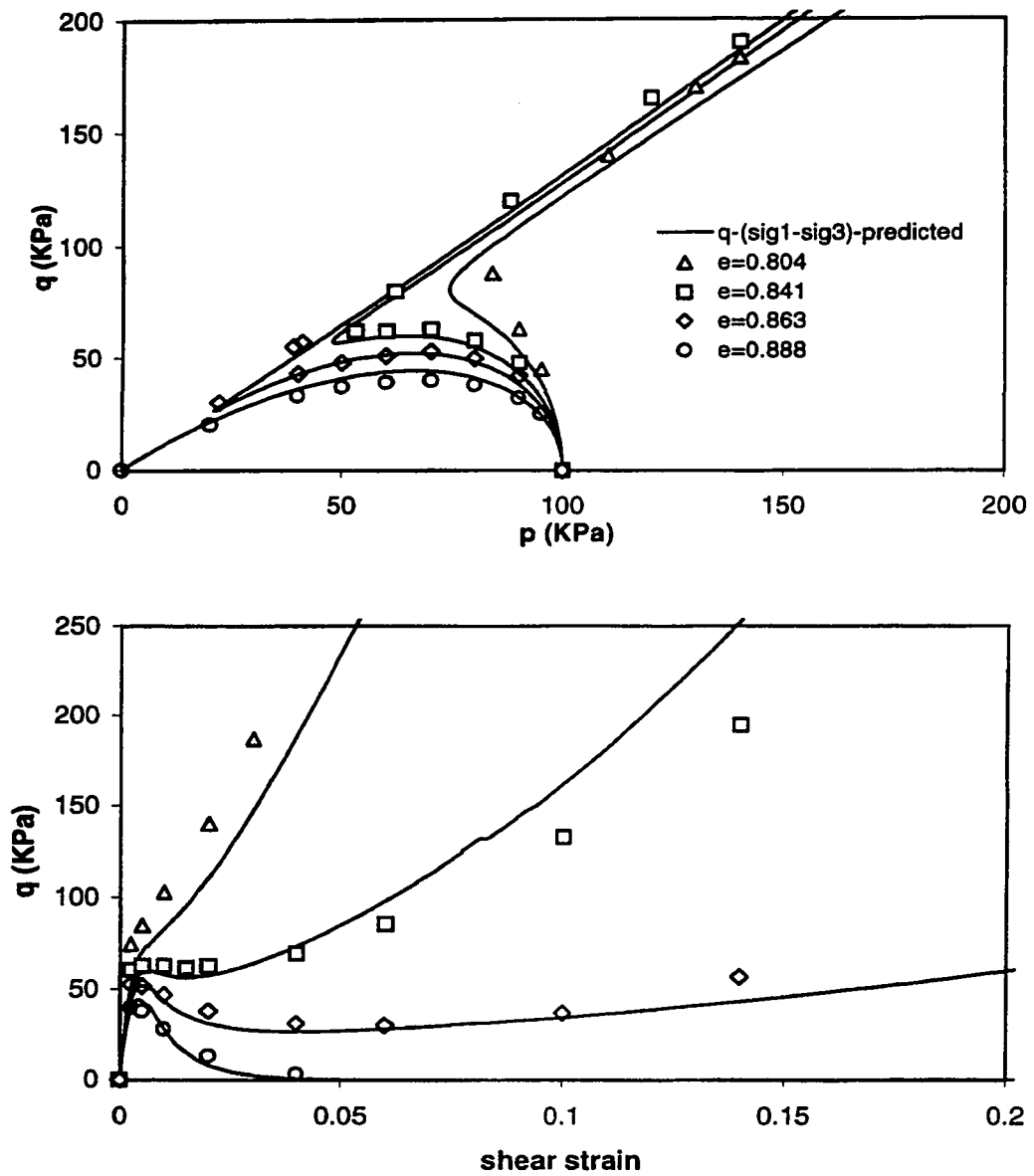


**Figure 6-17** Effect of void ratio on the undrained response of Toyoura sand in simple shear

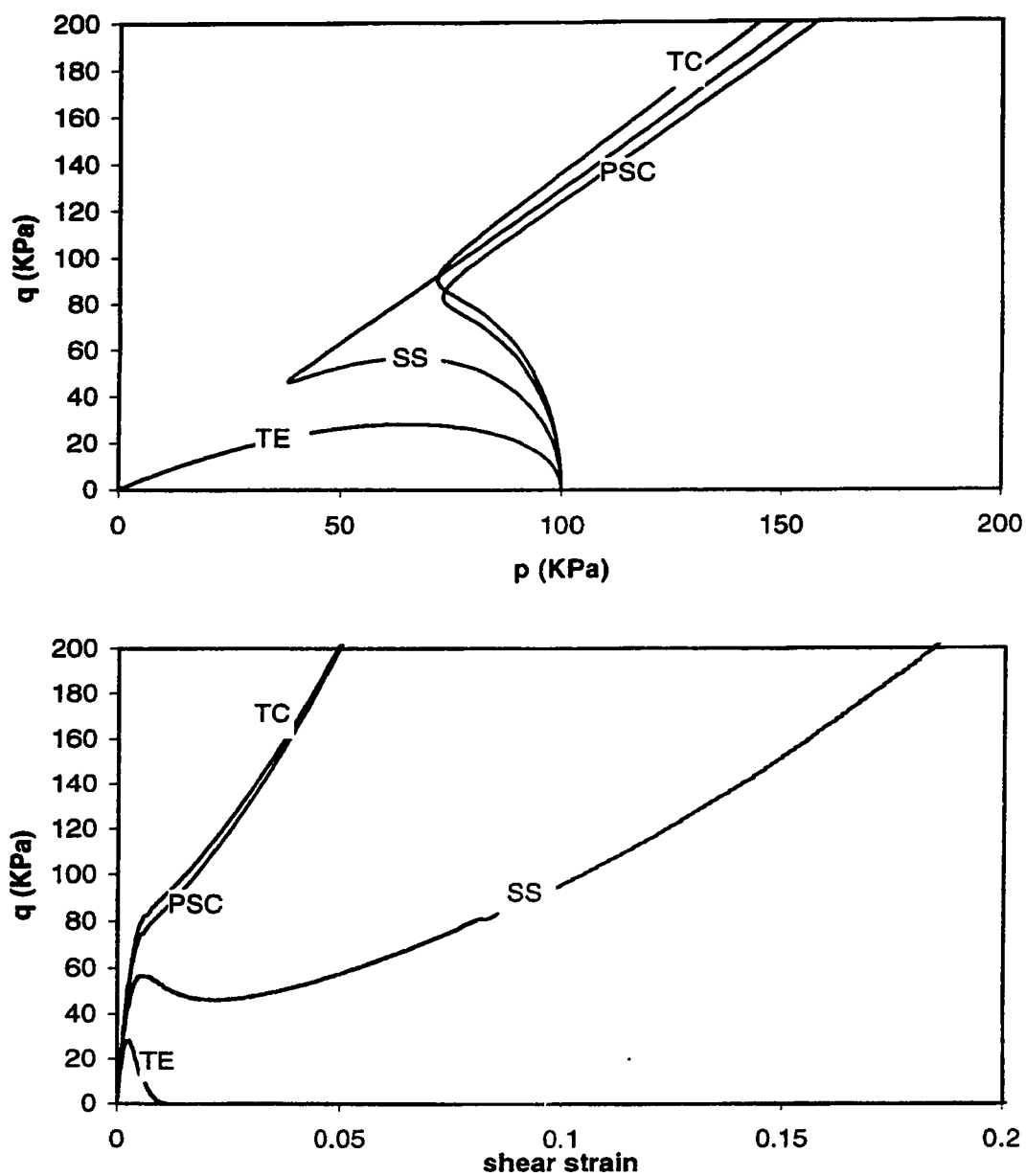


**Figure 6-18** Effect of mode of shearing on the undrained response of Toyoura sand with  $e=0.85$

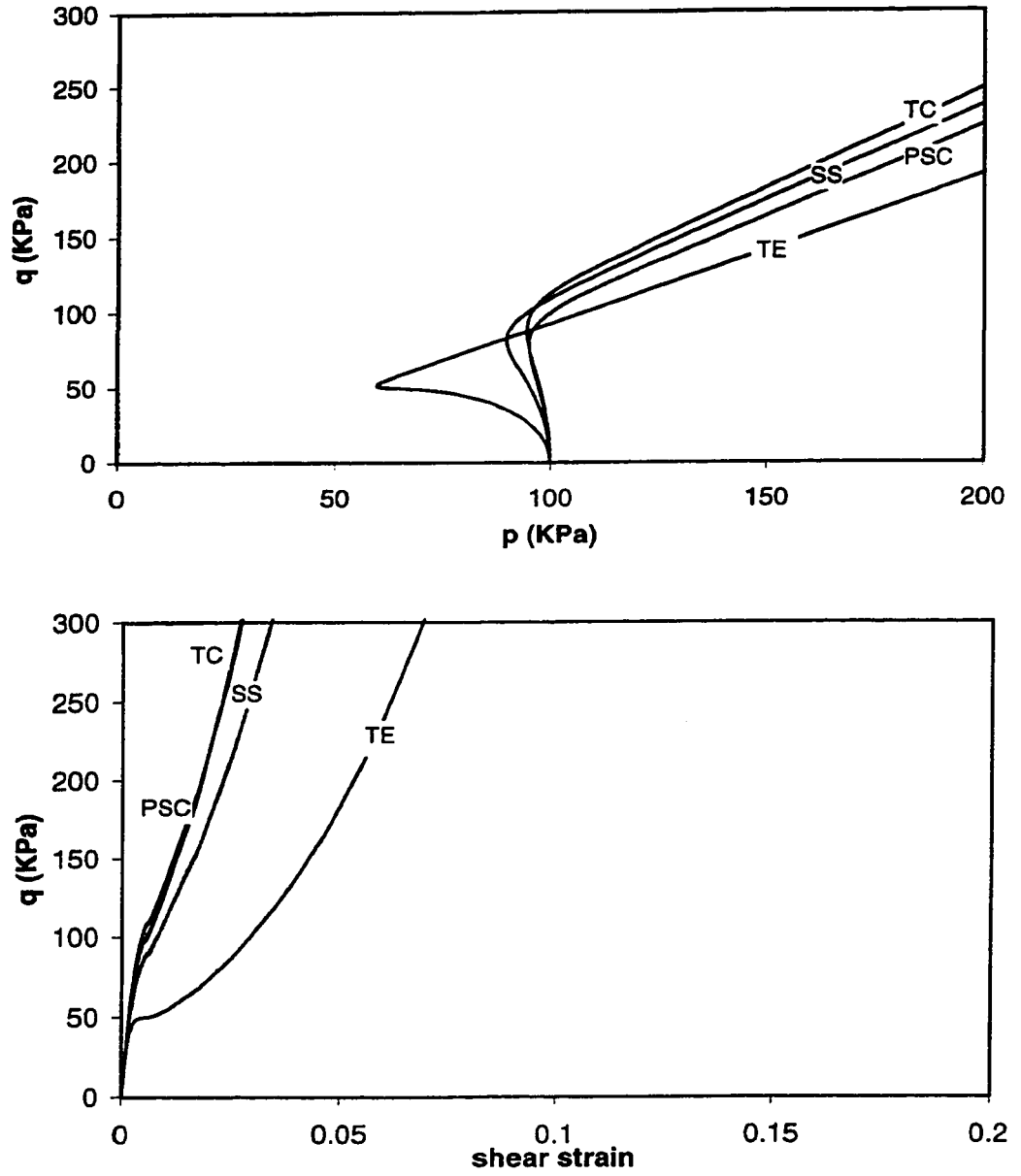


**Figure 6-19** Effect of mode of shearing on the undrained response of Toyoura sand with  $e=0.75$

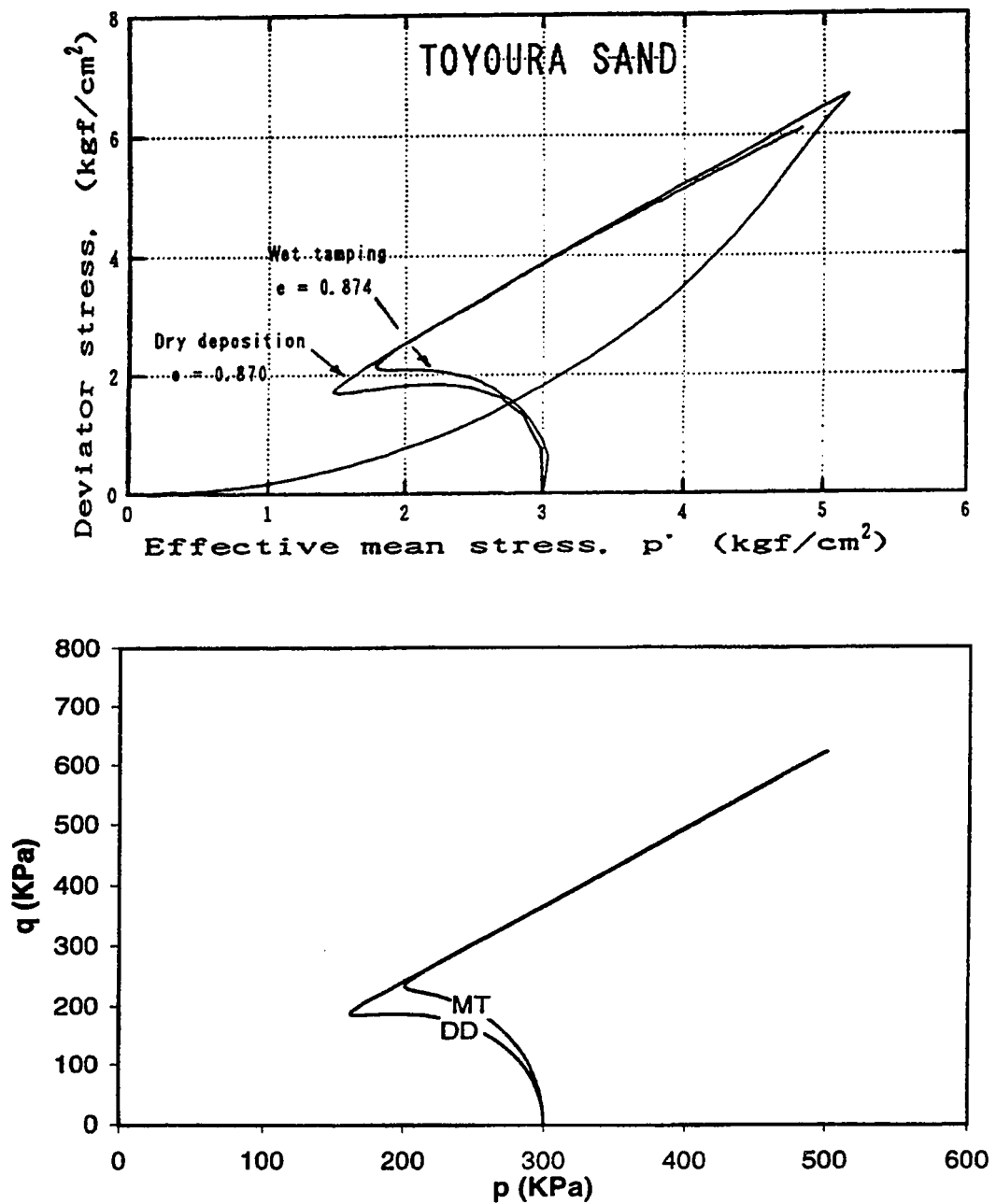


**Figure 6-20** Observed (top) and predicted (bottom) difference between the undrained effective stress path of Toyoura sand prepared by moist (wet) tamping (MT) and dry deposition (DD)

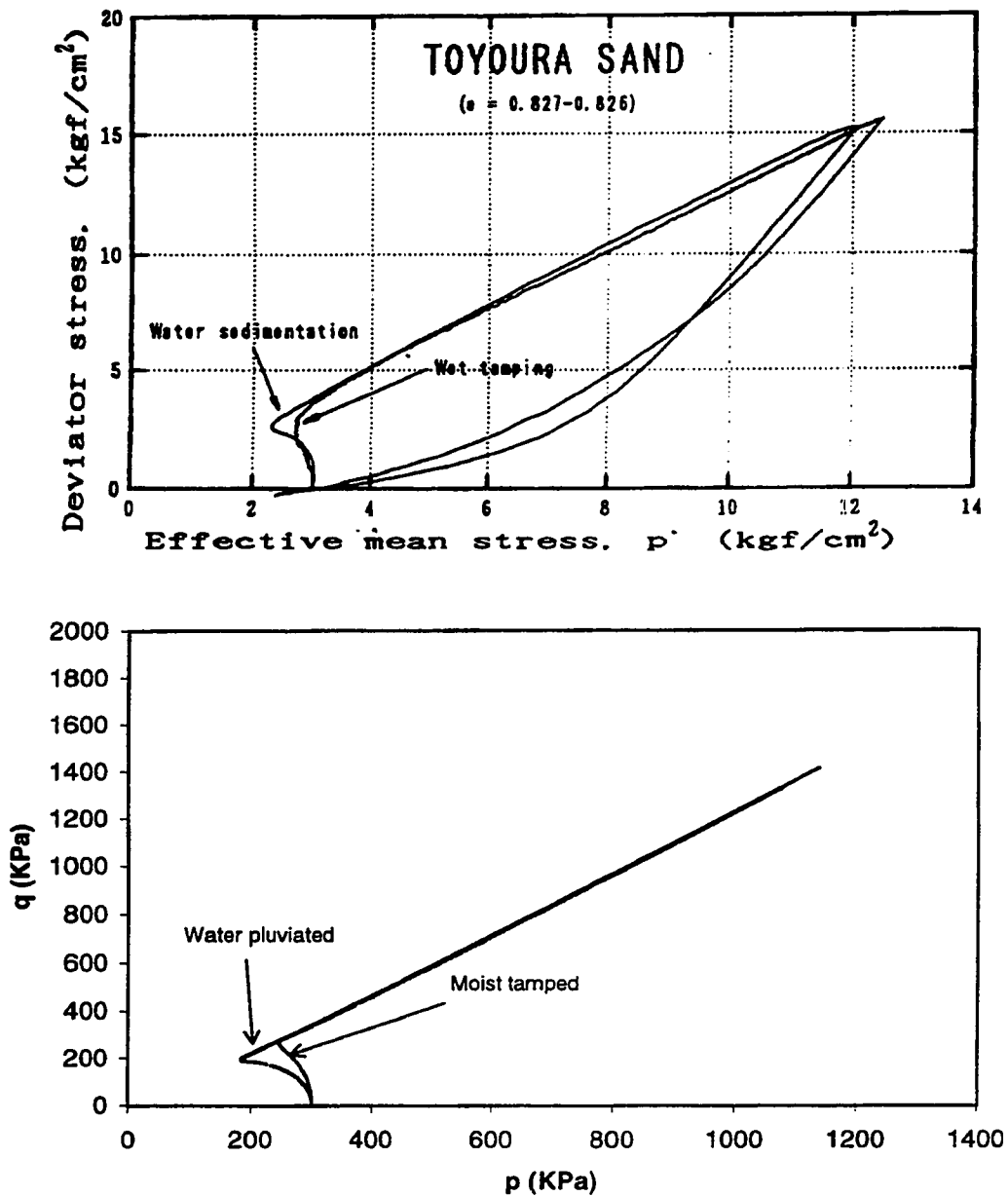


**Figure 6-21** Observed (top) and predicted (bottom) difference between the undrained effective stress path of Toyoura sand prepared by moist (wet) tamping (MT) and water pluviation (sedimentation) (WP).

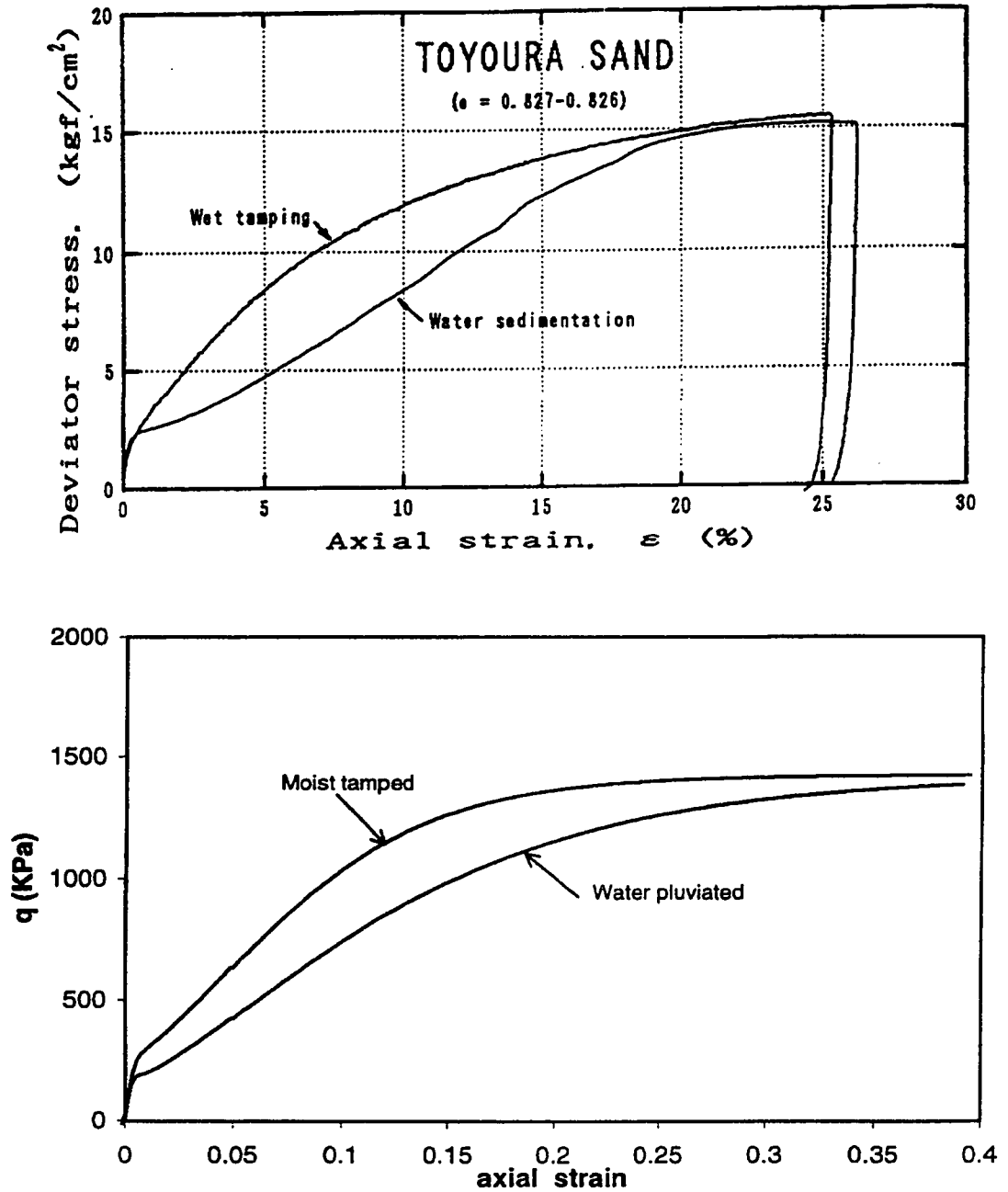


**Figure 6-22** Observed (top) and predicted (bottom) difference between the stress-strain behavior of Toyoura sand prepared by moist (wet) tamping and water pluviation (sedimentation).

## Appendix 6A: Formulation of the stress-strain relationship

Determination of the explicit stress-strain relationship is outlined below. Further details needed for the calculation of the variables can be found in Chapters 6 and 5.

### 6A-1 General stress conditions

Increments of stresses are related to increments of strain by Equations 6-27:

$$\dot{p} = K [\dot{\nu} - \langle L \rangle D] \quad \dot{s} = 2G [\dot{\epsilon} - \langle L \rangle u_p]$$

The above equations determine increments of stresses for given increments of total strain  $\dot{\nu}$  and  $\dot{\epsilon}$ , provided that  $u_p$ ,  $D$  and  $L$  are known. These variables can be determined from the following relationships:

a) Direction of loading:

$$3Q'' = \frac{\partial f}{\partial p} = \frac{M_\alpha^2}{2(pp_\alpha)^{1/2}} - \frac{2}{p}(\eta^2 - \alpha\eta)$$

$$Q' = \frac{\partial f}{\partial s} = \frac{1}{p} \left( \frac{3s}{p} - \sqrt{6\alpha} \right) - \left[ 1 - \left( \frac{p}{p_\alpha} \right)^{1/2} \right] \frac{\partial M_\alpha^2}{\partial s}$$

$$u_Q = \frac{Q'}{|Q'|} \quad \text{and we have} \quad u_P = u_Q$$

$$R = 3 \frac{Q''}{|Q'|} = \frac{\frac{\partial f}{\partial p}}{\left| \frac{\partial f}{\partial s} \right|}$$



**b) Dilatancy parameter D:**

$$D = \sqrt{\frac{2}{3}} A [ M_{PT,c} g(\theta) - \eta ] \quad \text{with} \quad A = \frac{9}{(9 - 2\eta M_{PT}) + 3M_{PT} \cos 3\theta}$$

$$M_{PT} = M_{PT,c} g(\theta) \quad \text{with} \quad g(\theta) = \frac{2c}{(1+c) - (1-c)\cos 3\theta} \quad \text{and} \quad c = \frac{M_{PT,e}}{M_{PT,c}}$$

$$M_{PT,c} = \frac{6 \sin \varphi_{PT,c}}{(3 - \sin \varphi_{PT,c})} \quad M_{PT,e} = \frac{6 \sin \varphi_{PT,e}}{(3 + \sin \varphi_{PT,e})}$$

$$\sin \varphi_{PT,c} = \sin \varphi_{cv} + k_{PT} \psi \quad \text{and} \quad \sin \varphi_{PT,e} = \sin \varphi_{cv} + a_{PT} + k_{PT} \psi$$

**c) Normalized loading index L:**

Since in the current model  $u_p = u_Q$ , we have  $u_p u_Q = 1$  and Equation 6-25 reduces to:

$$L = \frac{KR\dot{v} + 2Gu_Q\dot{e}}{H_n + KRD + 2G}$$

R and  $u_Q$  were determined in (a), and R was obtained in (b). The normalized plastic modulus  $H_n$  is obtained from the following relationships:

$$H_n = -\sqrt{\frac{2}{3}} \frac{1}{|Q|} \frac{\partial f}{\partial p_\alpha} \frac{\partial p_\alpha}{\partial |e^p|}$$

$$\text{with} \quad \frac{\partial f}{\partial p_\alpha} = -\frac{M_\alpha^2}{2p_\alpha} \left( \frac{p}{p_\alpha} \right)^{1/2} \quad \text{and} \quad \frac{\partial p_\alpha}{\partial |e^p|} = h(p_f - p_\alpha)$$

## 6A-2 Specialization for triaxial conditions:

For triaxial conditions, if the stress and strain variables defined in Chapter 5 and used in Appendix 5A are employed, the following equations can be obtained from Equation 6-27:

$$(a) dp = K [ d\epsilon_p - \langle L \rangle D ] \quad (b) dq = 3G [ d\epsilon_q - \sqrt{\frac{2}{3}} \langle L \rangle ]$$

in which 
$$D = \sqrt{\frac{2}{3}} A [ M_{PT} - \eta ]$$

$$A_c = 9/(9 - 2M_{PT,c} \eta + 3M_{PT,c}) \quad \text{for TC}$$

$$A_e = 9/(9 - 2M_{PT,e} \eta - 3M_{PT,e}) \quad \text{for TE}$$

and  $M_{PT,c}$  and  $M_{PT,e}$  can be obtained as given in (b) in Section 6A-1 above. The plastic (loading) index can be determined from:

$$L = \frac{KR(d\epsilon_p) + \sqrt{6}G(d\epsilon_q)}{H_n + KR D + 2G} \quad \text{with} \quad R = \sqrt{\frac{2}{3}} \frac{\partial f}{\partial p} \frac{\partial f}{\partial q}$$

$$\text{and} \quad \frac{\partial f}{\partial p} = \frac{M_\alpha^2}{2(pp_\alpha)^{1/2}} - \frac{2}{p}(\eta^2 - \alpha\eta) \quad \frac{\partial f}{\partial q} = \frac{2}{p}(\eta - \alpha)$$

The normalized hardening modulus can be obtained from the relationships given in part (c) of Section 6A-1 above. In this case we have:

$$|Q'| = \frac{\partial f}{\partial q} = \frac{2}{p}(\eta - \alpha)$$

## *Chapter 7*

# **7 Summary, conclusions and recommendations**

## **7.1 Summary and conclusions**

In this thesis, the constitutive behavior of sand was studied and a constitutive model for sand was formulated. The constitutive model was used to predict the behavior of sand over a wide range of densities and consolidation pressures subjected to a variety of loading conditions and modes of shearing. Emphasis was placed on modeling the behavior of loose collapsible sand and accounting for factors that were identified in the literature as having a particularly important effect on their behavior. After a brief introduction in Chapter 1 and a review of past literature in Chapter 2, the constitutive behavior of sands, in particular, their yielding behavior was examined in Chapters 3 and 4. Based on results of this examination, a constitutive model for sands was introduced which was presented and evaluated for triaxial conditions in Chapter 5, and for general stress conditions in Chapter 6.

The yielding behavior of sand was investigated in Chapter 3, and the suitability of some yield functions to represent the actual yielding of sand was evaluated. Changes in yield stresses with void ratio and anisotropic consolidation were also examined. For the capped yield surface used in this study, it was shown that an increase in void ratio resulted in a reduction in the stress ratio at the peak of the yield surface. Therefore, changes in yield stresses with void ratio could be accounted for, through changes in the stress ratio at the peak of the yield surface. Effects of anisotropic consolidation and

inherent anisotropy on the yielding behavior were also examined. The relationship between the stress state at the initiation of collapse, instability or undrained softening of loose sand, and the yielding stresses was investigated. Analysis of published experimental results and correlation of observations reported in the literature suggested that for very loose sand, collapse, instability or undrained softening may initiate upon reaching the yield surface. Changes in the stress state at the onset of collapse due to changes in the void ratio of the soil, the consolidation stresses and the loading condition were investigated by examining changes in the shape and size of the yield surface. The proximity of the yield surface and the undrained effective stress path (UESP) of very loose Ottawa sand was demonstrated. Based on the analysis of results of drained and undrained tests on very loose Ottawa sand, it was shown that the stress ratio at the peak of the yield surface can be approximated by the stress ratio  $M_p$  measured at the peak of the UESP. This result was used in Chapter 4 to investigate the yielding behavior of loose sand as explained below.

Variations of the stress ratio  $M_p$  with density, pressure, intermediate principal stress, direction of loading, anisotropic consolidation and soil fabric were examined and formulated in Chapter 4. These variations were then used to investigate the effects of the factors mentioned above on the yielding of sand. Published results of undrained loading of a variety of sands were used in this investigation. Comparisons were made between yield surfaces obtained using this procedure and those obtained in previously published studies, in which yield stresses were measured directly. These comparisons showed that both procedures resulted in similar effects of these factors on yielding stresses. Through the study of the variation of  $M_p$ , it was possible to account for and quantify the effects of various factors such as void ratio, intermediate principal stresses, direction of loading and soil fabric on the yielding behavior. Using conventional procedures to determine the effects of some of these factors on the yielding stresses can be very difficult. Model predictions presented in Chapters 5 and 6 suggested that effects of the factors mentioned above on the constitutive behavior of sand can be modeled using these yield surfaces.

Formulation of the variation of  $M_p$ , also made it possible to investigate quantitatively effects of the factors mentioned above on the susceptibility of loose sands to collapse and flow failure. Previous studies often investigated the collapse potential qualitatively and did not account for some of these effects. It was shown in Chapter 4 that when loose sand is sheared in TE, it is significantly more susceptible to collapse than when sheared in TC. In simple shear or plane strain loading, the susceptibility to collapse is intermediate between those of TC and TE. It was also shown in Chapter 4 that an increase in void ratio, or the angle  $\alpha_\sigma$  between the direction of soil deposition and the direction of application of the major principal stress, will also increase the potential for collapse significantly.

A critical state constitutive model for monotonic loading of sand was introduced in Chapters 5 and 6. Constitutive relationships and model predictions were presented in Chapter 5 for triaxial stress conditions. The constitutive relationships were extended in Chapter 6 to include loading in general stress conditions, and model predictions were presented for the response of sand to loading in such conditions. Yield surfaces obtained in Chapters 3 and 4 were used in developing the model.

The proposed model may be characterized by the following features:

- a- While the model is capable of predicting the behavior of sand over a wide range of densities, particular attention was paid to the formulation of the behavior of loose collapsible sand and accounting for the effects of factors that have greater influence on their behavior. The ability of the model to account for effects of factors such as direction of loading, direction of consolidation, mode of shearing, and soil fabric on the undrained response of loose sand was demonstrated.
- b- Through the use of a parameter  $M_p$ , the model quantifies and accounts for some effects that are important in the small to medium strain behavior of soils. Among these effects are the inherent anisotropy and soil fabric, which are often difficult to account for. The parameter  $M_p$  not only influences the yielding behavior, but

also affects the predicted plastic modulus through the form of the hardening rule that is employed in the model. The yield surface and the plastic modulus seem to be the most important elements of a constitutive model that are affected by anisotropy and soil fabric.

- c- The proposed model requires a set of 11 parameters plus the position of the ultimate state line to predict the behavior of sand over a wide range of void ratios and consolidation pressures. For Toyoura sand for which the most comprehensive data base was available, consolidation pressures for which model predictions were presented ranged between 4 kPa to 3000 kPa, a ratio of almost 1000. The samples for which responses were simulated ranged between very loose and very dense. Model predictions covered various directions of loading, directions of consolidation, modes of shearing, and soil fabrics.
- d- The model recognizes the existence of an ultimate state to which shearing processes converge. In the absence of sufficient experimental evidence and a definitive agreement among researchers, and in accordance with results of a number of experimental investigations, the model assumes that effects such as stress-induced anisotropy, inherent anisotropy, and soil fabric are eliminated at large strain. Significant differences, however, were predicted in sand behavior, due to some of these effects at smaller strain. These differences, which were consistent with observed experimental results, were mainly accounted for through the parameter  $M_p$ .
- e- The model uses a unique USL in predicting the behavior of sand subjected to different loading conditions and modes of shearing. In doing so, the unresolved controversy over the uniqueness of the USL is bypassed by taking into account effects of various factors that influence the behavior of sand in the small to medium levels of strain through other model parameters. Consequently, the USL affects the predicted behavior only at large strain.
- f- In accordance with experimental findings, directional properties of sand are divided into effects of stress-induced and inherent anisotropies. The two types of anisotropy are characterized by two separate and independent parameters, and the

ways in which the predicted behavior is influenced by the two types of anisotropy, are different from each other.

- g- The strength of sand at ultimate state was assumed to be independent of its initial state, while that at phase transformation (PT) was related to the state (i. e. void ratio and mean normal stress) of the soil. It was shown that this non-uniqueness of the strength at PT is embedded in Rowe's (1962) stress-dilatancy relationship. Use of the term "ultimate state" was made therefore, to refer to the ultimate condition at which continuous shearing under constant volume and stresses takes place, rather than the temporary condition at PT.
- h- The hardening rule is written such that increments of hardening are related to the state of the soil rather than its plastic shear strain. In contrast to "strain hardening" or "work hardening" formulations, in the current "state hardening" formulation knowledge of the current "state" of the soil is sufficient to predict the next increment of hardening. Therefore, the amount of shear strain experienced by the soil before reaching the current state is not needed in the hardening rule.
- i- Model parameters are related to well-known variables and concepts that are used in the characterization of strength and deformability of soils. Model parameters controlling soil strength at yielding, phase transformation and failure are determined in terms of friction angles, and those controlling deformability are related to deformation moduli. Physical meanings of parameters are clarified and methods by which they can be obtained from experiments, without the need for curve fitting or trial and error, are suggested.

Drained and undrained behaviors of Ottawa sand and Toyoura sand were predicted in Chapter 5 using the proposed model. The behavior of very loose Ottawa in a number of two-stage undrained-to-drained tests was predicted. In these two-stage tests, the strains that developed in the two stages belonged to different drainage conditions. The current "state hardening" formulation helped model the behavior without the need for the shear strain that is often needed in "strain hardening" or "work hardening" formulations. Observed and predicted results of these tests showed

that a small increase in shear stresses can cause a large increase in shear and volumetric strains when the sample is at a collapsible state.

The collapse of very loose, dry Ottawa sand in CDS tests was also modeled in Chapter 5. The model was used to predict the effect of density on the collapse potential in CDS tests. These predictions showed that as samples become denser, their susceptibility to collapse in CDS loading becomes smaller, until they no longer exhibit collapsive behavior. Modeling two-stage tests and CDS tests on very loose Ottawa sand showed that the model is able to simulate the behavior of very loose collapsible sands subjected to different stress paths. All the tests on Ottawa sand mentioned above, including some additional simulations of drained and undrained TC tests, were modeled using the same model parameters.

Drained and undrained responses of Toyoura sand in TC and TE tests were also modeled in Chapter 5. Model simulations and experimental results showed that significant differences may be observed between undrained responses of Toyoura sand to shearing in TC and TE. Void ratios, at which complete collapse of the sample occurred, were significantly different in TC and TE, and the model simulated these differences accurately. In agreement with experimental results, the model predicted undrained responses in TE that were significantly weaker than those in TC. Results of drained TE tests on Toyoura sand were not available. The model was used, therefore, to predict the results of such tests. Predicted response of Toyoura sand in drained tests showed that, compared to TC, significantly more contraction takes place before PT is reached in TE. However, the model predicted the same void ratio at ultimate state for both modes of shearing. Such large initial volumetric contraction may lead to complete collapse of the sample that is sheared in TE before PT is reached.

Model predictions shown in Chapter 5 suggested that some limitations of the available testing equipment might be responsible for some of the difficulties faced in reaching the ultimate state in TE tests. Apart from the occurrence of non-uniformities in TE tests that often makes results of such tests at larger strain unreliable, model predictions showed



that compared to TC, significantly more shear strain may be needed in TE tests before the ultimate state is reached. This is due to the larger volumetric contraction that is experienced by TE samples before the onset of any subsequent dilation, which brings the sample to the ultimate state.

Good agreement between observed and predicted response of loose and dense Toyoura sand consolidated anisotropically, and subjected to undrained shearing in TC was shown in Chapter 6. The effect of stress-induced anisotropic properties on the peak undrained shear strength of sand was also illustrated through model predictions. These predictions suggested that consolidating sand anisotropically in any direction can increase the peak strength of the sample, if it is sheared in the same direction, but decrease it, if sheared in the opposite direction. It was concluded therefore, that the direction of consolidation can have major effects on the susceptibility of sand to flow failure.

The influence of direction of loading was also investigated in Chapter 6. It was shown that the inherent anisotropy of sand, which is generally oriented in the direction of soil deposition, can have a significant effect on its drained and undrained responses. Observed and simulated behavior of Ham River sand and Toyoura sand showed that the drained response becomes more contractive and the undrained response becomes more strain-softening when loads are applied in directions that make larger angles with the direction of soil deposition (this angle was denoted by  $\alpha_{\sigma}$ ). Model predictions also showed that the void ratios at which complete collapse leading to zero strength occurs in undrained tests, increases with increases in  $\alpha_{\sigma}$ .

Differences in undrained responses of sand to shearing in various modes were investigated in Chapter 6 for loose and dense sand. These differences result from differences in intermediate principal stresses and directions of loading, corresponding to various modes of shearing. A major part of these differences resulted from the effect of direction of loading, and results of model predictions showed that shearing loose sand in modes that corresponded to higher values of  $\alpha_{\sigma}$  resulted in larger contractive tendencies.

Predicted response of loose Toyoura sand to undrained shearing exhibited increasing contractive behavior, as the mode of shearing changed in this order: TC, PSC, SS, PSE and TE. Model predictions, however, showed that changes in mode of shearing did not seem to affect the contractive potential of dense sand as much as that of loose sand. It is noted that dense sands do not experience large contractions at the beginning of their deformation, and before their subsequent dilation after the PT is reached. Changes in this small initial contraction due to changes in shearing mode or direction of loading therefore may not lead to significant differences in the undrained response.

The effects of the method by which sand samples are prepared before being tested were modeled at the end of Chapter 6. It was shown that these effects could be accounted for by selecting appropriate yield strengths for the different soil fabrics produced by different preparation methods. Changes in soil fabric were reflected in differences in the model parameters used to calculate the stress ratio  $M_p$ . Other model parameters were not changed with soil fabric. It was shown that differences in  $M_p$  produced predictions that differed from each other in the same way as the responses of samples prepared by different methods. In modeling the constitutive behavior of sand with different fabrics or structures, it may be possible therefore, to account for these differences through the use of appropriate yield variables, such as the stress ratio  $M_p$  used in the current model. It should be noted, however, that such variables are expected to be sensitive to any factor that influences the fabric or structure of the soil, including details of soil formation and subsequent physical processes experienced by the soil. Measurement of such variables, therefore, should be made from results of tests on undisturbed samples.

## 7.2 Recommendations

A number of areas in which further studies related to the current work is possible are listed below:

1. The constitutive model in its current state has not been evaluated for the response of sand to cyclic loading. The current formulation, however, can take into account effects of stress-induced anisotropy. Extension to cyclic loading is possible through the definition of a law that defines kinematic hardening or the use of bounding surface plasticity.
2. The model assumes that inherent anisotropy of the soil is eventually eliminated, and a unique ultimate state is finally reached at large strain. This is because while the yield surface can be strongly influenced by anisotropy, the ultimate state of the soil is governed by an isotropic failure criterion. This is also true for the effect of stress-induced anisotropy on the yielding behavior. It is assumed that as with the inherent anisotropy, the effect of stress-induced anisotropy on the yielding behavior remains unaltered by shearing, provided that the number and/or the size of the stress reversals is small. Sufficient experimental evidence regarding possible evolutions of soil anisotropies during shear, especially in the case of inherent anisotropy, was not available. However, formulation of changes in stress-induced anisotropy can be made in the context of cyclic loading, as mentioned earlier. In the current model, however, this was not attempted.
3. Accounting for the effect of fabric and structure on the constituting behavior of sand has always been a challenge. Some recent works on modeling the constitutive behavior of sand (e. g. Jefferies, 1993; Pestana, 1994) emphasized the importance of considering the effects of structure and fabric in modeling sand behavior. Incorporating such considerations into model formulations, however, has often been overlooked. It does not seem likely that quantifying and modeling such effects would be an easy and straightforward task. However, in view of the attempt made in the current model to quantify and account for these effects, it is beneficial to further evaluate the present approach by studying a wider variety of sands, and in particular, natural sands. Such evaluation may be performed by measuring stress ratios at peak  $M_p$  in sands with a wide range of structures and fabrics. Such exercises will also be useful in identifying other model elements that could possibly be affected by soil structure. The current exercise suggested that changes in soil fabric can be accounted for, by using appropriate values for

the stress ratio  $M_p$ . It is useful to examine the way in which this stress ratio changes when the structure of the soil is altered. Such studies can be helpful in selecting model parameters for in-situ soils that might have structures different from those of the samples that are reconstituted artificially in the laboratory.

4. Constitutive models are most useful when implemented in a numerical scheme and used to analyze soil structures subjected to various loading. It is useful, therefore, to use the model in a numerical scheme and examine the considerations that need to be accounted for in such implementations.
5. The model was used to predict the behavior of sands over a wide range of void ratios and consolidation pressures, using a unique set of parameters. In many in-situ tests, high stresses are applied to the ground during testing. However, soil properties derived from results of such tests are often needed to predict the response of soils at lower stresses. The model can be used in such cases to derive parameters from results of high-stress in-situ tests and use them to predict the response to actual low stress loading. The possibility of accounting for soil structure in the model may serve as an added benefit since many in-situ soils are structured. Use of the model in such exercises can help correlate soil properties obtained from in-situ tests with those derived from laboratory tests.
6. In many cases, natural soils are found in mixtures of sand, silt and clay. It is important in such instances to use constitutive models that are able to predict the behavior of a wide spectrum of soils. Therefore, extension of the current model to include the behavior of a wider range of soils can be important. The capped shape used for the yield surface in the current model provides adaptability to the behavior of clays. Such shape was used by Pestana (1994) to model the behavior clayey soils. Other model elements will also need to be evaluated in such an attempt.

**REFERENCES**

- Alarcon-Guzman, A., Leonards, G. A., and Chameau, J. L. 1988. Undrained monotonic and cyclic strength of sands. *J.Geotech.Engrg.ASCE*, **114**(10): 1089-1108.
- Anandarajah, A. and Dafalias, Y. 1986. Bounding Surface Plasticity, III: Application to Anisotropic Cohesive Clays. *Journal of Engineering Mechanics*, **112**(12): 1292-1318.
- Anderson, S. A. and Sitar, N. 1995. Analysis of rainfall-induced debris flows. *Journal of Geotechnical Engineering, ASCE*, **121**(7): 544-552.
- Anderson, S. A. and Riemer, M. F. 1995. Collapse of Saturated Soil Due to Reduction in Confinement. *Journal of Geotechnical Engineering, ASCE*, **121**(2): 216-219.
- Ayoubian, A. and Robertson, P. K. 1998. Void ratio redistribution in undrained triaxial extension tests on Ottawa sand. *Canadian Geotechnical Journal*, **35**(2): 351-359.
- Been, K. and Jefferies, M. G. 1985. A state parameter for sands. *Geotechnique*, **35**(2): 99-112.
- Been, K., Jefferies, M. G., and Hachey, J. 1991. The critical state of sands. *Geotechnique*, **41**(3): 365-381.
- Bellotti, R., Benoit, J., Fretti, C., and Jamiolkowski, M. 1997. Stiffness of Toyoura sand from dilatometer tests. *J.Geotech.Geoenvir.Eng.*, **123**(9): 836-846.
- Billam, J. 1971. Some aspects of the behavior of granular materials at high pressures. *Proc.of Roscoe Memorial Symp.*: 69-80.
- Bishop, A. W. 1966. The strength of soils as engineering materials. 6th Rankine Lecture. *Geotechnique*, **16**(2): 91-128.
- Bishop, A. W. 1971. Shear strength parameters for undisturbed and remoulded soil specimens. *Roscoe Memorial Symposium*: 3-58.
- Bishop, A. W. 1973. The Stability of Tips and Spoil Heaps. *Quarterly Journal of Eng.Geology*, **6**: 335-376.
- Bjerrum, L., Kringstand, S., and Kummeneje, O. 1961. The Shear Strength of a Fine Sand. *Proc.5th Int.Conf.Soil Mech.Found.Eng., Paris*, **1**: 29-37.
- Bolton, M. D. 1986. The strength and dilatancy of sands. *Geotechnique*, **36**(1): 65-78.
- Bopp, P. A. and Lade, P. V. 1997. Effects of Initial Density on Soil Instability at High Pressures. *Journal of Geotechnical and Geoenvironmental Engineering*, **123**(7): 671-677.

- Calladine, C. R. 1971. A microstructural view of the mechanical properties of saturated clay. *Geotechnique*, **21**: 391-415.
- Cambou, B. and Lanier, J. 1988. Induced Anisotropy in Cohesionless Soil: Experiments and Modelling. *Computers and Geotechnics*, **6**: 299-311.
- Canou, J., Bahda, F., Saitta, A., and Dupla, J. C. 1994. Initiation of Sand Liquefaction under Monotonic and Cyclic Loading. *Proc.XIII ICSMFE, New Delhi, India*: 1297-1300.
- Casagrande, A. 1936. Characteristics of Cohesionless Soils Affecting the Stability of Slopes and Earth Fills. *Journal of Boston Society of Civil Engineers*, Jan.: 13-32.
- Casagrande, A. 1970. On Liquefaction Phenomena. Lecture reported by Green and Ferguson, *Geotechnique*, **21**(3): 197-202.
- Casagrande, A. 1971. On Liquefaction Phenomena. *Geotechnique*, **11**(3): 197-202.
- Casagrande, A. 1975. Liquefaction and Cyclic deformation of sands - A critical Review. *Harvard Soil Mechanics Series*, No.88.
- Castro, G. 1969. "Liquefaction of sand". Ph.D.thesis, Harvard University.
- Castro, G. and Poulos, S. J. 1977. Factors Affecting Liquefaction and Cyclic Mobility. *Journal of Geotechnical Engineering, ASCE*, **103**(No. GT6): 501-516.
- Chan, D. H., Soroush, A., and Morgenstern, N. R. 1995. Numerical analysis of centrifuge modeling for the CANLEX experiment. *Proceedings of the 48th Canadian Geotechnical Conference, Vancouver*: 375-382.
- Chandler, H. W. 1990. A model for the deformation and flow of granular materials undergoing monotonic shear loading. *Geotechnique*, **40**(3): 379-388.
- Chern, J. 1985. Undrained response of saturated sands with emphasis on liquefaction and cyclic mobility. Ph.D.thesis University of British Columbia.
- Chillarige, A. V. 1995. Liquefaction and seabed instability in the Fraser River Delta. Ph D thesis, University of Alberta.
- Chillarige, A. V., Robertson, P. K., and Morgenstern, N. R. 1997. Evaluation of the in situ state of Fraser River sand. *Canadian Geotechnical Journal*, **34**(4): 510-519.
- Chu, J., Lo, S. C. R., and Lee, I. K. 1992. Strain Softening Behavior of a Dense Granular Soil in Strain Path Testing. *Journal of Geotechnical Engineering, ASCE*, **118**(2): 191-208.

- Chu, J., Lo, S. C. R., and Lee, I. K. 1993. Response of a Granular Soil During Strain Path Testing. *Modern approaches to plasticity* ed.D.Kolymbas, Rotterdam: Balkema.: 599-640.
- Courtney-Pratt, J. S. and Eisner, E. 1957. *Proc.Roy.Soc., Series*, **208**: 311.
- Crouch, R. S., Wolf, J., and Dafalias, Y. 1994. Unified critical state bounding surface plasticity model for soil. *J.Eng.Mech.*, **120**(11): 2251-2270.
- Cunning, J. C., Robertson, P. K., and Sego, D. C. 1995. Shear wave velocity to evaluate in-situ state of cohesionless soils. *Canadian Geotechnical Journal*, **32**: 848-858.
- Dafalias, Y. 1975. *On Cyclic and Anisotropic Plasticity*. Ph.D.thesis, University of California at Berkeley.
- Dafalias, Y. and Popov, E. P. 1975. *A Model of Nonlinearly Hardening Materials For Cyclic Loading*. *Acta Mechanica*, **21**: 173-192.
- Dafalias, Y. and Herrmann, L. R. 1982. *Bounding Surface Formulation of Soil Plasticity*. Chapter 10 in Pande, G.N.and Zienkiewicz, O.C.(eds.) *Soil Mechanics-Cyclic and Transient Loads*, Wiley: 253-282.
- Dafalias, Y. and Herrmann, L. R. 1986. *Bounding Surface Plasticity II: Application to Isotropic Cohesive Soils*. *Journal of Engineering Mechanics*, **112**(12): 1263-1291.
- di Prisco, C., Nova, R., and Lanier, J. 1993. A mixed isotropic kinematic hardening constitutive law for sand. *Modern approaches to plasticity* ed.D.Kolymbas, Rotterdam: Balkema.: 83-124.
- di Prisco, C. and Nova, R. 1994. *Stability Problems Related to Static Liquefaction of Loose Sand. Localization and Bifurcation Theory for Soils and Rocks*, Chambon, Desrues, Vardoulakis (ed.), Balkema: 59-70.
- di Prisco, C., Matiotti, R., and Nova, R. 1995. *Theoretical Investigation of the Undrained Stability of Shallow Submerged Slopes*. *Geotechnique*, **45**(3): 479-496.
- Drucker, D. C. 1951. *A More Fundamental Approach to Stress-Strain Relations*. *Proc.First U.S.Nat.Cong.Appl.Mech.*: 487-491.
- Drucker, D. C. and Prager, W. 1952. *Soil Mechanics and Plastic Analysis or Limit Design*. *Quarterly of Applied Mechanics*, **10**: 157-165.
- Drucker, D. C. 1956. *On Uniqueness on the Theory of Plasticity*. *Quart.Appl.Math.*, **14**: 35-42.
- Drucker, D. C., Gibson, R. E., and Henkel, D. 1957. *Soil Mechanics and Work Hardening Theories of Plasticity*. *Transactions of ASCE*, **122**: 338-346.

- Drucker, D. C. 1959. A definition of Stable Inelastic Material. *J.Appl.Mech.*, **26**: 101-106.
- Duffy, J. and Mindlin, R. D. 1957. Stress-strain relations and vibrations of a granular medium. *J.Appl.Mech.Trans.ASME*, **24**: 585-593.
- Faruque, M. O. and Zaman, M. M. 1991. On the concept of characteristic states of cohesionless soil and constitutive modeling. *Soils and Foundations*, **31**(2): 164-174.
- Ghaboussi, J. and Momen, H. 1979. Modeling and Analysis of Cyclic Behavior of Sand. *Soil Mechanics-Transient and Cyclic Loads*, edited by Pande, G. and Zienkiewicz, O.C., John Wiley and Sons.
- Ghaboussi, J. and Momen, H. 1982. Plasticity Model for Cyclic Behavior of Sands. *Pro.3rd Int.Conf.on Numerical Methods in Geomechanics, Aachen*.
- Graham, J., Noonan, M. L., and Lew, K. V. 1983. Yield states and stress-strain relationships in a natural plastic clay. *Canadian Geotechnical Journal*, **20**(3): 502-516.
- Griffiths, D. V. 1990. Failure Criteria Interpretation Based on Mohr-Coulomb Friction. *Journal of Geotechnical Engineering, ASCE*, **116**(6): 986-999.
- Gu, W. H., Morgenstern, N. R., and Robertson, P. K. 1993. Progressive failure of lower San Fernando dam. *Journal of Geotechnical Engineering, ASCE*, **119**(2): 333-348.
- Gudehus, G. 1973. Elastoplastische stoffgleichungen für trockenen sand. *Ingenieur-Archiv*, **42**: 151-169.
- Gutierrez, M., Ishihara, K., and Towhata, I. 1993. Model for the Deformation of Sand During Rotation of Principal Stress Direction. *Soils and Foundation*, **33**(3): 105-117.
- Hanzawa, H. 1980. Undrained Strength and Stability Analysis for a Quick Sand. *Soils and Foundation*, **20**(2): 17-29.
- Hardin, B. O. and Richart, F. E. Jr. 1963. Elastic wave velocities in granular soils. *J.Soil Mech.And Found.Engrg.Div.ASCE*, **89**(1): 33-65.
- Hardin, B. O. and Black, W. L. 1969. Closure to Vibration modulus of normally consolidated clay. *Journal of Soil Mechanics and Foundation Engineering Division, ASCE*, **95**(SM6): 1531-1537.
- Hardin, B. O. 1987. 1-D Strain in Normally Consolidated Cohesionless Soils. *Journal of Geotechnical Engineering, ASCE*, **113**(12): 1449-1467.



- Hill, R. 1958. A General Theory of Uniqueness and Stability in Elasto-plastic Solids. *J.Mech.Phys.Solids*, **6**: 236-249.
- Horn, H. M. and Deere, D. U. 1971. Frictional characteristics of minerals. *Proc.of the Roscoe Memorial Symposium*: 319-335.
- Horne, M. R. 1965. The Behavior of an Assembly of Rotund, Rigid Cohesionless Particles. *Proc.Royal Society, Series A*, **286**: 62-97.
- Hvorslev, M. J. 1937. Uber die Festigkeitseigenschaften Gestorter Bindiger Boden. *Ingeniorvidenskabelige Skrifter, A*, **45**: 159.
- Hyodo, M., Tanimizu, H., Yasufuku, N., and Murata, H. 1994. Undrained cyclic and monotonic triaxial behavior of saturated loose sand. *Soils and Foundations*, **34**(1): 19-32.
- Imam, R., Robertson, P. K., Chan, D. H., and Morgenstern, N. R. 1998. Constitutive modeling of loose collapsible soils. *Proceedings of the 51st Canadian Geotechnical Conference*.
- Imam, R., , Chan D. H., Robertson, P. K., and Morgenstern, N. R. 1998. Effect of loading direction on the constitutive behavior of sands. *Proceedings of the 51st Canadian Geotechnical Conference*.
- Ishihara, K., Tatsuoka, F., and Yasuda, S. 1975. Undrained deformation and liquefaction of sand under cyclic stresses. *Soils and Foundation*, **15**(1): 29-44.
- Ishihara, K. 1985. Stability of Natural Deposits During Earthquakes. Theme Lecture, *Proceeding of the XI ICSMFE*, **2**: 321-376.
- Ishihara, K., Verdugo, R., and Acacio, A. A. 1991. Characterization of cyclic behavior of sand and postseismic stability analyses. *Proc.9th Asian Regional conference on Soil Mech.and Found.Engrg.Bangkok*: 45-68.
- Ishihara, K. 1993. Liquefaction and flow failure during earthquakes. *Geotechnique*, **43**(3): 351-415.
- Iwan, W. D. 1967. On a Class of Models for the Yielding Behavior of Continuous and Composite Systems. *Journal of Applied Mechanics, ASME*, **34**: 612.
- Jaeger, J. C. 1971. Friction of rocks, and stability of rock slopes. 11th Rankine Lecture. *Geotechnique*, **21**(2).
- Jefferies, M. G. and Been, K. 1992. Undrained response of Nor-Sand. 45th Canadian Geotechnical Conference, Toronto, Canada.
- Jefferies, M. G. 1993. Nor-Sand: a simple critical state model for sand. *Geotechnique*, **43**(1): 91-103.

- Jiang, J. and Pietruszczak, S. 1988. Convexity of yield loci for pressure sensitive materials. *Computers and Geotechnics*(5): 51-63.
- Jovicic, V. and Coop, M. R. 1997. Stiffness of coarse grained soils at small strains. *Geotechnique*, **47**(3): 454-561.
- Kim, M. K. and Lade, P. V. 1988. Single Hardening Constitutive Model for Frictional Materials, I. Plastic Potential Function. *Computers and Geotechnics*, **5**: 307-324.
- Konrad, J. M. and Saint-Laurent, S. 1995. Laboratory testing of reconstituted and in-situ frozen specimens-Syncrude tailings sand, CANLEX Technical Report, Phase I, Activity 8C, Universite' Laval.
- Koppejan, A. W., Van Wamelen, B. M., and Weinberg, L. J. H. 1948. Coastal Landslides in the Dutch Province of Zeeland. *Proc.2nd Int.Conf.on Soil Mech.and Found.Eng.*, Rotterdam, Holland: 89-96.
- Lacy, S. J. and Prevost, J. H. 1987. Constitutive Model For Geomaterials. *Proc.of 2nd Int.Conf.on Constitutive Laws for Engineering Materials*, Tucson, Arizona: 1-12.
- Lade, P., Nelson, R. B., and Ito, Y. M. 1988. Instability of granular materials with nonassociated flow. *J.of Engrg.Mech.ASCE*, **114**(12): 2173-2191.
- Lade, P. 1992. Static instability and liquefaction of loose fine sandy slopes. *J.of Geotech.Engrg.ASCE*, **118**(1): 51-70.
- Lade, P. 1994. Creep effects on static and cyclic instability of granular soils. *J.of Geotech.Engrg.ASCE*, **120**(2): 404-419.
- Lade, P. V. and Duncan, J. M. 1973. Cubical triaxial tests on cohesionless soil. *J.of Soil Mech.and Foundations Division ASCE SM10*: 793-812.
- Lade, P. V. and Duncan, J. M. 1975. Elasto-plastic stress-strain theory for cohesionless soil. *J.of Geotech.Engrg.ASCE GT10*: 1037-1051.
- Lade, P. V. and Duncan, J. M. 1976. Stress-path dependent behavior of cohesionless soil. " *J.Of Geotech.Engrg.ASCE GT1*, **102**: 51-68.
- Lade, P. V. 1977. Elastoplastic stress-strain theory for cohesionless soil with curved yield surfaces. *Int.J.Solids and Structures*, **13**: 1019-1036.
- Lade, P. V. and Kim, M. K. 1988. Single hardening constitutive model for frictional materials II-Yield criterion and plastic work contours. *Computers and Geotechnics*, **6**: 13-29.
- Lade, P. V. 1992. Static Instability and Liquefaction of Loose Fine Sandy Slopes. *Journal of Geotechnical Engineering, ASCE*, **118**(1): 51-71.

- Lade, P. V., Bopp, P. A., and Peters, J. F. 1993. Instability of Dilating Sand. *Mechanics of Materials*, **16**: 249-264.
- Lade, P. V. 1994. Creep Effects on the Static and Cyclic Instability of Granular Soils. *Journal of Geotechnical Engineering, ASCE*, **120**(2): 404-419.
- Lade, P. V. and Prabucki, M. 1995. Softening and preshearing effects in sand. *Soils and Foundations*, **35**(4): 93-104.
- Lam, W. K. and Tatsuoka, F. 1988. Effects of initial anisotropic fabric and  $\sigma_2$  on the strength and deformation characteristics of sands. *Soils and Foundations*, **28**(1): 89-106.
- Manzari, M. T. and Dafalias, Y. F. 1997. A critical state two-surface plasticity model for sands. *Geotechnique*, **47**(2): 255-272.
- Matsuoka, H. 1974. Stress-strain relationships of sands based on the mobilized plane. *Soils and Foundations*, **14**(2): 47-61.
- Matsuoka, H. 1974. A microscopic study on shear mechanism of granular materials. *Soils and Foundations*, **14**(1): 29-43.
- Matsuoka, H. and Sakakibara, K. 1987. A constitutive model for sands and clays evaluating principal stress rotation. *Soils and Foundations*, **27**(4): 73-88.
- McKenna, G. T., Luternauer, J. L., and Kostaschuk, R. A. 1992. Large-Scale Mass Wasting Events on the Fraser River Delta Front Near Sand Heads, British Columbia. *Canadian Geotechnical Journal*, **29**(2): 151-156.
- Meyerhoff, G. G. 1951. The Ultimate Bearing Capacity of Foundations. *Geotechnique*, **2**: 301-332.
- Molenkamp, F. 1991. Material Instability for Drained and Undrained Behavior. Part 2: Combined Uniform Deformation and Shear Band Generation. *International Journal of Numerical and Analytical Methods in Geomechanics*, **15**: 169-180.
- Morgenstern, N. R. 1967. Submarine slumping and the initiation of turbidity currents. *Marine Geotechnique*, ed by Richards, Univ. of Illinois Press: 189-200.
- Morgenstern, N. R. 1994. Observations on the collapse of granular materials. "The Kersten Lecture" 42nd Annual Geotechnical Engineering Conference, Minneapolis, Minnesota.
- Moroto, Y. 1976. A new parameter to measure degree of shear deformation of granular materials in triaxial compression tests. *Soils and Foundations*, **16**(4): 1-10.
- Mroz, Z. 1967. On the Description of Anisotropic Hardening. *Journal of Mechanics and Physics of Solids*, **15**: 163-175.

- Mroz, Z, Norris, V. A., and Zienkiewicz, O. C. 1978. An Anisotropic Hardening Model for Soils and its Application to Cyclic Loading. *International Journal of Numerical and Analytical Methods in Geomechanics*, **14**(1): 203-221.
- Nakai, T. 1989. An isotropic hardening elastoplastic model for sand considering the stress path dependency in the three-dimensional stresses. *Soils and Foundations*, **29**(1): 119-137.
- Nova, R. 1977. On the Hardening of Soils. *Archives of Mechanics*, **29**(3): 445-458.
- Nova, R. and Wood, D. M. 1978. An experimental program to define the yield function for sands. *Soils and Foundations*, **18**(4): 77-86.
- Nova, R. and Wood, D. M. 1979. A constitutive model for sand in triaxial compression. *Int.J.Num.Anal.Meth in Geomech.*, **3**: 255-278.
- Nova, R. and Hueckel, T. 1981. A unified approach to the modeling of liquefaction and cyclic mobility of sands. *Soils and Foundations*, **21**(4): 13-28.
- Nova, R. 1988. *Sinfonietta Classica: An Exercise on Classical Soil Modelling*. Proc.Int.Workshop on Constitutive Equations For Granular non- Cohesive Soils, Saada A.and Bianchini G.Ed., Cleveland, July 1987: 501-520.
- Oda, M. 1972. The mechanism of fabric changes during compressional deformation of sand. *Soils and Foundations*, **12**(2): 1-18.
- Oda, M. and Konishi, J. 1974. Rotation of principal stresses in granular material during simple shear. *Soils and Foundations*, **14**(4): 39-53.
- Oda, M. 1975. On the Relation  $\tau/\sigma_v = K \tan \psi$  in the Simple Shear Test. *Soils and Foundations*, **15**(4): 35-40.
- Oda, M., Koishikawa, I., and Higuchi, T. 1978. Experimental study of anisotropic shear strength of sand by plane strain test. *Soils and Foundations*, **18**(1): 25-38.
- Oda, M. 1982. Experimental micromechanical evaluation of strength of granular materials: effect of particle rolling. *Mechanics of Materials* **1**: 269-283.
- Pastor, M., Zienkiewicz, O. C., and Leung, K. H. 1985. Simple model for transient soil loading in earthquake analysis. II. Non-associative model for sands. *Int.J.Num.Anal.Meth.Geomech.*, **9**: 477-498.
- Pastor, M., Zienkiewicz, O. C., and Chan, A. H. C. 1990. Generalized Plasticity and the Modeling of Soil Behavior. *International Journal of Numerical and Analytical Methods in Geomechanics*, **14**: 151-190.
- Pestana-Nascimento, J. M. 1994. A unified constitutive model for clays and sands. Ph D thesis, Massachusetts Institute of Technology.

- Pestana, J. M. and Whittle, J. A. 1995. Compression Model for Cohesionless Soils. *Geotechnique*, **45**(4): 611-631.
- Peters, J. F. 1991. Discussion of Instability of Granular Materials with Non-associated Flow. *Journal of Engineering Mechanics*, **117**(4): 934-936.
- Pietruszczak, S. and Mroz, Z 1981. Description of Mechanical behavior of Anisotropically consolidated Clays. *Mechanical Behavior of Anisotropic Solids*, J.P.(ed), Noordhoff.
- Pietruszczak, S. and Stolle, D. F. E. 1987. Modelling of sand behavior under earthquake excitation. *Int.J.for Num.And Analy.Meth.In Geomech.*, **11**: 221-140.
- Pietruszczak, S. and Stolle, D. F. E. 1987. Modeling of Sand Behavior Under Earthquake Excitation. *International Journal of Numerical and Analytical Methods in Geomechanics*, **11**: 221-240.
- Poorooshasb, H. B., Holubec, I., and Sherbourne, A. N. 1966. Yielding and flow of sand in triaxial compression: Part I. *Canadian Geotech.Journal*, **3**(4): 179-190.
- Poorooshasb, H. B. 1971. Deformation of sand in triaxial compression. *Proc.4th Asian Regional Conf.on Soil Mech.and Found.Engrg.*, Bangkok, **1**: 63-66.
- Poorooshasb, H. B. and Pietruszczak, S. 1985. On the Yielding and Flow of Sand, A Generalized Two Surface Model. *Computers and Geotechnics*, **1**: 33-58.
- Poorooshasb, H. B. and Pietruszczak, S. 1986. A Generalized Flow Theory For Sand. *Soils and Foundation*, **26**(2): 1-15.
- Poulos, S. J. 1971. *The Stress-Strain Curves of Soils*. Geotechnical Engineers, Inc., Winchester, Mass.
- Poulos, S. J. 1981. The steady state of deformation. *Journal of Geotechnical Engineering, ASCE*, **17**(No. GT5): 553-562.
- Pradel, D., Ishihara, K., and Gutierrez, M. 1990. Yielding and Flow of Sand Under Principal Stress Axes Rotation. *Soils and Foundation*, **30**(1): 87-99.
- Pradel, D. and Lade, P. V. 1990. Instability and Plastic Flow of Soils II: Analytical Investigation. *Journal of Engineering Mechanics*, **116**(11): 2551-2566.
- Prevost, J. H. 1977. Mathematical Modeling of Monotonic and Cyclic Undrained Clay Behavior. *International Journal of Numerical and Analytical Methods in Geomechanics*, **1**: 195-216.
- Prevost, J. H. 1978. Plasticity Theory for Soil Stress Strain Behavior. *Journal of Engineering Mechanics, ASCE*, **104**(EM5): 1177-1194.

- Prevost, J. H. 1985. A Simple Plasticity Model for Frictional Cohesionless Soils. *Journal of Soil Dynamics and Earthquake Engineering*, **4**(1): 9-17.
- Procter, D. C. and Barton, R. R. 1974. Measurement of the angle of interparticle friction. *Geotechnique*, **24**(4): 581-604.
- Riemer, M. F. 1992. The Effects of Testing Conditions on the Constitutive Behavior of Loose, Saturated Sands Under Monotonic Loading. PhD Thesis, University of California at Berkeley.
- Robertson, P. K. 1994. Suggested terminology for liquefaction. *Proceedings of the 47th Canadian Geotechnical Conference, Halifax*: 277-286.
- Roscoe, K. H., Schofield A.N., and Wroth, C. P. 1958. On the yielding of soils. *Geotechnique*, **8**(1): 22-53.
- Roscoe, K. H., Schofield, A. N., and Thurairajah, A. 1963. Yielding of clays in states wetter than critical. *Geotechnique*, **13**(3): 211-240.
- Roscoe, K. H. and Schofield, A. N. 1964. Discussion of Rowe 1963. *Jour. Soil Mech. Found. Div.*, **90**: 136.
- Roscoe, K. H. and Burland, J. B. 1968. On the Generalized Stress-Strain Behavior of Wet Clay. *Engineering Plasticity*, J. Heyman and F.A. Leckie (editors), Cambridge University Press, Cambridge, England: 535-609.
- Rowe, P. W. 1962. The stress-dilatancy relation for static equilibrium of an assembly of particles in contact. *Pro. of the Roy. Soc. A269*: 500-527.
- Rowe, P. W. 1969. The relation between the shear strength of sands in triaxial compression, plane strain and direct shear. *Geotechnique*, **19**(1): 75-86.
- Rowe, P. W. 1971. Theoretical meaning and observed values of deformation parameters for soil. *Stress-Strain Behavior of Soils, Proc. Roscoe Memorial Symposium*, Cambridge University, Foulis, Henley-on-Thames: 143-194.
- Sasitharan, S., Robertson, P. K., Sego, D. C., and Morgenstern, N. R. 1993. Collapse Behavior of Sand. *Canadian Geotechnical Journal*, **30**: 569-577.
- Sasitharan, S. 1994. Collapse behavior of very loose sands. Ph.D. thesis, University of Alberta.
- Sasitharan, S., Robertson, P. K., Sego, D. C., and Morgenstern, N. R. 1994. State Boundary Surface for Very Loose Sand and its Practical Implications. *Canadian Geotechnical Journal*, **31**: 321-334.
- Seed, H. B. 1983. Earthquake Resistant Design of Earth Dams. *Journal of Geotechnical Engineering, ASCE*, **1**: 41-64.

- Shibuya S. 1985. Undrained behaviour of granular materials under principal stress rotation. Ph D thesis, London University.
- Shibuya S. and Hight, D. W. 1987. On the stress path in simple shear. *Geotechnique*, **37**(4): 511-515.
- Skopek, P. 1994. Collapse behavior of very loose dry sand. Ph.D.thesis , The University of Alberta.
- Sladen, J. A., D'hollander, R. D., and Krahn, J. 1985. The liquefaction of sands, a collapse surface approach. *Canadian Geotec*, **22**: 564-578.
- Sladen, J. A., D'hollander, R. D., and Krahn, J. 1985. Back Analysis of The Nerlerk Berm Liquefaction Slides. *Canadian Geotechnical Journal*, **22**: 579-588.
- Sladen, J. A. and Handford, G. 1987. A potential systematic error in laboratory testing of very loose sands. *Canadian Geotechnical Journal*, **24**: 462-466.
- Symes, M. J., Gens, A., and Hight, D. W. 1984. Undrained anisotropy and principal stress rotation in saturated sand. *Geotechnique*, **34**(1): 11-27.
- Symes, M. J., Gens, A., and Hight, D. W. 1988. Drained principal stress rotation in saturated sand. *Geotechnique*, **38**(1): 59-81.
- Tabor, D. 1959. Junction growth in metallic friction: The role of combined stresses and surface contamination. *Proc.Roy.Soc., Series A* , No 251: 378-393.
- Tatsuoka, F. and Ishihara, K. 1974. Yielding of sand in triaxial compression. *Soils and Foundations*, **14**(2): 63-76.
- Tavenas, F., des Rosiers, J-P., Leroueil, S., LaRochelle P., and Roy, M. 1979. The use of strain energy as a yield and creep criterion for lightly overconsolidated clays. *Geotechnique*, **29**(3): 285-303.
- Terzaghi, K. 1925. *Erdbaumechanik*. Franz Deuticke, Vienna.
- Terzaghi, K. and Peck, R. B. 1948. *Soil Mechanics in Engineering Practice*. John Wiley and Sons, New York.
- Terzaghi, K. 1956. Varieties of Submarine Slope Failures. *Proc.8th Texas Conf.on Soil Mech.Found.Eng.*, U.of Texas, Austin: 1-41.
- Thomas, J. 1992. Static, Cyclic and Post-Liquefaction Undrained Behavior of Fraser River Sand. MSc.Thesis, University of British Columbia.
- Uchida, K. and Vaid, Y. P. 1994. Sand Behavior Under Strain Path Control. *Proc.XIII ICSMFE*, New Delhi, India: 17-20.

- Vaid, Y. P. and Chern, J. C. 1985. Cyclic and monotonic undrained response of saturated sands. *Advances in the art of testing soils under cyclic conditions*, ASCE Convention, Detroit, Mich.: 120-147.
- Vaid, Y. P., Chung, E. K. F., and Kuerbis, R. 1989. Preshearing and Undrained Response of Sand. *Soils and Foundation*, **29**(4): 46-61.
- Vaid, Y. P., Sivathayalan, S., Eliadorani, A., and Uthayakumar, M. 1996. Laboratory testing at UBC. CANLEX report dated April 1996.
- Vardoulakis, I. 1979. Bifurcation Analysis of the Triaxial Test on Sand Samples. *Acta.Mech.*, **38**: 219-239.
- Verdugo, R. and Ishihara, K. 1996. The steady state of sandy soils. *Soils and Foundations*, **36**(2): 81-91.
- Verdugo, R. L. 1992. Characterization of sandy soil behavior under large deformation. Ph D thesis, University of Tokyo.
- Vermeer, P. A. 1978. A Double Hardening Model for Sand. *Geotechnique*, **28**(4): 413-433.
- Whittle, A. J. 1993. Evaluation of a Constitutive Model for Overconsolidated Clays. *Geotechnique*, **43**(2): 289-315.
- Whittle, A. J. and Kavvadas, M. J. 1994. Formulation of the MIT-E3 Constitutive Model for Overconsolidated Clays. *Journal of Geotech.Eng.ASCE*, **120**(1): 173-198.
- Whittle, A. J., DeGroot, D. J., Ladd, C. C., and Seah, T. 1994. Model Prediction of Anisotropic Behavior of Boston Blue Clay. *Journal of Geotechnical Engineering. ASCE*, **120**(1): 199-224.
- Wood, D. M., Drescher, A., and Budhu, M. 1979. On the Determination of Stress State in the Simple Shear Apparatus. *Geotechnical Testing Journal*, **2**(4): 211-222.
- Wood, D. M. 1990. *Soil behavior and the critical state soil mechanics*. Cambridge university press: 239-241.
- Wood, D. M., Belkheir, K., and Liu, D. F. 1994. Strain softening and state parameter for sand modeling. *Geotechnique*, **44**(2): 335-339.
- Wride, C. and Robertson, P. K. 1997a. CANLEX - Phase I and III- Mildred Lake and J-Pit Sites.
- Wride, C. and Robertson, P. K. 1997b. CANLEX Phase II, Massey and Kidd sites, Fraser River Delta.



- Yamada, Y. and Ishihara, K. 1979. Anisotropic deformation characteristics of sand under three dimensional stress conditions. *Soils and Foundations*, **19**: 79-94.
- Yamamuro, J. 1996. Undrained sand behavior in axisymmetric tests at high pressures. *Journal of Geotech.Eng.ASCE*, **122**(2): 120-129.
- Yamashita, S., Shibuya, S., and Tanaka, H. 1997. A case study for characterizing undrained cyclic deformation properties in young sand deposit from in-situ and laboratory tests. *Soils and Foundations*.
- Yasufuku, N., Murata, H., Hyodo, M., and Hyde, A. F. L. 1991. A stress-strain relationship for anisotropically consolidated sand over a wide stress region. *Soils and Foundation*, **31**(4): 75-92.
- Yasufuku, N., Murata, H., and Hyodo, M. 1991. Yield characteristics of anisotropically consolidated sand under low and high stresses. *Soils and Foundations*, **31**(1): 95-109.
- Yoshimine, M. 1996. Undrained flow deformation of saturated sand under monotonic loading conditions. Ph D thesis, University of Tokyo.
- Zienkiewicz, O. C. and Mroz, Z 1984. Generalized Plasticity Formulation and Application to Geomechanics. *Mechanics of Engineering Materials*, Desai, C.S.and Gallagher, R.H.(eds.), Wiley, Chapter 33: 655-679.
- Zienkiewicz, O. C., Chan, A. H. C., Pastor, M., Paul, D. K., and Shiomi, T. 1990. Static and Dynamic Behavior of Soils: A Rational Approach to Quantitative Solutions. Part I. Fully Saturated Problems. *Proceedings of Royal Society, Series A.*, **429**: 285-309.
- Zienkiewicz, O. C., Huang, M., and Pastor, M. 1993. Numerical Prediction for Model No. 1. *Proc.Int.Conf.on The Verification of Numerical Procedures for the Analysis of Soil Liquefaction Problems*, held at the University of California, Davis, Balkema Press, Arulanandan, K.and Scott R.F.(editors), **1**: 259-274.